

REGULATION OF STALLED REPLICATION FORKS BY ATR

By

Frank Benjamin Couch, IV

Dissertation

Submitted to the Faculty of the
Graduate School of Vanderbilt University
in partial fulfillment of the requirements
for the degree of

DOCTOR OF PHILOSOPHY

in

Biochemistry

May, 2014

Nashville, Tennessee

Approved:

Professor David Cortez

Professor Bruce D. Carter

Professor Brandt F. Eichman

Professor Christine M. Eischen

Professor Scott W. Hiebert

To my family

and

To my amazing wife, Lindsay

ACKNOWLEDGEMENTS

This dissertation was made possible in part by funding from the Biochemical and Chemical Training for Cancer Research training program (NIH T32 CA09582) and the Kirschstein National Research Service Award (NIH F31 CA171586).

I would like to thank my mentor, Dr. David Cortez, for his support and training over the years. It seems as if he knows exactly how to strike the balance between providing guidance and letting students figure out their problems and grow as scientists. I also thank my committee, Dr. Bruce Carter, Dr. Brandt Eichman, Dr. Christine Eischen, Dr. Scott Hiebert, and Dr. Ellen Fanning, for their patience and guidance during my dissertation work.

I started graduate school in the interdisciplinary graduate program class of 2009, and I joined Dave's lab in 2010. It is amazing to me since that time to see how the lab has changed: only Dave, Gloria, and Nancy remain from when I joined. The students in the lab at the time that I joined, Edward Nam, Carol Bansbach, and Bianca Sirbu were invaluable as mentors and friends in the laboratory. I am indebted to each of them, as they all contributed to my dissertation in some way: Eddie laid much of the groundwork for the use of ATR inhibitors in our lab, Carol mapped and characterized SMARCAL1 phosphorylation sites, and I worked side by side with Bianca after she developed iPOND.

Since then, several new students have come along. Jessica Luzwick is our fiber labeling ninja, and she did all of the fiber labeling experiments that appear in this dissertation. Discussions with Akosua Badu-Nkansah about SMARCAL1 and ZRANB3 have been invaluable. Kami and Lisa, you are both talented, just remember to keep an open mind about things. You never know in what direction your data will lead.

I would also like to thank my parents who have always supported me through the ups and downs and drastic career trajectory changes that I've taken over the years. Most of all, though, I want to thank my beautiful wife, Lindsay, for all her love and support. Lindsay and I went on our first date less than a month after I joined Dave's lab in 2010. Since then she has been a constant source of support, and I'm not sure I could have finished this dissertation without her. I love you, Lindsay.

TABLE OF CONTENTS

	Page
DEDICATION.....	ii
ACKNOWLEDGEMENTS.....	iii
LIST OF TABLES.....	viii
LIST OF FIGURES.....	ix
LIST OF ABBREVIATIONS.....	xiii
 Chapter	
I. INTRODUCTION.....	1
DNA Replication.....	3
Origin Firing.....	3
Replication Elongation.....	4
Replication through chromatin.....	5
The DNA Damage Response.....	5
DSB Repair.....	8
Non-homologous end joining (NHEJ).....	9
Homology directed repair (HDR).....	9
DNA Damage Responsive Histone Modifications.....	13
The Replication Stress Response.....	14
Stalled Replication Fork Repair Pathways.....	14
1. Stabilization and restart or rescue.....	15
2. Repriming and post-replicative repair.....	15
3. Template switching or fork regression.....	17
4. DSB-mediated restart.....	21
Ataxia telangiectasia mutated and rad3-related (ATR).....	24
Essential Function of ATR.....	24
The S-phase checkpoint.....	25
ATR activation and the G2/M checkpoint.....	26
Function of MRE11 in ATR activation.....	27
ATR Stabilization of Replication Forks.....	29
SMARCAL1.....	30
SMARCAL1 Biochemistry.....	30
Annealing Helicases and Replication.....	33
Mechanism of Fork Remodeling.....	35
Crosstalk between ATR and SMARCAL1.....	37
II. MATERIALS AND METHODS.....	38
Antibodies (Western Blotting).....	38
Antibodies (Immunofluorescence).....	39

ATR inhibitor.....	40
Cell culture.....	40
Clonogenic survival.....	41
Fiber labeling.....	41
Fork regression assays.....	42
Flow Cytometry.....	43
In vitro kinase assay.....	44
Isolation of Proteins on Nascent DNA (iPOND).....	44
Native iPOND.....	46
Neutral COMET Assay.....	46
Plasmid constructs.....	47
Preparation of Fork Regression Substrates.....	48
Preparation of Fork Restoration Substrates.....	49
Pan-nuclear γ H2AX immunofluorescent assay.....	49
RBanneal PCR Program.....	50
RIPA Lysis for Western Blot.....	50
ssDNA immunofluorescent assays.....	50
SMARCAL1 Overexpression ssDNA Assay.....	53
SMARCAL1 ATPase assay.....	53
SMARCAL1 purification.....	54
Transfections.....	55
<i>Xenopus</i> cell free replication experiments.....	56
Extra Methods.....	56
[3H]Thymidine Incorporation Assay.....	56
BrdU Dot-Blot.....	57
Chromatin Fractionation.....	57
Plasmid-based Fork Regression Substrate Preparation.....	58
Plasmid Based Fork Regression Assay.....	59
Replication Intermediate Purification for Electron Microscopy.....	60
Yeast iPOND.....	61
III. ANALYSIS OF THE DNA DAMAGE RESPONSE AT STALLED REPLICATION FORKS.....	63
Preamble.....	63
Introduction.....	63
Results.....	65
Analysis of chromatin maturation using iPOND.....	65
Development of Native iPOND (n-iPOND).....	67
Analysis of Replisome Stability During Prolonged Replication Stress.....	70
DDR response at stalled replication forks.....	70
RAD51 accumulation at stalled replication forks.....	72
ATR Regulation of Stalled Replication Forks.....	74
γ H2AX spreading from stalled forks before and after fork collapse.....	74
Other DNA Damaging Agents.....	78
Discussion.....	80
IV. ATR PHOSPHORYLATES SMARCAL1 TO PREVENT REPLICATION FORK COLLAPSE.....	84
Introduction.....	84

Results.....	86
Acute ATR inhibition causes rapid cell death in cells experiencing replication stress.....	86
ATR inhibition deregulates replication timing control and causes replication fork collapse.....	90
ATR inhibition causes nascent-strand ssDNA formation.....	92
ATR prevents SLX4- and CtIP-dependent formation of DSBs and nascent-strand ssDNA at stalled forks.....	96
Nascent-strand ssDNA formation involves replication fork remodeling.....	99
Replication stress induces SMARCAL1 phosphorylation after it accumulates at stalled forks and binds DNA.....	108
S652 phosphorylation reduces SMARCAL1 activity.....	111
Too much SMARCAL1 activity in cells phenocopies the effect of ATR inhibition on fork collapse.....	119
Discussion.....	121
ATR as a drug target.....	123
Aberrant stalled fork processing when ATR is inactivated.....	125
Conclusions.....	128
V. BIOCHEMICAL MECHANISM OF SMARCAL1 TRANSLOCATION ON DNA.....	130
Introduction.....	130
Results.....	131
Development of a Biotin-Streptavidin Block Assay.....	137
Discussion.....	144
A Helicase Activity for SMARCAL1?.....	147
Avidin bound substrates reveal commonalities between fork regression enzymes.....	147
Function of Annealing Helicases in Replication.....	148
Conclusions.....	150
VI. DISCUSSION and FUTURE DIRECTIONS.....	153
Summary.....	153
iPOND and the DNA Damage Response.....	154
iPOND is a useful tool to study protein dynamics at stalled replication forks.....	154
ATR Regulation of Stalled Replication Forks.....	158
ATR and Fork Repair Pathways.....	161
Future Directions.....	162
Biochemistry of Annealing Helicases.....	164
Development of an assay for fork regression polarity.....	165
Comparison of SMARCAL1 and other annealing helicases.....	166
The Normal Function of Annealing Helicases.....	167
A Model for SMARCAL1 and ZRANB3 Function.....	168
Regulation of ZRANB3.....	171
Conclusions.....	171
REFERENCES.....	174

LIST OF TABLES

Table	Page
4.1 Oligonucleotides for substrate construction.....	129
5.1 Construction of Fork Regression Substrates.....	152

LIST OF FIGURES

Figure	Page
1.1. DNA replication through chromatin.....	6
1.2. DSBs activate DNA-PK, ATM, and ATR.....	7
1.3. Pathways of DSB Repair.....	10
1.4. ATM and MDC1 mediate spreading of γ H2AX from site of DSB.....	12
1.5. Stabilization and restart or rescue.....	16
1.6. Repriming and post-replicative repair.....	18
1.7. Fork regression and template switching.....	19
1.8. DSB-mediated recovery of stalled replication forks.....	22
1.9. G2/M Checkpoint.....	28
1.10. SMARCAL1 substrate preferences.....	32
1.11. Model for SMARCAL1 function in repair of stalled replication forks.....	34
3.1. Isolation of Proteins on Nascent DNA (iPOND).....	66
3.2. H4K5ac and H4K12ac are deacetylated with different kinetics after deposition due to reacetylation by HATs.....	68
3.3. Native isolation of proteins on nascent DNA (n-iPOND).....	69
3.4. Detection of polymerase subunits using iPOND.....	71
3.5. RAD51 accumulation during extended HU treatments is dependent on MRE11 nuclease activity.....	73
3.6. γ H2AX spreads along chromatin behind stalled replication forks.....	76
3.7. γ H2AX spreading is ATM/DNA-PK-dependent during extended HU treatments, but ATR-dependent during short HU treatments.....	77
3.8. Protein dynamics at CPT-damaged replication forks.....	79
4.1. Acute ATR inhibition causes rapid cell lethality.....	88

4.2.	Acute ATR inhibition causes an inability to complete DNA replication after a replication stress challenge.....	89
4.3.	ATR regulates DNA replication initiation and elongation.....	91
4.4.	Stalled replication forks collapse into double strand breaks when ATR is acutely inhibited.....	93
4.5.	ATR inhibition causes both nascent and parental ssDNA accumulation at stalled replication forks.....	94
4.6.	MUS81 is not required to generate DSBs or nascent-strand ssDNA after ATR inhibition.....	97
4.7.	SLX4 is required to generate DSBs and nascent-strand ssDNA at stalled forks when ATR is inhibited.....	98
4.8.	SLX1, GEN1, XPF are not required for nascent-strand ssDNA.....	100
4.9.	CtIP is required to generate nascent-strand ssDNA at stalled replication forks when ATR is inhibited.....	101
4.10.	EXO1, DNA2 are not required for nascent-strand ssDNA.....	102
4.11.	SMARCAL1 is required for the generation of nascent-strand ssDNA when ATR is inactivated in human cells.....	104
4.12.	FANCM, HLF are not required for nascent-strand ssDNA.....	105
4.13.	ZRANB3, BLM are not required for nascent-strand ssDNA.....	106
4.14.	xSMARCAL1 is required for the generation of nascent-strand ssDNA when ATR is inactivated in <i>Xenopus</i> egg extract.....	107
4.15.	ATR phosphorylates SMARCAL1 after SMARCAL1 binds to DNA at stalled forks.....	109
4.16.	SMARCAL1 mutants that cannot bind DNA retain their ability to localize to sites of stalled replication forks.....	110
4.17.	Mapping of SMARCAL1 phosphorylation sites.....	112

4.18.	SMARCAL1 S652 is phosphorylated by ATR in cells and <i>in vitro</i>	114
4.19.	SMARCAL1 phosphorylation on S173, S652, or S919 does not alter its ability to bind DNA or localize to stalled replication forks.....	116
4.20.	SMARCAL1 phosphorylation on serine 652 inhibits its ATP-dependent fork remodeling activity.....	117
4.21.	Mutation of S652 does not alter the DNA binding ability of SMARCAL1.....	118
4.22.	Phosphorylation of SMARCAL1 at S652 decreases its activity at DNA replication forks in cells.....	120
4.23.	Model for nascent-strand ssDNA generation at stalled forks.....	122
4.24.	CDK2 and CDC7 kinase inhibitors do not rescue ATRi toxicity.....	124
5.1.	Nicks and 1nt gaps have no effect on SMARCAL1 fork regression activity.....	133
5.2.	5nt and 10nt gaps on the leading template strand inhibit SMARCAL1 fork regression activity.....	134
5.3.	Effects of 10nt template strand gaps on UvsW and RecG fork regression activity	135
5.4.	Gapped fork regression intermediate resembles fork restoration substrate.....	136
5.5.	Substrates containing biotinylated nicks inhibit SMARCAL1 activity.....	138
5.6.	Nicked duplex DNA inhibits SMARCAL1 activity on no gap fork regression substrates.....	139
5.7.	Substrates containing biotin-dU bound to streptavidin inhibit SMARCAL1 fork regression activity.....	140
5.8.	Substrates containing biotin-dU bound to avidin inhibit SMARCAL1 fork regression activity.....	142
5.9.	Substrates containing biotin-dU bound to avidin inhibit ZRANB3 fork regression activity.....	143

5.10.	Substrates containing biotin-dU bound to avidin inhibit RecG fork regression activity.....	145
5.11.	Substrates containing biotin-dU bound to avidin inhibit UvsW fork regression activity.....	146
5.12.	Dual regression/restoration substrate design.....	151
6.1.	MRE11 and RAD51 interplay at stalled replication forks.....	156
6.2.	ATRi-induced pan-nuclear γ H2AX is DNA-PK-dependent.....	157
6.3.	SMARCAL1 activity is a balance between too much and too little.....	159
6.4.	Differential functions of SMARCAL1 and ZRANB3.....	170
6.5.	ZRANB3 contains similar linker sequence to SMARCAL1 including T264 in the same position as SMARCAL1 S652.....	172

LIST OF ABBREVIATIONS

53BP1	p53 binding protein 1
9-1-1	RAD9-HUS1-RAD1 complex
AAD	ATR activation domain
ALKB	Alkylation repair homolog
APH	Aphidicolin
ATM	Ataxia Telangiectasia mutated
ATP	Adenosine triphosphate
ATR	ATM and Rad3-related
ATRi	ATR inhibitor
ATRIP	ATR interacting protein
BLM	Bloom's syndrome protein, RecQ helicase-like
BRCA1	Breast cancer type 1 susceptibility protein
BRCA2	Breast cancer type 2 susceptibility protein
BrdU	5-bromo-2'-deoxyuridine
BSA	Bovine serum albumin
CAF-1	Chromatin assembly factor 1
CBP	CREBBP-associated factor
CDC6	Cell division cycle 6 homolog
CDC25	Cell division cycle 25 homolog
CDK	Cyclin-dependent kinase
CDT1	Chromatin licensing and DNA replication factor 1
ChIP	Chromatin immunoprecipitation
CHK1	Checkpoint kinase 1
CHK2	Checkpoint kinase 2

CldU	5-chloro-2'-deoxyuridine
CPT	Camptothecin
CtIP	CtBP[C-terminal binding protein]-interacting protein
DDK	DBF4-dependent kinase
DDR	DNA damage response
DMSO	Dimethyl sulfoxide
DNA	Deoxyribonucleic acid
DNA2	DNA replication helicase/nuclease 2
DNA-PK	DNA-dependent protein kinase
dNTP	Deoxynucleoside triphosphate
DSB	Double strand break
dsDNA	Double stranded DNA
EdU	5-ethynyl-2'-deoxyuridine
EME1	Essential meiotic structure-specific endonuclease 1
EXO1	Exonuclease 1
FANCM	Fanconi anemia, complementation group M
FAT	FRAP-ATM-TRRAP
FATC	FAT C-terminal
GEN1	GEN1 Holliday junction 5' flap endonuclease
GFP	Green fluorescent protein
GINS	Go-ichi-ni-san complex
H2AX	H2A histone family member X
γ H2AX	H2AX phosphorylated on serine 139
HARP	HepA-related protein
HAT	Histone acetyl transferase

HEAT	Huntingen, elongation factor 3, protein phosphatase 2A, yeast TOR1
HDR	Homology-directed repair
HLTF	Helicase like transcription factor
HR	Homologous recombination
HRR	HR repair
HU	Hydroxyurea
ICL	Interstrand crosslink
IdU	5-iodo-2'-deoxyuridine
iPOND	Isolation of proteins on nascent DNA
Mec1p	Mitosis entry checkpoint protein 1, ATR homolog
MCM	Minichromosome maintenance
MDC1	Mediator of DNA-damage checkpoint 1
MGMT	O-6-methylguanine-DNA methyltransferase
MMC	Mitomycin C
MMS	Methyl methanesulfonate
MOF	Ortholog of Drosophila males absent on the first
MRE11	Meiotic recombination 11 homolog
MRN	MRE11-RAD50-NBS1
mRNA	Messenger RNA
mTOR	Mammalian target of rapamycin
MUS81	MUS81 structure-specific endonuclease subunit
NBS1	Nijmegen Breakage Syndrome protein 1
NHEJ	Non-homologous end joining
ORC	Origin recognition complex
PAGE	Polyacrylamide gel electrophoresis

PARP	Poly ADP-ribose polymerase
PBS	Phosphate buffered saline
PCNA	Proliferating cell nuclear antigen
PIKK	Phosphoinositide-3-kinase-like kinase
PLK1	Polo-like kinase 1
POLA	DNA polymerase alpha
POLD	DNA polymerase delta
POLE	DNA polymerase epsilon
PRD	PIKK regulatory domain
Pre-RC	Prereplicative complex
PrimPol	DNA primase and polymerase
PTM	Post-translational modification
RAD51	RAD51 recombinase
RAP80	Receptor associated protein 80
REV1	REV1 homolog, DNA-directed polymerase
RING	Really interesting new gene
RNA	Ribonucleic acid
RNF4	RING finger protein 4
RNF8	RING finger protein 8
RNF168	RING finger protein 168
RPA	Replication protein A
RSR	Replication stress response
SDS	Sodium dodecyl sulfate
SF2	Helicase/translocase superfamily 2
SHPRH	SNF2 histone linker PHD RING helicase, E3 ubiquitin protein ligase

SIRT6	SIR2-like protein 6
SIOD	Schimke immunoosseous dysplasia
SLX1	SLX1 structure-specific endonuclease subunit
SLX4	SLX4 structure-specific endonuclease subunit
SMARCAL1	SWI/SNF, matrix associated, actin dependent regulator of chromatin A-like 1
SNF2H	Sucrose nonfermenting protein 2 homolog
SPO11	Sporulation 11
SWI/SNF	SWI/SNF DNA helicase/translocase family
SSB	Single strand break (DNA)
SSB	Single strand binding protein
SSC	Saline sodium citrate buffer
ssDNA	Single stranded DNA
SUMO	Small ubiquitin like modifier
TBE	Tris-borate-EDTA buffer
TBS	Tris buffered saline
Tip60	Lysine acetyltransferase 8
TLS	Translesion synthesis
TopBP1	Topoisomerase II-binding protein 1
TOPOIII	Topoisomerase III
Ub	Ubiquitin
UV	Ultraviolet radiation
WRN	Werner syndrome protein, RecQ helicase-like
XLF	Nonhomologous end-joining factor 1
XPF	Xeroderma Pigmentosum, complementation group F
XRCC4	X-ray repair complementing defective repair in Chinese hamster cells 4

ZRANB3

Zinc finger, RAN-binding domain containing 3

CHAPTER I

INTRODUCTION

DNA replication is a fundamental process for all life. With few exceptions, each of the trillions of cell divisions that occur in a human lifetime requires the accurate and complete duplication of all 6 billion base pairs of the human genome. Errors in replication can lead to mutations that contribute to cancer development. As if this alone were not enough of a challenge, replication takes place in the context of DNA damage. To counter this challenge to genome integrity, cells contain an innate machinery known as the DNA Damage Response (DDR), which coordinates cell cycle checkpoints, DNA repair activity, and replicative senescence or apoptosis to ensure that either the genetic material remains intact or the cell is removed from the actively cycling population.

Highlighting the importance of the DDR machinery, several proteins in this pathway, such as ATR (ATM- [Ataxia Telangiectasia Mutated] and Rad3-related) and CHK1, are essential for life (Brown and Baltimore 2000; de Klein et al. 2000), while mutations in others, such as MRE11 (Meiotic recombination 11 homolog), NBS1 (Nijmegen breakage syndrome protein 1), and CHK2 (Checkpoint kinase 2), cause disease syndromes associated with cancer (Hartlerode and Scully 2009). Many cancers have inactivated one or more DDR pathways, which allows mutations to accumulate and drive cancer progression (Hanahan and Weinberg 2011); however, these same cells may be more sensitive to inhibition of other DDR pathways – an example of synthetic lethality. The classic example of this is that BRCA1/2 (Breast cancer type 1/2 susceptibility protein) mutations sensitize cancer cells to PARP (Poly-ADP ribose polymerase) inhibitors (Bryant et al. 2005; Farmer et al. 2005). PARP inhibitors block single-strand break (SSB) repair. When the cell attempts to replicate these SSBs, they

are converted to double strand breaks (DSBs), which require homology directed repair (HDR). While normal cells have little problem with this, BRCA1 and BRCA2 are required for HDR; thus cells deficient for these genes accumulate unrepaired DSBs and die in the presence of PARP inhibitors (Helleday 2011). Alternatively, PARP inhibition may trap PARP on DNA repair intermediates which require BRCA1/2 to repair stalled replication forks that encounter these sites (Helleday 2011).

Replication stress arises any time a cell encounters difficulty replicating its DNA. UV light, alkylating agents, oxidative metabolic products, difficult to replicate sequences, and nucleotide imbalances can all cause replication stress (Cimprich and Cortez 2008; Zeman and Cimprich 2013). The oncogene-induced replication stress model posits that the genome instability that characterizes many cancer cells arises from replication stress (Halazonetis et al. 2008). As such, these same cells may have an increased dependence on replication stress response genes such as ATR and CHK1 (Charrier et al. 2011; López-Contreras et al. 2012; Reaper et al. 2011). For this reason, inhibitors of ATR and CHK1 may prove valuable anti-cancer agents and are currently in various stages of development (Chen et al. 2012; Fokas et al. 2014; Toledo et al. 2011a).

In this thesis, I will describe our studies of how ATR and SMARCAL1 function in the DNA damage response. In Chapter III, I will describe work done in collaboration with Bianca Sirbu to study the protein composition of stalled and collapsed replication forks using the iPOND technology. In Chapter IV, I will describe work done using an ATR inhibitor to probe the changes that occur during acute replication stress when ATR is absent. I also collaborated with Carol Bansbach-Robbins, who demonstrated that SMARCAL1 is regulated by phosphorylation. Together, we demonstrated that SMARCAL1 is regulated by ATR after DNA damage to prevent excess fork remodeling. Finally, in Chapter V, I will describe how I have built upon previous work described here and work by Rémy Bétous to understand at a deeper level the biochemistry of

SMARCAL1 and what the function of SMARCAL1 might be in cells. Finally, in Chapter VI, I will discuss what these results mean in the context of the literature and outline some future experiments. First, however, I will introduce several key concepts in DNA replication, the DNA damage response, and replication stress.

DNA Replication

Origin Firing

The process of duplicating the genome, known as DNA replication, involves several enzymatic activities and the coordinated action of several proteins, including helicases, polymerases, single-stranded binding proteins, topoisomerases, and various accessory factors. Bacterial replication is relatively simple, as bacteria contain a single circular chromosome with a single, well-defined origin of replication. In contrast, eukaryotes have multiple large linear chromosomes that initiate replication from multiple origins (O'Donnell et al. 2013).

The process of DNA replication actually begins in the G1 phase of the cell cycle. In eukaryotes, origins of replication are bound by the origin recognition complex (ORC), which consists of ORC1-6. These origins are controlled such that only a single round of replication occurs during each cell cycle. To accomplish this, the prereplicative complex (pre-RC), consisting of the ORC complex, CDC6 (cell division cycle 6 homolog), CDT1 (chromatin licensing and DNA replication factor 1), and two molecules of the MCM2-6 (minichromosome maintenance complex components 2-6) heterohexameric helicase, only assembles during G1. Once the cell enters S-phase, CDK (cyclin-dependent kinase) activity prevents further formation of the pre-RC through subcellular localization and degradation of pre-RC components CDC6 and CDT1 (Siddiqui et al. 2013).

At the onset of S-phase, CDKs and the DBF4/CDC7 kinase (or DBF4-dependent kinase, DDK) phosphorylate the pre-RC to allow recruitment of accessory factors CDC45 (cell division cycle 45) and the GINS complex (Go-ichi-ni-san complex). The origin can then 'fire', or unwind the DNA duplex to allow the MCM helicase to shift from its dsDNA-encircling mode to the active ssDNA-encircling mode and begin processive unwinding of the DNA duplex (Siddiqui et al. 2013).

Replication Elongation

The replicative helicases, DNA polymerase delta (POLD) and DNA polymerase epsilon (POLE), cannot initiate de-novo DNA synthesis, but must extend an existing DNA primer. To create these primers, DNA primase synthesizes an RNA primer, which DNA polymerase alpha (POLA) extends. After synthesis of a short DNA tract, the replicative polymerases can then take over DNA synthesis. On the leading strand, DNA synthesis is highly processive, aided by the proliferating cell nuclear antigen (PCNA) sliding clamp, which encircles the DNA and acts as a processivity factor for the polymerase. Because DNA synthesis occurs only in the 5' → 3' direction, lagging strand synthesis is discontinuous. Thus, the activity of POLA/Primase is required throughout the process of DNA synthesis to create primers for Okazaki fragments on the lagging strand (O'Donnell et al. 2013).

Intriguingly, PrimPol was recently identified as a second DNA priming activity capable of synthesizing DNA primers. Evidence so far suggests that PrimPol acts primarily at damaged replication forks to mediate repriming and tolerance of DNA lesions such as those induced by UV light (Mourón et al. 2013).

Replication through chromatin

Eukaryotic DNA is packaged into nucleosomes that contain the eight core histone proteins around which the DNA wraps. These nucleosomes are then packaged into higher order structures. As such, DNA replication takes place in the context of chromatin. Nucleosomes on the parental DNA must be removed and replaced on the daughter DNA strands (Fig 1.1). Additionally, half of the newly deposited histones will be newly synthesized, and thus will not contain the correct pattern of post-translational modifications (PTMs) that define the region of chromatin undergoing replication. The process through which these histones acquire the proper PTMs is called “chromatin maturation” (MacAlpine and Almouzni 2013).

The DNA Damage Response

The parts of the DDR that I will focus on here are the responses to double-strand breaks (DSBs) and replication stress (RSR). Both of these responses involve signaling from sensor kinases of the phosphoinositide-3-kinase-like kinase (PIKK) family: DNA-PK (DNA-dependent protein kinase) and ATM respond to DSBs, while ATR responds to both DSBs and replication stress. These PIKK family members share several important features. Structurally, the PIKKs consist of a large N-terminal domain of HEAT (Huntingen, Elongation factor 3, Protein phosphatase 2A, yeast TOR1) repeats followed by a FAT (FRAP-ATM-TRRAP) domain, kinase domain, PIKK regulatory domain (PRD), and FATC (FAT-C-terminal) domain (Lovejoy and Cortez 2009).

HEAT repeat domains typically mediate protein-protein or protein-DNA interactions, which is likely the case for ATM, ATR, and DNA-PK. Each of these proteins interacts with a protein activator: DNA-PK with KU70/80, ATM with the MRN (MRE11-RAD50-NBS1) complex, and ATR with ATRIP (ATR Interacting Protein) (Fig 1.2). While DNA-PK and ATM exist without their activators in solution, ATRIP is an

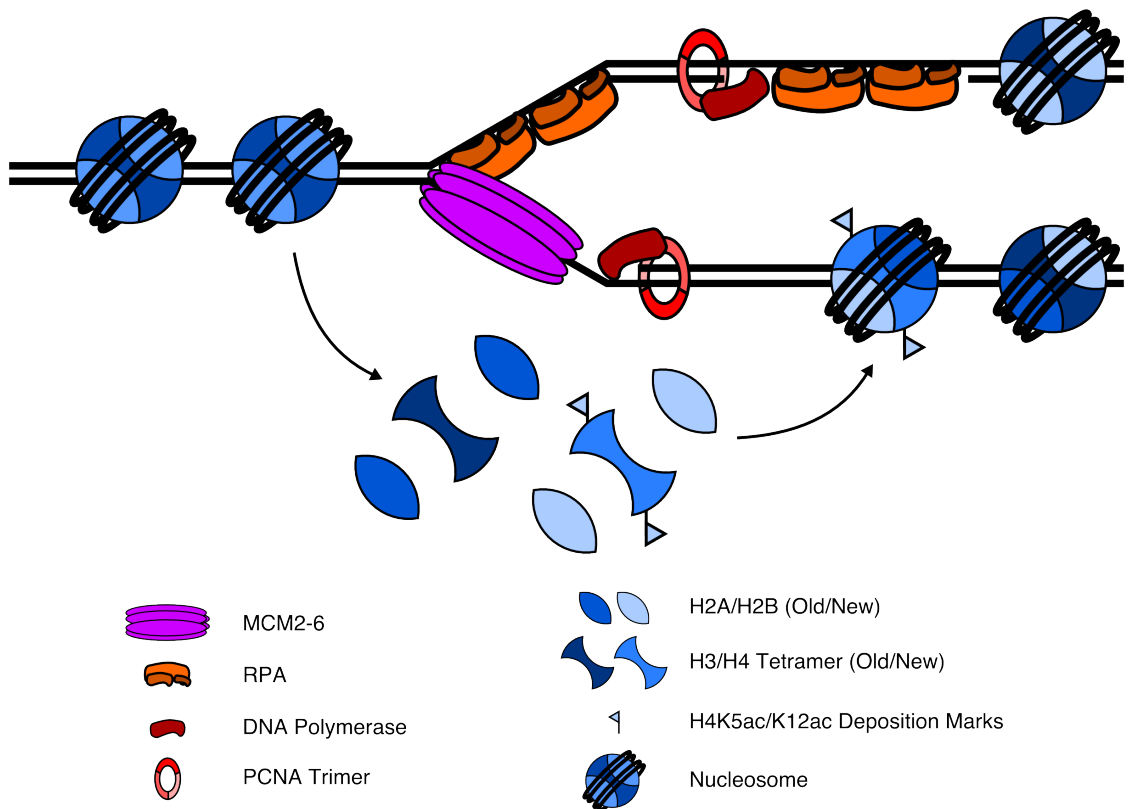


Figure 1.1 DNA replication through chromatin. As the MCM2-6 replicative helicase unwinds the DNA duplex, nucleosomes ahead of the replication fork are destabilized. RPA coats the unwound ssDNA on the lagging strand during Okazaki fragment synthesis. The PCNA sliding clamp serves as a processivity factor for DNA polymerases delta and epsilon. Following replication, histones are deposited to form nascent nucleosomes. Half of these deposited histones are newly synthesized and must be post translationally modified to reproduce the original chromatin state. This also includes removal of deposition marks H4K5 and H4K12 acetylation.

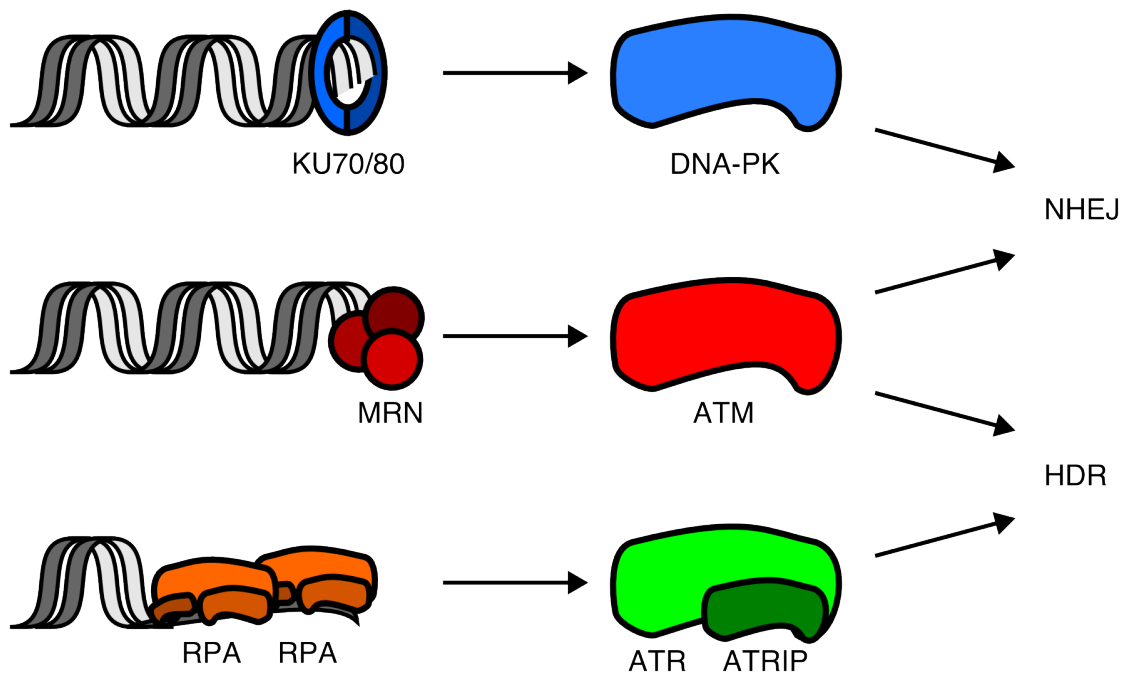


Figure 1.2 DSBs activate DNA-PK, ATM, and ATR. At a DSB, the KU heterodimer binds the DNA end and activates DNA-PK which coordinates NHEJ. If the ends cannot be directly ligated, the MRN complex displaces KU and leads to ATM activation. Minimal processing may lead to ligatable ends, allowing NHEJ to occur. Alternatively, the MRN complex initiates end resection to yield a 3' ssDNA tail. RPA bound to this tail activates ATR, which curbs end resection by phosphorylation of EXO1 and promotes homology-directed repair.

obligatory subunit of ATR: ATR and ATRIP purify as a stoichiometric complex and mutually depend on one another for protein stability (Cortez et al. 2001).

These proteins also require interactions in the PRD for maximal activation. While the KU heterodimer likely provides this interaction for DNA-PK, the situation is more complex for ATM and ATR. ATM requires acetylation by Tip60 in this region, while ATR requires interaction with the ATR activation domain (AAD) of TopBP1 (DNA Topoisomerase II-Binding Protein 1) (Lovejoy and Cortez 2009).

Finally, ATM and DNA-PK are regulated by auto-phosphorylation. DNA-PK extensively auto-phosphorylates, including several sites in the PQR cluster, which leads to increased activity, and the ABCDE cluster, which allows dissociation of the protein from DNA (Cui et al. 2005; Meek et al. 2008). ATM S1981 is an auto-phosphorylation site required for activation of ATM (Bakkenist and Kastan 2003). The Cortez lab has identified and characterized several potential auto-phosphorylation sites in ATR; however, it has not yet been demonstrated that these sites are phosphorylated by ATR in cells. One phosphorylation site, T1989, is damage-inducible and dependent on ATR activity. However, T1989 is followed by proline, not the PIKK consensus glutamine, and cannot be phosphorylated by ATR *in vitro*, and is thus unlikely to be an autophosphorylation site. Unlike ATM S1981, ATR T1989 is not critical for ATR activity, but marks an activated kinase and will likely prove a more direct and robust marker for ATR activation than CHK1 phosphorylation (Nam et al. 2011a).

DSB Repair

At genomic DSBs, meaning those not associated with a replication fork, there are two major pathways of repair, non-homologous end joining (NHEJ) and homology-directed repair (HDR; also known as: homologous recombination, HR; HR repair, HRR). I will not provide an extensive treatment of these pathways as, especially

in the case of HDR, these are complex pathways and not the primary concern of this dissertation (reviewed in Hartlerode and Scully 2009; Kakaroukas and Jeggo 2013). However, I do want to give a general overview and point out important details as we often gain insight into replication stress response pathways through comparison with DSB repair.

Non-homologous end joining (NHEJ)

The current model in the literature is that upon DSB formation, the KU70/80 heterodimer rapidly binds the DNA ends due to its high abundance and affinity. The KU heterodimer recruits and activates DNA-PK, which then coordinates rapid joining of the two DNA ends through recruitment of XRCC4, XLF, and DNA ligase IV (Fig. 1.3 and Kakaroukas and Jeggo 2013). In mammalian cells, most DSBs are repaired rapidly using this pathway; however, in S and G2 phases, when CDKs are active, this pathway can be passed over for HDR when the DSB occurs in a heterochromatic region or the DNA damage is too complex for simple ligation (Hartlerode and Scully 2009; Kakaroukas and Jeggo 2013).

Homology directed repair (HDR)

At DSBs which cannot be joined by NHEJ, DNA-PK is phosphorylated in the ABCDE (T2609) cluster, which allows DNA-PK to dissociate from DNA, a step required for HDR (Kakaroukas and Jeggo 2013; Shibata et al. 2011). Recruitment of the MRN complex activates ATM, which begins accumulation of a large number of proteins at the site of damage including MDC1, 53BP1, and BRCA1. Interestingly, ATM activity is required for DNA-PK T2609 phosphorylation, suggesting that ATM activation itself is the signal for the switch from DNA-PK to ATM signaling (Chen et al. 2007).

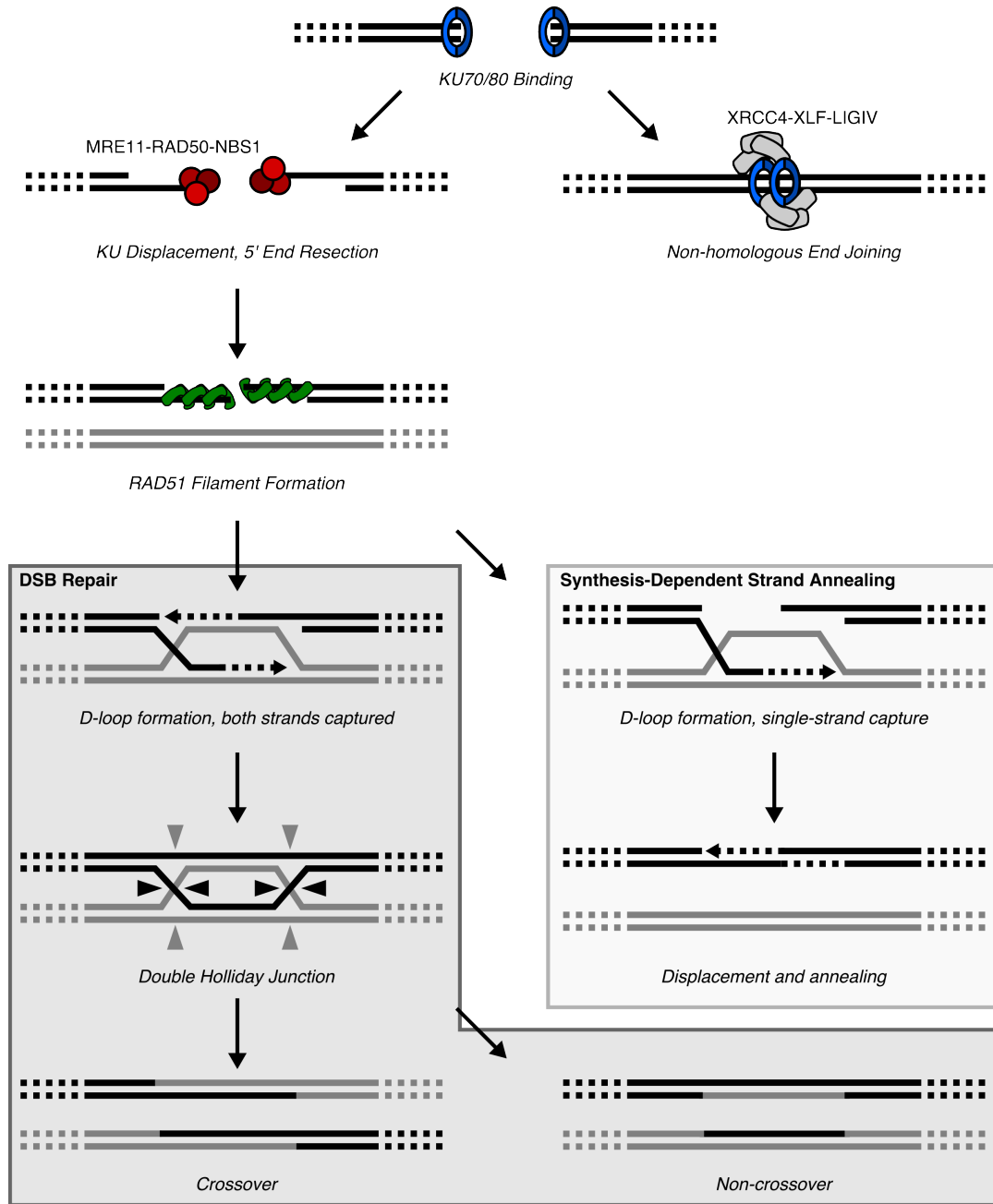


Figure 1.3 Pathways of DSB Repair. The KU heterodimer can bind and stabilize dsDNA ends. Rapid ligation through non-homologous end joining requires DNA ligase IV and XRCC4/XLF. Alternatively, the MRN complex can displace KU and promote 5' end resection. Extensive resection allows loading of RAD51 which can mediate strand invasion. If both strands are captured, the “DSB Repair” model predicts that DNA synthesis and ligation will form a double holliday junction, which can be dissolved by BLM-TOPOIII (not shown; non-crossover) or cleaved by Holliday junction resolvases to form crossover or non-crossover products. If only one strand is captured, the “Synthesis Dependent Strand Annealing” model predicts that after extension of the invading strand, the strand will be displaced and re-anneal to the exposed 3' tail of the other DSB end. Gap filling and ligation can then complete repair.

Of note, MDC1 binds to γ H2AX on the chromatin and serves as an additional binding site for the MRN complex (Chapman and Jackson 2008; Goldberg et al. 2003; Lukas et al. 2004; Spycher et al. 2008; Wu et al. 2008). ATM then binds this additional MRN and phosphorylates more H2AX molecules, which in turn allows more MDC1 binding. In this way, γ H2AX spreads from the site of damage throughout the entire surrounding region of chromatin, up to several megabases (Fig. 1.4 and Savic et al. 2009).

The critical decision point for the switch from NHEJ to HDR is resection initiation. This is a highly regulated process which requires CtIP and MRE11 (Kakaroukas and Jeggo 2013; You and Bailis 2010). CtIP is a highly modified protein that coordinates most cellular resection. CtIP requires phosphorylation by CDKs and deacetylation by SIRT6 to initiate resection (Huertas and Jackson 2009; Kaidi et al. 2010). At blocked ends, such as SPO11 cleavage sites in yeast, the MRE11 endonuclease incises the blocked strand internally to generate a free 5' end for resection. CtIP then directs extensive 5' resection that involves the EXO1, DNA2, and BLM proteins (Huertas and Jackson 2009; Kakaroukas and Jeggo 2013; Sartori et al. 2007). This extended 5' resection produces a 3'-ssDNA tail, which is rapidly bound by RPA. RPA coated ssDNA adjacent to a 5'-dsDNA junction is the activating structure for ATR. ATR activation restricts resection, likely through phosphorylation of EXO1, and promotes the completion of HDR. ATM and ATR phosphorylate BRCA2, and CHK1 phosphorylation of RAD51 is required for RAD51 recruitment to sites of damage (Ciccia and Elledge 2010). RAD51 displaces RPA, potentially through a SUMOylation regulated process, to form a filament on the 3' ssDNA tail in a BRCA2-dependent process. RAD51 then mediates strand exchange to form a D-loop (Ciccia and Elledge 2010).

Completion of HDR requires the activity of DNA polymerases to extend the invading strand. Finally, branch migration of the D-loop can displace the invading strand

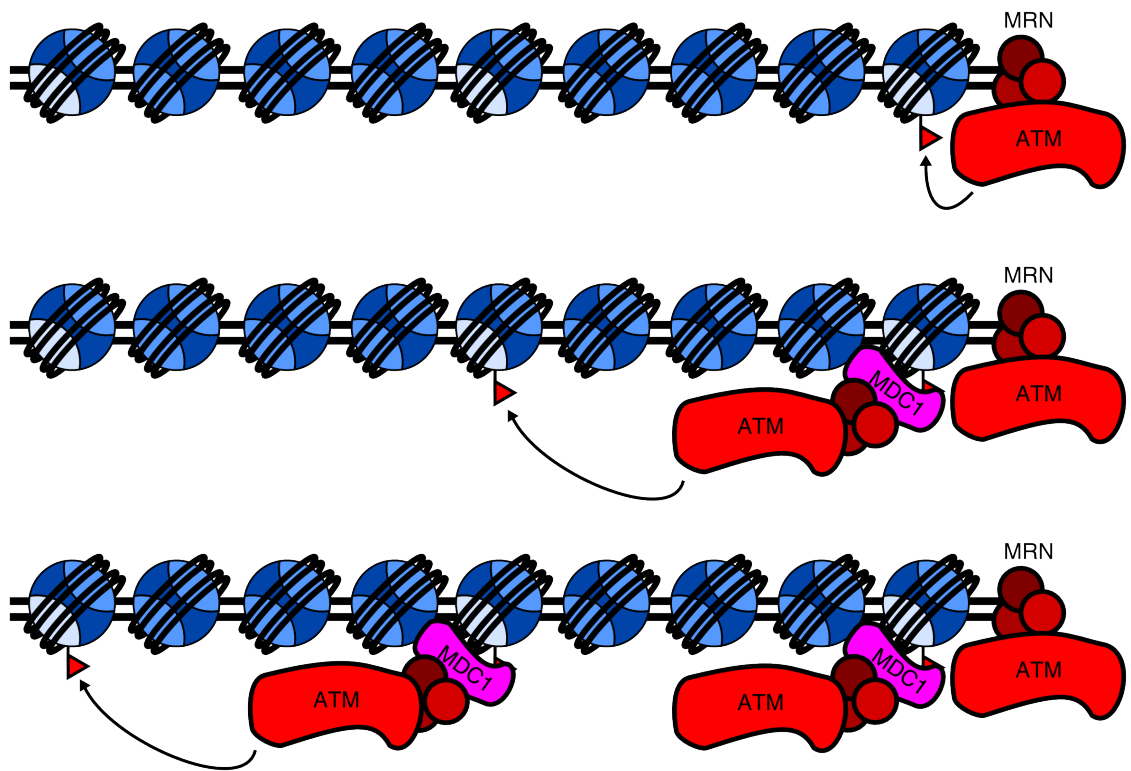


Figure 1.4 ATM and MDC1 mediate spreading of γ H2AX from site of DSB. MRN binds the DSB end and stimulates ATM phosphorylation of neighboring H2AX molecules (red flag represents phosphorylation; light oval represents H2AX containing H2A/H2B dimer). γ H2AX serves as a docking site for MDC1, which recruits additional MRN/ATM. This recruited ATM then phosphorylates additional H2AX molecules. This cycle can continue to spread γ H2AX throughout megabase regions of chromatin.

and allow completion of HDR by synthesis-dependent strand annealing – the extended 3' tail anneals to the 3' tail of the other DSB end – or annealing of the other 3' ssDNA tail to the displaced strand, which then forms a double Holliday junction (Ciccina and Elledge 2010; Hartlerode and Scully 2009). These double Holliday junctions can be resolved by the BLM/TOPOIII resolvase complex or several structure-specific nucleases in the cell such as SLX1/SLX4, GEN1, or MUS81/EME1 (Fig. 1.3 and Ciccina and Elledge 2010; Hartlerode and Scully 2009).

DNA Damage Responsive Histone Modifications

One area of interest is the interplay between histone PTMs and the DNA damage response. The use of chromatin immunoprecipitation (ChIP) and site-specific nucleases has allowed researchers to define several chromatin changes that occur near double strand breaks (DSBs) (Berkovich et al. 2008; Rodrigue et al. 2006; Rudin and Haber 1988; Soutoglou et al. 2007). The most obvious change in PTMs is phosphorylation of H2A variant H2AX on S139, known as γ H2AX, which occurs at DSBs and spreads into the entire chromatin domain surrounding the DSB (Berkovich et al. 2007; Savic et al. 2009).

A second chromatin modification that frequently occurs near DSBs is ubiquitination of H2A. This ubiquitination is catalyzed by RNF8 and RNF168, which require MDC1 for recruitment to break sites. Ub-H2A, in turn, allows recruitment of RAP80 and 53BP1 (Ciccina and Elledge 2010; Kakarougkas and Jeggo 2013).

Chromatin, especially compacted heterochromatin, presents a barrier to DSB repair. As such, it makes sense that in at least some cases, loosening of the chromatin must occur to allow repair. Indeed, this is the case, as MOF acetylates H4K16 and CBP and p300 catalyze acetylation of H3 and H4 to relax chromatin (Li et al. 2010; Sharma et al. 2010). It is unclear how these changes mimic those at a stalled replication fork, where

the situation is vastly different. The region of DNA immediately surrounding the replication fork is free of nucleosomes, while the daughter strands contain nucleosomes in various states of maturation. Our investigation into the link between chromatin maturation and the DDR will be described in Chapter III.

The Replication Stress Response

Replication stress arises from a variety of sources, both endogenous and exogenous. DNA lesions, insufficient nucleotides, difficult to replicate sequences, and collisions between replication and transcription machineries all cause replication stress. In many cases, replication stress results in stalling of replication forks. If these stalled forks remain unresolved, chromosomal rearrangements or cell death can occur when the cell attempts to enter mitosis (Cimprich and Cortez 2008; Zeman and Cimprich 2013).

Stalled Replication Fork Repair Pathways

Replication fork repair pathways have been extensively studied in lower organisms including bacteria and yeast. Technical limitations make studying replication fork repair difficult in higher eukaryotes, and so limits our knowledge of these pathways. Bacteria contain a single circular chromosome that initiates DNA replication at the *oriC* site. Two replication forks then proceed in opposite directions through the chromosome and meet in the terminator region. The Tus protein prevents passage of replication forks out of the terminator region (Duggin et al. 2008; Mulcair et al. 2006). Thus, replication fork restart is a critical process in bacteria because there is no possibility of rescue by the opposite replication fork. There are several possible fork restart mechanisms: (1) stabilization and restart or rescue; (2) repriming and post-replicative repair; (3) template switching or fork regression; and (4) DSB-mediated restart (Jones and Petermann 2012; Petermann and Helleday 2010; Yeeles et al. 2013). Note that these pathways are for a

'generic' lesion that blocks the polymerase but not the helicase. Interstrand crosslinks, which block the helicase, have a specialized repair pathway (that falls into category 4 listed above; reviewed in Deans and West 2011).

1. Stabilization and restart or rescue

The simplest replication fork restart pathway is simply to stabilize the replication machinery and await repair of the lesion or removal of the stressor (Fig. 1.5). For example, some alkylated bases can be directly repaired by ALKB or MGMT (Fu et al. 2012). REV1 is a translesion polymerase implicated in replication fork progression on damaged templates, possibly by performing translesion synthesis (TLS) directly at the stalled fork (Jones and Petermann 2012). In the case of nucleotide deprivation by hydroxyurea (HU) or polymerase inhibition with aphidicolin (APH), a stabilized stalled fork can directly restart after removal of the drug. Eukaryotes contain linear chromosomes with multiple origins of replication. As such, stalled replication forks can be rescued by replication from a nearby origin, possibly leaving a small patch of unreplicated DNA that can be filled in by TLS (Fig. 1.5).

2. Repriming and post-replicative repair

For some lesions, the replication fork machinery may simply skip over the lesion and continue on its way. For lagging strand lesions, this is accomplished simply by continuing normal DNA synthesis – the DNA priming activity is active on the lagging strand, and completion of one Okazaki fragment is not required to begin the next. A lesion on the leading strand, where DNA replication is more processive, would require repriming on the leading strand for bypass. This is indeed the case in *E. coli*, where DnaG repriming of the leading strand is the rate-limiting step for bypass of leading strand lesions (Yeeles and Marians 2013).

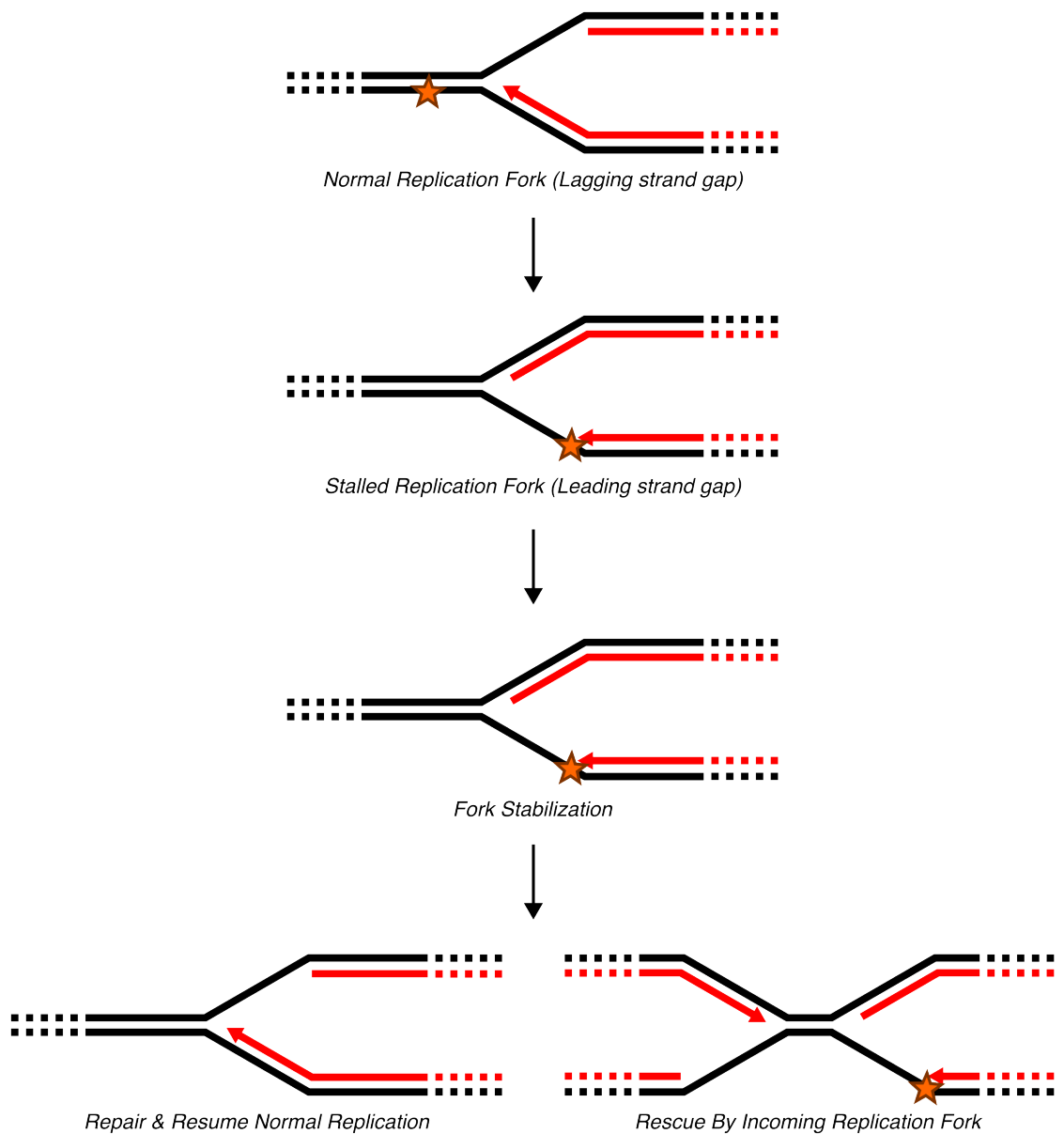


Figure 1.5 Stabilization and restart or rescue. The simplest method to deal with a stalled fork is to stabilize the replisome and wait for repair to occur or removal of a drug, then resume synthesis. In many cases, stabilization of a replication fork can allow a neighboring origin to fire and “rescue” the stalled fork by replicating up to the point where the fork stalled.

In mammals, PrimPol may provide this functionality. PrimPol-depleted human cells and *PrimPol*^{-/-} MEFs showed slower replication fork progression and decreased replication fork restart after UV irradiation (Mourón et al. 2013). Moreover, while PrimPol has both TLS and DNA primase activities, ablation of only the primase activity recapitulated the phenotypes of PrimPol deficiency (Mourón et al. 2013). This suggests that, indeed, repriming allows bypass of UV-induced lesions (Fig. 1.6).

Ubiquitination of the PCNA molecule adjacent to the lesion marks the lesion for post-replicative repair. Subsequent translesion synthesis can handle several types of lesions including alkylation damage induced by methyl methanesulfonate (MMS) and photo-crosslinked bases induced by UV (Ulrich and Walden 2010; Yeeles et al. 2013).

3. *Template switching or fork regression*

Template switching, using the opposite nascent strand as a template for DNA synthesis, is a potential error-free pathway to bypass template damage. The *S. cerevisiae* Rad5 and human orthologue HLF1 may be involved in such a process through their helicase activity (Lin et al. 2011; Motegi et al. 2008; Ulrich and Walden 2010). If this occurs post-replicatively, such as at a bypassed UV- or MMS-induced lesion, there are few conceptual problems to overcome, as unwinding by HLF1 could expose 3'-ssDNA, which could participate in strand exchange with the sister chromatid. A short patch of DNA synthesis could replicate past the lesion followed by D-loop dissolution and flap cleavage or gap filling as necessary (Fig. 1.7).

Template switching that occurs at the replication fork would involve fork regression, a more challenging biochemical problem. Fork regression has been a topic of interest in the DNA damage field for some time. This structure appears to occur frequently in *E. coli* in response to replication fork stalling and is invoked in many pathways of replication fork restart (Atkinson and McGlynn 2009). Single molecule

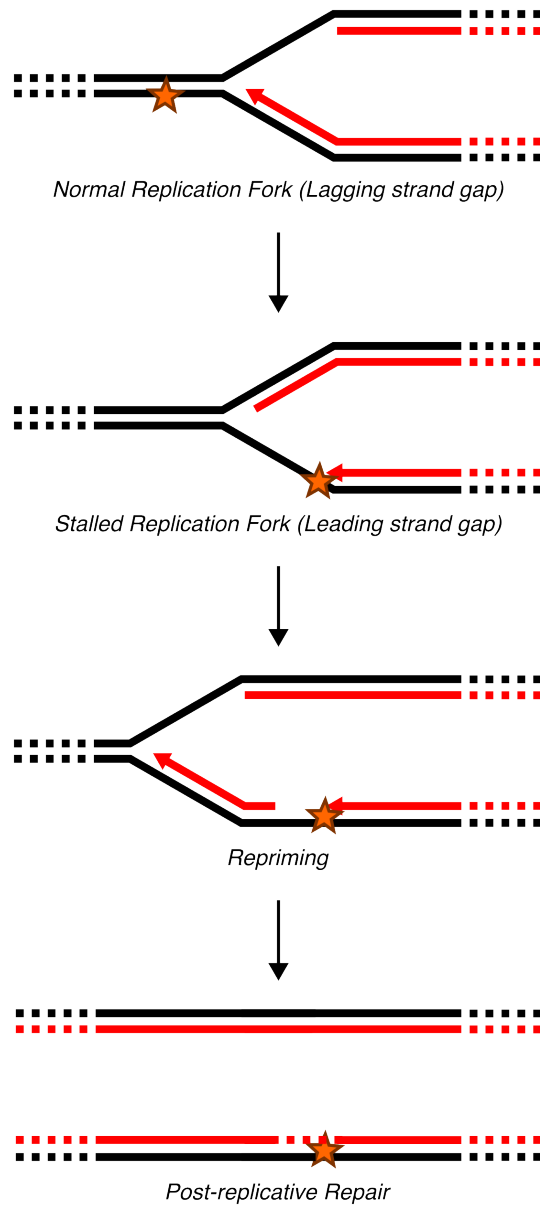


Figure 1.6 Repriming and post-replicative repair. After a lesion stalls the replication fork, functional uncoupling of the polymerase and helicase leads to excess ssDNA. Repriming activity on this ssDNA can allow the replisome to bypass the lesion. PCNA ubiquitination can then serve as a marker for translesion synthesis at the skipped region.

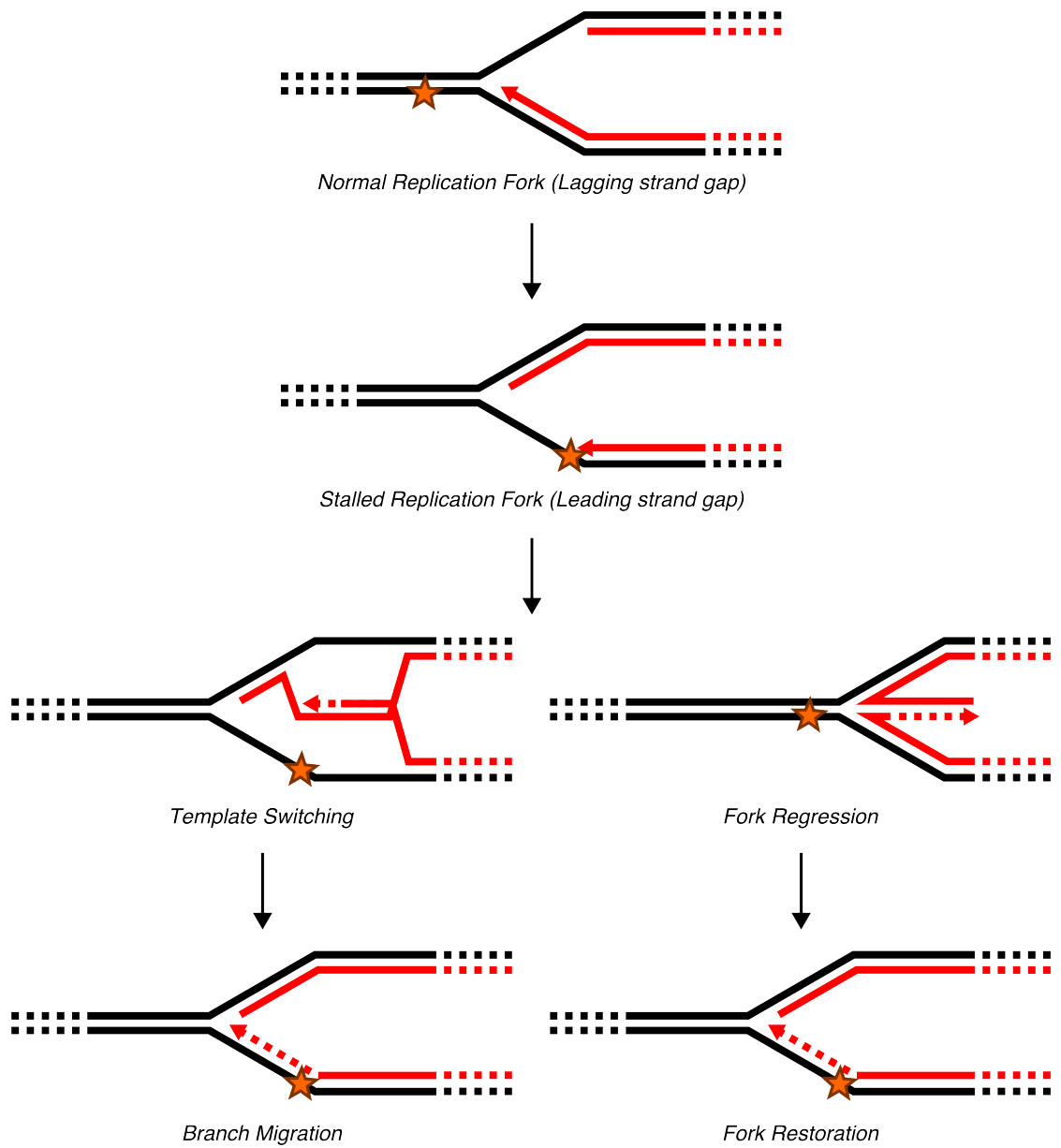


Figure 1.7 Fork regression and template switching. Nascent-nascent strand pairing, or template switching, can occur either at the replication fork, in the case of fork regression, or behind the replication fork if the stalled nascent strand invades the opposite nascent strand. Then, branch migration – either D-loop dissolution or fork restoration – restores the replication fork to its normal state, having synthesized past the lesion using the opposite nascent strand as a template.

studies of the T4 phage replication system demonstrated that the UvsW helicase allows the replisome to bypass a polymerase-blocking lesion using such a pathway. UvsW regresses the stalled replication fork, polymerization occurs using the opposite nascent strand as a template. UvsW subsequently restores the reversed fork (Manosas et al. 2012).

The situation in eukaryotes is less clear. In *S. cerevisiae*, fork regression occurs in checkpoint deficient cells and is associated with nucleolytic degradation of newly synthesized DNA and cell lethality (Cobb et al. 2003, 2005; Cotta-Ramusino et al. 2005; Sogo et al. 2002). However, the idea that this structure represents a repair intermediate rather than a pathogenic structure is bolstered by recent observations in mammalian cells. Both low-dose camptothecin (CPT) treatment and overexpression of oncogenes Cyclin E and CDC25A cause fork regression (Neelsen et al. 2013; Ray Chaudhuri et al. 2012). This suggests that fork regression is a frequent outcome of fork stalling, since these cells have otherwise intact checkpoint signaling.

Fork regression requires some combination of helicase or annealing activity that results in reannealing of the template DNA strands and annealing of the nascent strands to one another. This forms a Holliday junction-like structure. Several enzymes can perform this reaction *in vitro* including HLTF, BLM, WRN, SMARCAL1, ZRANB3, and FANCM (Achar et al. 2011; Bétous et al. 2012, 2013; Ciccia et al. 2012; Gari et al. 2008a, 2008b; Machwe et al. 2006, 2007; Ralf et al. 2006). Fork regression still presents a biochemical problem: what happens to the replisome during fork regression? It remains unclear whether the MCM helicase remains bound to the DNA, and if other replisome components, such as PCNA and the polymerases, also remain bound.

The T4 phage UvsW protein is a SWI/SNF family ATPase that supports template switching (Manosas et al. 2012). Beyond both belonging to the SWI/SNF family, SMARCAL1 and UvsW also share structural similarities: the HARP domains of

SMARCAL1 can substitute for the N-terminal MotA-like domain of UvsW (Aaron Mason and Brandt Eichman, unpublished observations). Both proteins have annealing helicase activity and can catalyze the regression of replication forks – annealing the two nascent strands – and the restoration of regressed forks – annealing the nascent strands back to their cognate template strands (Bétous et al. 2013).

In *E. coli*, replisomes at stalled forks have short half lives, and PriA- and PriC-dependent activities facilitate reloading of the replisome (Yeeles and Marians 2013; Yeeles et al. 2013). It is unclear whether the MCM helicase can be reloaded in such a mechanism. However, one recent report implies that this may be the case: FANCM promotes replication traversal across interstrand crosslinks (Huang et al. 2013). An interstrand crosslink cannot be bypassed by the MCM helicase – such a structure cannot be unwound. This implies that cells have either a mechanism for reloading the MCM helicase, can substitute an alternative helicase, or the MCM helicase has an unappreciated ability to bypass crosslinks, presumably by ring-opening and -closing.

4. DSB-mediated restart

Single cell organisms such as *E. coli* and *S. cerevisiae* have pathways known as break induced replication, which allow replication to initiate or resume from a DSB (Fig. 1.8 and Anand et al. 2013). In *S. cerevisiae*, this pathway can replicate long patches of DNA, up to the length of a chromosome arm (Anand et al. 2013). The best evidence for such a pathway in vertebrates comes from experiments in *Xenopus* egg extracts. In these experiments, replicating extracts were treated with nucleases to collapse replication forks into DSBs. Rad51 facilitated origin-independent replication restart (Hashimoto et al. 2011).

Several structure specific nucleases exist in cells which might facilitate break induced replication. MUS81 is most commonly linked to replication-associated DSBs,

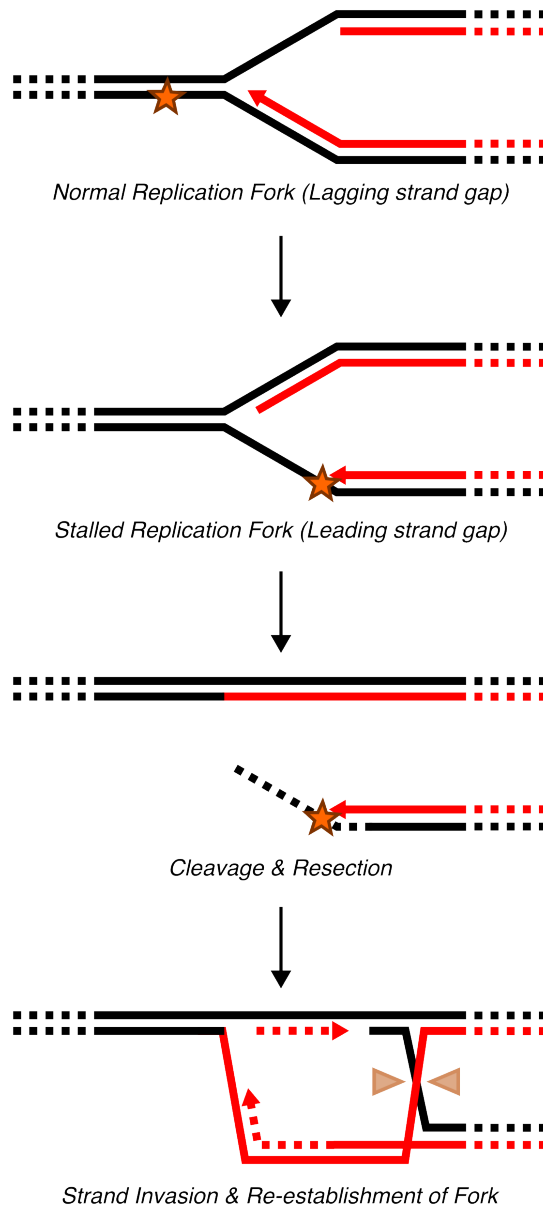


Figure 1.8 DSB-mediated recovery of stalled replication forks. A persistently stalled fork is cleaved by a structure-specific nuclease such as MUS81. After resection of the leading template strand, the leading nascent strand can invade the sister chromatid to form a new replication fork.

especially after depletion of SMARCAL1, WRN, and CHK1 (Bétous et al. 2012; Forment et al. 2011; Franchitto et al. 2008). MUS81 is the catalytic subunit of the MUS81-EME1/2 heterodimer. Unlike other structure-specific nucleases which cleave intact Holliday junctions efficiently, MUS81 prefers Holliday junction-like structures that resemble replication forks, especially those that have a free 5'-hydroxyl at the junction (Bastin-Shanower et al. 2003; Fricke et al. 2005; Osman and Whitby 2007).

MUS81 is also linked to DSB formation after treatment with camptothecin, a Topoisomerase I inhibitor, or extended (18-24h) treatments with hydroxyurea (HU) (Regairaz et al. 2011). MUS81-dependent DSBs occur in situations associated with fork collapse. Therefore, it is possible that these MUS81 DSBs are the cause of fork collapse, which is defined as the inability to resume replication at a stalled fork. However, co-depletion of WRN and MUS81 does not relieve the fork restart defect, suggesting that these DSBs are not the cause (Franchitto et al. 2008; Petermann et al. 2010). Furthermore, MUS81-deficient cells display hypersensitivity to cross-linking agents such as Mitomycin C (MMC) and cisplatin and impaired recovery of replication forks from HU, suggesting that DSB formation may be a critical step in at least some forms of repair (Hanada et al. 2007).

In the special case of interstrand crosslinks (ICLs), replication forks on either side of the ICL converge. Nucleolytic processing then “unhooks” the ICL and generates a two-ended DSB. Homology directed repair then completes repair past the lesion (Deans and West 2011). Likewise after a DSB occurs at a stalled replication fork, a combination of endo- and exonucleases, such as MRE11 and EXO1, could generate a 3' overhang to allow RAD51 loading and strand invasion. Branch migration and annealing of the leading template strand to the lagging template strand would then allow re-formation of the replication fork. In this case, further processing by endonucleases or BLM-TOPOIII is required to resolve the remaining Holliday junction (Fig. 1.8).

Of course, fork regression and DSB-mediated fork repair are by no means mutually exclusive ideas. In fact, it is entirely possible that regressed replication forks serve as substrates for structure-specific nucleases such as MUS81 or SLX1/SLX4 in order to generate DSBs. This is the case in *E. coli* where RecG-mediated fork regression allows cleavage by the RuvABC nuclease (McGlynn and Lloyd 2002).

Ataxia telangiectasia mutated and rad3-related (ATR)

ATR is the master regulator of the replication stress response (Cimprich and Cortez 2008). Upon replication fork stalling, ATR is activated and phosphorylates hundreds of substrates to effect the various functions of ATR, including replication fork stabilization, repression of dormant origins, and cell cycle arrest (Cimprich and Cortez 2008; Matsuoka et al. 2007). While many ATR substrates have been defined, and this signaling pathway is well studied, little is known about what happens to the DNA at stalled replication forks and how ATR regulates these changes.

Essential Function of ATR

ATR is an essential gene in replicating cells, but the essential function of ATR is a matter of some debate. It is possible that ATR is essential simply because all cells undergo some level of replication stress during each cell division cycle and ATR is required to handle this stress. Evidence from *S. cerevisiae* suggests that at least in yeast, regulation of origin firing is not the essential function. This is based on the observation that strains containing the *mec1-100* allele (Mec1 is the *S. cerevisiae* ortholog of *ATR*) are viable, yet unable to repress dormant origins (Paciotti et al. 2001; Zhong et al. 2013).

Edward Nam, a former graduate student in our lab, identified a separation of function mutant ATR (ATR-3A), which could perform the G2 checkpoint, but not S phase

functions of ATR. ATR-3A could prevent progression into mitosis following IR treatment, but the ATR-3A protein could not support viability in clonogenic survival assays or support resumption of DNA synthesis after release from HU treatment (Nam et al. 2011b). Taken together, these data suggest that the essential function of ATR is likely at the level of replication fork stability rather than regulation of origin firing or the G2 checkpoint.

Because ATR is essential, it is difficult to study the effects of ATR deletion at the replication fork level – the cells die over time as ATR levels decrease. However, the synthetic lethality concept has garnered support in recent years and several companies are directing efforts at developing inhibitors of ATR and ATR-pathway genes, such as CHK1. As such, we were able to obtain two such ATR inhibitor compounds, one from AstraZeneca called AZ20 (unpublished) and another published by Vertex, VE-821 (Reaper et al. 2011). In Chapter IV, I will describe how we utilized ATR inhibitors as tools to probe how ATR prevents replication fork collapse.

The S-phase checkpoint

ATR activation at stalled replication forks leads to a phenomenon known as the “S-phase checkpoint,” although this checkpoint differs from other cell cycle checkpoints in that the activities described do not directly prevent cell cycle transitions (Friedel et al. 2009). At any rate, the S-phase checkpoint activities of ATR are to promote replication fork stability, repress global origin firing, and promote local origin firing. While the latter goals may seem somewhat contradictory, it is important to note that some replication factors may be limiting, so firing random origins throughout the genome is not likely to resolve a fork stalling problem, but rather exacerbate it. In contrast, firing origins only locally may also titrate essential replication factors away from the stalled fork, but this stalled fork can then be rescued by replication from a nearby dormant origin. As such,

ATR only needs to prevent the replication fork from collapsing, rather than promote resumption of DNA synthesis.

Indeed, in CHK1 deficient cells, S-phase is shortened due to derepression of global origin firing. However, the replication rate of each individual replication fork is significantly slower due to titration of essential replication factors, such as dNTPs (Seiler et al. 2007). Origin firing requires phosphorylation of the MCM proteins by the DBF4-dependent kinase (DDK, consists of DBF4 and CDC7). DDK phosphorylation requires a 'priming' phosphorylation – normally administered by CDKs (Siddiqui et al. 2013). ATR activity inhibits CDK activity, so this priming activity is not available to global origins. However, ATR activity promotes PLK1 (Polo-like kinase 1) activity locally, which may override ATR signaling and allow replication initiation near the stalled fork (Cimprich and Cortez 2008).

ATR activation and the G2/M checkpoint

While DSBs require resection to expose ssDNA and activate ATR, the situation at replication forks is somewhat different. At an ongoing replication fork, ssDNA is produced constantly on the lagging DNA strand due to the discontinuous nature of DNA synthesis. When replication forks stall, which for our purposes means when the polymerase encounters a problem and stops inserting nucleotides, the polymerase and helicase become functionally uncoupled, and excess ssDNA is generated (Byun et al. 2005). The RPA coated ssDNA serves as an activating structure for ATR, which phosphorylates numerous substrates at the replication fork, including H2AX and the downstream checkpoint kinase CHK1 (Cimprich and Cortez 2008; Nam and Cortez 2011; Zeman and Cimprich 2013).

CHK1 phosphorylates CDC25, which targets CDC25 for degradation (Cimprich and Cortez 2008). CDC25 is a protein phosphatase that promotes cell cycle progression

by removing inhibitory phosphates on CDK1/2 (Boutros et al. 2006). ATR also phosphorylates and stabilizes p53, which in turn executes its transcription program, including expression of p21, an inhibitor of CDK activity, and leads to further inhibition of cell cycle progression (Tibbetts et al. 1999; Wang et al. 2008). This is known as the G2/M checkpoint, as CDK activity is required to proceed from G2 to M phase, which does not occur in wild type cells with DNA damage (Fig. 1.9 and Cimprich and Cortez 2008; Wang et al. 2009).

Function of MRE11 in ATR activation

Recent work has proposed a function for MRE11 in activation of ATR at stalled replication forks. At DSBs, MRE11 is required for ATR activation because MRE11-dependent resection is necessary to expose the ATR-activating ssDNA (Myers and Cortez 2006). However, the function of MRE11 in ATR activation at stalled forks is less clear. Functional uncoupling of the MCM helicase and DNA polymerase at a replication fork seems sufficient to form ssDNA, so why is MRE11 necessary?

Experiments in *X. laevis* egg extracts suggest that depletion of MRN or xMRE11 prevents maximal activation of ATR, and that depletion of xMRE11 also resulted in decreased xTOPBP1 recruitment to damaged chromatin. This suggests that MRE11 is required for full recruitment of TOPBP1 to damaged replication forks. Interestingly, xMRE11 recruitment of xTOPBP1 was independent of the 9-1-1 complex, and artificial targeting of the TOPBP1-AAD to ssDNA was sufficient to rescue ATR activation in MRE11-depleted extracts (Duursma et al. 2013). Another report also demonstrated in *X. laevis* egg extracts that MRE11 depletion prevented ATR activation via recruitment of TopBP1, and that this function of MRE11 required its nuclease activity (Lee and Dunphy 2013).

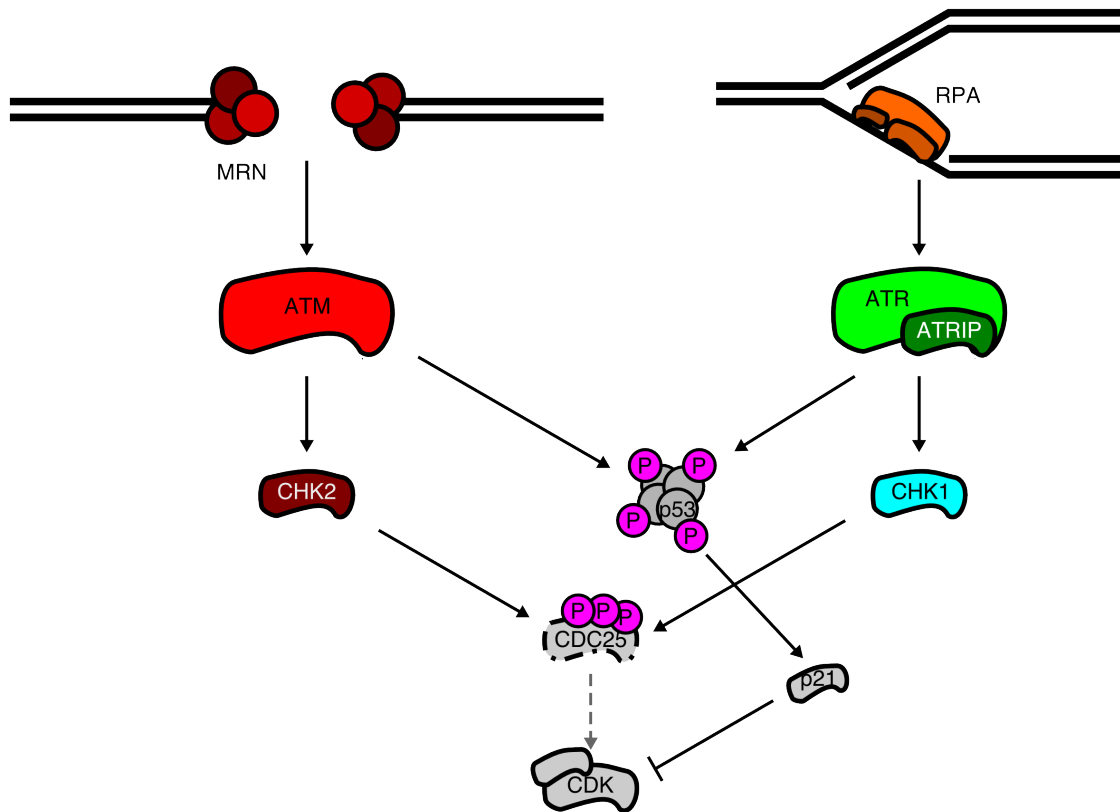


Figure 1.9 G2/M Checkpoint. At DSBs, ATM phosphorylates CHK2, which in turn phosphorylates CDC25. Alternatively, RPA coated ssDNA activates ATR, which phosphorylates CHK1. CHK1 can also phosphorylate CDC25. CDC25 phosphorylation by CHK1/2 targets it for degradation, which prevents CDC25-mediated dephosphorylation of CDKs. ATR and ATM also phosphorylate and stabilize p53, which triggers transcription of the p21 CKI, which inhibits CDK activity.

ATR Stabilization of Replication Forks

Mechanistically, it remains unclear how ATR stabilizes stalled replication forks. However, clues from lower organisms provide some insight. Unlike mammalian cells, *S. cerevisiae* have defined, sequence specific origins such that replisomes can be tracked as they progress along DNA by chromatin immunoprecipitation (ChIP). These studies revealed that in a *rad53Δ* background, replisome components dissociated from stalled forks (Lucca et al. 2004). These cells also accumulated regressed fork structures (Lucca et al. 2004; Sogo et al. 2002), and this phenotype was exacerbated in an *exo1Δ* background (Cotta-Ramusino et al. 2005). Deletion of the *S. cerevisiae* RecQ helicase, Sgs1, was synthetic lethal with the *mec1-100* allele, and these mutants had synergistic defects in maintenance of replisome components at stalled replication forks (Cobb et al. 2005). Taken together, these observations suggest that in *S. cerevisiae*, *mec1p* and *rad53p* stabilize replication forks to prevent dissociation of replication factors and fork regression.

X. laevis egg extracts depleted of ATR and ATM do not maintain POLE on chromatin during and after treatment with camptothecin (CPT) or mitomycin C (MMC), but not aphidicolin (Trenz et al. 2006). Moreover, recovery of DNA synthesis after removal of CPT or MMC required both MRE11 and ATM/ATR (Trenz et al. 2006). This suggests that the function of checkpoint signaling to maintain replisome integrity is conserved. Indeed, our lab and others demonstrated that one function of ATR is to prevent cleavage of replication forks by SLX4. Fork collapse in ATR-deficient cells involves replication fork remodeling by SMARCAL1 and degradation of replisome components by the PLK1 and RNF4 pathways (Couch et al. 2013; Ragland et al. 2013).

SMARCAL1

Carol Bansbach-Robbins, a former student in the Cortez lab, identified SMARCAL1 in a functional genomic screen for DDR proteins (Bansbach et al. 2009), and several other groups also identified SMARCAL1 as a genome maintenance protein (Ciccia et al. 2009; Yuan et al. 2009; Yusufzai and Kadonaga 2008). Depletion of SMARCAL1 from human cells produced increased γ H2AX and HU sensitivity. Intriguingly, over-expression of SMARCAL1 also produced γ H2AX, though depletion and over-expression present two different staining patterns: foci in the former case and pan-nuclear in the latter (Bansbach et al. 2009).

The γ H2AX produced in SMARCAL1-deficient cells is MUS81-dependent (Bansbach et al. 2009). While there is no direct physical evidence, one possible explanation is that in the absence of SMARCAL1 activity, cells accumulate regressed replication forks that serve as a substrate for nucleases such as MUS81. Another possibility is that SMARCAL1 is required to perform fork regression in some cases, and, absent this, MUS81 cleaves these forks. In fact, this may be the likely explanation, as MUS81 prefers to cleave substrates with a 5'-DNA end at the junction point (Bastin-Shanower et al. 2003; Fricke et al. 2005), which would occur at a "stalled" replication fork with ssDNA only on the leading strand. Regression of this replication fork would effectively hide the 5'-DNA end from MUS81 and prevent cleavage. Elucidating this will require DNA structural evidence to determine whether regressed forks accumulate in SMARCAL1- or MUS81-deficient cells.

SMARCAL1 Biochemistry

Biochemically, SMARCAL1 has several interesting properties. SMARCAL1 belongs to the SWI/SNF family of ATPases in helicase superfamily 2 (SF2) (Flaus et al. 2006). While these proteins share structural similarity with other helicases, such as the

RecQ family, they primarily have DNA translocase activity – sliding along double stranded DNA – and use accessory factors or other protein domains to determine substrate specificity and activity (Singleton et al. 2007).

For example, SNF2H exists in a complex with accessory factors that confer chromatin remodeling activity and allow SNF2H to couple ATP hydrolysis with nucleosome sliding (Gangaraju and Bartholomew 2007). Similarly, the N-terminal region of SMARCAL1 contains an RPA binding motif and two HARP (HepA-related protein) domains. The RPA binding motif is required for SMARCAL1 localization to replication foci in cells, and the HARP domains are required for DNA binding and ATP hydrolysis. In fact, the ATPase core and adjacent HARP domain (HARP2) form the enzymatic core of the protein and are sufficient for enzymatic activity *in vitro* (Bétous et al. 2012).

Unlike many other SWI/SNF family members which bind dsDNA, SMARCAL1 binds to DNA that contains dsDNA and ssDNA regions. These structures include dsDNA with ssDNA gaps, ssDNA extensions, or more complex structures such as 3- and 4-way junctions that do not have overt ssDNA. In the latter case, SMARCAL1 may bind to ssDNA at the junction that results from breathing of the structure (Bétous et al. 2012).

A talented biochemist in the Cortez lab, Rémy Bétous, set out to define the substrate specificity of SMARCAL1. To do this, he utilized substrates that resembled “normal” and “stalled” replication forks, which contain an ssDNA gap at the fork on either the lagging or leading strand, respectively (Fig. 1.10A). Rémy determined that in the absence of RPA, SMARCAL1 preferred to perform fork regression on the “normal” fork substrate; however, RPA stimulated SMARCAL1 activity on the “stalled” fork substrate and inhibited SMARCAL1 activity on the “normal” fork substrate, inverting the preference. This suggests that in a cell, one function of SMARCAL1 may be to regress stalled replication forks (Bétous et al. 2013).

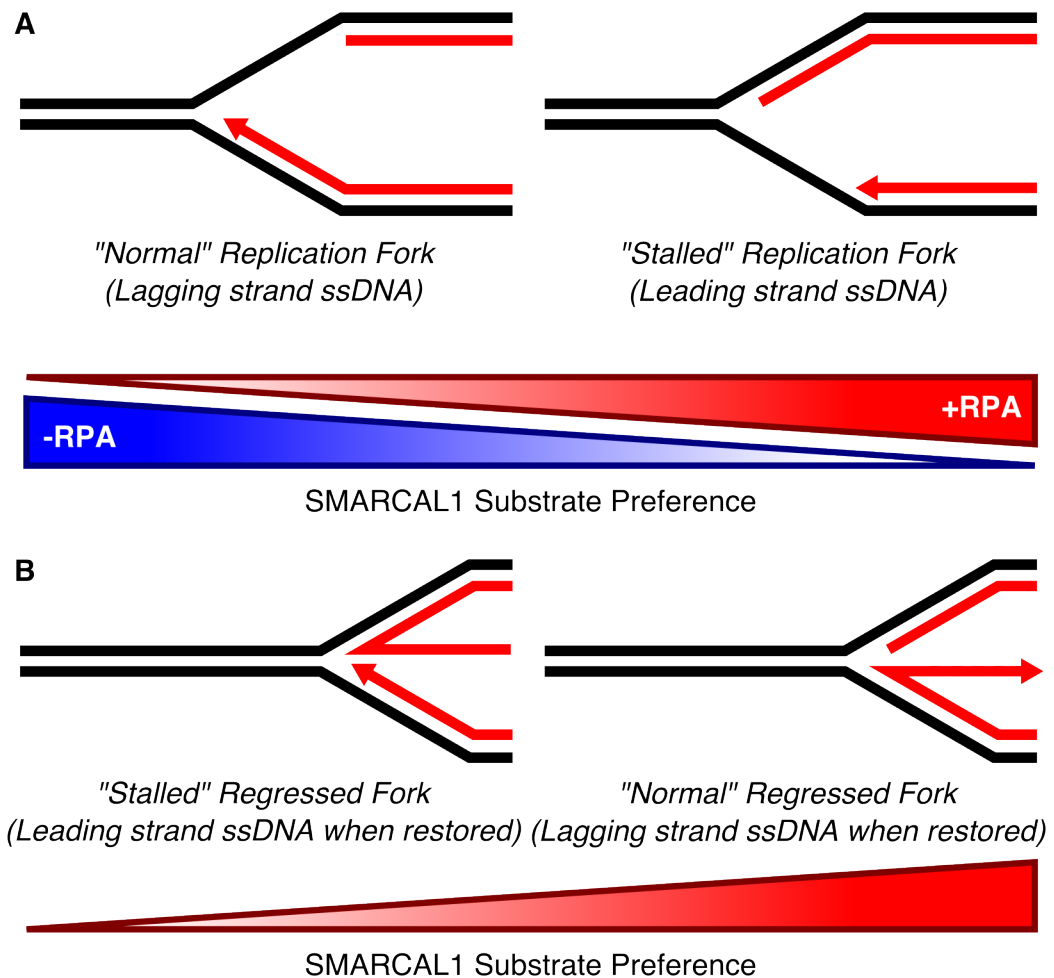


Figure 1.10 SMARCAL1 substrate preferences. (A) In the absence of RPA, SMARCAL1 prefers a fork regression substrate that resembles a “normal” replication fork – lagging strand ssDNA. However, in the presence of RPA, SMARCAL1 prefers a substrate that resembles a “stalled” replication fork – ssDNA on the leading strand. (B) SMARCAL1 prefers to restore model regressed forks with a longer leading strand than lagging strand, such that when restored, the fork resembles a “normal” fork – lagging strand ssDNA. RPA enforces this preference by inhibiting SMARCAL1 on the stalled fork substrate and strongly stimulating SMARCAL1 on the normal fork substrate.

Conversely, Rémy also determined that using substrates that mimic regressed normal and stalled forks, SMARCAL1 preferred to restore a “normal” fork compared to a “stalled” fork, and that RPA strongly stimulated SMARCAL1 fork restoration on a regressed “normal” fork substrate (Fig. 1.10B). This suggests a cycle of regression and restoration wherein SMARCAL1 may regress a stalled fork, repair occurs through some mechanism that produces a “normal” regressed fork, which SMARCAL1 then restores (Fig. 1.11 and Bétous et al. 2013). Such a mechanism is not unprecedented, as UvsW can perform such activities in an *in vitro* T4 replication assay (Manosas et al. 2012).

Annealing Helicases and Replication

Human cells contain at least two annealing helicases: SMARCAL1 and ZRANB3 (Bansbach et al. 2010; Ciccina et al. 2009, 2012; Postow et al. 2009; Yuan et al. 2009, 2012; Yusufzai and Kadonaga 2008, 2010). Both of these are DNA-stimulated ATPases that catalyze strand annealing and RPA displacement *in vitro*. Cells depleted of either enzyme have increased γ H2AX foci, and mutations in SMARCAL1 are associated with the human disease Schimke Immunoosseous Dysplasia (SIOD) (Bansbach et al. 2010; Boerkoel et al. 2002). The biological function of these proteins in the cell remains a mystery. However, annealing helicase activity is highly conserved, as the T4 phage UvsW and *E. coli* RecG proteins perform similar *in vitro* activities.

The question remains, however, why more than one annealing helicase? While these enzymes have a similar biochemical activity, some biochemical and genetic evidence suggests that they have at least some distinct functions in cells. Depletion of either protein alone results in γ H2AX foci and sensitivity to replication stress. However, simultaneous depletion of both proteins results in further sensitivity to camptothecin (Ciccina et al. 2012). Genetically, this suggests that these proteins function in separate

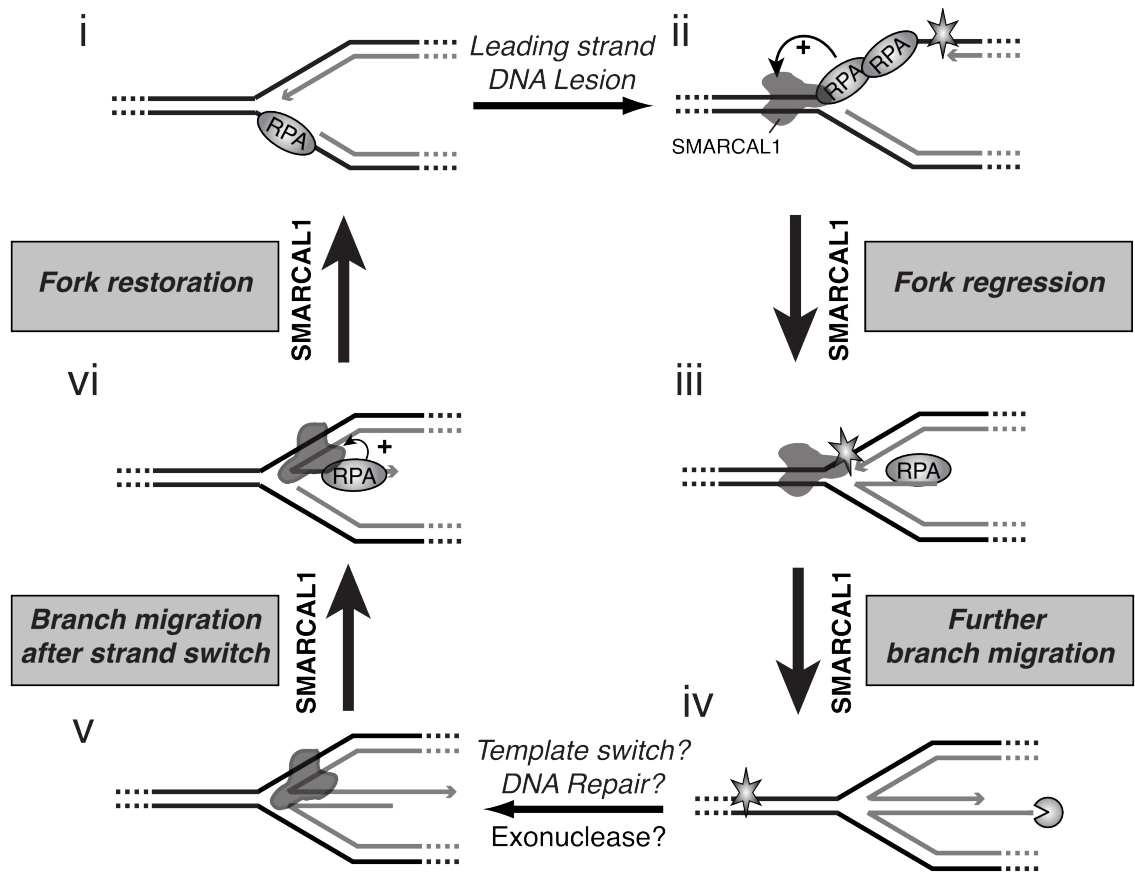


Figure 1.11 Model for SMARCAL1 function in repair of stalled replication forks. (i) A leading strand DNA lesion stalls the replication fork. (ii) RPA bound to the leading strand stimulates SMARCAL1 fork regression activity. (iii) SMARCAL1 further branch migrates the initially regressed fork. (iv) DNA replication and/or repair can occur on the regressed fork and exonuclease activity may digest the regressed lagging strand. (v) SMARCAL1 branch migrates the replication fork until only the ssDNA overhang remains (vi) RPA stimulates SMARCAL1 restoration of a regressed fork with the leading strand overhang exposed. Figure is from (Bétous et al. 2013).

pathways. Unfortunately, due to the inherent limitations of siRNA, we cannot make a definitive statement based on this evidence alone.

SMARCAL1 and ZRANB3 also have distinct modes of recruitment. SMARCAL1 contains an RPA32 binding domain at the N-terminus of the protein which is required for localization to replication foci and to complement the γ H2AX phenotype (Bansbach et al. 2009). In contrast, ZRANB3 contains both a PIP box and an APIM motif, which interact with PCNA, and its NZF domain interacts with ubiquitin (Ciccina et al. 2012). As such, ZRANB3 is recruited to replication foci through its interaction with poly-ubiquitinated PCNA.

One possibility is that ZRANB3 participates in template switching, which makes sense given that it binds to poly-ubiquitinated PCNA, which is thought to regulate template switching (Motegi et al. 2008; Unk et al. 2010; Zeman and Cimprich 2012). ZRANB3 can perform D-loop dissolution and branch migration *in vitro*, and depletion of ZRANB3 leads to increased sister chromatid exchanges (Ciccina et al. 2012). These activities suggest an anti-recombinase function for ZRANB3. One component of which could be dissolving template-switching intermediates. SMARCAL1 is recruited and stimulated by RPA on certain substrates, which could reflect a cellular function in regressing and restoring damaged replication forks (Bétous et al. 2013).

Mechanism of Fork Remodeling

One important open question for these enzymes is the biochemical mechanism by which they translocate on DNA to remodel substrates. Unfortunately, there is little structural data on either SMARCAL1 or ZRANB3. However, structural studies of RecG in complex with forked DNA are illustrative (Singleton et al. 2001). While this structure does not show the contacts that the ATPase domain makes with the template DNA strands, clearly the so-called wedge domain of RecG inserts into the fork junction. This suggests

that RecG translocates along the parental duplex toward the fork junction and uses the wedge domain to displace the nascent strands and produce annealing (Singleton et al. 2001). The DNA protection footprint of RecG indicates that RecG protects the template duplex in the region near the junction (Tanaka and Masai 2006).

Rad54 is another member of the SWI/SNF family involved in D-loop migration during HR. A structure of the ATPase domain of *S. solfataricus* Rad54 bound to dsDNA shows that the ATPase A lobe of Rad54 binds to the 3' → 5' strand, while the ATPase B lobe makes contacts with the opposite strand. The protein itself spans the minor groove. Given the 3' → 5' translocase polarity of Rad54 and DNA binding activity of only the ATPase A domain, Rad54 likely translocates along the 3' → 5' strand (Dürr et al. 2005).

NS3 is a herpes virus helicase of the SWI/SNF family. Crystal structures with various ATP-analogues that mimic transition states allowed structural insight into how these enzymes couple ATP hydrolysis to translocation. This study revealed that the NS3 ATPase A domain makes contact with the nucleic acid and that conformational changes induced during the ATPase cycle shift one nucleotide from one binding site to another, allowing the protein to move along the backbone (Gu and Rice 2010).

What is known for SMARCAL1 is that it has opposite substrate preferences to RecG in the absence of RPA, and Rémy Bétous's footprinting studies demonstrated that SMARCAL1 primarily protects the leading template strand immediately upstream of the fork junction (Bétous et al. 2013). This suggests that SMARCAL1 may bind and translocate along the leading template strand in the 5' → 3' direction. We hypothesize, therefore, that SMARCAL1 would be more sensitive to lesions on the leading template strand and tolerant of those on the lagging template strand. I will explore this hypothesis in Chapter V.

Crosstalk between ATR and SMARCAL1

ATR phosphorylates and regulates a number of replication stress proteins, and Carol Bansbach determined that this includes SMARCAL1. She identified several ATR consensus phosphorylation sites ([S/T]Q) in SMARCAL1 and found that S173, S652, and S919 are damage-inducible. SMARCAL1 purified from HU-treated cells is less active as an ATPase, and the phosphomimetic S652D mutant is less active *in vitro* and is less able to produce the pan-nuclear γ H2AX overexpression phenotype of SMARCAL1 in cells (Couch et al. 2013). The link between SMARCAL1 and ATR will be further explored in Chapter IV.

CHAPTER II

MATERIALS AND METHODS

Antibodies (Western Blotting)

Antibody	Sp.	Dilution	Company	Cat. No.	Notes
ATRIP 403	Rbt	1:3000	Cortez		
ATRIP C	Rbt	1:1000	Cortez		
ATRIP N	Rbt	1:1000	Cortez		
BrdU	Ms	1:1000	BD	555627	
CAF1/p60	Rbt	1:2000	Bethyl	A301-085A	
CDK9	Rbt	1:1000	Cell Signaling	C12F7	
Chk1 (G-4)	Ms	1:1000	Santa Cruz	sc-8408	
Chk1pS317	Rbt	1:1000	Cell Signaling	2344S	
Chk2	Rbt	1:2000	Cortez		
Chk2pT68	Rbt	1:1000	Cell Signaling	2661S	
CtIP	Rbt	1:500	Abcam	ab70163	
Cyclin K	Rbt	1:500	Bethyl	A301-939A-1	Not great
DNA-PK	Ms	1:200	Santa Cruz	SC-5282	
DNA-PKpS2056	Rbt	1:2000	Abcam	ab18192	
DNA-PKpT2609	Ms	1:1000	Abcam	ab18356	
GAPDH	Ms	1:50,000	Millipore	MAB374	
H1 (AE-4)	Ms	1:200	Millipore	05-457	5% Milk, overnight
H2AX (non-phospho)	Rbt	1:5000	Bethyl	A300-082A	
γH2AX (JBW301)	Ms	1:1000	Millipore	05-636	
H2B	Rbt	1:5000	Abcam	ab1790	
H3	Rbt	1:5000	Abcam	ab46765	
H3 "pan acetyl"	Rbt	1:2500	Millipore	06-599	
H3K9me1	Rbt	1:2500	Millipore	07-450	
H3K56ac	Rbt	1:1000	Abcam	ab76307	
H4	Ms	1:5000	Abcam	ab31830	

H4K5ac	Rbt	1:1000	Abcam	ab51997	
H4K12ac	Rbt	1:2000	Active Motif	39166	
H4K20me1	Rbt	1:1000	Active Motif	39727	
HA	Ms	1:3000	Covance	MMS-101P	
HP1 α	Rbt	1:1000	Active Motif	39296	Didn't work
HP1 β	Goat	1:1000	Bethyl	A300-019A	Didn't work
Ku80	Rbt	1:1000	Abcam	ab33242	
MCM2	Ms	1:10,000	BD	39289	
MDC1	Rbt	1:500	Bethyl		
MDC1	Rbt	1:1000	From J. Chen	MC879	
MRE11	Ms	1:1000	Gene Tex	GTX30294	
MUS81	Ms	1:1000	Novus	NBP1-00609	
ORC2	Rbt	1:5000	BD	559266	
PCNA	Rbt	1:200	Santa Cruz	SC-7907	
RAD51	Ms	1:250	Abcam	ab213	
RAD51 (H-92)	Rbt	1:200	Santa Cruz	sc-8349	
RPA32	Rbt	1:1000	Bethyl	A300-244A	
RPA32pS4S8	Rbt	1:1000	Bethyl	A300-245A	
RPA32pS33	Rbt	1:1000	Bethyl	A300-246A	
RPA70	Rbt	1:1000	Cell Signaling	2267	
SLX4	Rbt	1:1000	Bethyl	A302-269A-1	
SMARCAL1	Rbt	1:5000	Bethyl	A301-616A	
SMARCAL1 909	Rbt	1:1000	Open		
SMARCAL1 pS652	Rbt	1:1000 + 1:500 non-phospho peptide (5 mg/mL stock)	Bethyl		Preincubate antibody and peptide 1h; only works after IP
WRN	Rbt	1:1000	Bethyl	A300-239	
ZRANB3	Rbt	1:1000	From J. Chen		

Antibodies (Immunofluorescence)

Antibody	Species	Dilution	Company	Cat. No.	Notes
53BP1	Rbt	1:500	Bethyl	A300-272A	
BrdU	Ms	1:50	BD	555627	3% BSA-PBS, 1h at 37°
"CldU" (BrdU)	Rbt	1:100	Abcam	ab6326	
"IdU" (BrdU)	Ms	1:100	BD	347580	

RAD51 (H-92)	Rbt	1:500	Santa Cruz	sc-8349	3% BSA + 0.1% Tween-20 / PBS
RAD51	Rbt	1:400	Calbiochem	PC130	
γ H2AX (JBW301)	Ms	1:10000	Millipore	05-636	5% BSA-PBS
γ H2AX	Rbt	1:9000	Cortez		

ATR inhibitor

The VE-821 ATR-selective inhibitor (Reaper et al. 2011) was synthesized by the Vanderbilt Institute for Chemical Biology Chemical Synthesis facility and used in most experiments. ATR inhibition in *Xenopus* extracts was achieved with 64 μ M 4-{4-[(3R)-3-methylmorpholin-4-yl]-6-[4-(methylsulfonyl)piperidin-4-yl]pyrimidin-2-yl}-1H-indole (Foote et al. 2010, Patent no. WO2010073034), synthesized by CheminPharma. The minimum concentration needed to achieve a near-complete block of ATR-dependent CHK1 phosphorylation was determined and used in all experiments. This concentration did not inhibit ATM, DNA-PKcs, or mTOR kinases ((Reaper et al. 2011); data not shown).

Cell culture

Name	Media	Source	Notes
U2OS	DMEM + 7.5% FBS		
RPE-hTERT	DMEM/F12 + 10% FBS, 0.348% sodium bicarbonate, 2mM L-glutamine		
293T	DMEM + 7.5% FBS		
HCT116	McCoy's + 10% FBS		
MUS81 ^{-/-} HCT116	McCoy's 5A + 10% FBS	(Shimura et al. 2008)	
HLTF ^{-/-} and ^{+/+} MEFs	DMEM + 15% FBS + 2mM L-glutamine + 55 μ M	(Motegi et al. 2008)	

	β -mercaptoethanol + pen/strep		
Werner syndrome cells (hTERT)	DMEM + 7.5% FBS + pen/strep	(Oshima et al. 2002)	
FANCM ^{-/-} HCT116	McCoy's + 7.5% FBS + pen/strep	(Wang et al. 2013b)	
BSC40	DMEM + 7.5% FBS	Ellen Fanning	Monkey cells for permissive SV40 infection

Clonogenic survival

U2OS cells were seeded onto 60-mm cell culture plates at 200–5000 cells per plate in triplicate. The following day, cells were treated with drug, washed, and released into fresh growth medium for 10–14 days prior to staining with methylene blue.

Fiber labeling

The day before, split cells onto a 6 well plate so that they will be 60-70% confluent on the day of the experiment (~200,000 RPE-hTERT cells per well). Label with 20 μ M IdU for 20 minutes, rinse twice with equilibrated HEPES buffered saline, treat with 2 mM HU or 3 μ M ATRi, then label with 100 μ M CldU (Sigma) for 20 minutes. Harvest cells by trypsinizing in 300 μ L/well trypsin at room temperature. Resuspend in 500 μ L media, transfer to eppendorf tube, and pellet by centrifuging at 2000 rcf for 2-3 minutes. Aspirate and resuspend cells in ice cold PBS to about 1,000,000 cells/mL (200-300 μ L typically). Dilute labeled cells 1:3 with non-labeled cells. Spot 2 μ L of cell suspension on a microscope slide and add 10 μ L of spreading buffer (200 mM Tris-HCl, pH 7.4, 0.5% SDS, 50 mM EDTA) to the cells on the slide for 6 minutes. Then, tilt the slides to 15 degrees to stretch the DNA fibers. (Note: mark in pencil where you deposited the cells. You can put at least 2 spots on one slide, I typically do 3 slides per sample). Air dry for at

least 40 minutes. Fix for 2 minutes in 3:1 methanol:acetic acid in coplin jars. Do this in the hood. Air dry the slides in the hood for about 20 minutes. Slides can be stored up to 5 days at 4°.

Denature the DNA with 2.5N HCl for 30 minutes in coplin jars. Rinse 3 times with PBS in the coplin jars. Block for 1 hour with 10% goat serum in PBS + 0.1% Triton X-100 (Serum solution should be sterile filtered. Can be reused if you add sodium azide and keep at 4°). Stain for 1 hour with rat anti-CldU (Abcam, ab6326; 1:100 dilution) and mouse anti-IdU (Becton Dickinson, 347580; 1:100 dilution) diluted in PBS containing 10% goat serum and 0.1% triton X-100. Do this by placing 200µL drops of antibody on parafilm. Invert the slide and place atop, taking care to eliminate bubbles. Rinse 3 times in PBS in a coplin jar. Stain with secondary antibodies (Alexa-594 goat anti-rat IgG and Alexa-488 goat anti-mouse (Invitrogen); 1:350 dilutions). Rinse 3 times in PBS. Air dry, dark. Mount whole slide coverslips with 110µL Prolong gold (no DAPI!). Dry overnight.

To find the spots with DNA, start with the 100X objective over the pencil marks. Move over to the slide area, zoom out fully, then focus on the speckles, which are typically in the same plane as the DNA. Search around for the DNA. Take at least 10 pictures per condition, really 5-10 pictures per drop, so that you have plenty. You can only measure tracks that are straight and do not overlap. Measure at least 100 tracks per condition.

Fork regression assays

Fork regression assays were completed with 3nM of gel purified, labeled fork regression DNA substrate containing a leading strand gap and 3nM of SMARCAL1 protein in reaction buffer (40mM Tris (pH=7.5), 100mM KCl, 5mM MgCl₂, 100µg/ml BSA, 2mM ATP and 2mM DTT). Reactions were terminated by the addition of 3X stop buffer (0.9%

SDS, 50mM EDTA, 40% glycerol, 0.1% bromophenol blue, and 0.1% xylene cyanol). Samples were separated on 8% polyacrylamide (19:1) 1X TBE gels. The gels were dried and quantified using a Molecular Imager FX (Bio Rad). Sequences of oligonucleotides used to make substrates are listed in Tables 4.1 and 5.1.

Flow Cytometry

Seed ~300,000 cells in a 6-well dish the previous day. Label cells for 40 minutes with 10 μ M BrdU. Trypsinize and collect. Spin for 5 minutes at 1000rpm to pellet. Transfer to a 1.5mL microcentrifuge tube with cold PBS. Spin 5 minutes at 300 rcf. Resuspend in 1mL cold 70% ethanol. Leave on ice 60 minutes or at -20° indefinitely. Spin 5 minutes at 1800 rcf. Aspirate supernatant. Add 1mL 0.5% BSA/PBS (BSA needs to be in all the washes from now on or the ethanol fixed cells will not pellet and resuspend properly) and resuspend. Spin 5 minutes at 1800 rcf. Aspirate supernatant. Add 1mL 2N HCl + 0.5% Triton X-100 in PBS. Incubate 30 minutes at room temperature. Spin and aspirate (5 minutes at 1800 rcf from now on). Add 1mL 0.1M sodium borate and resuspend. Incubate 2 minutes. Spin and aspirate. Wash with 1mL 0.5% BSA/PBS. Spin and aspirate. Add 100 μ L BrdU antibody solution (1:50 Alexa-488 conjugated mouse anti-BrdU [MoBu-1] in 0.5% BSA/PBS + 0.5% Tween-20). Resuspend. Incubate 30 minutes at room temperature in the dark. Spin and aspirate. Wash with 1mL 0.5% BSA/PBS. Spin and aspirate. Resuspend in 0.5-1mL of PBS with 5 μ g/mL propidium iodide and 1:200 RNase A from Sigma. Incubate 2 hours at 37° or overnight at room temperature, dark. Pass through fine nylon mesh (Sefar Nitex 90 μ m mesh). If not staining BrdU, after wash following 70% ethanol fixation, resuspend in PBS containing 25 μ g/ml propidium iodide and 1:200 RNase A. Pro tip: use P1000 with a yellow tip on top of the blue tip to aspirate, this gives greater control so that you don't aspirate your pellets. Also, when resuspending, always rake the tubes across a test tube rack before

adding the next solution to break up the pellet. Also, getting good separation of your BrdU positive and negative cells requires some finagling with the FL1 voltage and compensation settings. It's also probably a good idea to optimize the amount of antibody for your specific cell line/numbers.

In vitro kinase assay

GST-S652 protein contains amino acids 645-661 of SMARCAL1 inserted into pBG101. GST-His' protein is produced from the pBG101 vector without insertion of SMARCAL1 amino acids. It is larger than GST-S652 since there is no stop codon to prevent translation through the polylinker. Both proteins were purified from *E. coli* using glutathione sepharose. Kinase reactions were performed with hyperactive ATR(S1333A)-ATRIP purified from human cells and incubated with the TOPBP1 AAD protein as previously described (Mordes et al. 2008).

Isolation of Proteins on Nascent DNA (iPOND)

The iPOND procedure was carried out as described previously (Sirbu et al. 2011, 2012):

EdU-labeled sample preparation: HEK 293T cells (approximately 1.5×10^8 cells/sample – 3-4 15cm dishes) were incubated with 10-12 M EdU (Vanderbilt Synthesis Core). For pulse chase experiments with thymidine (Sigma), EdU-labeled cells were washed once with temperature and pH-equilibrated media containing 10 M thymidine to remove the EdU, then chased into 10 M thymidine. Other chemicals were added to the cell cultures at the following concentrations: HU (Sigma, 3mM), HAT inhibitor anacardic acid (Enzo, 30 M), HDAC inhibitor FK228 (kindly provided by Dineo Khabele, 100nM), Mre11 inhibitor Mirin (Sigma, 100 M), ATM inhibitor (KU55933, 10 M, AstraZeneca), DNA-PK inhibitor (KU57788, 1 M, AstraZeneca), caffeine (ICN Biomedicals, 10mM), AZ20 ATR inhibitor (3 M, AstraZeneca), ATR inhibitor (VE821, 5 M, Reaper et al. 2011). DMSO was used as a vehicle control where appropriate.

After labeling, cells were crosslinked in 1% formaldehyde/PBS for 20 min (10 minutes works fine) at room temperature, quenched using 0.125M glycine, and washed three times in PBS. Collected cell pellets were frozen at -80°C, then resuspended in 0.25% Triton X/PBS to permeabilize. Pellets were washed once with 0.5% BSA/PBS and once with PBS prior to the click reaction.

Cells were incubated in click reaction buffer for 1-2h at a concentration of 2×10^7 cells/ml of click reaction buffer (2h is better when using these reagents instead of the Invitrogen kit). The click reaction buffer is PBS containing 2mg/mL sodium ascorbate, 2 mM copper (II) sulfate (CuSO_4), and 1 M photocleavable biotin-azide (Kim et al. 2009) (kindly provided by Ned Porter). DMSO was added instead of biotin-azide to the negative control samples (no clk in all figures). Cell pellets were washed once with 0.5% BSA/PBS and once with PBS.

Cells were then resuspended in lysis buffer containing 1% SDS, 50mM Tris (pH 8.0), 1 g/mL leupeptin and 1 g/mL aprotinin. Samples were sonicated (Micro-tip, Misonix 4000) using the following settings: 13-16 Watts (~30% amplitude), 20 s constant pulse, 40-59 sec pause for a total of 4-5 min. (Note: this is the official protocol. What I actually do is two 40 second pulses, and rotate through each sample so that I don't have any down time. I wipe off the tip between each sample). Samples were centrifuged at 13,200rpm for 10 min, filtered through a 90 micron nylon mesh, and diluted 1:1 (v/v) with PBS containing 1 g/mL leupeptin and 1 g/mL aprotinin prior to purification.

Streptavidin-agarose beads (Novagen) were washed 1:1 (v/v) two times in lysis buffer and one time in PBS (The protocol calls for 100 μL beads per 10 million cells. I use about one-fourth of that with good results). Washed beads were incubated with the samples at 4°C in the dark for 14-20 hours (Huzefa Dungrawala showed that 1h at room temperature also works well). The beads were washed one time with lysis buffer, once with 1M NaCl, then twice with lysis buffer. Captured proteins were eluted and crosslinks reversed in SDS sample buffer (add 1:1 to the beads) by incubating for 25 min at 95°C. Collect lysate by poking a hole in the bottom of the tube with a hypodermic needle, then

spin at low speed into another tube (you recover ~1.5x volume this way). Proteins were resolved on SDS-PAGE and detected by immunoblotting. In most cases, quantitative immunoblotting was performed using the Odyssey infrared imaging system.

Native iPOND

Native iPOND is performed the same as normal iPOND with the following modifications: samples are lysed with in Cell Lysis buffer (10mM Tris [pH 8.0], 2mM MgCl₂, 1% NP-40) and vortexing 5 times for 5 seconds with 5 seconds between pulses. Nuclei are then collected by centrifugation at 100 rcf for 5 minutes at 4°. The nuclei are washed twice in 5mL Cell Lysis buffer without NP-40 and resuspended in ice cold Nuclei buffer (15mM Tris [pH 8], 0.125M Sucrose, 15mM NaCl, 40mM KCl, 0.5mM Spermidine, 0.15mM Spermine) at 2,500,000 cells/mL then added to Click reactions (formula is the same). After Click reactions, nuclei are again collected by centrifugation at 100 rcf for 5 minutes at 4° and resuspended at 2,000,000 cells/mL. Add EDTA to 1mM and CaCl₂ to 2mM. Warm to 37° in a water bath and add Micrococcal Nuclease (NEB) to 20 Kurntz units per 1,000,000 cells. Incubate at 37° for 3.5 minutes. Add EDTA to 2mM to quench reactions. Collect by centrifugation. Extract chromatin by resuspending nuclei in ice cold Extraction Buffer (1X PBS containing 350mM NaCl, 2mM EDTA, and 0.1% Triton X-100) at 5,000,000 cells per 3mL. Rock for 2h to overnight at 4°. Centrifuge at 16,000 rcf for 5 minutes at 4° to remove insoluble material. Wash and add 20 L Streptavidin Agarose beads (Novagen). Pulldown is the same as the normal iPOND – incubate overnight, wash the beads, and elute by boiling in 2X sample buffer.

Neutral COMET assay

The neutral COMET assays were performed in accordance with the manufacturer's (Trevigen) instructions:

The day before, plate 150,000 U2OS cells/well in 6-well dishes. Make sure to plate cells for 30 minutes of 1µM CPT and untreated as positive and negative controls,

respectively. Treat cells as necessary then harvest by trypsinization, pellet, and resuspend at 200,000 cells/mL in cold PBS. Pre-warm low melting temperature agarose (LM Agarose, Trevigen) on 95° heat block until thawed, then place in 42° water bath. Mix 10µL cells + 100µL agarose, pipette 50µL into one well of a Trevigen COMET slide. Spread around to make sure agarose is completely covering the well using the pipette tip. Plate 2 wells per condition. Allow to polymerize for 20 minutes at 4°. Immerse slides in pre-chilled lysis buffer (Trevigen) at 4° for 1 hour. Wash by immersion in 50mL pre-chilled TAE for 30 minutes at 4°. Place in large horizontal electrophoresis tank and fill with TAE until buffer is at least 0.5cm above the slides. Electrophorese for 1 hour at 1 V/cm (20V) at 4°. Rinse with deionized water. Immerse in DNA precipitation solution (1M ammonium acetate in ethanol; this stuff is quite pungent, use it in the hood) for 30 minutes at room temperature. Immerse in 70% ethanol for 30 minutes at room temperature. Dry at 45° for 10-15 minutes in the hybridization oven. Store overnight if desired before staining. Stain with 100µL SYBR Green for 30 minutes. Remove and allow to dry for 30 minutes. View the slides with the 10X objective on our Zeiss scope and take pictures. I usually try for ~5 cells per picture, 20 pictures per well so that you can measure at least 100 cells per condition with CometScore software (look in my folder on our backup drive to find the free version).

Plasmid constructs

POLE2-HA and POLE3-HA retroviral vectors were generated by gateway cloning. pENTR POLE2 and pENTR POLE3 were recombined with pLPCX-GW-HA3X (pDC1127) to generate a C-terminal HA-tagged POLE2 and POLE3 retroviral vectors. pDC1127 was created by subcloning a 3XHA epitope into pLPCX between the Not1 and Cla1 restriction sites, then subcloning the gateway cassette containing attR1, ccdB gene, and attR2 as an EcoRV fragment between EcoR1 and Not1 sites.

Preparation of Fork Regression Substrates

Oligo labeling: I usually label the lagging nascent strand (LagN42 in this case). Each 10 μ L labeling reaction should contain 10 μ M oligo, 1x T4 polynucleotide kinase buffer, 0.5 μ L T4 PNK, 0.5 μ L-2 μ L γ -[32P]-ATP. Incubate for 1 hour at 37 $^{\circ}$, then purify on a G25 column (GE). To use the G25 columns, mix the resin well before opening and removing the cap. Spin at 2,800 rpm in an Eppendorf tabletop centrifuge for 1 minute. Add up to 50 μ L of sample. Spin another 2 minutes at 2,800 rpm.

Annealing forks: Anneal each arm of the replication fork separately. In 20 μ L total, mix 7 μ L of LagP62 at 10 μ M with 9 μ L LagN42* (labeled) in 1x SSC. Separately, in 20 μ L total, mix 7 μ L LeadP62 at 20 μ M and 7 μ L LeadN42 at 20 μ M, also in 1X SSC. Also create the product at this step: 2.5 μ L LagN42* and 7.5 μ L LeadN42 at 5 μ M in 1X SSC. Use the RBanneal PCR program to anneal these (RBanneal is designed to prevent secondary structure formation; see program below). Next, add 20 μ L of the leading strand and 20 μ L of the lagging strand to 4.5 μ L of 10X annealing buffer (400mM Tris [pH 7.5], 50mM MgCl₂, 20mM DTT, 1mg/mL BSA, 200mM KCl). Incubate 20-30 minutes on a 37 $^{\circ}$ heat block. Turn off the heat block at the beginning of the incubation. It will cool to about 30 $^{\circ}$ by the end of the incubation.

Gel purification: Add 6x loading dye to the annealed substrate and load into 2 wells of a pre run 5% acrylamide (37.5:1) 0.25X TBE gel (pre-run 100V, 60 minutes). Run for 60 minutes at 100V. Place gel in saran wrap, expose to film for 1 minute, and cut out the band. Place in 3500 MWCO dialysis bag with 1mL 0.25X TBE. Electroelute in ethidium bromide-free gel box in 0.25X TBE for 80 minutes at 80V. Massage the bag and transfer the liquid to 1.5mL eppendorf tubes. Concentrate using Amicon Ultra 4 (10,000 MWCO) columns (add 0.5mL, spin for 5 minutes at 14,000 rcf, discard flowthrough and repeat until only ~50 μ L remain, invert column in fresh collection tube and spin 2 minutes

at 1,000 rcf). Then G25 column purify and add Tris pH 7.5 to 40mM and MgCl₂ to 5mM. Aliquot and store at -80°.

Preparation of Fork Restoration Substrates

This is similar to preparation of fork regression substrates except that the first annealing mixture should contain RD62-P, RG62-P, and ResG30. After RAnneal, add RD62-N2.6 and anneal in annealing buffer before gel purification. Note: this is the lagging gap fork restoration substrate. Use ResD30 and RG62-N2.6 for the leading gap fork restoration substrate.

Pan-nuclear γ H2AX immunofluorescent assay

U2OS cells were transfected with GFP-SMARCAL1 encoding vectors (pLEGFP-C1, Clontech) using Fugene HD (Promega) according to the manufacturer's instructions. Twenty-four hours after transfection the cells were seeded into 96-well CellCarrier plates (Perkin Elmer). Forty-eight hours after transfection the cells were washed once with PBS, fixed with 3% paraformaldehyde solution and permeabilized with 0.5% triton X-100 for 10 minutes at 4 degrees. Fixed cells were then incubated with mouse anti- γ H2AX antibody followed by Cy5-conjugated secondary antibody. After washing, the cells were incubated with DAPI then imaged on an Opera automated confocal microscope (Perkin Elmer) using a 20X water immersion objective. Columbus software (Perkin Elmer) was used to define nuclei and calculate the mean intensity per nucleus for GFP and γ H2AX.

RBanneal PCR Program

1. 95° for 30 seconds.
2. 95° (-3° per cycle) for 40 seconds.
3. 97° (-3° per cycle) for 40 seconds.
4. 96° (-3° per cycle) for 40 seconds.
5. GOTO 2, 24X. (25 total cycles).
6. 12° forever.

RIPA Lysis for Western Blot

Resuspend cells in RIPA buffer (50mM Tris [pH 8.0], 150mM NaCl, 0.1% SDS, 0.5% sodium deoxycholate, 1% Triton X-100, 1mM DTT, 1µg/mL aprotinin, 1µg/mL leupeptin) about 2:1 v/v. Incubate 30 minutes, then pellet at 16,000 rcf for 5 minutes to remove insoluble material. Move supernatant to a new tube, quantitate protein by Biorad DC protein assay. Separate proteins by SDS-PAGE and detect by Western blot.

ssDNA immunofluorescent assays

To detect parental-strand ssDNA, the cells were labeled for 20 hours with 10 µM BrdU then released into fresh growth media for 2 hours prior to addition of drugs. To detect nascent-strand ssDNA, the cells were labeled for 10 minutes with 10 µM BrdU immediately prior to addition of drugs. 3mM HU was added with 5 µM ATRi. Next, the cells were washed once with PBS, permeabilized with 0.5% triton X-100 for 10 minutes at 4 degrees, fixed with 3% paraformaldehyde/2% sucrose solution for 10 minutes, and blocked for 15 minutes in 3% BSA-PBS. Fixed cells were then incubated with mouse anti-BrdU antibody (BD Pharmingen) for 60 minutes at 37 degrees followed by Alexa-488 goat anti-mouse (Invitrogen) secondary antibody. Images were collected using a Zeiss camera at a constant exposure time and quantitated with Cell Profiler (<http://www.cellprofiler.org>).

CellProfiler Pipeline:

1. LoadImages:

File type to be loaded:individual images
File selection method:Text-Exact match
Number of images in each group?:3
Type the text that the excluded images have in common:GFP+DAPI
Analyze all subfolders within the selected folder?:None
Input image file location:Default Input Folder\x7C.
Check image sets for missing or duplicate files?:No
Group images by metadata?:No
Exclude certain files?:Yes
Specify metadata fields to group by:
Select subfolders to analyze:
Image count:2
Text that these images have in common (case-sensitive):DAPI
Position of this image in each group:hoe
Extract metadata from where?:None
Regular expression that finds metadata in the file name:None
Type the regular expression that finds metadata in the subfolder path:None
Channel count:1
Group the movie frames?:No
Grouping method:Interleaved
Number of channels per group:2
Load the input as images or objects?:Images
Name this loaded image:OrigBlue
Name this loaded object:Nuclei
Retain outlines of loaded objects?:No
Name the outline image:NucleiOutlines
Channel number:1
Rescale intensities?:Yes
Text that these images have in common (case-sensitive):GFP
Position of this image in each group:h2ax
Extract metadata from where?:None
Regular expression that finds metadata in the file name:None
Type the regular expression that finds metadata in the subfolder path:None
Channel count:1
Group the movie frames?:No
Grouping method:Interleaved
Number of channels per group:2
Load the input as images or objects?:Images
Name this loaded image:OrigGreen
Name this loaded object:Nuclei
Retain outlines of loaded objects?:No
Name the outline image:NucleiOutlines
Channel number:1
Rescale intensities?:Yes

2. IdentifyPrimaryObjects:

Select the input image:OrigBlue
Name the primary objects to be identified:Nuclei

Typical diameter of objects, in pixel units (Min,Max):60,150
Discard objects outside the diameter range?:Yes
Try to merge too small objects with nearby larger objects?:No
Discard objects touching the border of the image?:Yes
Select the thresholding method:Otsu PerObject
Threshold correction factor:1
Lower and upper bounds on threshold:0.0,1.0
Approximate fraction of image covered by objects?:10%
Method to distinguish clumped objects:Intensity
Method to draw dividing lines between clumped objects:Intensity
Size of smoothing filter:10
Suppress local maxima that are closer than this minimum allowed distance:5
Speed up by using lower-resolution image to find local maxima?:Yes
Name the outline image:None
Fill holes in identified objects?:Yes
Automatically calculate size of smoothing filter?:Yes
Automatically calculate minimum allowed distance between local maxima?:Yes
Manual threshold:0.0
Select binary image:Otsu Global
Retain outlines of the identified objects?:No
Automatically calculate the threshold using the Otsu method?:Yes
Enter Laplacian of Gaussian threshold:.5
Two-class or three-class thresholding?:Two classes
Minimize the weighted variance or the entropy?:Weighted variance
Assign pixels in the middle intensity class to the foreground or the background?:Foreground
Automatically calculate the size of objects for the Laplacian of Gaussian filter?:Yes
Enter LoG filter diameter:5
Handling of objects if excessive number of objects identified:Continue
Maximum number of objects:500
Select the measurement to threshold with:None

3. MeasureObjectIntensity:

Hidden:2
Select an image to measure:OrigBlue
Select an image to measure:OrigGreen
Select objects to measure:Nuclei

4. ExportToSpreadsheet:

Select or enter the column delimiter:Comma (",")
Prepend the output file name to the data file names?:Yes
Add image metadata columns to your object data file?:No
Limit output to a size that is allowed in Excel?:No
Select the columns of measurements to export?:Yes
Calculate the per-image mean values for object measurements?:Yes
Calculate the per-image median values for object measurements?:Yes
Calculate the per-image standard deviation values for object measurements?:Yes

Output file location:Default Output Folder\x7C.
 Create a GenePattern GCT file?:No
 Select source of sample row name:Metadata
 Select the image to use as the identifier:None
 Select the metadata to use as the identifier:None
 Export all measurements, using default file names?:No
 Press button to select measurements to
 export:Image\x7CCount_Nuclei,Image\x7CFileName_OrigGreen,Image\x7CFileName_OrigBlue,Nuclei\x7CIntensity_MeanIntensity_OrigGreen,Nuclei\x7CIntensity_MeanIntensity_OrigBlue,Nuclei\x7CIntensity_IntegratedIntensity_OrigGreen,Nuclei\x7CIntensity_IntegratedIntensity_OrigBlue,Nuclei\x7CLocation_Center_Y,Nuclei\x7CLocation_Center_X,Nuclei\x7CNumber_Object_Number
 Data to export:Image
 Combine these object measurements with those of the previous object?:No
 File name:Image.csv
 Use the object name for the file name?:No
 Data to export:Nuclei
 Combine these object measurements with those of the previous object?:No
 File name:Nuclei.csv
 Use the object name for the file name?:No

SMARCAL1 Overexpression ssDNA Assay

Transfect cells with SMARCAL1 cDNA as in the pan-nuclear γ H2AX immunofluorescence assay. 24 hours after transfection, add 10 μ M BrdU. Harvest and process for ssDNA detection 48 hours after transfection.

SMARCAL1 ATPase assay

ATPase assays were performed as described previously with a splayed arm DNA substrate (Bétous et al. 2012). Make ATPase buffer (20mM HEPES [pH 7.6], 100mM KCl, 5mM MgCl₂, 3% glycerol, 0.25mg/mL BSA, 0.05M EDTA, 0.5mM DTT, 0.01% NP-40). Each ATPase reaction should contain 0.24 μ L γ -[³²P]-ATP, 100nM cold ATP, SMARCAL1 (around 8nM), splayed arm substrate (RBanneal [see program above] GTCGCTGCCCTAATCTGGCTTGCTAGGACATCTTTGCCGAGGTAGACCCG and CGGGTCTACCTCGGCAAAGATGTCCTAGCAATGTAATCGTCTATGTCGTG) and buffer up to 10 μ L total. Incubate at 30° for 1 hour, place on ice, then spot 1 μ L on a TLC plate.

Migrate 45 minutes with 1M formic acid/0.5M LiCl buffer in equilibrated chromatography tank. Dry overnight, then expose to a K-screen and quantitate on the Phosphorimager.

SMARCAL1 purification

Flag-SMARCAL1 was purified from HEK293T cells following transient transfection or from insect cells after baculovirus infection as described previously (Bétous et al. 2012).

Insect cell purification: Thaw pellets on ice for 1 hour. While thawing, prepare lysis buffer (20mM Tris [pH 7.5], 150mM NaCl, 0.1mM EDTA, 0.2mM PMSF, 1µg/mL aprotinin, 1µg/mL leupeptin, 0.1% Triton X-100) and add 20 mL to each pellet. Once thawed, pipette up and down to resuspend the pellets. Transfer to high speed centrifuge tubes (ensure the weight of each is within 10% of one another). Centrifuge 25000 rcf for 10 minutes at 4°. Decant supernatant into another centrifuge tube. Centrifuge 25000 rcf for 10 minutes at 4°. Decant supernatant into a 50mL conical ("cleared lysate"). Wash 250µL anti-FLAG M2 beads (Sigma; use the red ones so you can see them) with lysis buffer twice. Add the beads to the cleared lysate and incubate on the rotator in the cold room for at least 2 hours. Centrifuge at 1200 rcf for 1 minute at 4° to pellet the beads. Transfer the beads to a microcentrifuge tube. Wash once with lysis buffer, once with 0.1M KCl solution (10mM HEPES [pH 7.6], 100mM KCl, 20% Glycerol, 0.2mM EDTA, 0.01% NP40, 1mM DTT, 0.2mM PMSF, 1.5mM MgCl₂), once with 0.1M KCl solution + 0.5M LiCl, and twice more with 0.1M KCl solution. After washes, elute with 250µg/mL FLAG peptide in 0.1M KCl solution by rotating 15 minutes in the cold room (probably just do 2x 200µL elutions). Centrifuge eluates at 1200 rcf for 1 minute to remove any remaining beads. Use a gradient gel to check that you got protein. If desired, concentrate and rinse on a 50,000Da MWCO concentrating column. Aliquot and flash freeze. Store at -80°.

Flag-SMARCAL1 from HEK293T: Harvest 2 15cm dishes per condition. Rinse cell pellet with PBS, then lyse in 2mL NETN buffer (100mM NaCl, 20mM Tris [pH 8], 0.5mM EDTA, 0.5% NP-40, 1mM DTT, 10mM Sodium Fluoride, 0.2mM PMSF, 25mM β -glycerophosphate, 1 μ g/mL aprotinin, 1 μ g/mL leupeptin). Centrifuge at 16,000 rcf for 15 minutes at 4°. Immunoprecipitate 16 μ g protein with 30 μ L anti-FLAG M2 beads (Sigma) equilibrated with NETN. Incubate 3 hours at 4° on rotator. Wash 3 times with NETN buffer, once with NETN buffer + 0.5M LiCl, and twice with SMARCAL1 buffer (20mM HEPES [pH 7.6], 20% glycerol, 100mM KCl, 1.5mM MgCl₂, 1mM DTT, 0.2mM EDTA, 0.2mM PMSF, 0.01% NP-40). Elute in 30 μ L SMARCAL1 buffer + 300 μ g/mL FLAG peptide for 1 hour on ice. Endogenous SMARCAL1 was purified using the same procedure with SMARCAL1 909 antibody and Protein A beads.

Transfections

siRNA transfections were performed using either RNAiMax (Invitrogen), HiPerfect (Qiagen) or Dharmafect 1 (Dharmacon) at a final siRNA concentration of 10 μ M. siRNAs were purchased from Dharmacon or Ambion.

RNAiMax

- W/S cells: 3.2 μ L lipid for 210,000 cells.
- U2OS cells: 4.8 μ L lipid for 210,000 cells.
- RPE cells: 3.2 μ L lipid for 128,000 cells.

HiPerfect

- U2OS cells: 12 μ L lipid for 300,000 cells.

Dharmafect 1

- U2OS cells: 3.2 μ L lipid for 127,500 cells.

Xenopus cell free replication experiments

Xenopus low speed extract was prepared as described (Lebofsky et al. 2009). Immunodepletion of xSMARCAL1 was carried out by incubation of serum with Protein A-Sepharose Fast Flow beads (GE Healthcare) at a 1:1 ratio for 1.5 h at 4°C, and the resulting beads were mixed with extract at a 3:1 extract/bead ratio for 1 h at 4°C. 10 mg/ml rabbit IgG (Sigma-Aldrich) was incubated with Protein A-beads for mock depletions at a 1:10 ratio. For nuclei spindowns, extracts (20 µl) were transferred to 1 ml dilution buffer (30% glycerol, 150 mM KCl, 0.5% Triton X-100, 80 mM PIPES pH 6.8, 1 mM MgCl₂, 1 mM EGTA) and 1 ml of fixation buffer (30% glycerol, 0.5% Triton X-100, 80 mM PIPES pH 6.8, 1 mM MgCl₂, 1 mM EGTA, 4% formaldehyde) was added. The resulting 2 mL was then layered on top of a glycerol cushion (40% glycerol, 80 mM PIPES pH 6.8, 1 mM MgCl₂, 1 mM EGTA) and spun at 3500 rpm for 15 min in a JS-4.2 rotor. Nuclei were washed with TBS and blocked in TBS+1% BSA overnight. BrdU antibody (Santa Cruz, IIB5) was added for 5 h, followed by alexa-594 goat anti-mouse (Invitrogen). Mean BrdU signal intensity was quantitated using ImageJ.

Extra Methods

[3H]Thymidine Incorporation Assay

Adapted from (Coward et al. 1998). Plate about 500,000 cells in a 12-well dish the previous day. Add 10µL of 0.1µCi/µL [3H]Thymidine in PBS (1 µCi/mL final) to the media. Incubate for at least 10 minutes. Carefully remove the media with 1mL pipette. Wash with 1mL PBS. Aspirate. Add 1mL ice cold 5% Trichloroacetic acid. Place at 4° or on ice for 30 minutes. (Note: It's okay to leave cells at 37° in the incubator if you aren't harvesting all the wells at the same time). Remove the TCA and wash with 1mL PBS.

Add 500 μ L freshly prepared 0.5N NaOH/0.5% SDS at room temperature. Pipette up and down and add to scintillation vials. Add 3mL EcoScint fluid. Shake vigorously until phases are mixed (not cloudy). Allow to sit a few hours or overnight before counting. I used the scintillation counter in the Wagner lab. Note: make sure to keep blue pads under everything while you're working. You can't detect [3H] with a Geiger counter, so this will prevent you from accidentally spreading it everywhere.

BrdU Dot-Blot

Cut two pieces of Whatman paper to the size of the dot-blot manifold. Cut one piece of Nytran membrane to the same size. Pour 6x SSC to a depth of 0.5cm and place the Nytran membrane on top. Allow it to sit for 10 minutes before submerging. Wet one piece of Whatman paper with 6x SSC and place on the manifold. Place the membrane on top of the Whatman paper. Adjust all samples to 200-400 μ L in 6x SSC using 20x SSC and deionized water. (Note: I usually load 150-200ng of DNA). Apply 500 μ L 6x SSC to all wells of the manifold. Apply vacuum such that it takes about 5 minutes for the liquid to be sucked through. Apply the samples. Remove membrane from the manifold and dry on a fresh piece of Whatman paper overnight. Crosslink using on the Stratalinker auto-crosslink setting (120,000 μ J) with 265nm light. Block for 30 minutes with 5% milk in TBST. Incubate on the rocker in 1% milk/TBST containing 1:1000 mouse anti-BrdU from BD for 1 hour. Wash four times with TBST. Incubate on the rocker in 1% milk/TBST containing the Licor anti-mouse 800 secondary at 1:10,000 for 1 hour. Wash four times with TBST. Then rinse with TBS. Scan on the Odyssey scanner.

Chromatin Fractionation

Adapted from: (Wysocka et al. 2001). Harvest 10,000,000-20,000,000 cells using a cell scraper. Spin down at 300 rcf for 2 minutes. Wash pellet with PBS, spin again at 300 rcf

for 2 minutes. Repeat wash. Resuspend cell pellet in 200 μ L Buffer A (10mM HEPES [pH 7.9], 10mM KCl, 1.5mM MgCl₂, 0.34M sucrose, 10% glycerol, 1mM DTT, protease inhibitors). Add Triton X-100 to a final concentration of 0.1%. Incubate on ice for 8 minutes. Centrifuge at 1,300 rcf for 5 minutes at 4°. Separate supernatant (fraction S1) from pellet (nuclei; P1). Clarify S1 by high speed centrifugation at 20,000 rcf for 5 minutes at 4° (I usually just do 16,000 rcf). Separate the supernatant (fraction S2) and discard the pellet. Wash P1 once with Buffer A and lyse for 30 minutes in 100 μ L Buffer B (3mM EDTA, 0.2mM EGTA, 1mM DTT, protease inhibitors). Centrifuge at 1,700 rcf for 5 minutes at 4°. Separate supernatant (S3) from pellet (chromatin; P3). Wash P3 once with Buffer B and resuspend in SDS sample buffer, boil for 10 minutes. Separate proteins by SDS-PAGE and analyze by Western blot.

Plasmid-based Fork Regression Substrate Preparation

Prepare pG46 and pG68 plasmid DNAs. Digest 150 μ g of pG46 with Nt.BbvCI and 150 μ g of pG68 with Nb.BbvCI (use 50 μ g DNA and 25 μ L enzyme in 500 μ L reactions). Incubate for 1 hour at 37° then add 2 μ L calf intestinal phosphatase to the pG46 reactions for 20 minutes at 37°. Heat at 80° for 10 minutes then immediately add buffer PBI (from Qiagen kit). Purify each reaction (3 each) on a Qiagen PCR purification kit and calculate the molar concentration (1 μ g of each is 0.57 μ mol). Digest 2 μ L of pG46/pG68 products with 1 μ L SpeI to check gap (SpeI will not cleave gapped plasmid). Digest pG68 product with XhoI (10 μ L in each of 2 reactions) for 1 hour at 37° then use Qiagen PCR kit again – elute each reaction in 30 μ L. Ensure linearity on agarose gel. Label pG46 product with γ -[³²P]-ATP (use 12 μ L [³²P]ATP and 4 μ L T4 polynucleotide kinase) for 2 hours at 37°. Purify on G25 columns (GE). Prepare 10x annealing buffer (500mM Tris-HCl [pH 7.5], 100mM MgCl₂, 50mM DTT). Anneal labeled pG46 product and XhoI-digested pG68 in

1X annealing buffer: 30 seconds at 80° then 20 minute cooldown to 53° in the hybridization oven. Turn the oven off and allow to cool for 20 minutes. Store at -80°.

Thaw the annealed substrate, add 6x loading dye (7.5% ficoll, 15% glycerol, xylene cyanol, bromophenol blue). Prepare 0.6% agarose gel in 0.25X TBE (22mM Tris, 22mM Boric acid, 500µM EDTA). Load ~45µL per well (about 14 wells total). Run until the dye bands are well separated. Expose to film, then excise the band and place in two dialysis bags (3500 MWCO) with 3mL 0.25X TBE each. Electroelute in 0.25X TBE for 60-70 minutes at 90V. Massage the bag then add Tris (pH 7.5) to 10mM. Transfer to (4) 1.5mL tubes and add 1µL MgCl₂ to each. Speedvac (2.0 mmHg, no heat) until about 50µL remains in each tube (about 200µL total). Split into 10µL aliquots and freeze at -80°.

To quantitate the substrate, pour a 5% acrylamide (37.5:1) gel in 1X TBE (89mM Tris, 89mM Boric acid, 2mM EDTA). Load 2µL of 1.185-15nM dilution series of labelled pG46 and 2µL of substrate. Run at 100V for 90 minutes. Dry overnight and quantitate on Phosphorimager.

Plasmid Based Fork Regression Assay

Dilute SMARCAL1 to desired concentrations (150nM works well) and substrate (1.6nM final) in replication fork buffer (20mM Tris-HCl [pH 7.5], 50mM KCl, 5mM MgCl₂, 1mM DTT, 130µg/mL BSA, 2.5mM ATP or ATPγS). Add 5µL of 10X substrate and 10X SMARCAL1 stock to 40µL replication fork buffer and incubate 20 minutes at 37°. Add 5µL of 60mM MgCl₂ + 110mM ATPγS to stop reactions. Mix 9µL of reaction with 1µL of 50% glycerol or AvrII, EcoRI, Sapl, or AlwNI and further incubate 30 minutes at 37°. Add 5µL STOP buffer (0.9% SDS, 50mM EDTA, 30% glycerol, dye). Load 10µL on 6% acrylamide (37.5:1) gel in 1X TBE. Run for 100 minutes at 80V. Dry overnight. AlwNI product is 836bp; Sapl, 329bp; EcoRI, 86bp; AvrII, 36bp.

Replication Intermediate Purification for Electron Microscopy

Plate 5,000,000 cells per dish in 10 centimeter dishes the previous day. Label cells for 10 minutes with 10 μ M BrdU then treat as necessary. Harvest by trypsinization. Wash once with cold PBS and resuspend in 10mL cold PBS.

Transfer to a 6cm dish on ice. Add 0.5mL of 200 μ g/mL Trioxsalen (TMP) in ethanol. Mix and incubate 5 minutes on ice. Irradiate in Stratalinker for 5 minutes with 365nm light for 5 minutes. Add TMP and crosslink 4 times total. Purify genomic DNA using the Qiagen Blood & Tissue kit. The DNA can be stored overnight at 4°. Digest 16 μ g of DNA for each sample with 5 μ L NdeI in 450 μ L total volume for 3 to 5 hours. Adjust volume to 600 μ L with 5M NaCl and TBS-300 (10mM Tris [pH 8.0], 300mM NaCl) to yield a final NaCl concentration of 300 μ M.

BND-Cellulose stock should be prepared ahead of time at 0.1g/mL in TBS-300. This will require lots of vortexing and pipetting up and down with a cut pipette tip to yield a mostly homogeneous solution. Using a cut pipette tip, add 1mL BND-Cellulose solution to an empty Bio-rad Poly-Prep Chromatography column. Allow the liquid to drain through completely. Pre-wash the column 6 times with 1mL TBS-800 (10mM Tris [pH 8.0], 800mM NaCl). Add the liquid rapidly so that the BND-cellulose gets resuspended in it. Equilibrate the column 6 times with 1mL TBS-300, again adding rapidly. Allow the column to drain completely, but don't let it dry out.

Bind digested DNA to the column by adding it to the column and gently tapping the column to resuspend the BND-cellulose. Incubate 30 minutes at room temperature with agitation every 10 minutes. Collect and save the flow-through. Elute the dsDNA by adding 1 mL TBS-800. Collect the flow through and repeat once. Elute the replication intermediates by adding 600 μ L TBSC-1000 (10mM Tris [pH 8.0], 1M NaCl, 1.8% w/v caffeine). Incubate 10 minutes with agitation every 5 minutes. Collect the eluate, which should contain replication intermediates.

Load the eluate onto a Microcon YM-100 column (100,000 kDa MW cutoff). Centrifuge at 2400 rcf for 5 minutes. Add 200 μ L TE. Centrifuge at 850 rcf for 3 minutes. Repeat. Continue to spin until only 10-30 μ L remain. Turn column upside down in a fresh collection tube. Quick spin twice up to 9500 rcf (hold down the button until ~9500rcf, then release). Load 1-2 μ L onto an agarose gel to quantitate DNA. Residual caffeine in the prep precludes A260 quantification. Proceed to dot blot to confirm the presence of BrdU.

Yeast iPOND

Inoculate a 25mL overnight culture the previous day. Use this culture to inoculate 50-100mL 0.1OD culture. Grow to 0.56OD, add 200 μ g/ μ L EdU 1:500 to a final concentration of 400 μ g/mL. Grow for 60 minutes at 30° with shaking (target is 0.8 OD600 at the end of the labeling). Add 37% formaldehyde to a final concentration of 1%. Incubate on rotator for 20 minutes at room temperature. Quench by adding 1.25M glycine to a final concentration of 125mM. Incubate 10 minutes on rotator at room temperature. Split as necessary. Pellet (3000rpm for 2 minutes) and wash twice with equal volume water. Resuspend in 1mL water, transfer to a 2mL microcentrifuge tube, pellet, discard supernatant, and store at -80°.

Resuspend in 1600 μ L lysis buffer (1% Triton X-10, 50mM Tris [pH 8.0]). Divide into four 2-mL tubes and add acid washed beads until only a tiny amount of volume remains atop the beads. Bead beat six times, 30 seconds per step. Incubate on ice 1 minute between steps. Poke a hole in the bottom of the tube and spin into 15mL tube at 2000 rpm. Resuspend lysate and transfer to a microcentrifuge tube. Check lysis efficiency by looking at 5 μ L under the microscope. Broken cells appear as “ghosts” - very light and faint compared to unbroken cells. Save 1% for gel (“pre-click”).

Resuspend in click reactions – 500µL per 2 OD (1x Click buffer, xx Biotin-azide, 1x Click additive, 2mM CuSO₄). Rotate for 2 hours in dark at room temperature. Add 20% SDS to a final concentration of 0.5%. Save 1% for gel (“post-click”). Sonicate until clear – 30% amplitude, 20 second pulses, 1 minute on ice between pulses). Save 1% for gel (“post-sonication”). Spin at 16000 rcf for 5 minutes. Collect the supernatant and transfer to a fresh tube. Centrifuge again at 16000 rcf for 15 minutes. Pass through a FACS membrane into a fresh tube. Wash 10uL Novagen Streptavidin agarose beads per OD. Wash two times with 1mL lysis buffer then once with 1mL PBS. Resuspend 1:1 in PBS. Save 1% of the lysate as “input” before adding beads. Add beads and incubate overnight at 4°, dark. Spin at 1800 rcf for 5 minutes, transfer supernatant to another tube. Transfer beads to fresh tubes using 1mL lysis buffer. Incubate beads for 5 minutes on rotator, then discard supernatant. Wash three times with 1mL lysis buffer. Add 2x sample buffer 1:1 to the beads and boil for 25 minutes. Resolve proteins by SDS-PAGE and detect by Western blotting.

CHAPTER III

ANALYSIS OF THE DNA DAMAGE RESPONSE AT STALLED REPLICATION FORKS[†]

Preamble

I joined the Cortez laboratory in May 2010 just after Bianca Sirbu developed iPOND (isolation of proteins on nascent DNA) and was fortunate enough to collaborate on two of her publications (Sirbu et al. 2011, 2012). As such, this chapter draws primarily from the first of these publications, and I have borrowed heavily from this work and focused the discussion here on areas where I made primary contributions. I have also included several unpublished experiments where I have adapted the protocol to specific applications, such as native iPOND and damaging agents other than HU.

Introduction

Human cells replicate billions of base pairs of DNA during each cell cycle. While much of the cellular machinery involved in this process has been identified, much still remains unknown. DNA replication must be faithful and complete. Insufficient nucleotide precursors, difficult to replicate sequences, and DNA lesions challenge the fidelity of replication. Failure to overcome these challenges can lead to mutations that contribute to the development of cancer. To deal with challenges to genome integrity, the cell contains machinery known as the DNA damage response (DDR). The DDR activities that respond to replication stress, appropriately termed the replication stress response (RSR), coordinate replication fork stabilization, cell cycle progression, and completion of DNA synthesis (Cimprich and Cortez 2008; Harper and Elledge 2007).

[†] Parts of this chapter were published in (Sirbu et al. 2011).

In comparison to the cellular response to DSBs, we know relatively little about the replication stress response. Numerous proteins accumulate at stalled replication forks and these forks can be repaired in a number of ways, likely dependent on the context, type, and severity of damage. However, we know little about the interplay between these pathways and how they are regulated.

At a DSB, there are extensive modifications to the surrounding chromatin including destabilization of nucleosomes, chromatin remodeling, and histone post-translational modifications (van Attikum and Gasser 2009; Morrison and Shen 2009; Rossetto et al. 2010; Venkitaraman 2010). These changes increase access to the repair machinery and recruit proteins involved in repair and DDR signaling. The extent to which chromatin changes at a stalled fork mimic those at a double-strand break is unknown.

Replication provides a unique landscape and set of challenges compared to a DSB. The immediate vicinity of the replisome lacks nucleosomes. Also, half of the histones on the nascent DNA are newly synthesized and require changes in post-translational modifications to restore the proper chromatin structure (MacAlpine and Almouzni 2013). Finally, several mechanisms exist to recover stalled replication forks, which necessitate the recruitment of multiple enzymatic activities and perhaps different chromatin changes (Yeeles et al. 2013).

Our lack of knowledge is in part due to the unique challenges of studying the replication stress response in the mammalian system. Engineering site-specific nucleases with unique cleavage sites into the mammalian genome allows researchers to use chromatin immunoprecipitation (ChIP) to monitor changes in protein dynamics at a single DSB (Berkovich et al. 2008; Rodrigue et al. 2006; Rudin and Haber 1988; Soutoglou et al. 2007).

Thus far, the only site-specific analysis of active and stalled replisomes in mammalian cells was achieved using an episome containing an interstrand crosslink

(Shen et al. 2009). Unlike lower organisms, mammalian cells lack efficient, sequence-specific origins which makes tracking the location of any single replisome in a mammalian cell impossible and limits the utility of ChIP-based technologies. We have addressed this technical limitation by developing the iPOND methodology. Briefly, we utilized the thymidine analog 5-ethynyl-2'-deoxyuridine (EdU) (Salic and Mitchison 2008) which contains an alkyne functional group. Covalent linkage to a biotin-azide using click chemistry (Moses and Moorhouse 2007) facilitates single-step purification of the EdU-labeled nascent DNA and associated proteins at replication forks (Fig. 3.1). We demonstrated previously that iPOND can detect replication proteins with as little as 2.5 minutes of EdU labeling, which suggests resolution on the order of 2-6kb (Sirbu et al. 2011). iPOND permits the isolation and analysis of proteins at active, stalled, and collapsed replication forks.

The development of iPOND allows us to ask new questions about the DDR at replication forks. While previous analyses were sufficient to demonstrate much of the protein recruitment and phosphorylation events that occur at stalled replication forks, iPOND allows us to investigate these events with a higher degree of spatial and temporal resolution. Therefore, we endeavored to describe in detail the protein recruitment and PTM changes that occur over time at stalled and collapsed replication forks.

Results

Analysis of chromatin maturation using iPOND

Maturation of the new chromatin requires addition and removal of histone post-translational modifications. Newly synthesized histone H4 is acetylated on two lysines (5 and 12), and these evolutionarily conserved marks are removed after

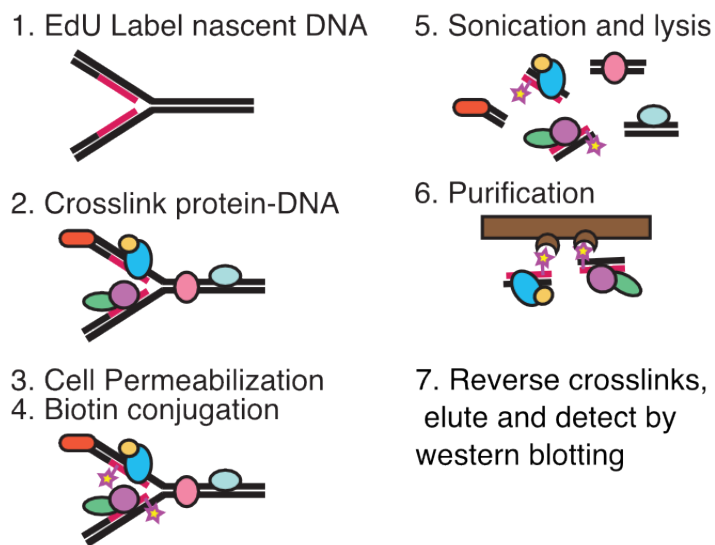


Figure 3.1 Isolation of Proteins on Nascent DNA (iPOND). (1) Cells are incubated with Thymidine analogue 5'-Ethylnyl-3'-deoxyuridine (EdU) to label nascent DNA. (2) Formaldehyde crosslinks protein-DNA complexes. (3) Cells are permeabilized using Triton X-100. (4) Click chemistry covalently links EdU and Biotin-azide. (5) Cells are sonicated to release small fragments of DNA bound to proteins. (6) Streptavidin resin allows single-step, high-affinity purification of biotin tagged protein-DNA complexes. (7) Reverse formaldehyde crosslinks to elute and detect by Western blotting.

deposition (Sobel et al. 1995; Taddei et al. 1999). Therefore, we monitored removal of these marks as a surrogate for chromatin maturation. Our time course experiments indicate that H4K5ac is removed rapidly and H4K12ac deacetylation is slightly delayed (Fig. 3.2A). The delay in K12 deacetylation could be due to the activity of chromatin-associated histone acetyl transferases (HATs) that promote the acetylation of this site in some chromatin domains. Indeed, in the presence of the non-selective HAT inhibitor anacardic acid the rate of H4K12 deacetylation became identical to H4K5 with a half-life of less than 20 minutes (Fig. 3.2B). We also observed that replication fork stalling with HU did not alter the rate of H4 deacetylation. Therefore, replication fork progression can be uncoupled from chromatin maturation (Sirbu et al. 2011).

Development of Native iPOND (n-iPOND)

Another application of iPOND is to study the chromatin context of the replication fork under a variety of conditions. One limitation in this regard is the use of a formaldehyde crosslinking step. Incomplete removal of this crosslinker interferes with these analyses by destroying antibody epitopes and altering the m/z ratio of proteins, making detection of PTMs difficult. Therefore, we developed an alternative methodology called Native iPOND (n-iPOND) to address these limitations.

Native iPOND differs from iPOND in that we omitted the cross-linking step and used micrococcal nuclease (MNase) in lieu of sonication to solubilize the chromatin after the Click chemistry step. Proteins bound to these fragments can be purified and detected by Western blot (Fig. 3.3). We successfully purified histones using the n-iPOND technology, and we envision that future studies will use n-iPOND to catalog histone modifications at replication forks under a variety of conditions. While the n-iPOND protocol reported in (Sirbu et al. 2012) is unoptimized and has a low experimental yield,

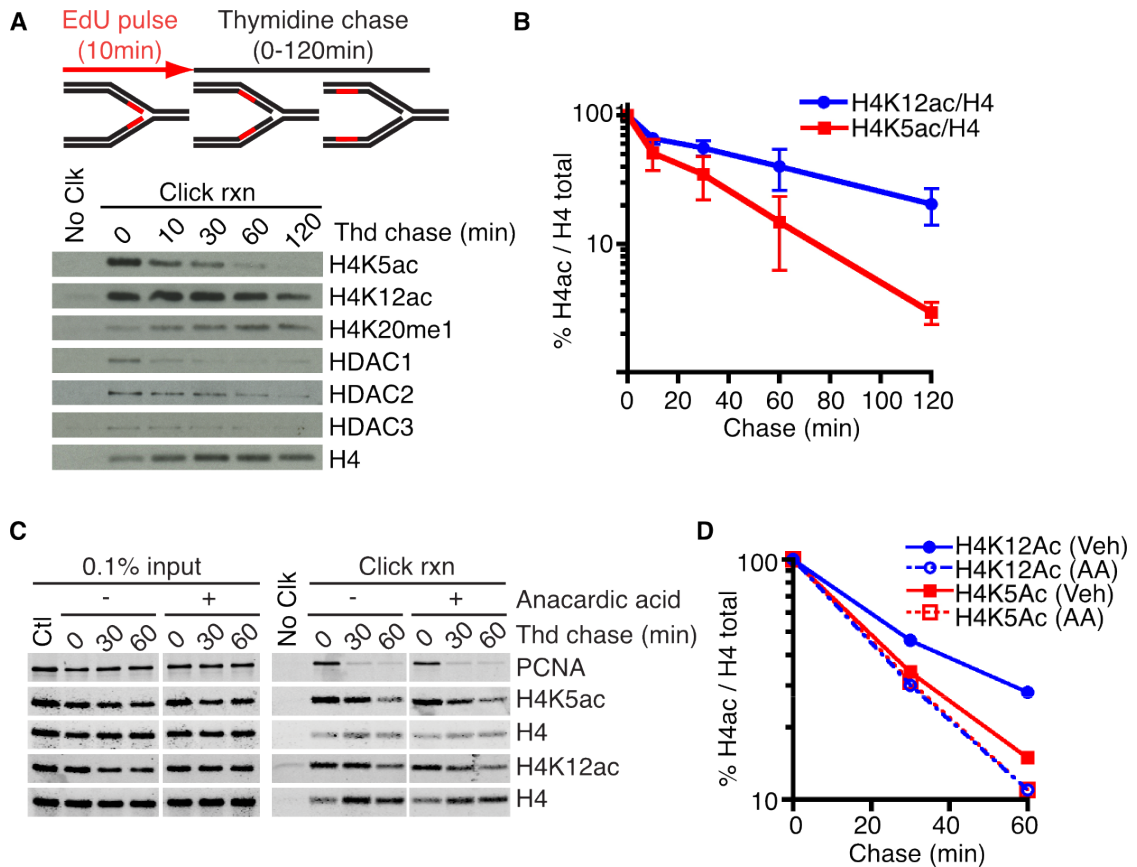


Figure 3.2 H4K5ac and H4K12ac are deacetylated with different kinetics after deposition due to reacetylation by HATs. (A) Cells were labeled with EdU for 10 minutes followed by a chase into thymidine containing media for the indicated times prior to performing iPOND. (B) Quantitation of H4 acetylation levels compared to total H4 in the click reaction samples from three independent experiments. Error bars indicate standard deviation. (C) Cells were labeled with EdU for 10 minutes followed by a chase into thymidine containing media in the presence or absence of 30 μ M anacardic acid for the indicated times prior to performing iPOND. (D) Quantitation of H4 acetylation levels compared to total H4 in the click reaction samples from three independent experiments. Error bars indicate standard deviation. Data for panels A and B were produced by Bianca M. Sirbu and Frank B. Couch.

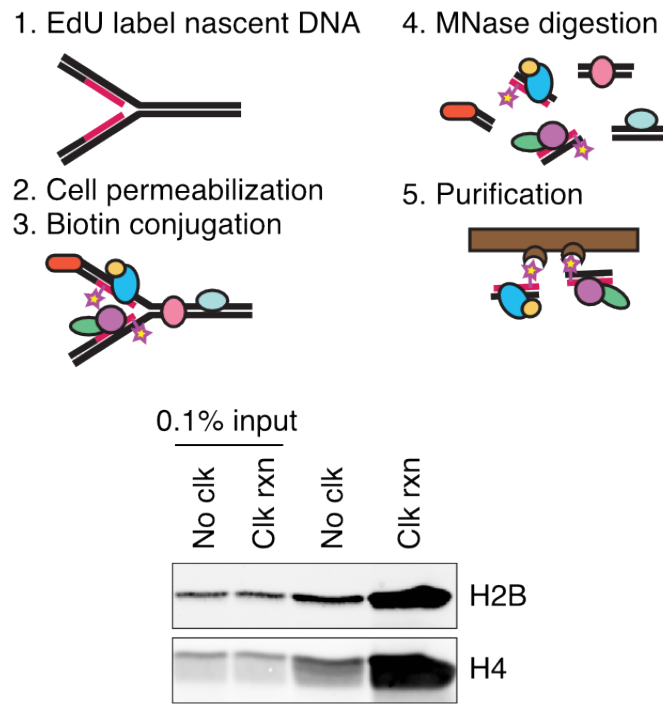


Figure 3.3 Native isolation of proteins on nascent DNA (n-iPOND). (1) Cells were labeled with EdU for 60 minutes, (2) permeabilized with Triton X-100, then (3) biotin conjugated using click chemistry. (4) Chromatin fragments were solubilized using Mnase, followed by (5) purification with streptavidin agarose. Purified proteins were separated by SDS-PAGE and visualized by Western blotting with antibodies to H2B and H4.

another group has since improved the n-iPOND protocol (Leung et al. 2013). This improved protocol will likely enable further studies of chromatin modifications.

Analysis of Replisome Stability During Prolonged Replication Stress

Unfortunately, iPOND coupled to SDS-PAGE and Western blot requires highly-specific, high-affinity antibodies, especially for proteins of low abundance. To detect such proteins, for example polymerase subunits, we engineered cell lines that stably express tagged versions of these proteins. Using these cell lines, we detected two subunits of polymerase epsilon: POLE2 and POLE3 (Fig. 3.4A).

In lower organisms such as *S. cerevisiae* and *X. laevis*, certain types of replication stress lead to disassembly of the replisome as measured by dissociation of polymerases from DNA (Cobb et al. 2003; Trenz et al. 2006). We hypothesized that replisome disassembly also occurs in human cells in response to prolonged replication stress induced by HU. To test this hypothesis, we labeled cells expressing POLE3-HA for 10 minutes with EdU then added HU for 0, 1, or 8 hours before purifying replication fork associated proteins using iPOND. We observed a modest decrease in POLE3 captured at both timepoints. This suggests that while some replisome disassembly may occur, this is not a major event during HU treatments of 8 hours or less (Fig. 3.4B), and this result can be explained by replication termination events that occur during this time. Further experimentation can elucidate whether the replisome is destabilized under other damage conditions and if and how ATR regulates this process.

DDR response at stalled replication forks

HU treatment causes DDR activation to stabilize the stalled fork and induce a cell cycle checkpoint. Previous studies suggest that HU-stalled forks remain stable and competent to resume DNA synthesis for several hours; however, eventually the stalled

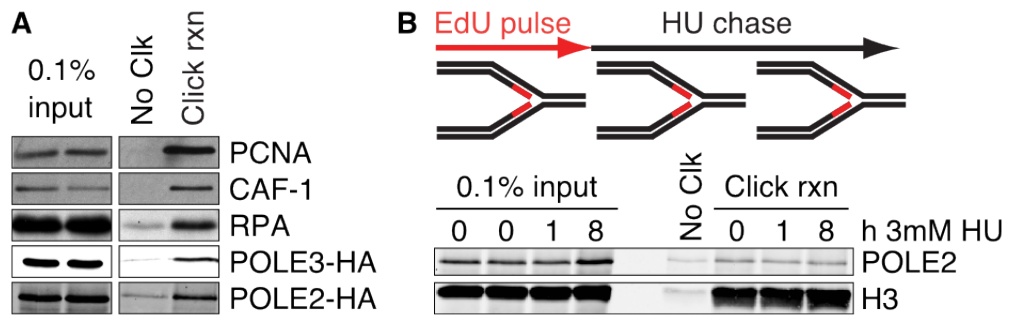


Figure 3.4 Detection of polymerase subunits using iPOND. (A) Cells expressing HA-tagged versions of POLE2 or POLE3 were labeled with EdU for 10 minutes prior to performing iPOND. (B) Cells expressing POLE2-HA were labeled with EdU for 10 minutes then HU was added to 3mM for the indicated times prior to performing iPOND. Data were produced by Jordan T. Feigerle under the direction of Frank B. Couch.

fork collapses and double-strand breaks form (Hanada et al. 2007; Petermann et al. 2010). Using iPOND, we demonstrated that PCNA and CAF-1 decrease after HU addition to a steady state level of 20-30% of that found at elongating forks, likely due to unloading of PCNA from completed Okazaki fragments (Sirbu et al. 2011). Moreover, we detected rapid phosphorylation of RPA on S33 followed by S4-S8 at later timepoints (Fig. 3.5A), consistent with phosphorylation of S33 by ATR and S4-S8 by DNA-PK (Anantha et al. 2007; Sirbu et al. 2011). We detected phosphorylation of H2AX at the earliest timepoints of HU tested, 10 minutes (Sirbu et al. 2011), well before evidence of DSB formation (Petermann et al. 2010). Finally, we monitored accumulation of DSB proteins and detected MRE11, RAD51, and KU80 (Fig 3.5A). While we observed low levels of these proteins at early timepoints, we detected a shift in the DDR between 2 and 4 hours of HU treatment that resulted in hyperaccumulation of these proteins, suggesting the formation of DSBs (Fig. 3.5A and Sirbu et al. 2011).

RAD51 accumulation at stalled replication forks

With similar kinetics to the shift from ATR- to ATM/DNA-PK-dependent H2AX phosphorylation, we observed increased accumulation of the DSB proteins MRE11, RAD51, and KU70/80 at stalled replication forks (Fig. 3.5A and Sirbu et al. 2011). At DSBs, MRE11-dependent end-resection is required to load RAD51 (Mimitou and Symington 2009). At collapsed forks, RAD51 may function to promote recombination-based methods to re-establish the replication fork (Anand et al. 2013; Errico and Costanzo 2010). To test whether the loading of RAD51 at stalled forks also requires MRE11, we treated cells with the MRE11 nuclease inhibitor mirin (Dupré et al. 2008). Although the early recruitment of RAD51 occurred independently of MRE11, the late accumulation required MRE11 activity (Fig. 3.5B), suggesting that end-resection of the parental DNA strand promotes this loading. The timing of MRE11 recruitment also

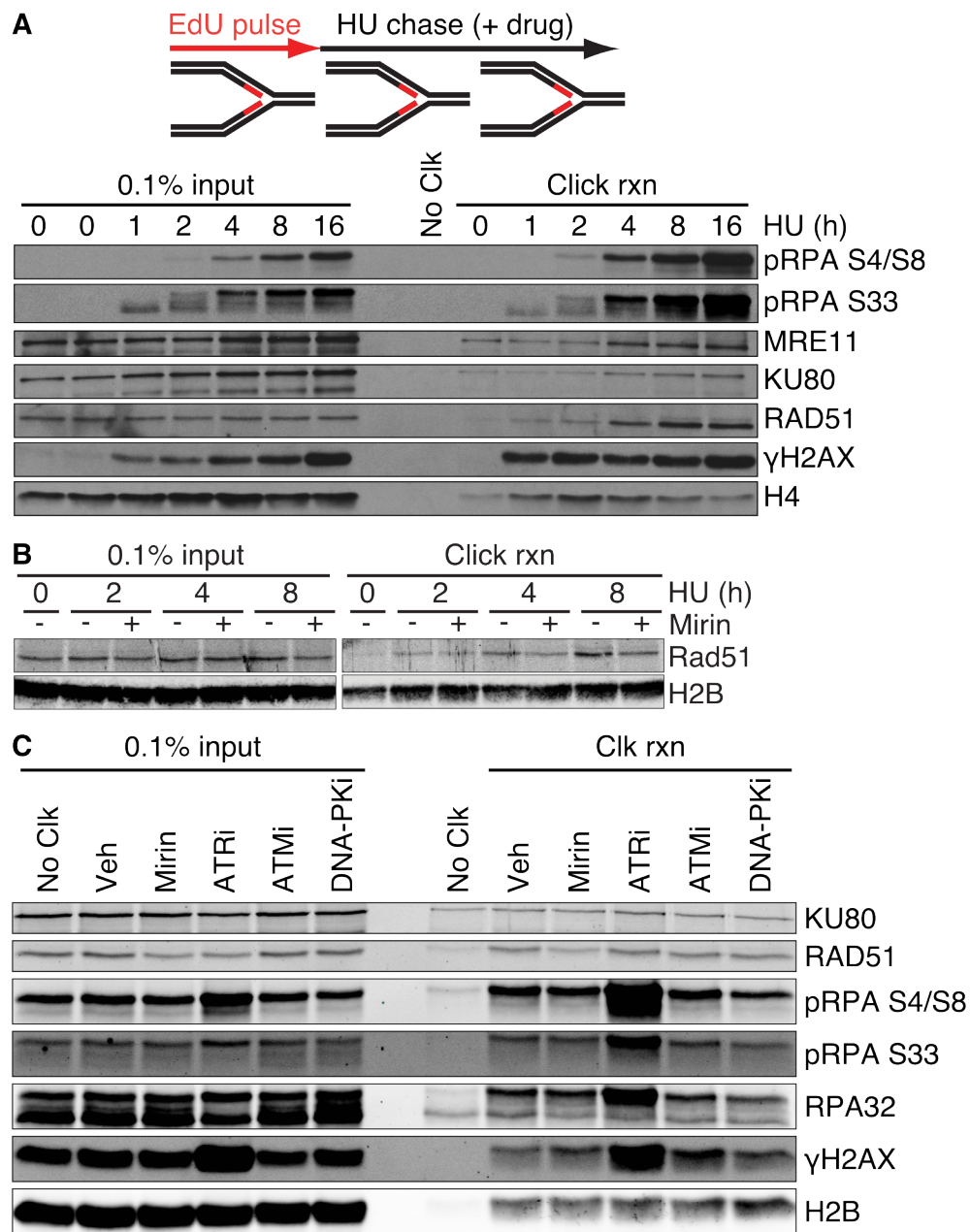


Figure 3.5 RAD51 accumulation during extended HU treatments is dependent on MRE11 nuclease activity. (A) Cells were labeled with EdU for 10 minutes then HU was added to 3mM for the indicated times prior to performing iPOND. (B) Cells were labeled with EdU for 10 minutes then HU was added to 3mM in the presence or absence of 100μM mirin for the indicated times prior to performing iPOND. (C) Cells labeled with EdU for 10 minutes were treated with 3mM HU for 8 hours. Mirin (100μM), ATRi (AZ20, 3μM), ATMi (KU55933, 10μM), and DNA-PKi (NU7441, 1μM) were added at the same time as HU. Data for panel A were produced by Bianca M. Sirbu.

correlated with a large increase in RPA S4/S8 phosphorylation (Sirbu et al. 2011), which was previously linked to end-resection at camptothecin-damaged forks (Sartori et al. 2007).

ATR Regulation of Stalled Replication Forks

ATR is the master regulator of the response to replication fork stalling. While ATR phosphorylates hundreds of substrates at stalled replication forks, how ATR regulates the DDR at stalled replication forks to preserve genome integrity remains unclear (Cimprich and Cortez 2008; Nam and Cortez 2011). Therefore, we next investigated whether RAD51 accumulation is ATR-dependent. Using the ATR inhibitor AZ20 from AstraZeneca, we observed that RAD51 accumulation remains unchanged regardless of ATR signaling after 8 hours of HU treatment (Fig. 3.5C). This suggests that the observed shift in the DNA damage response that results in increased RAD51 accumulation does not require ATR signaling. Inhibition of ATM or DNA-PK also had no effect on RAD51 accumulation (Fig. 3.5C).

Interestingly, we noticed an increase in the RPA and γ H2AX purified at the stalled replication forks when ATR was inhibited. iPOND likely only purifies RPA molecules immediately adjacent to the newly synthesized DNA strand (Sirbu et al. 2011); therefore, the increase in RPA purification indicates that the nascent strand likely became single stranded and bound by RPA. Since we also observed increased γ H2AX, this may occur through DSB formation and resection of the template strand to expose ssDNA on the newly synthesized strand. This topic will be revisited in Chapter IV.

γ H2AX spreading from stalled forks before and after fork collapse

We noticed that the rapid phosphorylation of H2AX near the fork saturates within 30 minutes; however, global levels continue to increase (Sirbu et al. 2011). Therefore,

we hypothesized that the global increase stems from γ H2AX spreading from the stalled fork as is observed near double-strand breaks (Berkovich et al. 2007; Savic et al. 2009). To test this hypothesis we first labeled cells with EdU, then chased with thymidine for various lengths of time to extend the distance between the EdU-labeled fragment and the fork, and finally added HU to stall the fork. A detailed analysis revealed that the density of γ H2AX gradually declined as a function of distance from the stalled fork (Fig. 3.6). Compared to the saturated density at the fork, the γ H2AX density decreased approximately two-fold for every 15 minutes of thymidine chase time when cells were treated with HU for one hour. By two hours, we observed increased γ H2AX density in all chromatin segments analyzed suggesting that γ H2AX spreading contributes significantly to the global change in γ H2AX levels.

To examine the chromatin at a single location distant from the fork, we repeated this experiment holding the thymidine chase time constant at 30 minutes and treated with HU for varying times. We observe a steady increase in γ H2AX at this distance from the fork with increasing times of HU treatment (Fig. 3.6B). Importantly, these results indicate considerable spreading of the γ H2AX signal even shortly after fork stalling. Assuming a conservative rate of fork elongation of 1kb/min, these data imply that within one hour of fork stalling γ H2AX spreads to include a large domain containing tens of thousands of base pairs of DNA.

To identify the kinase(s) that phosphorylate H2AX adjacent to the stalled fork and that promote spreading, we utilized small molecule kinase inhibitors. The selective DNA-PK and ATM inhibitors NU7441 (Leahy et al. 2004) and KU55933 (Hickson et al. 2004) had minimal effects on the spreading or total levels of γ H2AX induced by a short (30-60min) HU treatment (Sirbu et al. 2011). However, these inhibitors did significantly reduce γ H2AX levels in cells treated with HU for 4 hours (Fig. 3.7A). These results indicate that DNA-PK/ATM contributes to maintenance and spreading of γ H2AX at

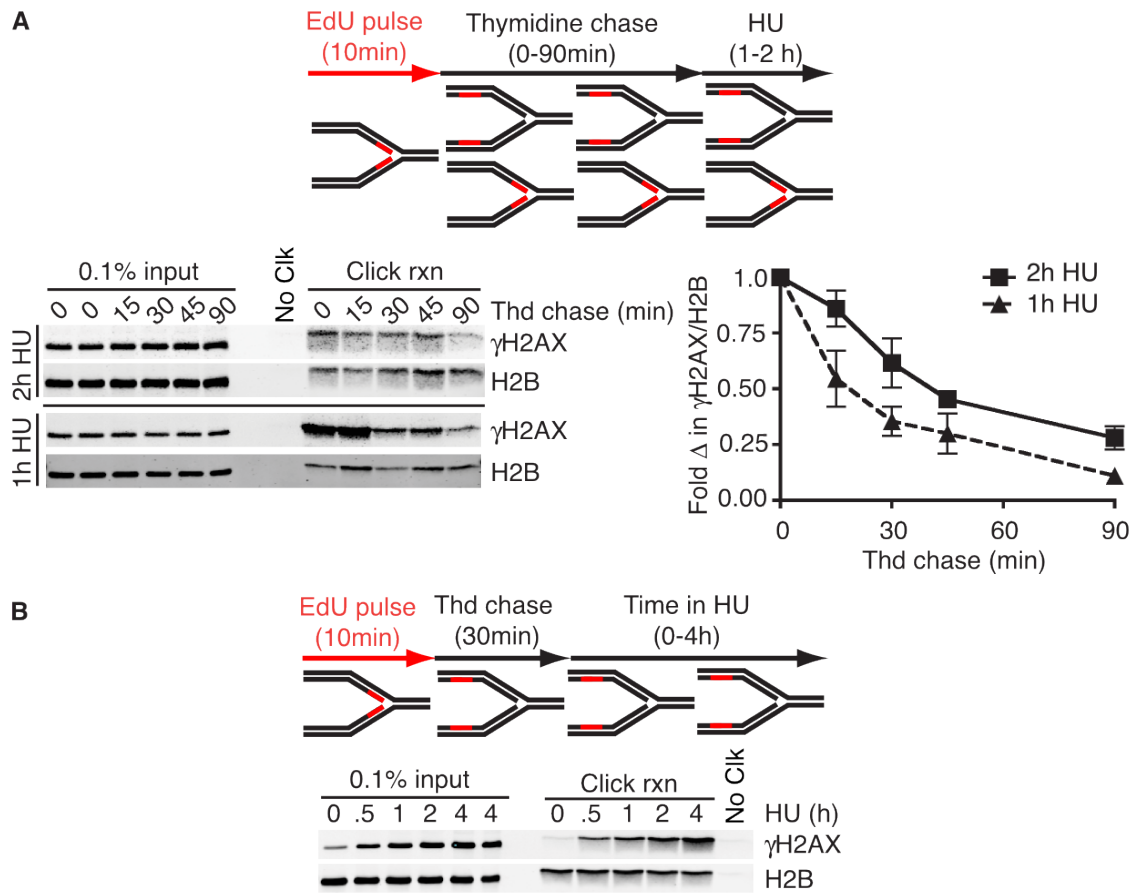


Figure 3.6 γ H2AX spreads along chromatin behind stalled replication forks. (A-B) Cells were labeled with EdU for 10 minutes then chased into thymidine containing media for the indicated times before addition of 3mM HU for the indicated times prior to performing iPOND. (A) Graphed values are the mean and standard deviation of fold change in the ratio of γ H2AX to H2B compared to the 0 minute thymidine chase from 3 independent experiments for the 2h HU timepoints and 2 independent experiments at the 1h HU timepoints.

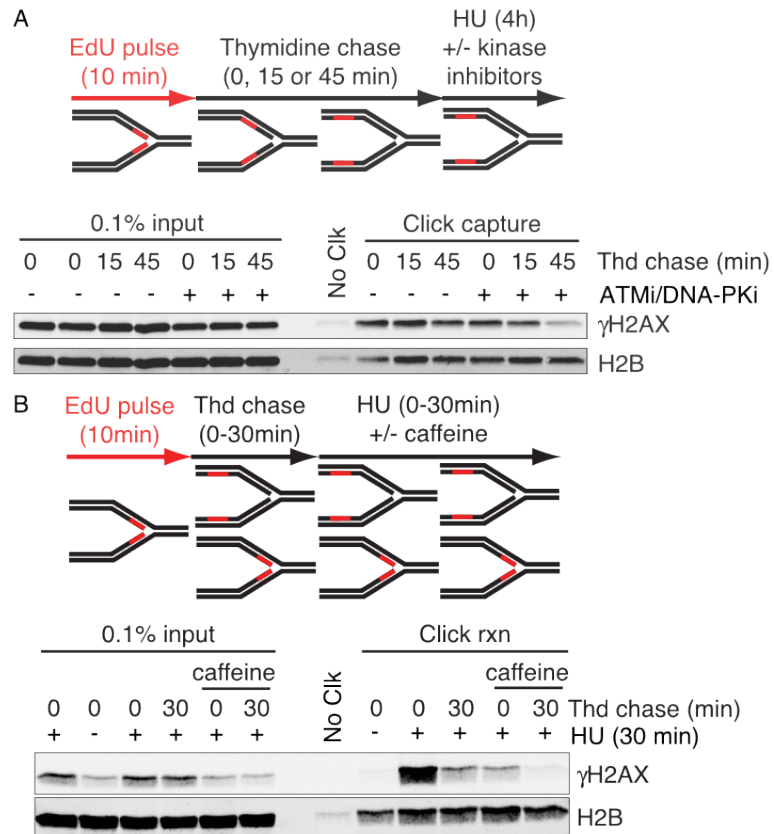


Figure 3.7 γ H2AX spreading is ATM/DNA-PK-dependent during extended HU treatments, but ATR-dependent during short HU treatments. Cells labeled with EdU for 10 minutes were chased into thymidine followed by treatment with HU. The length of thymidine and HU treatments are indicated. (A) DNA-PK (NU7441, 1 μ M) and ATM (KU55933, 10 μ M) inhibitors were added at the same time as HU in the indicated samples. (B) Caffeine (10mM) was added at the same time as HU in the indicated samples.

persistently stalled forks. In contrast, treatment with caffeine, which preferentially inhibits ATR (Sarkaria et al. 1999), significantly reduced γ H2AX formation and spreading shortly after the fork is stalled (Fig. 3.7B). These results are consistent with a model in which ATR phosphorylates H2AX at a stalled fork and promotes initial spreading. At later time points, likely after DSB formation, ATM and DNA-PKcs maintain and further propagate the H2AX phosphorylation.

Other DNA Damaging Agents

HU is not the only DNA damaging agent that causes replication stress. Camptothecin (CPT), a Topoisomerase I poison, causes replication-dependent DSBs. These DSBs likely arise from either cleavage of replication forks stalled by topological strain or through polymerase run-off at CPT-induced SSBs (Pommier 2006; Ray Chaudhuri et al. 2012). Unlike HU, CPT does not rapidly stall every fork in the cell, rather, in CPT-treated cells, replication forks proceed more slowly as they encounter topological strain or SSBs and collapse asynchronously.

We utilized two different experimental protocols to label and purify replication fork associated proteins in CPT treated cells. First, we treated cells with CPT for increasing times up to one hour and added EdU to the media for the final 15 minutes of treatment. Using this methodology, we detected decreasing amounts of H2B and PCNA with increasing CPT treatment times. This likely reflects the general slowing of replication during CPT treatment (Regairaz et al. 2011). In this instance, however, we detected an increase in RPA phosphorylated on S4-S8, consistent with DSB formation (Fig. 3.8A and Sartori et al. 2007).

Alternatively, we treated cells for one hour with CPT and added EdU for increasing labeling times at the end of CPT treatment. In this case, we detected increasing H2B over time, indicating that replication forks do progress detectably in CPT

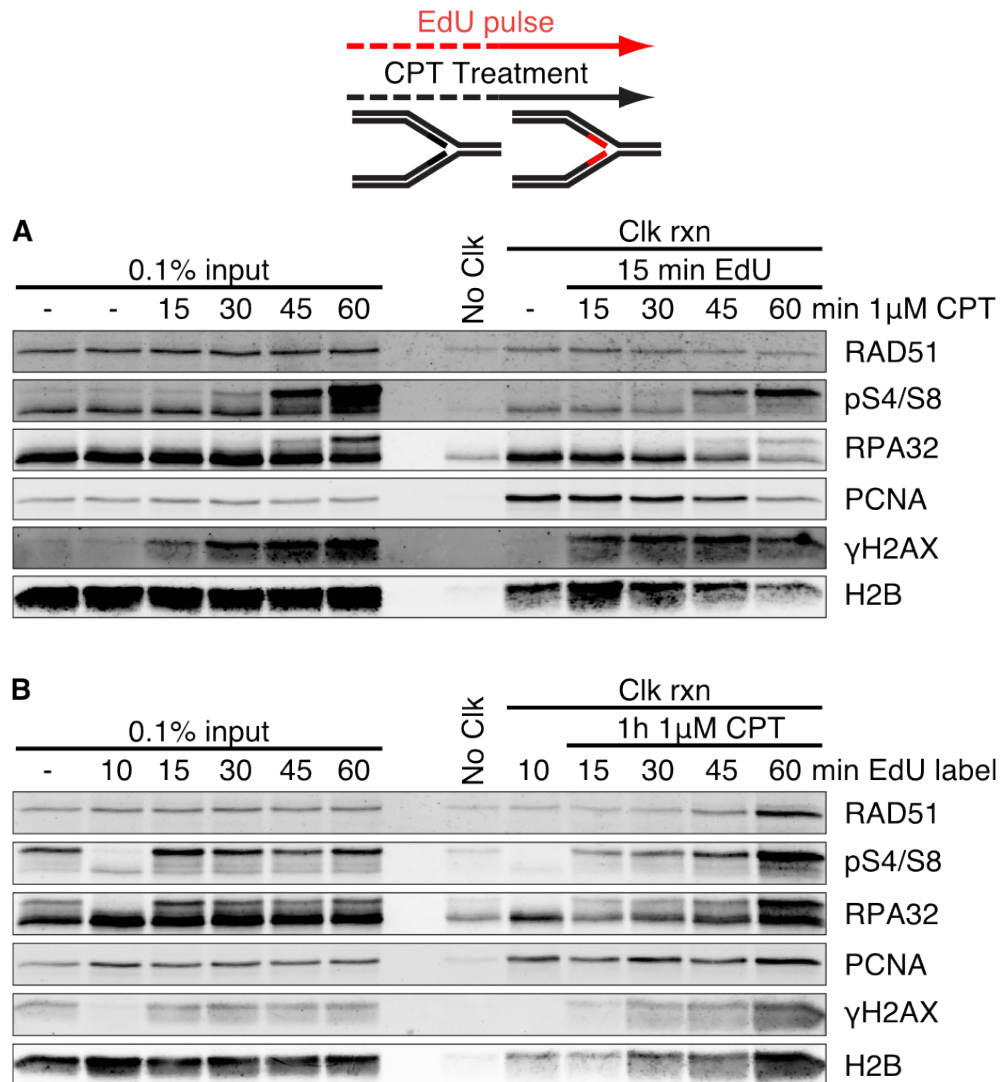


Figure 3.8 Protein dynamics at CPT-damaged replication forks. (A) Cells were treated with 1 μM CPT for indicated times and labeled with EdU for the final 15 minutes of CPT treatment prior to performing iPOND. (B) Cells were treated with 1 μM CPT for 1 h and labeled with EdU for the indicated times at the end of CPT treatment prior to performing iPOND.

treated cells. However, we detect only a modest increase in PCNA, suggesting that the number of new replication forks labeled is low, consistent with a checkpoint response. Similarly to HU treated, ATR inhibited cells, we detect a marked increase in RPA32 and RAD51 indicative of ssDNA on the newly synthesized DNA strand. Furthermore, the RPA32 purified is largely phosphorylated on S4/S8 (Fig. 3.8B). Taken together, these suggest that, consistent with previous reports, CPT generates DSBs at replication forks, and iPOND can detect the changes in protein recruitment and PTMs that occur at these forks.

Discussion

Here, we described the first investigation into the DNA damage response using the iPOND methodology. The advantage of iPOND over similar previous methods, such as CldU immunoprecipitation, is increased resolution and background. Compared to iPOND, which can detect replication fork proteins with only 2.5 minutes of EdU labeling, the CldU immunoprecipitation method used a 40 minute labeling time (Petermann et al. 2010). Furthermore, iPOND is compatible with stringent wash conditions such as 1M NaCl and 1% SDS and does not require a denaturation step to expose an antibody epitope.

Using iPOND, we monitored chromatin maturation by following removal of the deposition marks H4K5ac and H4K12ac. Consistent with previous reports, H4K5ac and H4K12ac were deacetylated at different rates. Furthermore, we demonstrated that the difference in deacetylation rates was entirely due to reacylation of H4K12 using the nonspecific HAT inhibitor anacardic acid (Fig. 3.2). Our analysis provides higher spatial and temporal resolution than previous methods and begins to elucidate the chromatin changes that occur as chromatin is reassembled behind replication forks. We developed the native iPOND methodology to enable future studies of chromatin PTMs (Fig. 3.3).

iPOND is also more sensitive than previous methods of studying replication-associated proteins. Previous studies largely relied on immunofluorescent (IF) imaging to track protein localization. While useful, immunofluorescence has the significant disadvantages of low resolution and low sensitivity. For example, proteins that exist at only single copy levels at replication forks cannot be tracked with IF. In contrast, iPOND technology has dramatically improved sensitivity, allowing us to detect even proteins such as polymerases. Furthermore, combining iPOND with pulse-chase methods provides high spatial and temporal resolution of protein dynamics. Finally, iPOND also facilitates analysis of post-translational modifications, which is often impossible with IF due to poor antibody quality or specificity.

We are able to detect molecules expected to be present at only one or two copies per fork, such as polymerase subunits, using iPOND (Fig 3.4). In lower organisms, some DNA damaging agents cause dissociation of replisome components (Cobb et al. 2003; Trenz et al. 2006). Therefore, we tested whether extended treatment with HU caused replisome disassembly in mammalian cells. Our results indicate that this does not occur in response to HU; however, whether other damaging agents cause disassembly and whether ATR regulates this process remain open questions.

iPOND is an ensemble methodology, thus while it does not provide information about any single replication fork, iPOND provides an average picture of events in different cells at stalled forks throughout the genome in a population of cells. Using iPOND, we detected several DDR proteins including KU80 and MRE11 prior to addition of any exogenous damaging agents (Fig 3.5A). The idea that KU80 travels with the replication fork is not without precedent (Shao et al. 1999), and several groups have recently suggested a function for the MRN complex in ATR activation at stalled replication forks (Duursma et al. 2013; Kobayashi et al. 2013; Lee and Dunphy 2013).

The interplay between RAD51 and MRE11 at stalled replication forks has seen several recent developments. The Costanzo group demonstrated that in *S. cerevisiae*, depletion or inhibition of RAD51 leads to increased ssDNA gaps behind the replication fork in an MRE11-dependent process (Hashimoto et al. 2010). Furthermore, the Jasin group found that in the absence of BRCA2/RAD51, the newly synthesized DNA strands shorten during HU treatment in an MRE11-dependent manner. This suggests that at persistently stalled replication forks, MRE11 performs limited resection that allows BRCA2-RAD51 loading. In the absence of BRCA2 or RAD51, MRE11 resection continues unimpeded and produces detectable shortening of DNA fibers using fiber labeling (Schlacher et al. 2011).

Interestingly, we observed a shift in the DDR between 2 and 4 hours of HU treatment. This occurs well before evidence of DSB formation, which requires in excess of 12 hours of treatment (Petermann et al. 2010). While we cannot exclude the possibility that DSB detection methods lack sufficient sensitivity to detect breaks at these times, another possibility is that fork regression occurs to form a Holliday junction-like structure. To distinguish between these possibilities would require direct evidence of fork regression in response to HU and identification of the enzymatic requirements, such as SMARCAL1 activity. Replication stress caused by camptothecin treatment or oncogene overexpression can induce this structure in mammalian cells (Neelsen et al. 2013; Ray Chaudhuri et al. 2012). The extruded nascent strand duplex resembles a DSB end and may recruit typical DSB proteins such as KU70/80, MRE11, and RAD51. RAD51 assembly at persistently stalled forks depends on MRE11 activity, suggesting a requirement for end-resection (Fig. 3.5B). This end-resection is likely either on the template DNA strand of a DSB or limited to the extruded arms of a regressed fork, since we continued to capture EdU-labeled DNA and associated proteins. In either case,

resection would yield a 3' overhang of newly synthesized DNA, which could be used in recombination-based methods of fork repair and restart (Petermann and Helleday 2010).

Prominent changes in the response to replication stress include protein phosphorylation. Importantly, our data indicate that H2AX phosphorylation spreads to a large chromatin domain early in the response to fork stalling. This early phosphorylation is catalyzed by ATR and is unlikely to be due to the processing of the fork into a double-strand break intermediate. Our data is consistent with previous analyses implicating both ATR-dependent (Ward and Chen 2001) and –independent (Brown and Baltimore 2003; Gilad et al. 2010) H2AX phosphorylating activities in response to fork arrest. Most models of ATR function suggest it is only active when bound to the single-stranded DNA at the stalled fork through an ATRIP-RPA interaction (Cimprich and Cortez 2008), but our data indicate that ATR helps spread the γ H2AX signal. One possibility is that the early spreading of γ H2AX is due to looping of the newly synthesized chromatin that brings it into proximity of ATR. Alternatively, ATR may have a method of spreading its signal beyond the immediate single-stranded DNA vicinity similar to the ability of active ATM to spread along the double-stranded DNA away from the DSB end (You et al. 2007). MDC1 may be involved in such a process (Ichijima et al. 2011; Wang et al. 2011).

iPOND is also useful for studies of protein dynamics at replication forks damaged with other agents. We demonstrated that iPOND can detect accumulation of RPA, RAD51, and γ H2AX at CPT-damaged replication forks. We also detect RPA32 phosphorylated on S4/S8, indicative of DSB formation and DNA-PK activation. Using iPOND, we conducted a high resolution, temporal analysis of protein dynamics at replication forks in mammalian cells. These analyses provide us with a molecular picture of how replication stress response proteins accumulate at stalled replication forks and some indications as to the function of ATR in this process.

CHAPTER IV

ATR PHOSPHORYLATES SMARCAL1 TO PREVENT REPLICATION FORK COLLAPSE†

Introduction

Every cell division cycle, cells must accurately and completely replicate their genome. Errors in replication result in mutations and chromosomal rearrangements that contribute to tumorigenesis. Replication stress caused by DNA lesions, insufficient nucleotides, or even collisions of replication and transcriptional machineries increases the chance of errors. However, replication stress also activates a DNA damage response (DDR) that slows cell cycle progression and promotes DNA repair to ensure accurate duplication of the genome.

The DDR kinase Ataxia-telangiectasia and Rad3-related (ATR), a member of the phosphoinositol 3-kinase-like kinase (PIKK) family, coordinates much of the cellular response to replication stress (Cimprich and Cortez 2008; Nam and Cortez 2011). ATR is activated upon replication fork stalling and uncoupling of the replicative helicase and polymerase (Byun et al. 2005). Once activated, ATR phosphorylates hundreds of substrates to induce the replication checkpoint and promote fork repair.

ATR is essential for cell viability, and hypomorphic ATR mutations cause the rare disease Seckel syndrome characterized by growth retardation, microcephaly and other developmental problems (O'Driscoll et al. 2003). ATR is thought to be a good drug target for cancer therapy because its function is especially critical in replicating tumor cells, which have elevated levels of replication stress due to activated oncogenes and frequent loss of the G1 checkpoint (Reaper et al. 2011; Schoppy et al. 2012; Toledo et al. 2011b).

† This chapter was published in (Couch et al. 2013).

The mechanism by which ATR selective inhibitors kill cells is unknown but is likely linked to the replication fork stabilization and repair activities of ATR instead of its G2 checkpoint function (Nam et al. 2011b; Toledo et al. 2011a). Defining these mechanisms is important for the development of ATR pathway inhibitors for cancer treatment.

Replication fork repair is a complex process that can proceed through multiple pathways depending on the cause, persistence, and genomic context of the replication stress. These mechanisms include fork stabilization to allow completion of replication by a converging replication fork, lesion bypass, template-switching through recombination or fork reversal, and double-strand break (DSB)-mediated restart (Branzei and Foiani 2010). Many enzymes participate in these activities including helicases, DNA translocases, nucleases, and specialized polymerases. ATR can phosphorylate many of these enzymes; however, the mechanisms by which it promotes fork stabilization, repair, and cell viability remain largely unknown.

One ATR substrate that acts at stalled forks is SMARCAL1 (also known as HARP) (Bansbach et al. 2009; Postow et al. 2009). SMARCAL1 binds branched DNA structures and can catalyze DNA annealing, branch migration, fork regression, and fork restoration (Bétous et al. 2012, 2013; Ciccia et al. 2012; Yusufzai and Kadonaga 2008). SMARCAL1 is recruited to stalled forks through an interaction with replication protein A (RPA) (Bansbach et al. 2009; Ciccia et al. 2009; Yuan et al. 2009; Yusufzai et al. 2009), which directs it to regress stalled forks with a leading strand gap and restore a normal fork structure (Bétous et al. 2013). Both overexpression and siRNA-silencing of SMARCAL1 cause replication-associated DNA damage (Bansbach et al. 2009). Furthermore, loss of function mutations in SMARCAL1 cause the human disease Schimke immunosseous dysplasia that is characterized by growth defects, renal failure, immune deficiencies and predisposition to cancer (Baradaran-Heravi et al. 2012; Boerkoel et al. 2002; Carroll et al. 2013). How ATR phosphorylation of SMARCAL1

regulates its genome maintenance functions at a damaged fork has not been investigated.

Using a selective ATR inhibitor, we demonstrate that acute inhibition of ATR kinase activity perturbs the timing of replication initiation, impairs fork elongation rates, and causes rapid lethality in S-phase cells experiencing replication stress. Stalled forks collapse when ATR is inhibited due to SLX4-dependent endonuclease cleavage, which yields DSBs and the CtIP-dependent appearance of single-stranded template and nascent DNA strands. Excessive SMARCAL1 activity is partly responsible for this aberrant fork processing. ATR phosphorylation of a conserved SMARCAL1 serine regulates SMARCAL1 and is one mechanism by which ATR maintains genome integrity during DNA replication. Thus, our results provide a mechanistic description of fork collapse in mammalian cells and define a specific enzymatic pathway responsible for this collapse. They also explain why both too much and too little SMARCAL1 causes replication-associated DNA damage emphasizing the need to properly regulate this replication fork repair enzyme. Finally, these data provide insights into the mechanism of action of ATR inhibitors which are being developed to treat cancers with high levels of dependency on this replication-stress response pathway.

Results

Acute ATR inhibition causes rapid cell death in cells experiencing replication stress

Conditional deletion of ATR in dividing mouse or human cells causes cell death as the mRNA and protein levels decay over time (Brown and Baltimore 2000; Cortez et al. 2001; de Klein et al. 2000). The gradual nature of these genetic loss-of-function experiments precludes an analysis of the immediate effects of ATR deficiency. To overcome this technical challenge, we utilized a selective ATR kinase inhibitor to

examine how cells respond to acute and transient ATR inhibition. In this analysis, 39% of asynchronous cultured U2OS cells were no longer able to form colonies after a 10-hour treatment with a concentration of ATR inhibitor sufficient to block phosphorylation of CHK1, and 71% of cells were inviable after 20 hours of treatment (Fig. 4.1A).

Acute treatment with the combination of ATRi and replication stress induced by the ribonucleotide reductase inhibitor hydroxyurea (HU) caused a greater reduction in viability than either drug alone (Fig. 4.1A-B). Notably, 5 hours of treatment with HU and ATRi caused a 55% reduction in viability. This percentage corresponds approximately to the proportion of cells in S-phase at the onset of treatment plus the cells that enter S-phase during the 5-hour treatment. ATR inhibition is synergistic with HU: at the 20-hour time point, the combination of HU+ATRi gave an experimental response (99% decrease in viability) greater than the additive effect predicted from HU alone and ATRi alone (89%).

To determine how rapidly the cell lethality occurs, we treated U2OS cells with or without HU and ATRi for up to 5 hours. While HU alone or ATRi alone had only modest effects at earlier time points, the combination of HU and ATRi caused a 30% decrease in colony forming ability within 45 minutes of treatment (Fig. 4.1C-D). Since HU treatment is expected to affect primarily S-phase cells, we tested whether these cells could recover from this treatment and complete DNA replication. By flow cytometry, at least 20% of cells treated with HU and ATR inhibitor for 5 hours failed to complete DNA synthesis 24 hours after release into fresh growth media compared to only 7% of controls (Fig. 4.2A). After a 16 hour HU treatment, this fraction of lagging cells increased to at least 65% of ATR inhibited cells compared to only 15% of controls (Fig. 4.2B). Thus, ATR is required during an acute replication stress challenge to ensure that cells can recover, complete DNA synthesis, and retain long-term viability.

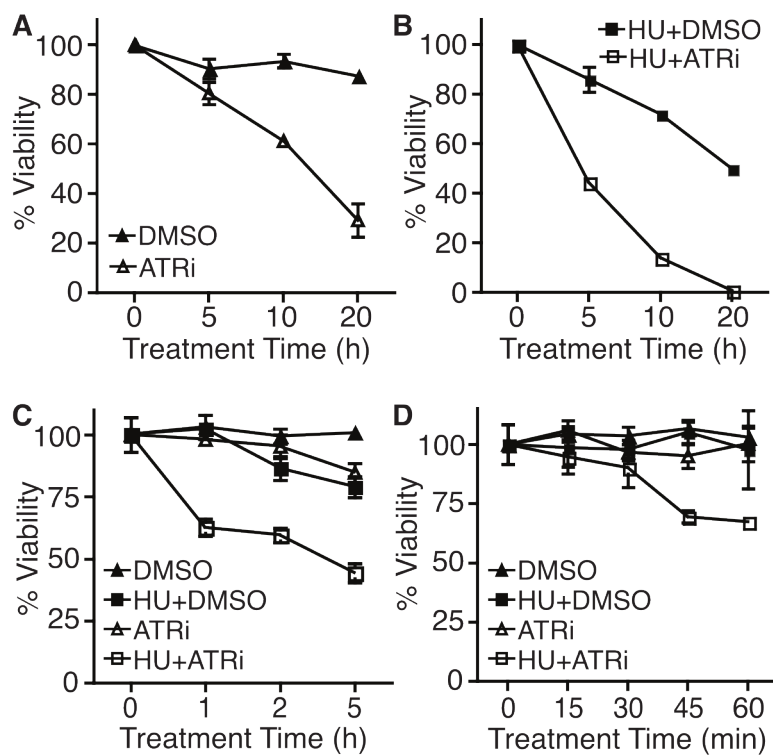


Figure 4.1 Acute ATR inhibition causes rapid cell lethality. (A-D) U2OS cells were treated with DMSO, 5 μ M ATRi, and/or 3mM HU for the indicated times and released into fresh growth media for 10-14 days. Colonies were visualized by methylene blue staining. Results shown are mean \pm standard error of the mean (SEM) of at least two independent experiments.

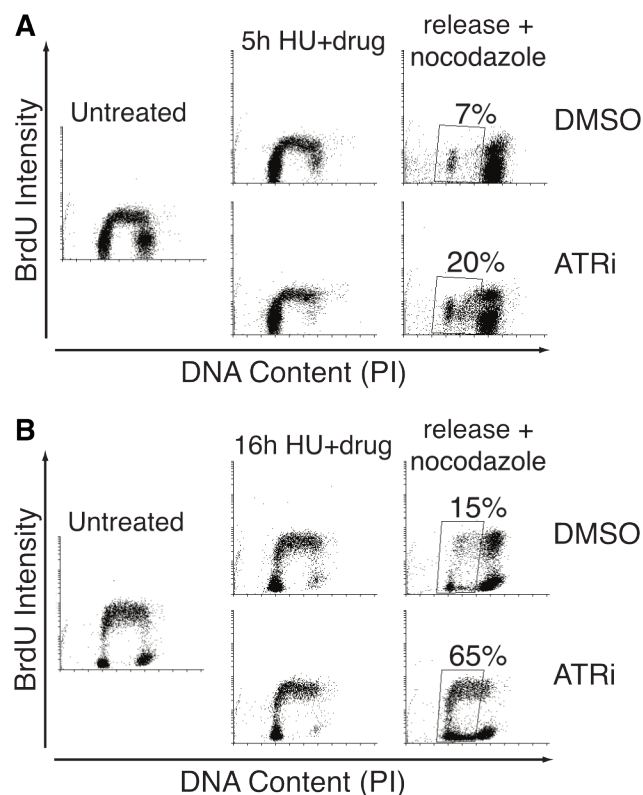


Figure 4.2 Acute ATR inhibition causes an inability to complete DNA replication after a replication stress challenge. RPE-hTERT cells were labeled with 20 μ M BrdU for 20 minutes, treated with 3mM HU for 5 (A) or 16 (B) hours in the presence or absence of 5 μ M ATRi, and then released into fresh growth media containing 1 μ g/ml nocodazole for 24 hours prior to harvesting. Cells were then fixed, acid denatured, stained with BrdU antibodies and propidium iodide, and analyzed by flow cytometry. Plots were made using Cyflogic software.

ATR inhibition deregulates replication timing control and causes replication fork collapse

To understand the cause of the rapid lethality when ATR is inhibited, we utilized fiber labeling to examine DNA replication. Cells were labeled with IdU (green) for 20 minutes then CldU (red) for 20 minutes in the presence or absence of ATRi during both labeling periods. ATR inhibition caused the CldU fiber length to decrease to approximately half the length of controls, which indicates slower replication fork elongation (Fig. 4.3A). CHK1 inhibition causes a similar slowing of fork elongation, which was attributed to deregulation of origin firing (Seiler et al. 2007). This also appears to be the case after ATR inhibition since we observed a large increase in the number of origins in the ATRi sample compared to controls (Fig. 4.3B).

Recovery of DNA synthesis after transient replication block is also dependent on ATR function. We labeled cells with IdU, blocked replication with high concentrations of HU in the presence or absence of ATRi, then removed the drugs and labeled with CldU. The CldU-labeled replication tracks were significantly shorter in the ATR inhibited condition compared to controls (Fig. 4.3C). Furthermore, ATR inhibition causes a large increase in the number of forks that cannot restart and collapse entirely during the HU-treatment with no CldU incorporation after release (Fig. 4.3D). Origins were also de-repressed under these conditions (Fig. 4.3E).

Similar experiments in cells lacking BRCA2 function found that the IdU-labeled tracks synthesized prior to HU addition undergo shortening, which indicates degradation of the newly synthesized DNA strands after fork stalling (Schlacher et al. 2011). We did not observe this phenotype in the ATRi samples indicating that ATR is not required in this BRCA2-RAD51-dependent fork protection pathway (Fig. 4.3F).

To examine what is happening to the stalled forks when ATR is inhibited, we first examined the levels of DNA damage in ATRi-treated cells. H2AX phosphorylation (γ H2AX) provides an indirect marker for DNA damage since it is phosphorylated at

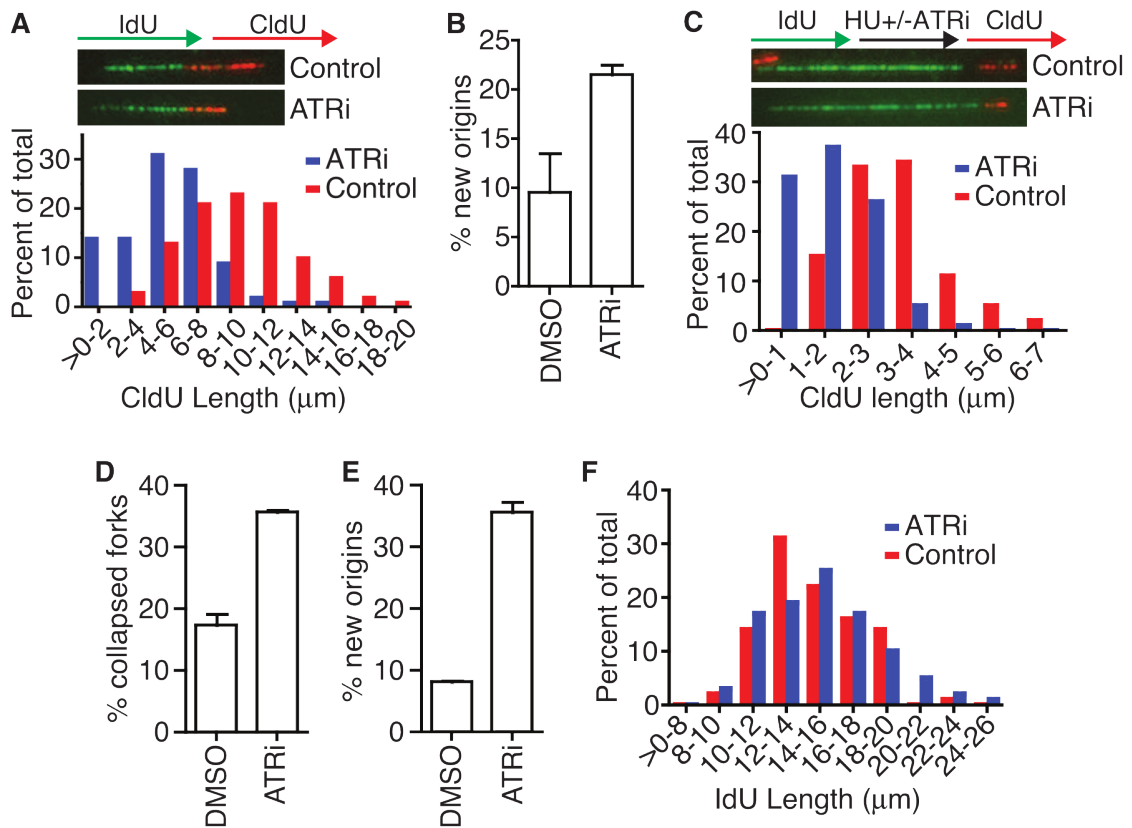


Figure 4.3 ATR regulates DNA replication initiation and elongation. (A and B) RPE-hTERT cells were labeled with IdU for 20 minutes then with CldU for 20 minutes in the presence of DMSO (red bars) or 5μM ATRi (blue bars) during both labeling periods before harvesting for fiber labeling. (A) Representative replication tracks and quantification of the length of CldU (red) tracks in dual-labeled tracks are shown. (B) Origin initiation was scored as the percentage of red-only tracks. (C-F) RPE-hTERT cells were labeled with IdU for 20 minutes, treated with 2mM HU for 2 hours in the presence of DMSO (red bars) or 5μM ATRi (blue bars), then labeled with CldU for 20 minutes before harvesting for fiber staining. Representative images and quantification of CldU (C) and IdU (F) track lengths in dual-labeled fibers are shown. (D) Percentage of collapsed forks (green-only tracks) and (E) newly initiated origins (red-only tracks) were quantitated. In all experiments data was collected from several experimental samples with high quality DNA fibers. Error bars are SEM. Data were produced by Jessica Luzwick.

stalled forks and at DSBs. As expected, HU treatment alone causes low but detectable levels of γ H2AX, which increase over time (Fig. 4.4A-B). In the presence of ATRi, γ H2AX is absent at the earliest time points of HU treatment indicating that ATR is required to phosphorylate H2AX near stalled replication forks consistent with previous observations (Sirbu et al. 2011). However, by 1 hour in HU the γ H2AX in ATR inhibited cells exceeds that in controls. At this time point a few cells display large, poorly defined γ H2AX foci but most contain a pan-nuclear staining pattern without discernable foci suggesting rapid spreading through the chromatin. These data suggest the activation of the DSB-sensing kinases ATM and DNA-PKcs between 30 and 60 minutes of HU treatment when ATR is inhibited. Indeed, we detected elevated RPA32 S4/S8 phosphorylation (a DNA-PK-dependent phosphorylation site), and CHK2 T68 phosphorylation (an ATM-dependent phosphorylation site) in ATR inhibited cells compared to controls with similar kinetics to γ H2AX (Fig. 4.4C). Thus, a DSB may form at the stalled fork generating the ATM and DNA-PKcs activating signal.

To provide direct evidence of DSB formation, we utilized a neutral COMET assay. The combination of HU and ATRi treatment caused an increase in COMET tail moment compared to controls similar to what is caused by high-dose camptothecin treatment (Fig. 4.4D) confirming DSB formation and replication fork collapse in ATR inhibited cells.

ATR inhibition causes nascent-strand ssDNA formation

To confirm that the γ H2AX and RPA32 hyper-phosphorylation that happens in cells treated with HU and the ATRi occur at replication forks, we utilized iPOND (Sirbu et al. 2011, 2012). iPOND uses click chemistry to conjugate biotin to a nucleoside analog (EdU) incorporated in newly synthesized DNA thereby permitting a single-step purification of proteins near the replication fork. As expected, the γ H2AX is associated with the newly synthesized DNA strands (Fig. 4.5A). Additionally, we observed a striking

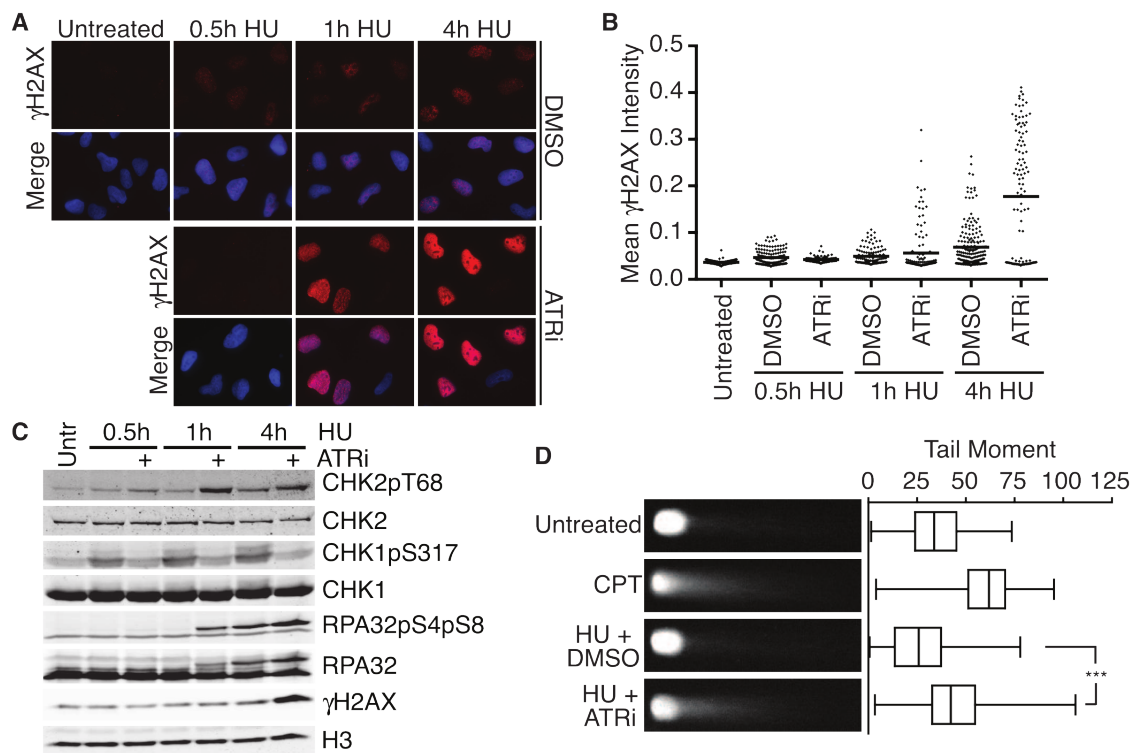


Figure 4.4 Stalled replication forks collapse into double strand breaks when ATR is acutely inhibited. (A and B) U2OS cells were treated with 3mM HU in the presence or absence of 5 μ M ATRi for the indicated times before preparation for immunofluorescence using anti- γ H2AX antibodies. Dot-plot of mean γ H2AX intensity per nucleus is shown in (B). (C) U2OS cells were treated with 3mM HU in the presence or absence of 5 μ M ATRi for the indicated times. Following treatment, cell lysates were separated by SDS-PAGE then immunoblotted to detect the indicated proteins and phosphorylation levels. (D) U2OS cells were treated for 1h with 1 μ M CPT or 4h with 3mM HU in the presence or absence of 5 μ M ATRi. Neutral COMET assay was performed and at least 100 individual cells were scored for tail moment using CometScore software. Representative images and box-and-whisker plot are shown. Samples were compared with one-way ANOVA ($p < 0.0001$). Bonferroni's Multiple Comparison test was used as a follow up to compare untreated vs. CPT ($p < 0.0001$) and HU+DMSO vs. HU+ATRi ($p < 0.0001$).

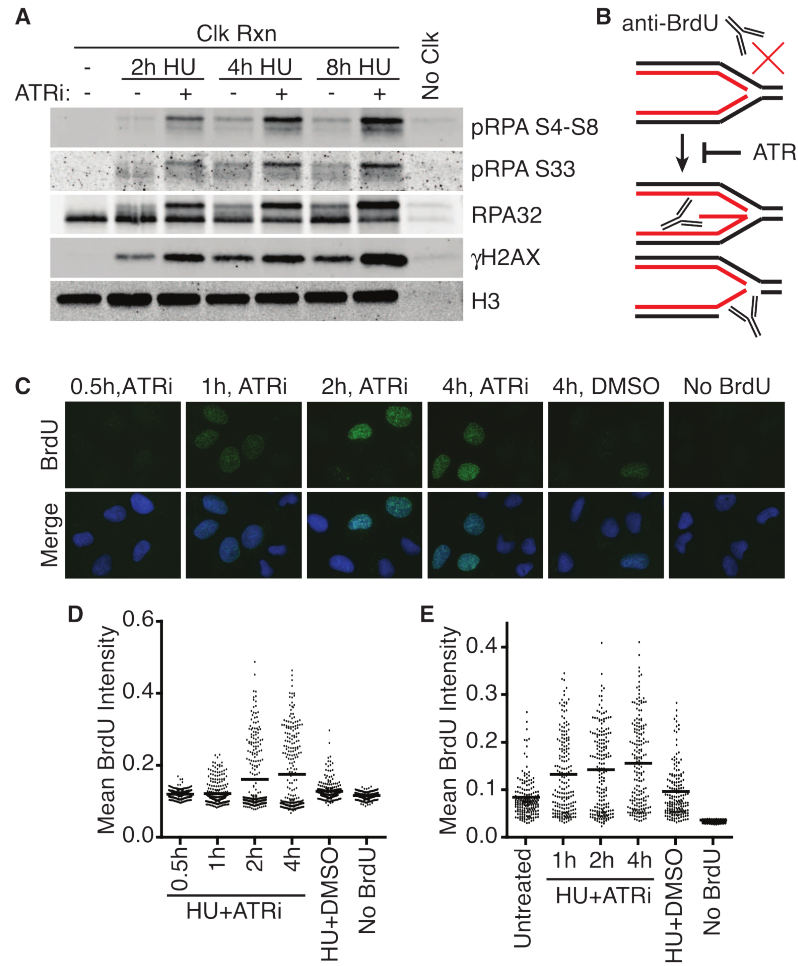


Figure 4.5 ATR inhibition causes both nascent and parental ssDNA accumulation at a stalled replication forks. (A) 293T cells were labeled with EdU for 10 minutes prior to addition of 3mM HU and 5 μ M ATRi as indicated. Samples were processed for iPOND and captured proteins were separated by SDS-PAGE then immunoblotted. (B) Model for nascent-strand ssDNA assay. Black and red lines indicate template and nascent DNA strands, respectively. Without DNA denaturation, BrdU antibodies will not recognize intact replication forks but will recognize the labeled, nascent DNA when single-stranded. (C and D) The newly synthesized DNA in replicating U2OS cells was labeled for 10 minutes with 10 μ M BrdU before addition of 3mM HU and 5 μ M ATRi as indicated. “No BrdU” sample is 4h HU+ATRi treatment without BrdU pre-labeling. “DMSO” samples were labeled with BrdU and treated with 3mM HU for 4h. After the indicated treatment times, cells were fixed and stained with antibodies against BrdU without DNA denaturation to selectively detect nascent-strand ssDNA. Representative images are shown in (C) and a dot-plot of mean BrdU intensity per nucleus is shown in (D). (E) Parental DNA in replicating U2OS cells was labeled by the addition of 10 μ M BrdU for 20 hours followed by a chase into normal growth media for 2 hours before addition of 3mM HU and 5 μ M ATRi for the indicated times. “DMSO” samples were labeled with BrdU and treated with 3mM HU for 4h. Cells were fixed and stained with antibodies against BrdU without DNA denaturation to selectively detect parental-strand ssDNA. Dot-plot of mean BrdU intensity per nucleus is shown. Data for panel A were produced by David Cortez and Frank B. Couch.

accumulation of hyperphosphorylated RPA purified with the nascent DNA when ATR is inhibited (Fig. 4.5A). Quantitative mass spectrometry following the iPOND purification also confirmed an increase in total RPA in the HU+ATRi conditions (B Sirbu and D Cortez, unpublished observation). iPOND only purifies RPA bound to or immediately adjacent to the EdU-labeled nascent strand and therefore does not detect an increase in RPA in cells treated with HU alone (Sirbu et al. 2011). Thus, the increased abundance of RPA in the iPOND samples may suggest that the EdU-labeled nascent strand becomes single-stranded and bound to RPA when ATR is inhibited.

To directly test whether the nascent strand becomes single-stranded at stalled forks in the absence of ATR activity, we developed an assay to selectively detect nascent-strand ssDNA using a short (10 minute) BrdU incubation immediately before stalling forks with HU. Under non-denaturing conditions, the BrdU antibody selectively recognizes ssDNA (Fig. 4.5B). Treatment with HU and DMSO vehicle resulted in little BrdU staining (Fig. 4.5C, see “4h, DMSO” image). Conversely, treatment with HU and ATR inhibitor resulted in robust BrdU staining, indicating that the nascent strand becomes ssDNA (Fig. 4.5C-D). The nascent-strand ssDNA became detectable after 1 hour of treatment and increased dramatically after 2 and 4 hours (Fig. 4.5C-D). The timing of nascent-strand ssDNA formation correlates with the cellular lethality and γ H2AX hyper-phosphorylation caused by ATR inhibition.

We also tested whether ATR inhibition caused the appearance of parental-strand ssDNA at the replication fork. After labeling overnight with BrdU, we released cells into fresh growth media for 2 hours before treating with HU with or without ATR inhibitor. As expected, some parental-strand ssDNA forms during HU treatment alone compared to untreated; however, much more parental-strand ssDNA forms in the ATR inhibited condition, indicating that ATR inhibition results in increased nascent- and parental-strand ssDNA (Fig. 4.5E). Thus, fork collapse when ATR is inactivated is characterized by

double-strand breaks and a large increase in ssDNA consisting of both the template and newly synthesized DNA strands.

ATR prevents SLX4- and CtIP-dependent formation of DSBs and nascent-strand ssDNA at stalled forks

We reasoned that the nascent-strand ssDNA could be generated from template-strand resection after DSB formation, branch migration of the stalled fork to yield a reversed fork structure with unequal length nascent DNA strands, or both (Fig. 4.5B). The MUS81 structure-specific endonuclease generates DSBs during persistent exposure to replication stress agents or in response to silencing or inhibition of replication fork repair proteins such as WRN, SMARCAL1, and CHK1 (Bétous et al. 2012; Forment et al. 2011; Franchitto et al. 2008; Hanada et al. 2007). Therefore, we tested whether siRNA depletion of MUS81 affects DSB formation in HU/ATRi treated cells. Surprisingly, MUS81-depleted cells showed no difference in γ H2AX or DSB formation compared to controls (data not shown and Fig. 4.6A). We also failed to observe a change in HU/ATRi-induced ssDNA formation with MUS81 knockdown or in MUS81-deficient HCT116 cells (Fig. 4.6B-C).

Multiple other structure-specific nucleases exist in mammalian cells. SLX4 is a molecular scaffold which functions as the structural subunit of the SLX4-SLX1 Holliday junction resolvase and coordinates the SLX1, XPF, and MUS81 nucleases (Fekairi et al. 2009; Svendsen et al. 2009). In contrast to MUS81, silencing SLX4 by siRNA largely abrogated DSB formation in HU+ATRi treated cells (Fig. 4.7A). Furthermore, SLX4 depletion also resulted in a large decrease in nascent-strand ssDNA formation (Fig. 4.7B-C). This result is not due to a change in the S-phase population (Fig. 4.7D). Furthermore, the response in the nascent-strand ssDNA assay correlates with SLX4 knockdown efficiency indicating it is not an off-target effect of the siRNA (Fig. 4.7E).

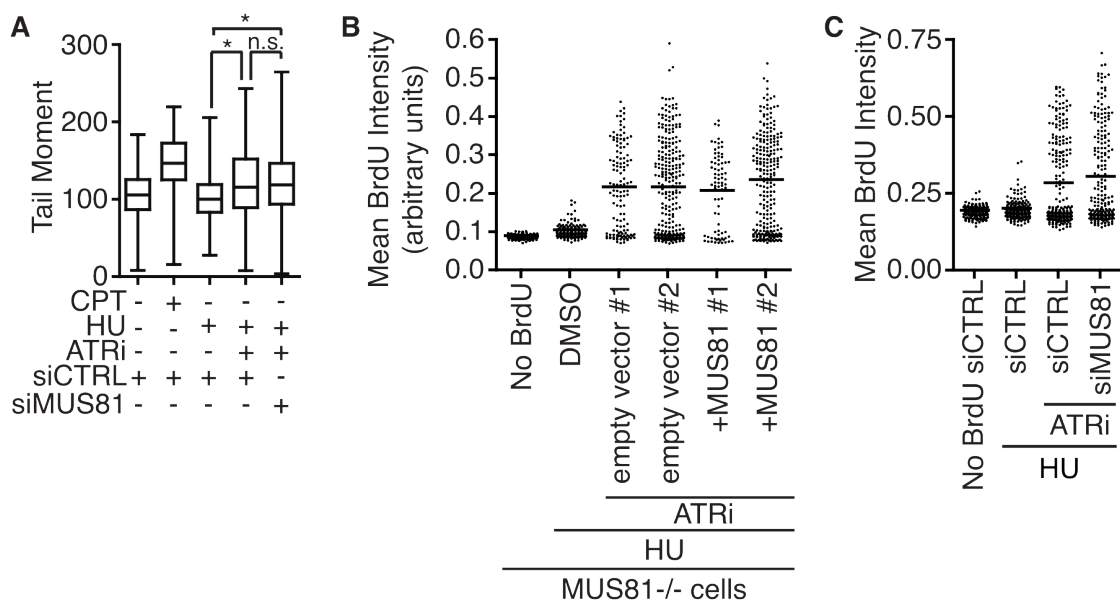


Figure 4.6 MUS81 is not required to generate DSBs or nascent-strand ssDNA after ATR inhibition. (A) U2OS cells were transfected with MUS81 or control siRNA prior to treatment for 1h with 1 μ M CPT or 4h with 3mM HU in the presence or absence of 5 μ M ATRi. A neutral COMET assay was performed. Samples were compared with one-way ANOVA ($p < 0.0001$). Bonferroni's Multiple Comparison test was used as a follow up to compare siCTRL HU+DMSO vs siCTRL HU+ATRi ($p < 0.0001$), siCTRL HU+DMSO vs siMUS81 HU+ATRi ($p < 0.0001$), and siCTRL HU+ATRi vs siMUS81 HU+ATRi ($p > 0.05$). (B) Two independent clones of MUS81^{-/-} cells containing either an empty vector or expressing a MUS81 cDNA were treated with HU and the ATRi as indicated. The cells were then labeled with 10 μ M BrdU for 20 minutes and stained with BrdU antibodies in non-denaturing conditions to visualize ssDNA. There is no significant difference among any of the ATRi-treated samples. (C) U2OS cells were transfected with control or MUS81-targeting siRNA. Transfected cells were labeled with 10 μ M BrdU for 10 minutes before addition of 3mM HU and 5 μ M ATRi for 4 hours. Samples were then processed to quantitate nascent-strand ssDNA. Representative dot-plot of mean BrdU intensity per nucleus is shown.

Silencing SLX1, XPF, MUS81, or the GEN1 nuclease individually had no consistent effect on nascent-strand ssDNA formation (Figs. 4.6C and 4.8). Thus it is likely that multiple SLX4-coordinated nucleases function redundantly to process HU stalled replication forks when ATR is inhibited.

Once the fork is cleaved, ssDNA could be generated by DNA end-resection. CtIP promotes resection at DSBs through multiple exonucleases (Paull 2010). Silencing CtIP significantly reduced the amount of nascent-strand ssDNA with 3 of 4 siRNAs, and the fourth siRNA decreased nascent-strand ssDNA in all experiments but did not reach statistical significance (Fig. 4.9A-B). CtIP protein levels decreased to nearly undetectable levels with all four siRNAs, and the change in nascent-strand ssDNA intensity is not due to a change in the S-phase population of these cells (Fig. 4.9C-D). These results suggest that at least some of the ssDNA that accumulates at stalled forks when ATR function is inhibited is generated by end-resection. Knockdown of individual exonucleases including EXO1 and DNA2 alone did not result in any change in nascent-strand ssDNA consistent with redundancy in end-resection mechanisms (Fig. 4.10).

Nascent-strand ssDNA formation involves replication fork remodeling

We next asked whether any fork processing steps occur upstream of SLX4-dependent cleavage. Specifically, we hypothesized that fork remodeling enzymes may be needed to generate a reversed replication fork structure that looks like a Holliday junction (or “chicken foot”), which is a preferred substrate for SLX4-dependent endonucleases. Therefore, we tested whether nascent-strand ssDNA formation depends on enzymes known to catalyze replication fork regression. SMARCAL1 is a DNA translocase that can anneal DNA strands and perform replication fork regression at stalled forks with leading strand gaps (Bétous et al. 2012, 2013). Silencing SMARCAL1

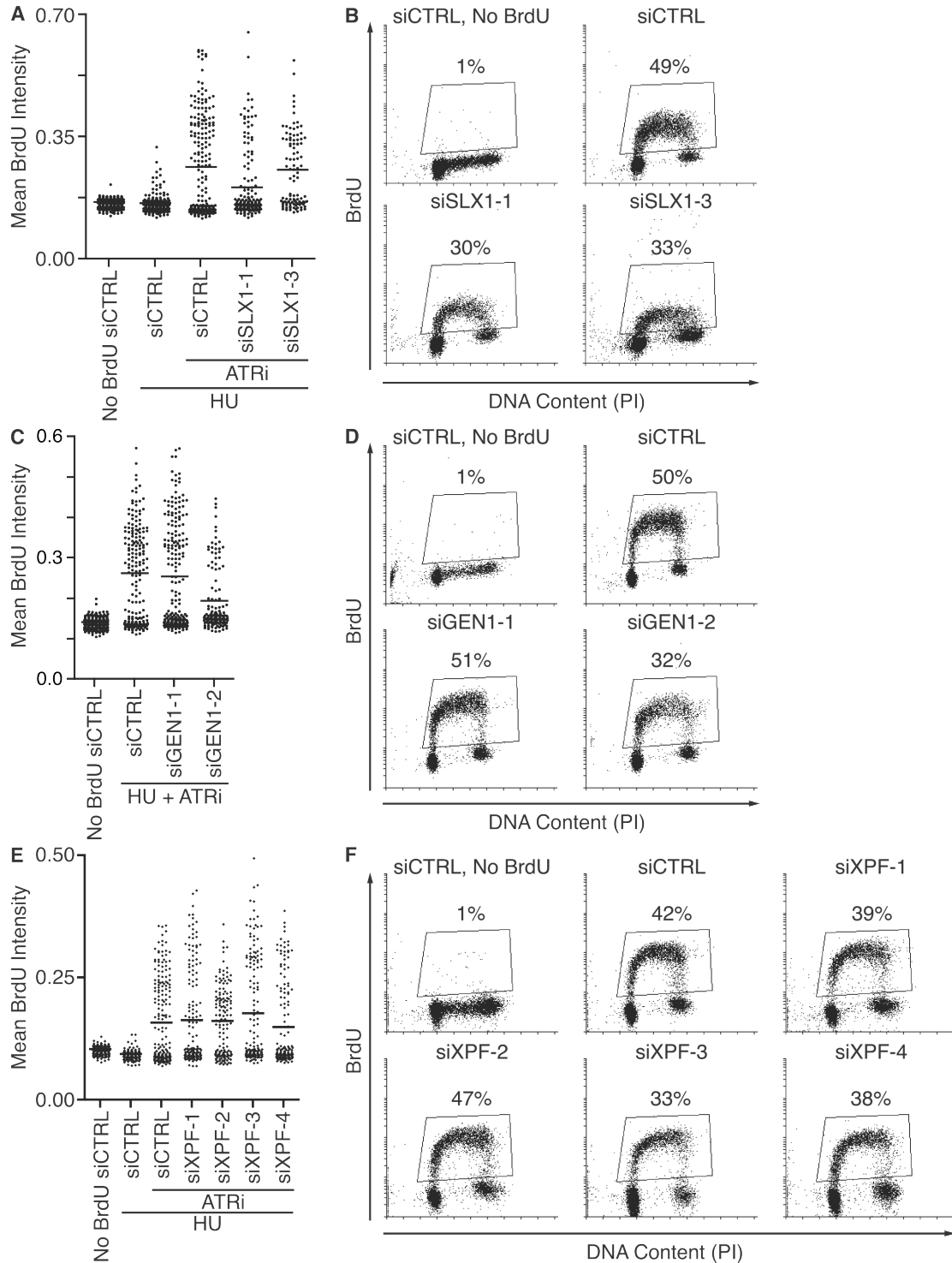


Figure 4.8 SLX1, GEN1, XPF are not required for nascent-strand ssDNA. U2OS cells were transfected with control or siRNA targeting SLX1, GEN1, or XPF. (A, C, E) Transfected cells were labeled with 10 μ M BrdU for 10 minutes before addition of 3mM HU and 5 μ M ATRi for 4 hours to measure nascent-strand ssDNA or (B, D, F) labeled with 10 μ M BrdU for 40 minutes to measure percentage of cells in S-phase. Any apparent decreases in nascent-strand ssDNA can be explained by cell cycle perturbations.

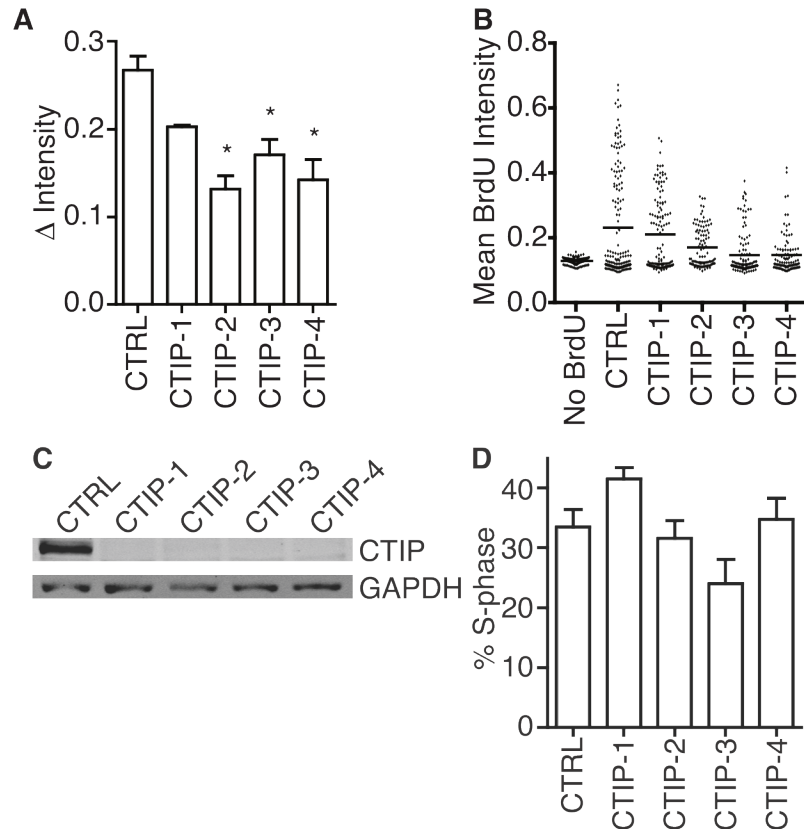


Figure 4.9 CtIP is required to generate nascent-strand ssDNA at stalled replication forks when ATR is inhibited. U2OS cells were transfected with non-targeting or CtIP siRNA. (A-B) Transfected cells were labeled with 10 μ M BrdU for 10 minutes before addition of 3mM HU and 5 μ M ATRi for 4 hours. Samples were then processed to detect nascent-strand ssDNA. (A) Quantitation of percent of nuclei containing nascent-strand ssDNA (mean \pm SEM of three experiments, * indicates $p < 0.05$). (B) Dot-plot of mean BrdU intensity per nucleus for a representative experiment is shown. (C) Transfected cells were harvested and lysed. Lysates were separated by SDS-PAGE and immunoblotted with antibodies to detect CtIP or GAPDH. (D) Transfected cells were labeled for 40 minutes with 10 μ M BrdU before harvesting for ethanol fixation, acid denaturation, and staining with BrdU antibodies and propidium iodide to measure the percentage of cells in S-phase. Values represent mean \pm SEM of four independent replicates.

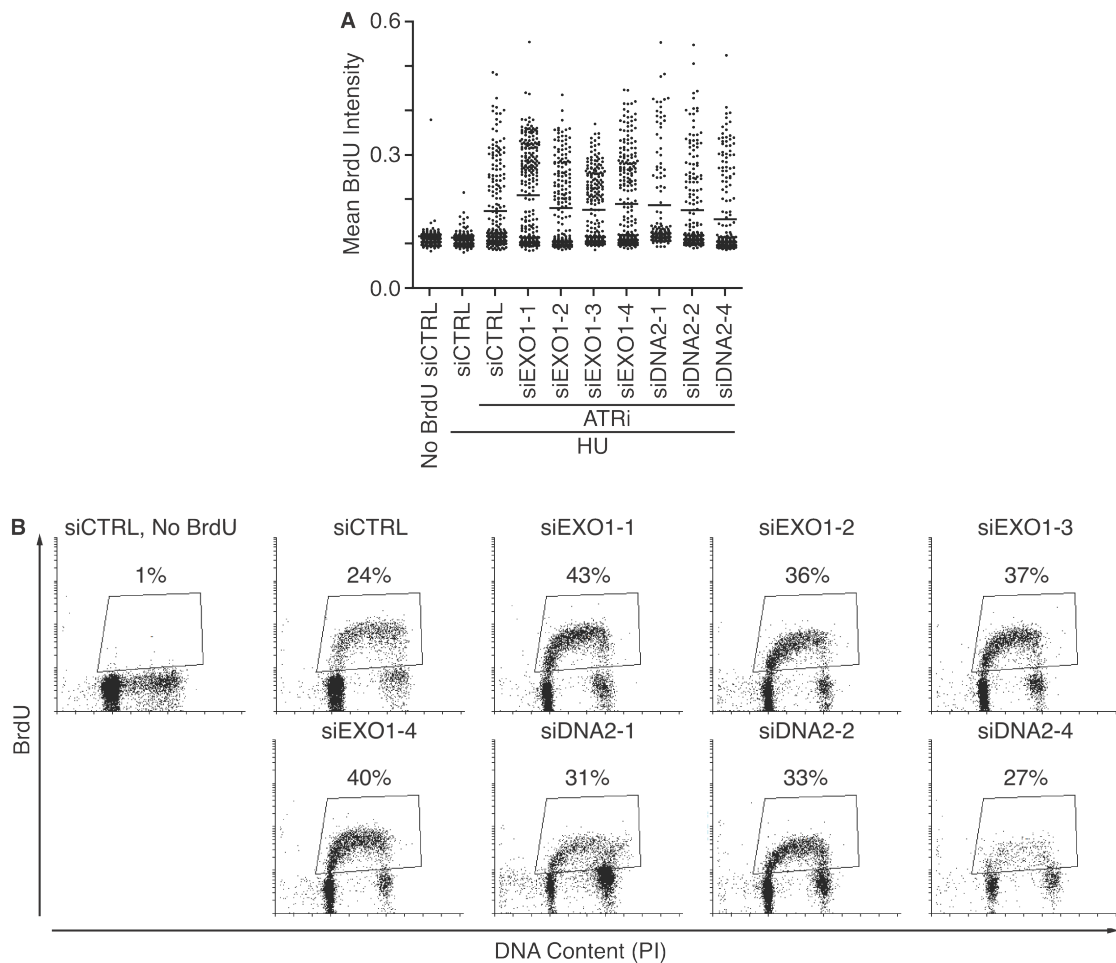


Figure 4.10 EXO1, DNA2 are not required for nascent-strand ssDNA. U2OS cells were transfected with control or siRNA targeting EXO1 or DNA2. (A) Transfected cells were labeled with 10 μ M BrdU for 10 minutes before addition of 3mM HU and 5 μ M ATRi for 4 hours to measure nascent-strand ssDNA or (B) labeled with 10 μ M BrdU for 40 minutes to measure percentage of cells in S-phase. Although DNA2-4 siRNA causes a decrease in nascent strand ssDNA (panel A), this correlates with a decrease in the S-phase population.

with four siRNAs decreases nascent-strand ssDNA positive cells compared to controls (Fig. 4.11). Silencing other enzymes capable of catalyzing fork regression including FANCM, HLTF, ZRANB3, and BLM did not decrease nascent-strand ssDNA (Figs. 4.12 and 4.13).

To further confirm the requirement of SMARCAL1 in the fork collapse associated with ATR inactivation, we examined whether a similar phenotype could be observed in the *Xenopus* cell-free replication system. In this system, replication of sperm chromatin in the presence of the DNA polymerase inhibitor aphidicolin causes ATR activation due to polymerase and helicase uncoupling (Byun et al. 2005). Pre-labeling the newly synthesized DNA strands with BrdU allowed us to observe the appearance of nascent-strand ssDNA either when camptothecin (CPT) was added to promote fork collapse or when ATR was inhibited in the presence of aphidicolin (Fig. 4.14A-C). Depleting xSMARCAL1 from the replicating extracts prevented the nascent-strand ssDNA generation only in the context of ATR inhibition with aphidicolin (Fig. 4.14A-C). xSMARCAL1 depletion had no effect on CPT-induced ssDNA or the activation of the ATR checkpoint (Fig. 4.14D). Thus, just as in mammalian cells, xSMARCAL1 is at least partially responsible for the aberrant replication fork processing in the *Xenopus* cell-free system when ATR is inactivated.

These data suggest that when ATR is not active, SMARCAL1 remodels stalled replication forks, and thereby provides a substrate for endonuclease cleavage and DNA end-resection. Silencing SMARCAL1 in the mammalian system only yielded a partial suppression of the ssDNA phenotype indicating other mechanisms may also be important.

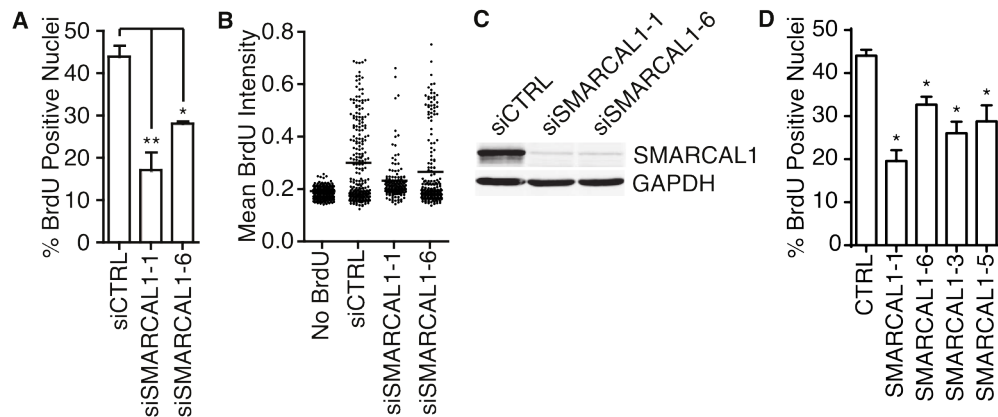


Figure 4.11 SMARCAL1 is required for the generation of nascent-strand ssDNA when ATR is inactivated in human cells. (A-B) U2OS cells were transfected with control or SMARCAL1 siRNA then labeled with 10 μ M BrdU for 10 minutes before addition of 3mM HU and 5 μ M ATRi for 4 hours. Samples were then processed to quantitate nascent-strand ssDNA. (A) Bars represent mean \pm SEM of percent BrdU positive cells across at least 5 experiments. (* $p < 0.005$, ** $p < 0.001$) (B) Representative dot-plots of mean BrdU intensity per nucleus. (C) U2OS cells transfected with control or SMARCAL1 siRNA were harvested and lysed. Lysates were separated by SDS-PAGE and immunoblotted with antibodies to detect SMARCAL1 or GAPDH. (D) Four siRNAs against SMARCAL1 were transfected into U2OS cells. Transfected cells were labeled with 10 μ M BrdU for 10 minutes before addition of 3mM HU and 5 μ M ATRi for 4 hours. Samples were then processed to quantitate nascent-strand ssDNA. Bars represent mean and SEM of 3 replicates. (* $p < 0.05$).

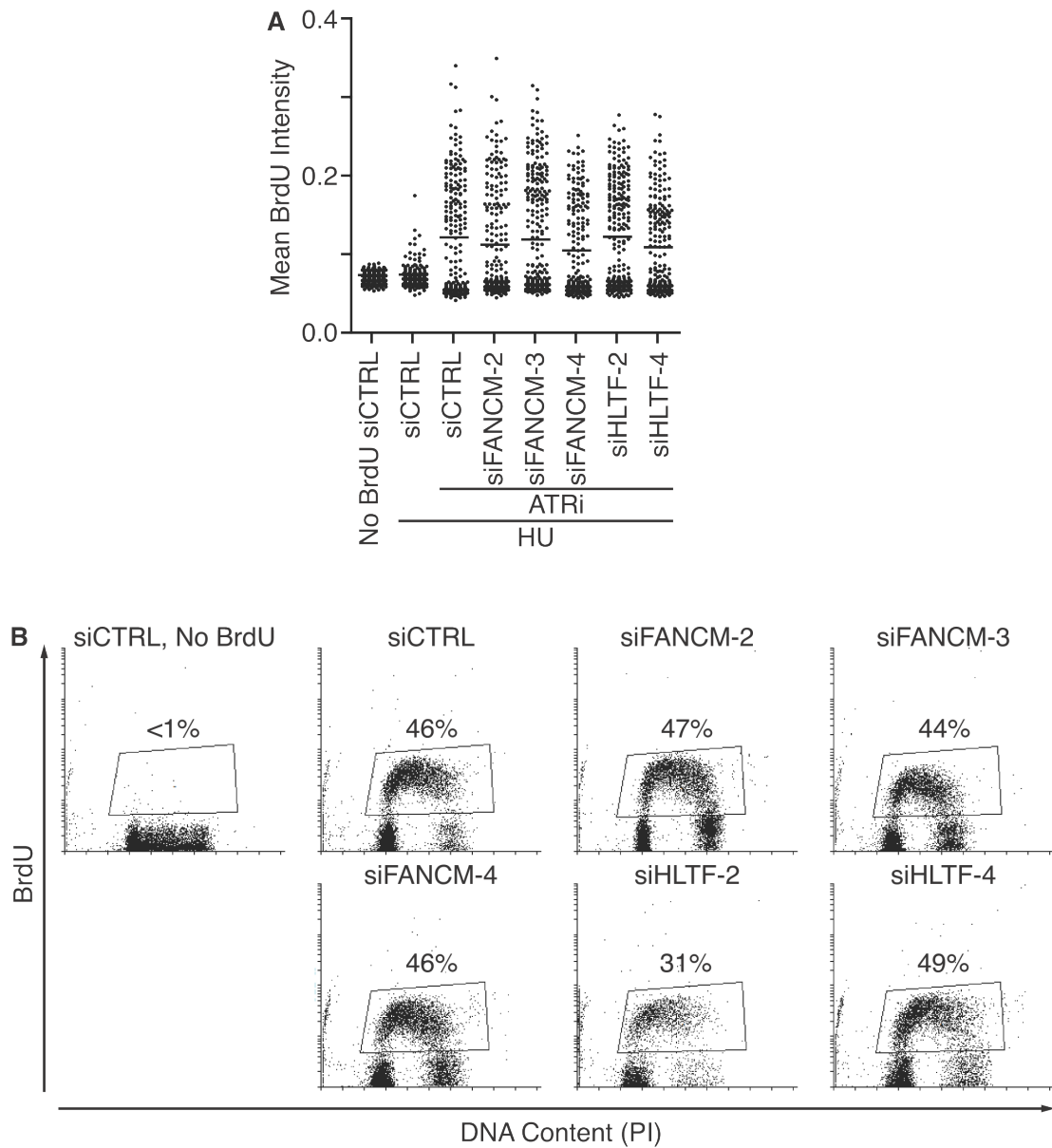


Figure 4.12 FANCM, HLTF are not required for nascent-strand ssDNA. U2OS cells were transfected with control or siRNA targeting FANCM or HLTF. (A) Transfected cells were labeled with 10 μ M BrdU for 10 minutes before addition of 3mM HU and 5 μ M ATRi for 4 hours to measure nascent-strand ssDNA or (B) labeled with 10 μ M BrdU for 40 minutes to measure percentage of cells in S-phase.

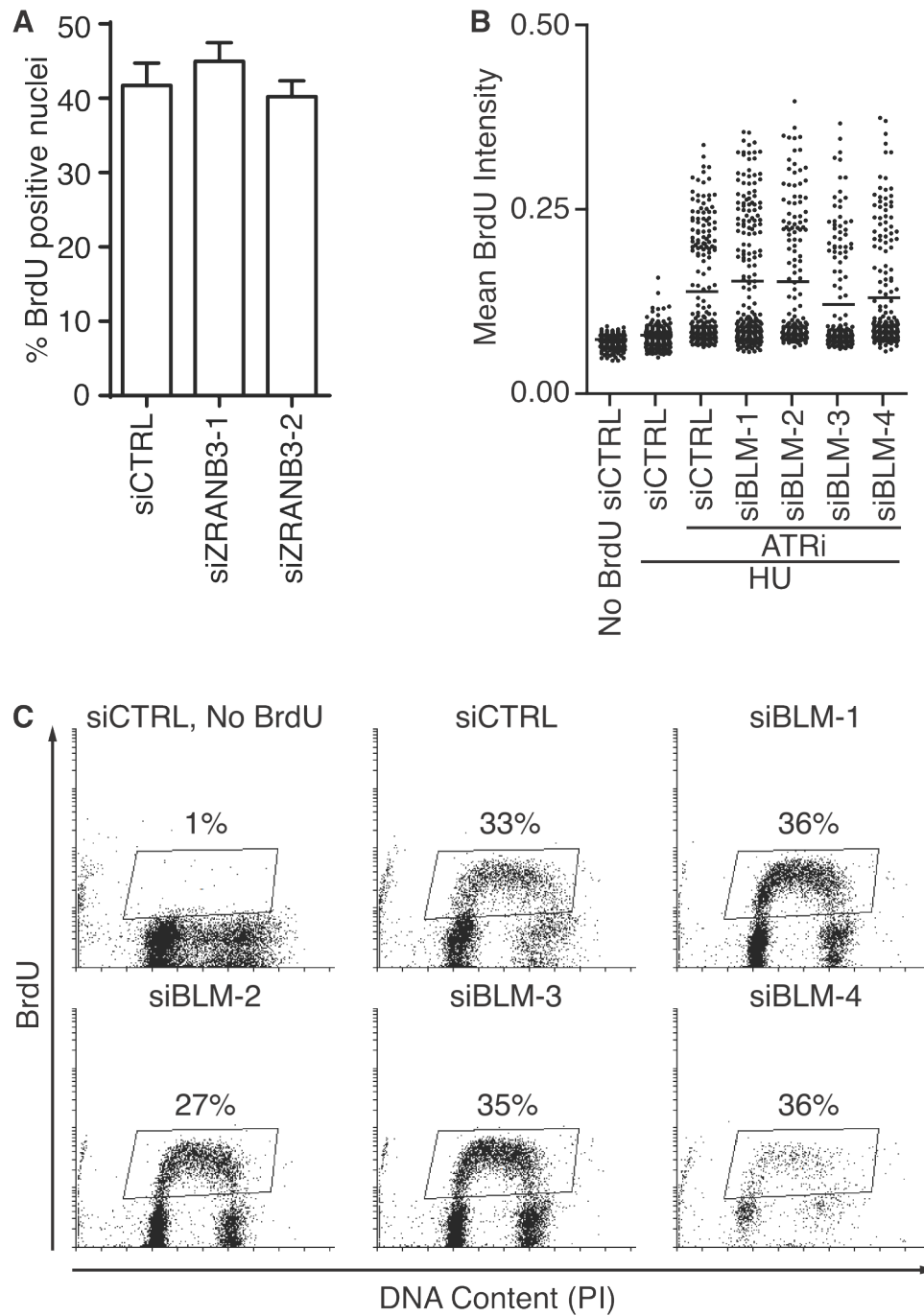


Figure 4.13 ZRANB3, BLM are not required for nascent-strand ssDNA. U2OS cells were transfected with control or siRNA targeting ZRANB3 or BLM. (A-B) Transfected cells were labeled with 10 μ M BrdU for 10 minutes before addition of 3mM HU and 5 μ M ATRi for 4 hours to measure nascent-strand ssDNA or (C) labeled with 10 μ M BrdU for 40 minutes to measure percentage of cells in S-phase. (A) Bars represent mean and SEM of 3 replicates.

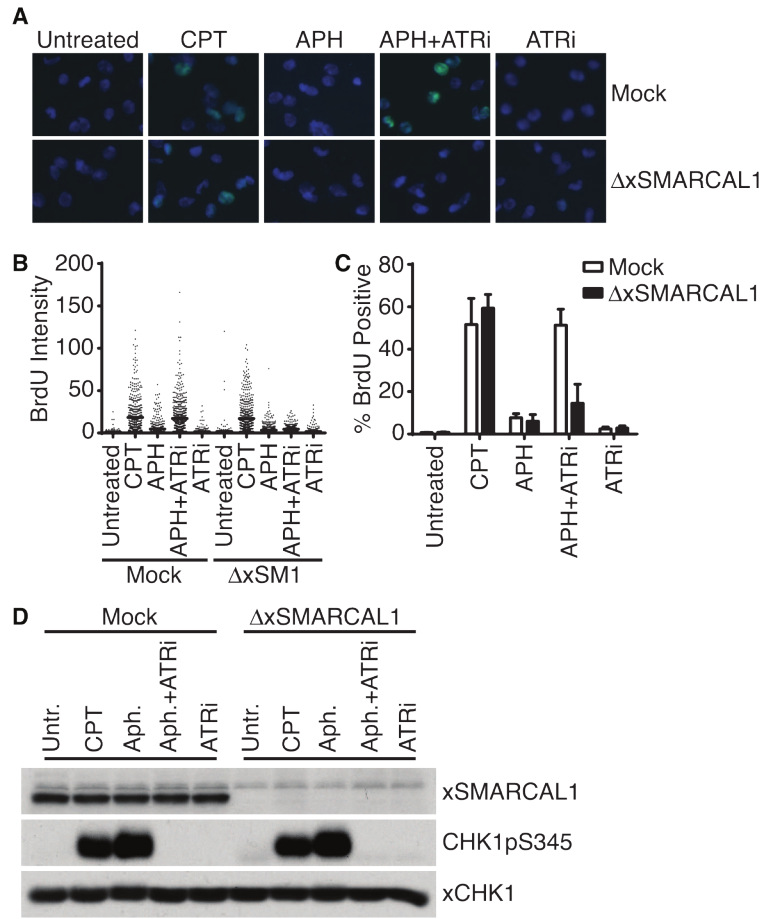


Figure 4.14 xSMARCAL1 is required for the generation of nascent-strand ssDNA when ATR is inactivated in *Xenopus* egg extract. Sperm chromatin (4000 nuclei/ μ l) was replicated in low speed *Xenopus* extract containing DMSO or ATR inhibitor. After 10 minutes, extracts were labeled with 50 μ M BrdU for 20 minutes prior to addition of DMSO, 50 μ M camptothecin (CPT), or 100 μ M aphidicolin (APH) as indicated. 60 minutes after addition of chromatin, nuclei were fixed and spun down onto coverslips through a glycerol cushion. Where indicated extracts were either mock or xSMARCAL1 depleted. Nuclei from extracts were processed to quantitate nascent-strand ssDNA. (A) Representative images of BrdU staining from each sample. (B) Representative dot-plots of BrdU intensity per nucleus measured using ImageJ. (C) Quantitation (mean \pm SEM) of percent BrdU positive nuclei across three independent experiments. (D) Extracts were harvested, separated by SDS-PAGE and immunoblotted with antibodies to detect xSMARCAL1, CHK1 pS345, or xCHK1. These data were produced by Robert Driscoll.

Replication stress induces SMARCAL1 phosphorylation after it accumulates at stalled forks and binds DNA

One mechanism to explain these results is that ATR prevents aberrant fork processing by directly regulating SMARCAL1. The lack of effect of xSMARCAL1 depletion on CPT-induced ssDNA formation would be consistent with this mechanism since ATR is active in these circumstances. ATR can phosphorylate SMARCAL1 (Bansbach et al. 2009), but the functional consequences have not been described. Therefore, we investigated whether SMARCAL1 phosphorylation is a mechanism by which ATR stabilizes stalled replication forks.

SMARCAL1 phosphorylation in response to replication stress can be monitored by a pronounced gel mobility shift of the endogenous protein ((Bansbach et al. 2009) and Fig. 4.15A). GFP-SMARCAL1 protein expressed at near endogenous levels in HEK293T cells also is phosphorylated in response to HU (Fig. 4.15A). SMARCAL1 localizes to stalled forks via an interaction between its N-terminus and RPA2 (Bansbach et al. 2009; Ciccia et al. 2009; Yuan et al. 2009; Yusufzai et al. 2009). However, abrogation of stalled fork localization with a mutant that does not bind RPA (Δ N) caused a loss of damage-dependent phosphorylation indicating SMARCAL1 must be in proximity to the stalled fork to be phosphorylated (Fig. 4.15B). Deletion or point mutations in the SMARCAL1 HARP1 domain decrease but do not eliminate DNA binding (Bétous et al. 2012), and decrease damage-dependent SMARCAL1 phosphorylation (Fig. 4.15B). Deletion or mutation of the HARP2 domain eliminates DNA binding (Bétous et al. 2012) and eliminates phosphorylation (Fig. 4.15B). These HARP mutants retain the ability to localize to stalled forks (Fig. 4.16), indicating that both localization and DNA binding are required for damage-dependent phosphorylation. Thus, phosphorylation occurs after SMARCAL1 is positioned to catalyze fork remodeling. However, the ability of SMARCAL1 to translocate on DNA is not a prerequisite for phosphorylation since the

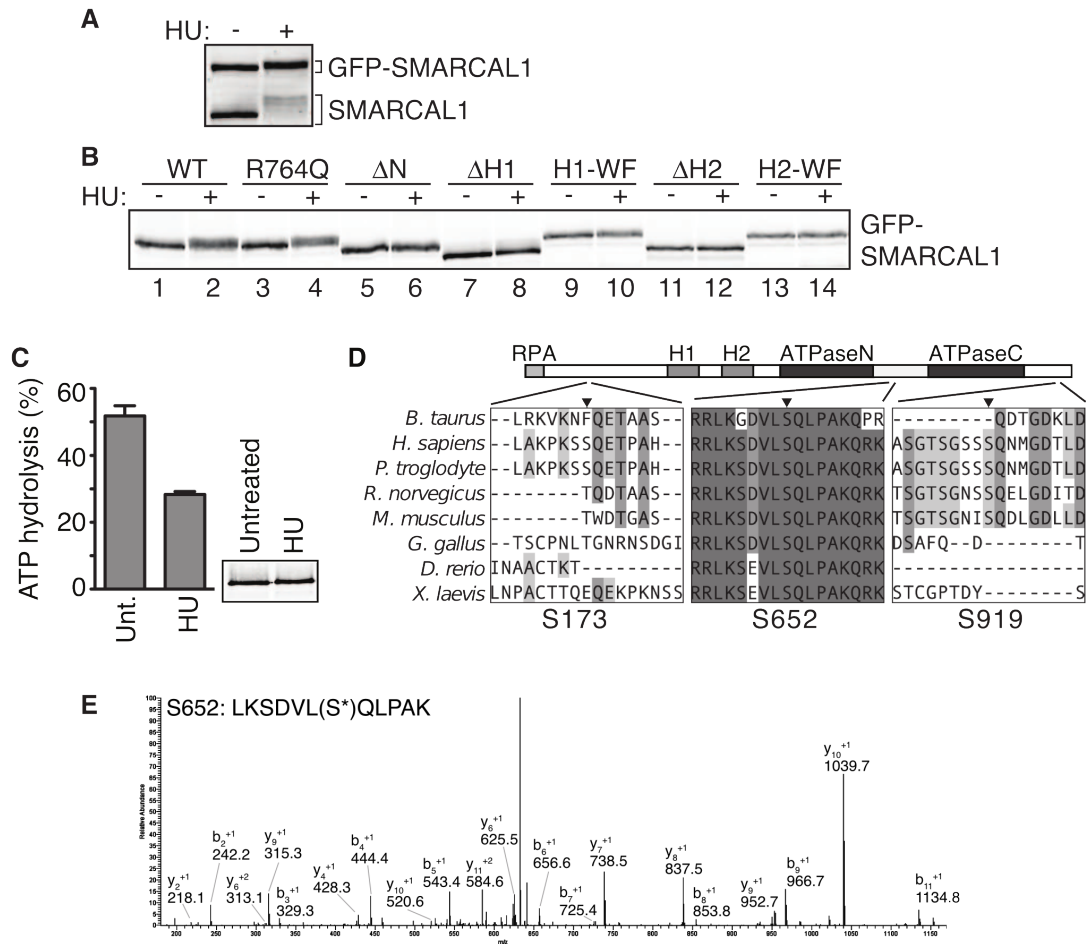


Figure 4.15 ATR phosphorylates SMARCAL1 after SMARCAL1 binds to DNA at stalled forks. (A and B) HEK293T cells were transfected with small amounts of GFP-SMARCAL1 wild type (WT) and mutant expression vectors to minimize overexpression. Δ H1 and Δ H2 are deletions of the HARP1 and HARP2 domains, respectively, while H1-WF and H2-WF are point mutants in each HARP domain (Bétous et al. 2012). Cells were treated with 2mM HU for 16h where indicated prior to lysis, separation by SDS-PAGE, and immunoblotting with SMARCAL1 antibody. (C) SMARCAL1 was purified from untreated (unt.) or HU-treated (16h, 2mM) HEK293T cells and used to measure ATPase activity in the presence of 5nM forked DNA substrate. Error bars are standard deviation from three experiments ($p = 0.0007$, two-tailed unpaired t-test). The inset is an immunoblot showing equal amounts of protein used in each condition. The purified protein was treated with lambda phosphatase before immunoblotting to eliminate the gel mobility shift and allow more accurate quantitation of protein concentration. (D) ClustalW was used to align SMARCAL1 from the indicated organisms. The position of the phosphorylated SQ residues S173, S652, and S919 relative to protein domains is depicted. (E) SMARCAL1 was purified from HU-treated HEK293T cells, trypsinized, and analyzed by tandem mass spectrometry. Shown is one of several spectra that correspond to phosphorylated S652. These data were produced by Carol Bansbach.

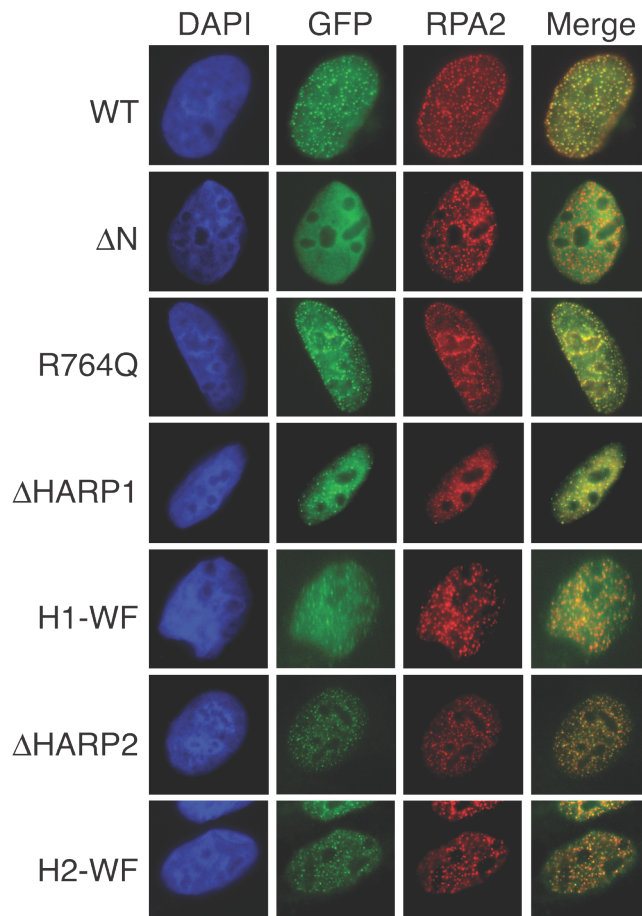


Figure 4.16 SMARCAL1 mutants that cannot bind DNA retain their ability to localize to sites of stalled replication forks. U2OS cells transfected with GFP-SMARCAL1 vectors were treated with HU for five hours, fixed and stained with antibodies to RPA2 and imaged for GFP, RPA and DAPI. Representative images are shown. None of the mutations except the RPA binding mutant (ΔN) caused a difference in the percentage of cells containing SMARCAL1 foci. $\Delta HARP1$ and $\Delta HARP2$ are deletions of the HARP1 and HARP2 domains, respectively, while H1-WF and H2-WF are point mutants in each HARP domain (Bétous et al. 2012). R764Q is a catalytically inactive mutant (Yusufzai and Kadonaga 2008). These data were produced by Carol Bansbach.

ATPase-deficient R764Q mutant exhibits the same mobility shift as the wild-type protein in response to HU (Fig. 4.15B).

S652 phosphorylation reduces SMARCAL1 activity

To test the functional significance of damage-dependent phosphorylation we isolated SMARCAL1 before and after exposure to HU. Phosphorylated SMARCAL1 isolated from HU-treated cells retains only 50% activity compared to SMARCAL1 isolated from untreated cells (Fig. 4.15C). This suggests that HU-dependent post-translational modifications inactivate SMARCAL1. This difference in activity is not due to a difference in cell cycle stage induced by HU since the cells were synchronized and released into S-phase prior to the experiment.

Next, we utilized mass-spectrometry and phosphopeptide mapping to identify damage-induced phosphorylation sites. Mass spectrometry of SMARCAL1 purified from HU-treated cells identified phosphorylation of S652, which lies within a consensus sequence (SQ) for the ATR kinase (Fig. 4.15E) on a linker between the two lobes of the SMARCAL1 ATPase domain (Fig. 4.15D). We identified two additional SQ phosphorylation sites (S173 and S919) through phosphopeptide mapping (Fig. 4.17). These phosphorylation sites are within poorly conserved, unstructured regions near the N- and C-termini, respectively (Fig. 4.15D).

Since S652 is highly conserved, we raised phosphopeptide specific antibodies to this phosphorylation site. These antibodies show that S652 phosphorylation is increased in response to HU (Fig. 4.18A). Phosphorylation is largely ATR-dependent in cells (Fig. 4.18B), and purified ATR can phosphorylate S652 in an in vitro kinase assay (Fig. 4.18C).

To determine whether these phosphorylation sites are functionally important, we tested whether phosphorylation alters SMARCAL1 localization or biochemical functions.

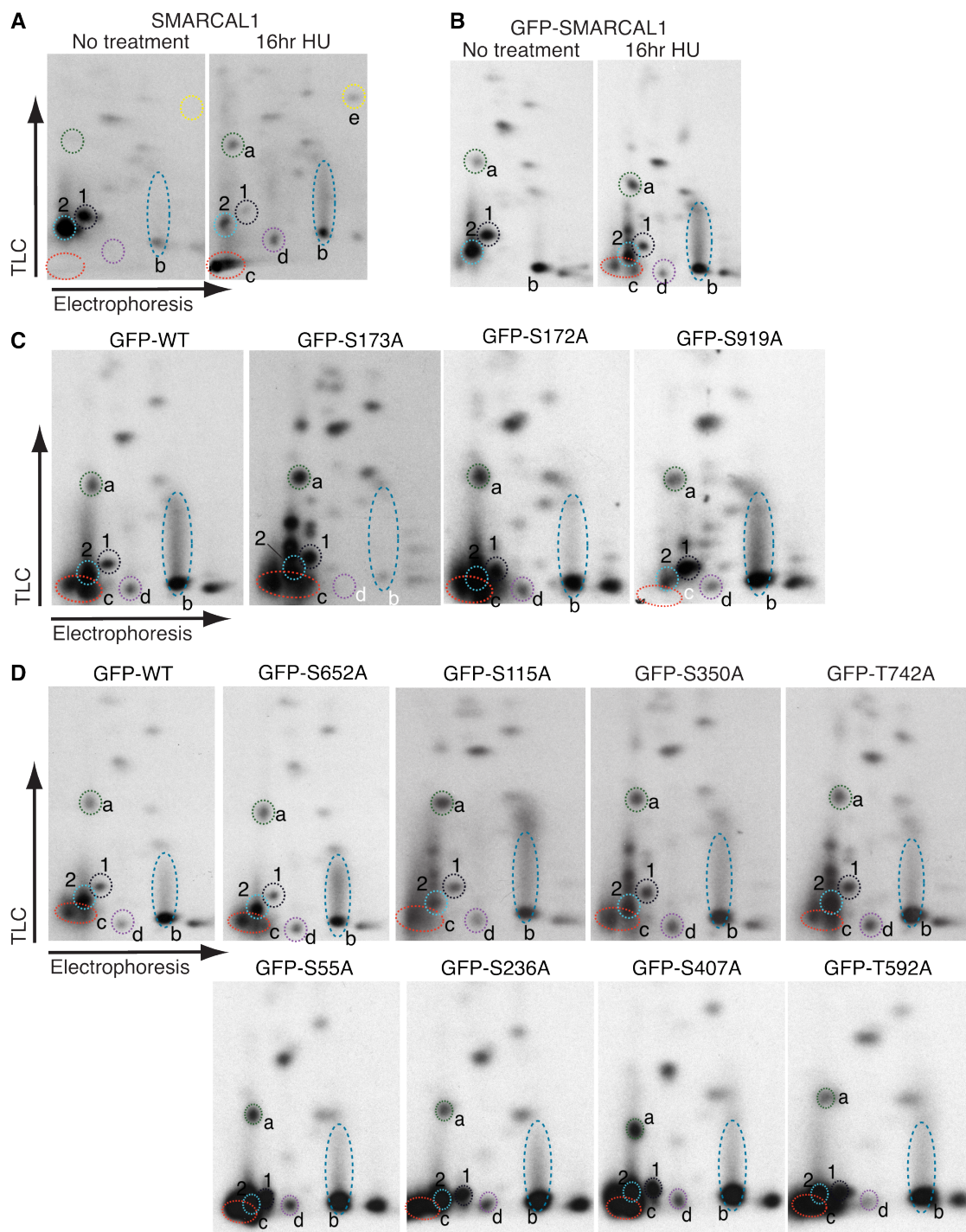


Figure 4.17 Mapping of SMARCAL1 phosphorylation sites. To determine and map additional sites of phosphorylation, we utilized two-dimensional phosphopeptide mapping on thin layer cellulose plates. (Continued on next page)

Figure 4.17 Mapping of SMARCAL1 phosphorylation sites (cont'd). (A) First the phosphopeptide map of endogenous SMARCAL1 was determined before and after treatment with HU. Several SMARCAL1 phosphopeptides are detected when SMARCAL1 is purified from ³²P-orthophosphate-labeled cells. After HU treatment phosphopeptides 1 and 2 decrease in intensity, phosphopeptide b increases, and several new phosphopeptides (a, c, d, and e) appear. (B) Similar patterns of phosphorylation are evident on GFP-SMARCAL1 with the exception that phosphopeptide e is not visible. We next examined the phosphopeptide patterns of GFP-SMARCAL1 mutant proteins purified from orthophosphate-labeled cells. (C) We first examined S172 and S173 since a tryptic peptide containing a phosphoserine at one of these two positions was identified in our mass spectrometry experiments. Mutation of S172 to alanine did not change the phosphopeptide pattern; whereas, mutation of S173 to alanine eliminated phosphopeptide d and greatly reduced phosphopeptide b. Thus, S173 is a major site of phosphorylation after DNA damage. It is likely phosphorylated by the PIKK family of kinases since it matches the consensus for ATR and ATM phosphorylation (SQ). (C and D) To identify the other damage-induced phosphorylation sites, each candidate SQ or TQ in SMARCAL1 was mutated to alanine. (C) Mutation of S919 to alanine eliminated phosphopeptide c indicating S919 is phosphorylated in cells. S919 is contained within a very large tryptic peptide that contains 14 potential sites of phosphorylation (EGSDMELLEASESFDPGSASGTSGSSSQNMGDTLDESSLTASPQK). In the 2D mapping, peptides that have variable numbers of phosphorylated residues typically yield a complicated pattern with multiple spots on a diagonal. Furthermore, large peptides move only short distances from the origin and increasing phosphorylation retards the mobility even further. Thus, we believe phosphopeptides 1, 2, and c are actually the same peptide with one, two, or three phosphates respectively. This interpretation explains the proportional decrease in intensity of phosphopeptides 1 and 2 when c is increased in HU-treated cells. The large size of this phosphopeptide may also explain our inability to observe it by mass spectrometry. (D) We did not observe any consistent change in the phosphopeptide map after mutation of any of the other SQ or TQ motifs. The lack of a change in the map when S652 is mutated to alanine was surprising given the mass spectrometry data indicating this SQ site is phosphorylated on endogenous SMARCAL1 in HU-treated cells. We suspect S652 is on phosphopeptide e which is only visible on the endogenous SMARCAL1 map and not on the maps from the GFP-SMARCAL1 protein. The small size and charge of the predicted S652 tryptic peptide (SDVLSQLPAK) are consistent with the migration of phosphopeptide e in both dimensions on the TLC plate. These data suggest S652 is not efficiently phosphorylated on the exogenous GFP-SMARCAL1 protein. These data were produced by Carol Bansbach.

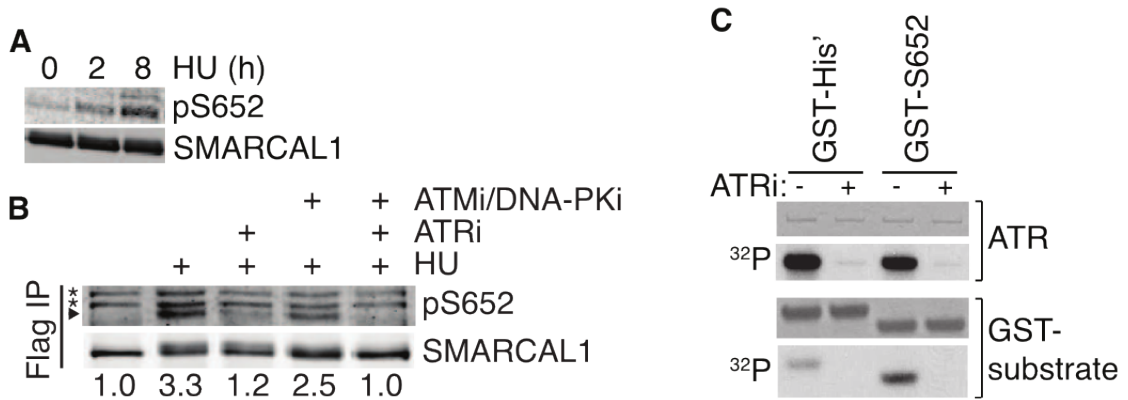


Figure 4.18 SMARCAL1 S652 is phosphorylated by ATR in cells and *in vitro*. (A and B) HEK293T cells were transfected with Flag-SMARCAL1 and treated with HU for the indicated times. Kinase inhibitors were added as indicated. Flag-SMARCAL1 was immunoprecipitated from cell lysates, separated by SDS-PAGE and immunoblotted with either total SMARCAL1 antibody or pS652-specific antibody. Asterisks indicate non-specific bands. Images were captured and quantitated relative to total SMARCAL1 using an Odyssey imaging system. (C) Purified ATR-ATRIP complex phosphorylates a GST-S652 peptide *in vitro*. ATRi was added where indicated to ensure specificity of the kinase in the reaction. Shown are images of a coomassie stained gel to visualize the amount of ATR and GST protein in the reactions or an autoradiogram (³²P) of the gel to visualize phosphorylation. Data for panel A were produced by Carol Bansbach. Data for panel C were produced by David Cortez.

Phosphorylation of S173, S652, or S919 does not regulate SMARCAL1 localization to stalled replication forks since neither non-phosphorylatable nor phospho-mimetic mutations in these residues alter their ability to co-localize with RPA foci in response to DNA damage (Fig. 4.19). Mutations of S173 or S919 also did not affect the DNA stimulated ATPase activity of SMARCAL1 (Fig. 4.20A-B). In contrast, the phospho-mimetic S652D mutant is a much less active DNA-stimulated ATPase compared to the wild-type (Fig. 4.20C-D), even though it has indistinguishable DNA binding activity (Fig. 4.21). The extent of ATPase inhibition caused by the phospho-mimetic mutation is similar to the inhibition of SMARCAL1 observed after HU-treatment (Fig. 4.15C), suggesting that S652 phosphorylation is a major mechanism by which SMARCAL1 is inhibited in cells exposed to persistent replication stress. Combining the S173D, S652D, S919D mutations did not further alter SMARCAL1 activity (data not shown), and mutation of S652 to alanine had no effect on SMARCAL1 activity indicating the serine itself is not required for function.

Consistent with its reduced ATPase activity, we also observed a significant reduction in the ability of the phospho-mimetic S652D SMARCAL1 to catalyze fork regression compared to the S652A or wild-type proteins indicating that SMARCAL1 phosphorylation at S652 limits its ability to perform branch migration (Fig. 4.20E-F). Combined with the observation that SMARCAL1 must first bind DNA before it can be phosphorylated, these data are consistent with a model in which SMARCAL1 initially is recruited to a damaged fork, binds the DNA to perform a fork remodeling activity, and then is phosphorylated on S652 to regulate this activity.

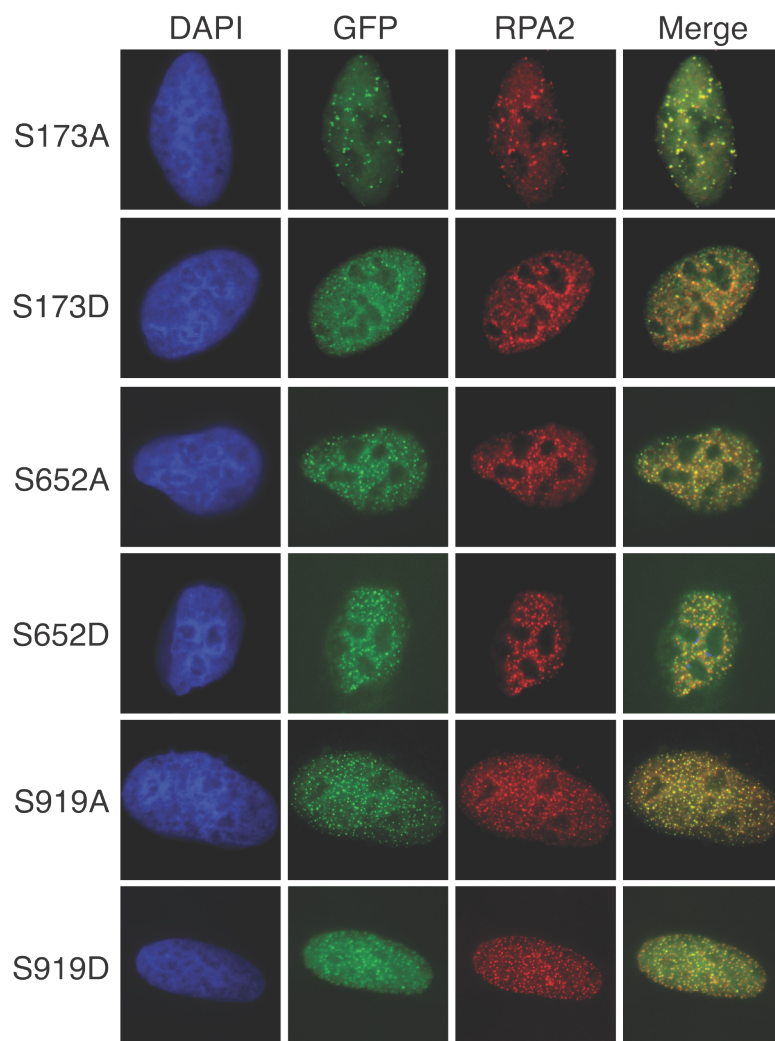


Figure 4.19 SMARCAL1 phosphorylation on S173, S652, or S919 does not alter its ability to bind DNA or localize to stalled replication forks. U2OS cells transfected with GFP-SMARCAL1 expression vectors encoding non-phosphorylatable or phosphorylation-mimetic mutations were treated with HU for five hours, fixed and stained with antibodies to RPA2 and imaged for GFP, RPA and DAPI. Representative images are shown. None of the mutations altered the percentage of cells exhibiting GFP-SMARCAL1 and RPA co-localization. Data were produced by Carol Bansbach.

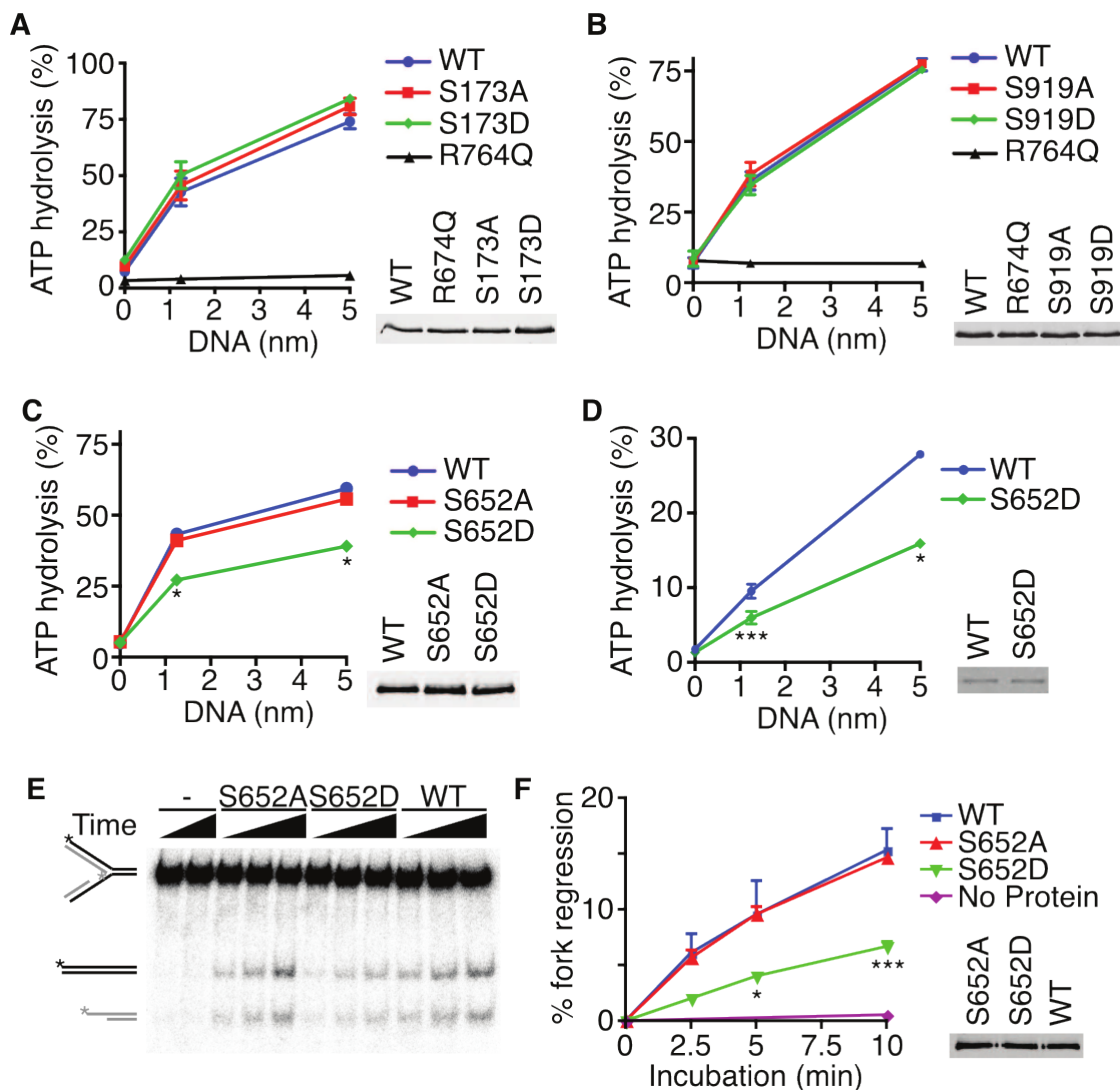


Figure 4.20 SMARCAL1 phosphorylation on serine 652 inhibits its ATP-dependent fork remodeling activity. (A-D) The indicated Flag-SMARCAL1 proteins were purified from HEK293T cells (A-C) or baculovirus infected insect cells (D), and their ATPase activity measured in the presence of increasing concentrations of splayed arm DNA substrate. The insets in (A-C) are representative immunoblots, and the inset in (D) is a coomassie stained gel showing equal amount of wild-type and mutant SMARCAL1 proteins used. Error bars in all panels represent SEM (n=3) and in many cases were smaller than the symbol. * $p < 0.0002$, ** $p < 0.002$, *** $p < 0.05$. (E-F) The fork regression activity of purified SMARCAL1 proteins was assayed on a model replication fork substrate schematized on the far left. (See Table 4.1 for details). (E) A representative DNA gel and (F) quantitation of three independent experiments (mean and SEM) are shown. Inset is a representative immunoblot showing equal amount of wild-type and mutant SMARCAL1 proteins. Data for panels A-D were produced by Carol Bansbach. Proteins used in panels E-F were purified by Clint Carroll. Lead-gap substrate used in panels E-F was purified by Rémy Bétous.

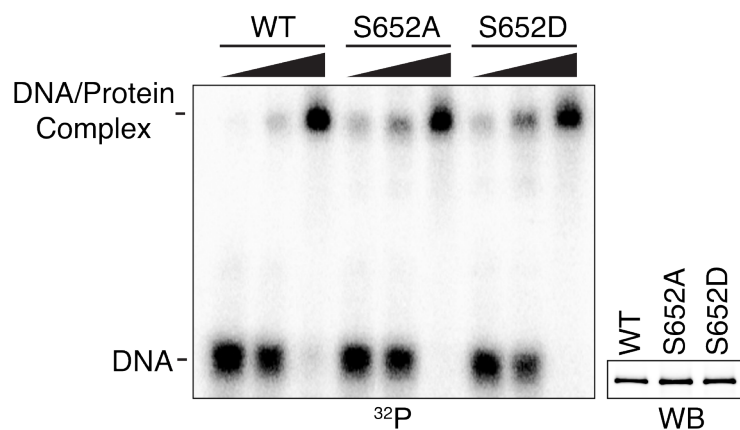


Figure 4.21 Mutation of S652 does not alter the DNA binding ability of SMARCAL1. Increasing amounts of wild-type, S652A, or S652D mutant SMARCAL1 proteins were incubated with a radio-labeled splayed arm DNA substrate. Complexes were separated by electrophoresis on a polyacrylamide gel and imaged by autoradiography. WB=western blot showing that equal levels of the proteins were used in the assay. Data were produced by Clint Carroll.

Too much SMARCAL1 activity in cells phenocopies the effect of ATR inhibition on fork collapse

To confirm that ATR-dependent SMARCAL1 phosphorylation also inhibits SMARCAL1 activity in cells at stalled replication forks, we used an assay that measures the consequences of uncontrolled SMARCAL1 activity. Expression of wild type SMARCAL1 from a strong promoter causes the induction of γ H2AX throughout the nucleus in a pan-nuclear pattern (Fig. 4.22A-C, and Bansbach et al. 2009) similar to what is observed when ATR is inhibited in HU-treated cells (Fig. 4.4A) supporting a functional link between ATR and SMARCAL1. The induction of pan-nuclear γ H2AX by overexpressed SMARCAL1 is dependent on DNA replication, the ability of SMARCAL1 to localize to stalled forks, and its enzymatic activity (Bansbach et al. 2009). Like ATR inhibition, overexpression of SMARCAL1 causes increased levels of single-stranded DNA at replication forks (Fig. 4.22D-E). Furthermore, just as is the case with ATR inhibition, knockdown of SLX4, but not MUS81, resulted in a decrease in ssDNA formation in cells expressing SMARCAL1 (Fig. 4.22E). Taken together, these data indicate that the phenotype of cells overexpressing SMARCAL1 is similar to that induced when ATR is inhibited as predicted if ATR phosphorylates SMARCAL1 as a mechanism of limiting its activity and preventing fork collapse.

If ATR-catalyzed S652 phosphorylation decreases SMARCAL1 activity to prevent aberrant fork processing then the S652D phospho-mimetic mutation should yield a protein that is less capable of inducing the pan-nuclear γ H2AX phenotype. Indeed, overexpression of GFP-SMARCAL1 S652D induces significantly less pan-nuclear H2AX phosphorylation compared to the wild type protein (Fig. 4.22A-B). We did observe some cells with pan-nuclear γ H2AX when S652D is overexpressed; however, those cells contained on average twice the amount of S652D protein overexpression compared to

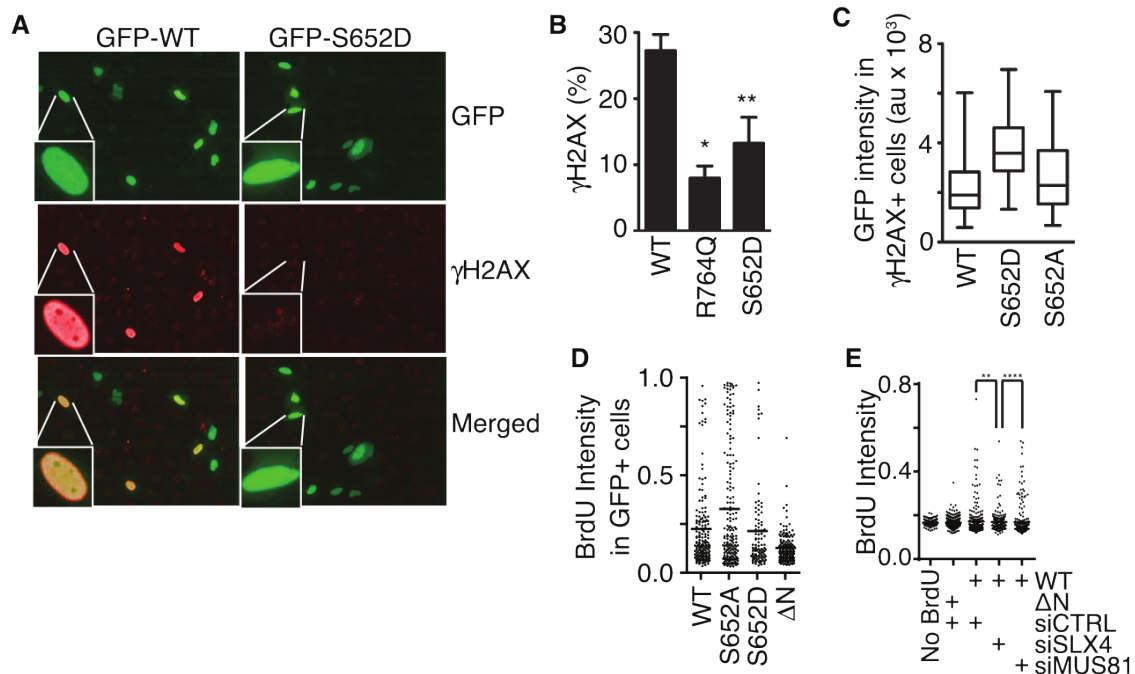


Figure 4.22 Phosphorylation of SMARCAL1 at S652 decreases its activity at DNA replication forks in cells. (A-C) GFP-SMARCAL1 wild type and mutant proteins were over-expressed in U2OS cells. Cells were stained with DAPI to mark the nucleus and antibodies to γ H2AX. Images were acquired using an Opera automated confocal microscope and the levels of GFP-SMARCAL1 and γ H2AX levels were quantitated in each nucleus using Columbus software. (A) Representative images. (B) Data represent the percent of cells expressing between 500-2500 arbitrary units (a.u.) of GFP-SMARCAL1 that contain a mean γ H2AX intensity of greater than 1000 a.u. Error bars represent SEM from three independent experiments; * $p = 0.0007$, ** $p = 0.023$. (C) The expression level of GFP-SMARCAL1 (as measured by GFP intensity) in each cell that had γ H2AX intensity of greater than 1000 arbitrary units is plotted in box and whisker format; Significantly higher GFP-SMARCAL1 S652D protein levels were needed to induce γ H2AX than either wild-type or S652A protein ($p < 0.0001$). (D) GFP-SMARCAL1 proteins with the indicated mutations were expressed in U2OS cells. BrdU was added to the culture media 16h prior fixation and staining in non-denaturing conditions to measure the total level of ssDNA. The mean intensity (a.u.) of BrdU staining per GFP-SMARCAL1 expressing cell is graphed. The line indicates the mean value in each population (Mann-Whitney test S652A vs. S652D, $p = 0.013$). (E) GFP-SMARCAL1 proteins were expressed in U2OS. These cells were then transfected with control, MUS81 or SLX4 siRNA. BrdU was added to the culture media 16h prior fixation and staining in non-denaturing conditions to measure the total level of ssDNA. The mean intensity (a.u.) of BrdU staining per cell is graphed. The line indicates the mean value in each population (Mann-Whitney test siCTRL vs siSLX4, $p = 0.0012$; siSLX4 vs siMUS81, $p < 0.0001$). Data for panels A-C were produced by Carol Bansbach. Data for panels D-E were produced by Gloria Glick.

the level of the wild type or S652A proteins needed to induce pan-nuclear γ H2AX (Fig. 4.22C).

Finally, consistent with our model, we also found that overexpression of the S652D SMARCAL1 protein yielded less single-stranded DNA than the S652A mutant although it does remain slightly more active than a SMARCAL1- Δ N protein that cannot localize to stalled forks because it lacks an RPA binding domain (Fig. 4.22D). These data suggest that S652 of SMARCAL1 is one of the ATR phosphorylation targets necessary to prevent fork collapse and emphasize the need for properly regulating SMARCAL1 to achieve successful stalled fork stabilization and repair.

Discussion

Our data is consistent with a specific model of how ATR prevents fork collapse in the context of replication stress (Fig. 4.23). ATR maintains the integrity of the replication fork through regulation of several proteins including direct phosphorylation of S652 of SMARCAL1. If properly regulated, SMARCAL1 participates in maintaining fork stability and promoting fork restart. However, in the absence of ATR regulation, SMARCAL1 catalyzes excessive replication fork reversal or other DNA remodeling that generates a substrate for the SLX4-dependent Holliday junction endonucleases. These enzymes cleave the reversed replication fork into a one-ended DSB which CtIP-dependent endonucleases further process into ssDNA of both the parental and nascent strands. Consistent with this model, fork reversal is observed in replication checkpoint-deficient *S. cerevisiae* cells in response to replication stress (Lopes et al. 2001) although no responsible yeast enzymes have been identified. In addition, nucleases process stalled forks in checkpoint defective yeast cells (Cotta-Ramusino et al. 2005). This model also explains why both too little and too much SMARCAL1 in a cell causes replication fork collapse (Bansbach et al. 2009). Finally, the activity of unregulated SMARCAL1 in

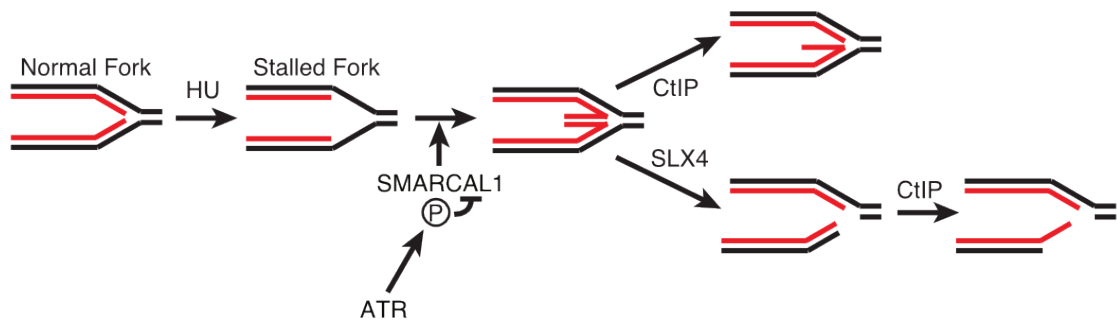


Figure 4.23 Model for nascent-strand ssDNA generation at stalled forks. Black and red lines represent template and nascent strands, respectively. HU causes uncoupling of the replicative helicase and polymerases, resulting in template-strand ssDNA at the replication fork. ATR prevents aberrant fork remodeling by the SMARCAL1 enzyme. In the absence of ATR-dependent SMARCAL1 S652 phosphorylation, a Holliday-junction like structure may persist at the fork and is cleaved by SLX4-dependent nucleases generating a double-strand break. CtIP-dependent nucleases then resect the break yielding nascent-strand ssDNA. CtIP may also process a reversed fork structure prior to SLX4 cleavage which could contribute to the nascent-strand ssDNA formation.

causing fork collapse is not limited to mammalian cells since we also observed it in a *Xenopus* cell-free replication system when ATR is inhibited.

ATR as a drug target

The essential function of ATR to maintain cell viability is linked to its requirement to complete DNA replication and separable from its G2 checkpoint activity (Nam et al. 2011b). Defining how ATR promotes the completion of DNA replication is essential to understand the major pathway that controls genome integrity in S-phase and to identify the mechanism of action of ATR-directed drugs. Our data indicate that acute ATR inhibition results in a rapid decrease in the rate of fork elongation. This effect likely results from loss of checkpoint control of origin firing leading to a decrease in elongation rates due to depletion of essential replication factors such as nucleotides or replication proteins. The deregulation of origin timing is unlikely to be cell lethal by itself since it happens within 20 minutes of adding the ATRi but loss of cell viability requires several hours without additional genotoxic agents. Furthermore, suppression of origin firing by the addition of CDK2 or CDC7 inhibitors did not improve the viability of ATRi-treated cells (Fig. 4.24). More likely the essential function of ATR is to stabilize or repair stalled replication forks, which collapse when ATR is inhibited. Deregulated origin firing would exacerbate this problem by creating additional stalled forks. Consistent with this interpretation, viability is lost within 45 minutes in cells treated with both ATRi and HU. The increase in irreversible replication fork collapse, concomitant formation of DSBs, and excess ssDNA when ATR is inactivated suggests improper enzymatic processing of the stalled fork DNA. These fork-processing events may be largely unsuccessful attempts to repair the damaged fork.

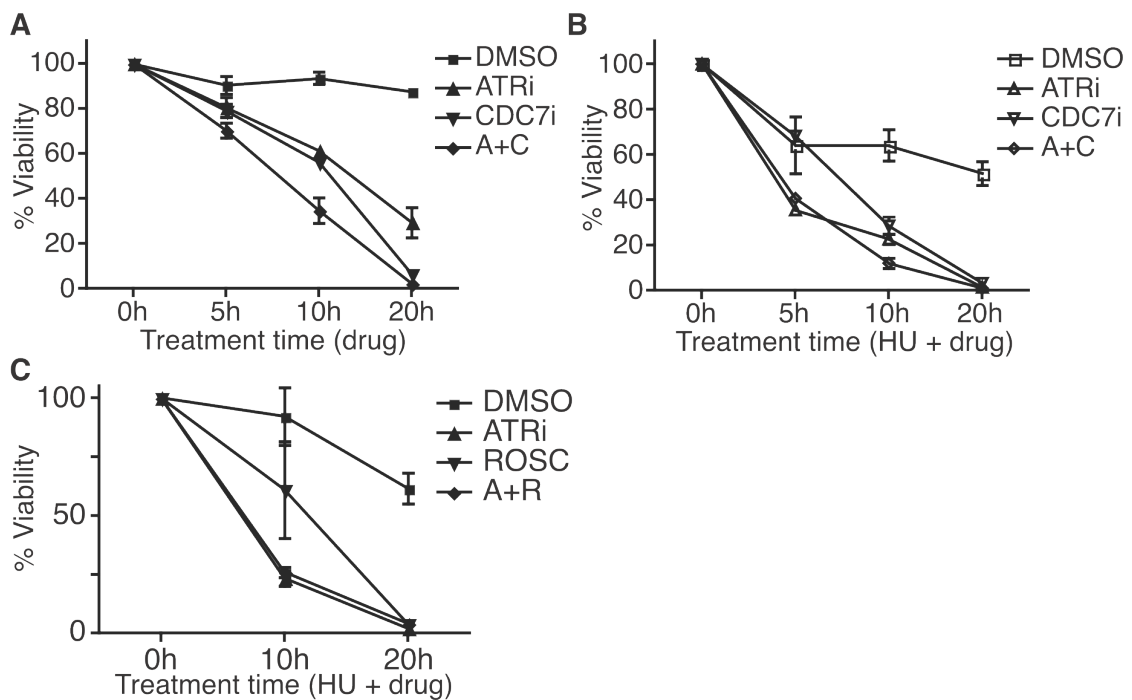


Figure 4.24 CDK2 and CDC7 kinase inhibitors do not rescue ATRi toxicity. (A-C) U2OS cells were treated with DMSO, 5 μ M ATRi, 5 μ M CDC7i (PHA 767491, Sigma), or ATRi + CDC7i in the absence (A) or presence (B) of 3mM HU for the indicated times. (C) U2OS cells were treated with DMSO, 5 μ M ATRi, 30 μ M Roscovitine (Sigma), or ATRi + Roscovitine in the presence of 3mM HU for the indicated times. (A-C) After treatment, cells were released into fresh growth media for 10-14 days. Colonies were visualized by methylene blue staining. Results shown are mean \pm SEM of at least two independent experiments.

Aberrant stalled fork processing when ATR is inactivated

Previous studies implicated the MUS81 endonuclease as an enzyme that cleaves persistently stalled replication forks after several hours of HU treatment leading to the appearance of high levels of γ H2AX (Hanada et al. 2007). MUS81 was also reported to generate DNA damage in cells treated with a CHK1 inhibitor (Forment et al. 2011). However, we found no effect of MUS81 on the generation of DSBs in cells treated with the ATRi. Instead, we observed a strong dependency on SLX4. Furthermore, we found that SLX4 is required for nascent-strand ssDNA formation. SLX4 is a scaffolding protein for several endonucleases including MUS81, SLX1, and XPF (Fekairi et al. 2009; Svendsen et al. 2009). Since we did not observe a significant effect of silencing any of these nucleases individually, our data suggests that more than one of them may function redundantly to cleave stalled forks when ATR is inhibited. CtIP-dependent exonucleases then process the cleaved fork to generate nascent-strand ssDNA. SLX4 depletion yields a complete loss of DSBs as measured by the COMET assay, but only a partial suppression of the nascent-strand ssDNA. Therefore, it is possible that CtIP also directs resection of a stalled, regressed fork when ATR is inhibited prior to DSB formation, thereby generating a nascent-strand ssDNA overhang with or without SLX4-dependent cleavage.

A preferred substrate of SLX4-dependent endonucleases resembles a Holliday junction, which can form at a stalled fork either due to torsional stress or enzymatic processing. Our data are consistent with enzymatic processing of the fork by the SMARCAL1 fork regressing enzyme to generate a preferred substrate for SLX4-dependent cleavage when ATR is inhibited. ATR phosphorylates SMARCAL1, and previous studies indicate that excess SMARCAL1 activity causes replication fork problems (Bansbach et al. 2009). Thus, the fork remodeling activities of SMARCAL1 promotes fork repair in some cases, but can threaten genome stability if not properly

regulated. SMARCAL1 is not needed for fork collapse in all circumstances. For example, our data indicate that CPT treatment induces fork collapse and ssDNA formation independently of xSMARCAL1. Since ATR would be active in CPT-treated cells, SMARCAL1 would be appropriately regulated.

Consistent with our model we find that phosphorylated SMARCAL1 purified from cells treated with HU is significantly less active than SMARCAL1 purified from untreated cells. We identified three damage induced phosphorylation sites on SMARCAL1 including S652, which is phosphorylated by ATR. Phospho-mimetic mutations in S652 yield a protein that is significantly less active in catalyzing ATP hydrolysis and fork reversal in vitro and also less active in cells. S652 lies within the linker between the two RecA lobes of the ATPase domain. Flexibility of this linker is needed for conformational changes required for catalysis (Dürr et al. 2005; Lewis et al. 2008; Sprouse et al. 2006). Since S652 phosphorylation does not impair SMARCAL1 localization or DNA binding activity, we suspect that phosphorylation of the linker reduces the ability of SMARCAL1 to undergo this conformational change and thereby inhibits its translocase activity. SMARCAL1 phosphorylation requires it to first localize to the stalled fork and bind DNA. Thus, SMARCAL1 likely acts at damaged forks prior to ATR-dependent phosphorylation, which serves as a mechanism of limiting its activity.

Overexpression of active SMARCAL1 causes pan-nuclear γ H2AX staining. This effect requires localization of SMARCAL1 to replication forks and its enzymatic activity. The exact source of this staining pattern is not clear although it forms well before there is any evidence of apoptosis, it is chromatin-associated (data not shown), and is also observed in cells treated with ATRi and HU. Thus, our data suggest that it is linked to the aberrant fork processing and collapse that occurs when ATR cannot regulate SMARCAL1. Consistent with this interpretation, the phospho-mimetic S652D SMARCAL1 protein is less capable of inducing this phenotype and is less active as a

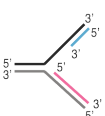
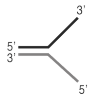
fork regression enzyme. Furthermore, like ATR inhibition, SMARCAL1 overexpression also induces SLX4-dependent excess ssDNA formation at stalled forks and this effect is alleviated by a phosphomimetic mutation in S652.

Another prediction of our model is that the S652A mutant should retain too much activity in HU-treated cells perhaps generating some fork collapse events even when ATR is not inhibited (assuming S652 phosphorylation is not completely redundant with other mechanisms). Unfortunately, since SMARCAL1 overexpression causes significant perturbations to DNA replication on its own and the S652 site does not appear to be regulated properly on the exogenously expressed SMARCAL1 wild-type protein (Fig. 4.17), we have been unable to do effective genetic complementation experiments to examine the effect of the S652A mutant on fork collapse and ssDNA generation. Future experiments either knocking in the mutation into the genome or using expression systems with native promoter and gene structures will be needed.

Neither SMARCAL1 nor SLX4 silencing completely prevents nascent-strand ssDNA formation caused by ATR inhibition suggesting additional aberrant fork processing events remain to be identified. The lack of complete suppression by SMARCAL1 silencing may also be due to the competing increase in ssDNA generated due to the need for some properly regulated SMARCAL1 protein to protect stalled forks. In addition, it seems likely that additional mechanisms regulate the activity of SMARCAL1. Our phosphopeptide maps indicate that S652, S173, and S919 are the major HU-induced phosphorylation sites on SMARCAL1; however mutation of all three serines to alanines does not eliminate the HU-induced mobility shift of the protein on SDS-PAGE gels (data not shown). Thus, there must be additional regulatory post-translational modifications that could also contribute to SMARCAL1 regulation. Finally, the ATR inhibitor may not completely block all ATR activity so the results observed may not be equivalent to a complete loss of ATR function.

Conclusions

ATR signaling has long been known to regulate DNA replication and prevent fork collapse based largely on studies in yeast. However, the molecular mechanisms of what ATR does to prevent fork collapse and even what fork collapse is in mammalian cells are not well understood. Our data define an ATR-dependent replication fork protection mechanism in human cells that is critical for genome maintenance and cell viability. These studies also help define the mechanism of action of ATR-targeted therapeutic agents. Specifically, combinations of selective ATR pathway inhibitors with either intrinsic or added replication stress provides a rapid mechanism of cancer cell killing due at least in part to aberrant processing of stalled replication forks.

Assays	Substrate structures	Lengths (Nt)	5' to 3' oligonucleotide sequences
Fork regression		122	CGTGACTTGATGTTAACCCCTAACCCCTAAGATATCGCGT <u>TA</u> TCAGAGTGTGAGGATACATGTAGG CAATTGCCACGTGTCTATCAGCTGAAGTTGTTTCGCGACGTGCGATCGTCGCTGCGACG
		122	CGTCGCAGCGACGATCGCACGTCGCGAACAACCTTCAGCTGATAGACACGTGGCAATTGCCTA CATGTATCCTCACACTCTGA <u>AT</u> ACGCGATATCTAGGGTTAGGGTTAACATCAAGTCACG
		52	CGTCGCAGCGACGATCGCACGTCGCGAACAACCTTCAGCTGATAGACACGTGG
		82	TCAGAGTGTGAGGATACATGTAGGCAATTGCCACGTGTCTATCAGCTGAAGTTGTTTCGCGACG TGCGATCGTCGCTGCGACG
ATPase		30	CCAGTGAATTGTTGCTCGGTACCTGCTAAC
		30	GACATTTGATACCGAGCAACAATCACTGG

Bolded and underlined letters indicate mismatched bases between parental strands (fork regression assay) to suppress spontaneous branch migration.

Table 4.1 Oligonucleotides for substrate construction.

CHAPTER V

BIOCHEMICAL MECHANISM OF SMARCAL1 TRANSLOCATION ON DNA

Introduction

During DNA replication, replication forks frequently encounter DNA damage which causes replication stress. One potential repair intermediate is the regressed fork in which the two nascent strands pair as the branch point migrates in the reverse direction of replication fork movement. This four way junction resembles a Holliday junction and may serve as an intermediate in several repair pathways.

SMARCAL1 is a DNA-stimulated ATPase capable of rewinding RPA-coated bubbles and performing both fork regression and restoration *in vitro*. Depletion of SMARCAL1 causes DNA damage and sensitivity to replication stress (Bansbach et al. 2009; Ciccia et al. 2009; Postow et al. 2009; Yuan et al. 2009), and over-expression of SMARCAL1 also causes DNA damage (Bansbach et al. 2009; Couch et al. 2013). SMARCAL1 belongs to the SWI/SNF family of the helicase-like protein superfamily 2 (SF2), which includes several other enzymes capable of *in vitro* fork regression including UvsW, ZRANB3, and RecG (Atkinson and McGlynn 2009; Singleton et al. 2007). While we have characterized several genetic phenotypes of SMARCAL1, we still do not fully understand the biochemistry of the enzyme. Therefore, we will compare SMARCAL1 to the more well characterized UvsW and RecG and the related human annealing helicase, ZRANB3.

To better understand how annealing helicases help preserve genome integrity, we conducted a biochemical study of how leading and lagging template strand lesions affect SMARCAL1 activity, and we compared the activities of UvsW, RecG, and ZRANB3 in these assays. Two lines of evidence suggest a translocation polarity for SMARCAL1.

First, nuclease footprinting assays demonstrated that SMARCAL1 binds the dsDNA of the parental duplex primarily on the leading template strand (Bétous et al. 2013). Second, our collaborator Maria Manosas determined that in a single molecule assay using a DNA hairpin controlled by magnetic tweezers, a region of reversed polarity on the parental leading strand more strongly inhibited SMARCAL1 activity than on the parental lagging strand, suggesting that SMARCAL1 binds the leading strand (M. Manosas, personal communication – similar to experiments in Manosas et al. 2013). Therefore, we hypothesized that SMARCAL1 binds and tracks the leading template strand of DNA during fork regression.

To test this hypothesis, we created model replication fork substrates containing modifications on the leading or lagging template strands. These modifications included nicks, gaps, and biotinylation. Using substrates containing biotinylated deoxyuridine in either the leading, lagging, or both template strands, we compared SMARCAL1, ZRANB3, UvsW, and RecG. We determined that these enzymes were similarly inhibited by avidin bound to the leading template strand. This suggests that while this assay likely does not measure translocation polarity, these enzymes use a common mechanism for fork regression.

Results

The biochemical properties of other dsDNA translocases have been defined using gapped dsDNA to determine the polarity and step-size of these enzymes (Deindl et al. 2013; Stanley et al. 2006; Whitehouse and Stockdale 2003). While SMARCAL1 is not known to translocate on dsDNA alone, we reasoned that constructing fork regression substrates containing template-strand gaps would provide insight into how this enzyme functions and what lesions SMARCAL1 can and cannot tolerate in the cell.

First, we constructed substrates containing a nick or 1 nucleotide gap on either the leading or lagging template strand. None of these substrates had any effect on SMARCAL1 activity (Fig. 5.1). This suggests that the step size of SMARCAL1 is greater than 1 nucleotide. Next, we constructed substrates with 5 or 10 nucleotide gaps on either template strand. In both cases, a gap on the leading strand inhibited SMARCAL1 activity approximately 2-fold, which suggests a step-size less than or equal to 5 nucleotides (Fig. 5.2).

Next, we tested UvsW and RecG in this assay. While SMARCAL1 and UvsW are structurally similar enzymes (Aaron Mason and Brandt Eichman, unpublished observations), UvsW was unaffected by the leading strand lesion. Instead, the lagging strand gap inhibited UvsW activity, consistent with the reported 3' → 5' polarity of UvsW (Nelson et al. 2009). On the other hand, lesions on either strand inhibited RecG to some extent, though the extent of inhibition was greater when the gap was placed on the leading template strand (Fig. 5.3).

Both RecG and UvsW have strand-switching capability (Manosas et al. 2013). Template strand gaps did not inhibit SMARCAL1 activity completely in either orientation. Although our results suggest a 5' → 3' polarity, one alternative explanation for this limited inhibition is that SMARCAL1 may switch strands after encountering the lesion. Once the fork junction is migrated to the gap, this intermediate resembles the fork restoration substrates used previously. In fork restoration assays, SMARCAL1 prefers substrates where the leading nascent strand is longer than the lagging nascent strand (Bétous et al. 2013). The leading template strand gap substrate used here resembles a fork restoration substrate with a longer lagging nascent strand, and vice versa (Fig. 5.4A). Once SMARCAL1 migrates these substrates to the template strand gap, SMARCAL1 may complete the reaction through translocation on a different strand (Fig. 5.4B).

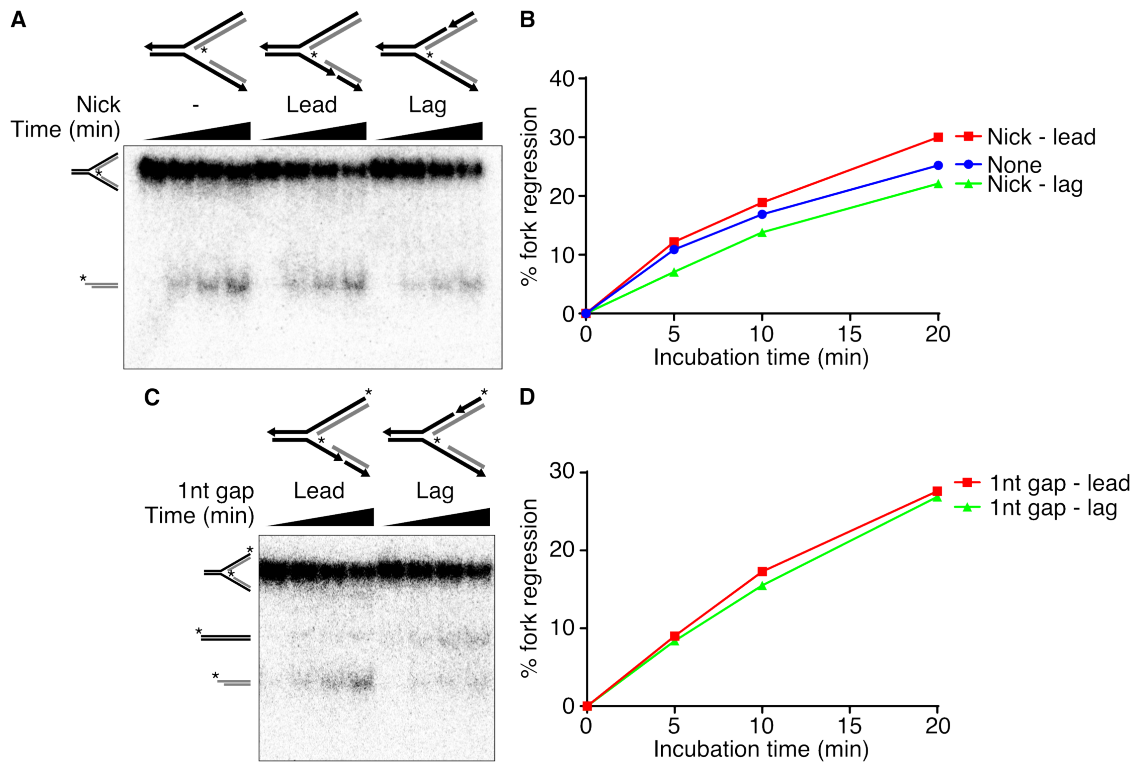


Figure 5.1 Nicks and 1nt Gaps Have No Effect on SMARCAL1 Fork Regression Activity. (A-B) Leading gap substrates (3nM) containing no modification (“None”), a leading strand nick (“Lead”), or a lagging strand nick (“Lag”) were incubated with SMARCAL1 (3nM) at 30°C for 5, 10, or 20 minutes. DNA products were analyzed by native gel electrophoresis (A) and phosphorimager quantitation (B). (C-D) Leading gap substrates (3nM) containing a 1nt gap on the leading (“Lead”) or lagging (“Lag”) template strand were incubated with SMARCAL1 (3nM) at 30°C for 5, 10, or 20 minutes. DNA products were analyzed by native gel electrophoresis (C) and phosphorimager quantitation (D). Graphs are from a single experiment (n=1). Oligos: (No mod) LeadP122 + LagP122 + LeadD52 + LagG82; (Lead nick/gap) LeadP84/LeadP83 + LeadP38 + LagP122 + LeadD52 + LagG82; (Lag nick/gap) LeadP122 + LagP38 + LagP84/LagP83 + LeadD52 + LagG82.

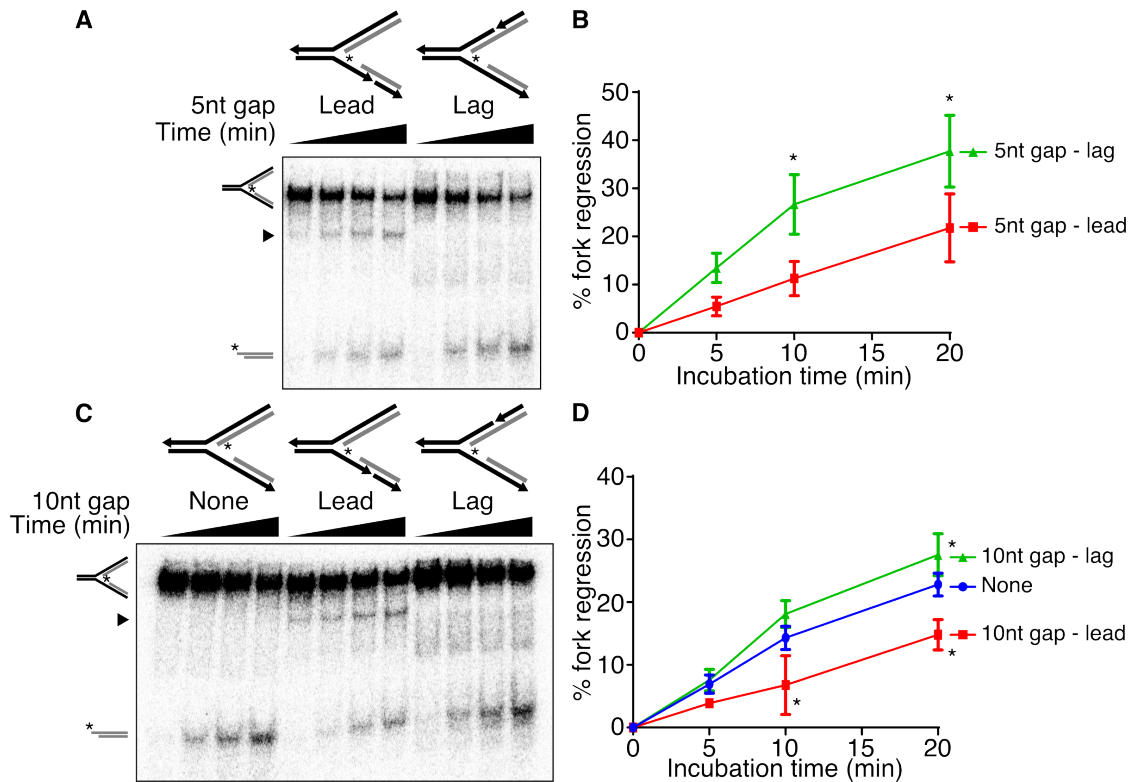


Figure 5.2 5nt and 10nt Gaps on the Leading Template Strand Inhibit SMARCAL1 Fork Regression Activity. (A-B) Leading gap substrates (3nM) containing a 5nt gap on the leading (“Lead”) or lagging (“Lag”) template strand were incubated with SMARCAL1 (3nM) at 30°C for 5, 10, or 20 minutes. DNA products were analyzed by native gel electrophoresis (A) and phosphorimager quantitation (B). (C-D) Leading gap substrates (3nM) containing a 10nt gap on the leading (“Lead”) or lagging (“Lag”) template strand or unmodified substrate (“None”) were incubated with SMARCAL1 (3nM) at 30°C for 5, 10, or 20 minutes. DNA products were analyzed by native gel electrophoresis (C) and phosphorimager quantitation (D). (A, C) Arrow indicates alternative product that likely lacks leading nascent strand and the smaller leading template fragment. (B, D) Graphs represent mean and standard deviation of 3 replicates. (* $p < 0.05$). Oligos: (No mod) LeadP122 + LagP122 + LeadD52 + LagG82; (Lead 5/10nt gap) LeadP79 + LeadP38/LeadP33 + LagP122 + LeadD52 + LagG82; (Lag nick/gap) LeadP122 + LagP38/LagP33 + LagP79 + LeadD52 + LagG82.

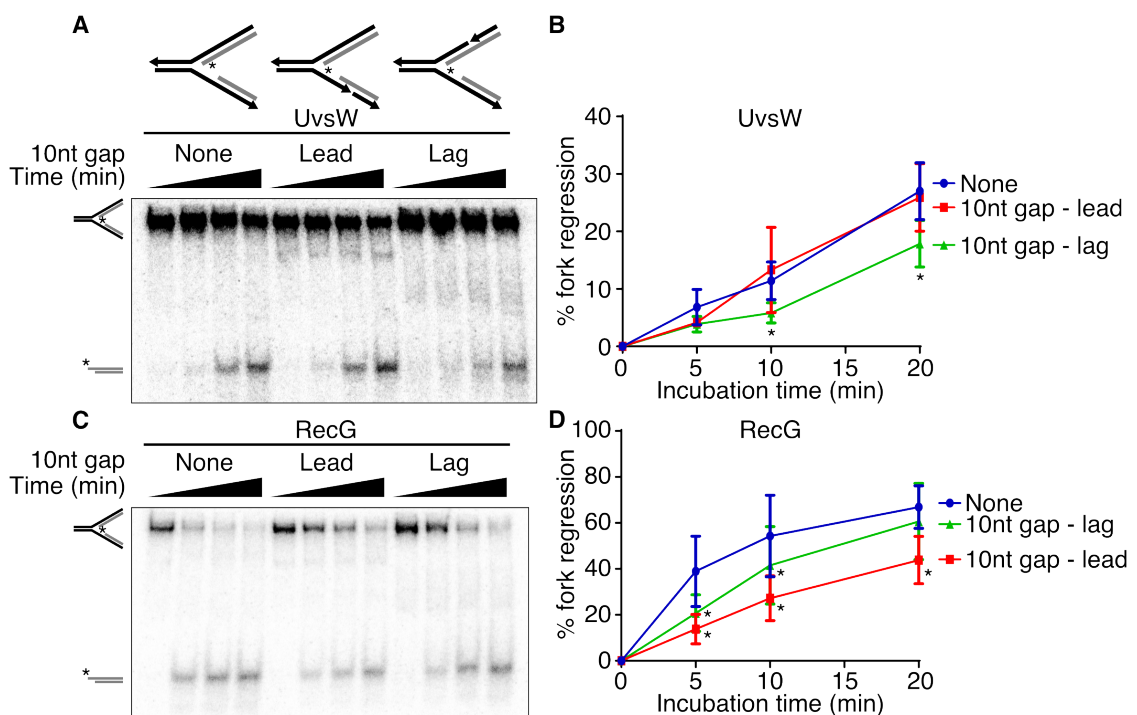


Figure 5.3 Effects of 10nt Template Strand Gaps on UvsW and RecG Fork Regression Activity. Leading gap substrates (3nM) containing a 10nt gap on the leading (“Lead”) or lagging (“Lag”) template strand or unmodified substrate (“None”) were incubated with UvsW (3nM; A-B) or RecG (50pM; C-D) at 30°C for 5, 10, or 20 minutes. DNA products were analyzed by native gel electrophoresis (A, C) and phosphorimager quantitation (B, D). (B, D) Graphs represent mean and standard deviation of 3 replicates. (* $p < 0.05$). Oligos: (No mod) LeadP122 + LagP122 + LeadD52 + LagG82; (Lead 5/10nt gap) LeadP79 + LeadP38/LeadP33 + LagP122 + LeadD52 + LagG82; (Lag nick/gap) LeadP122 + LagP38/LagP33 + LagP79 + LeadD52 + LagG82.

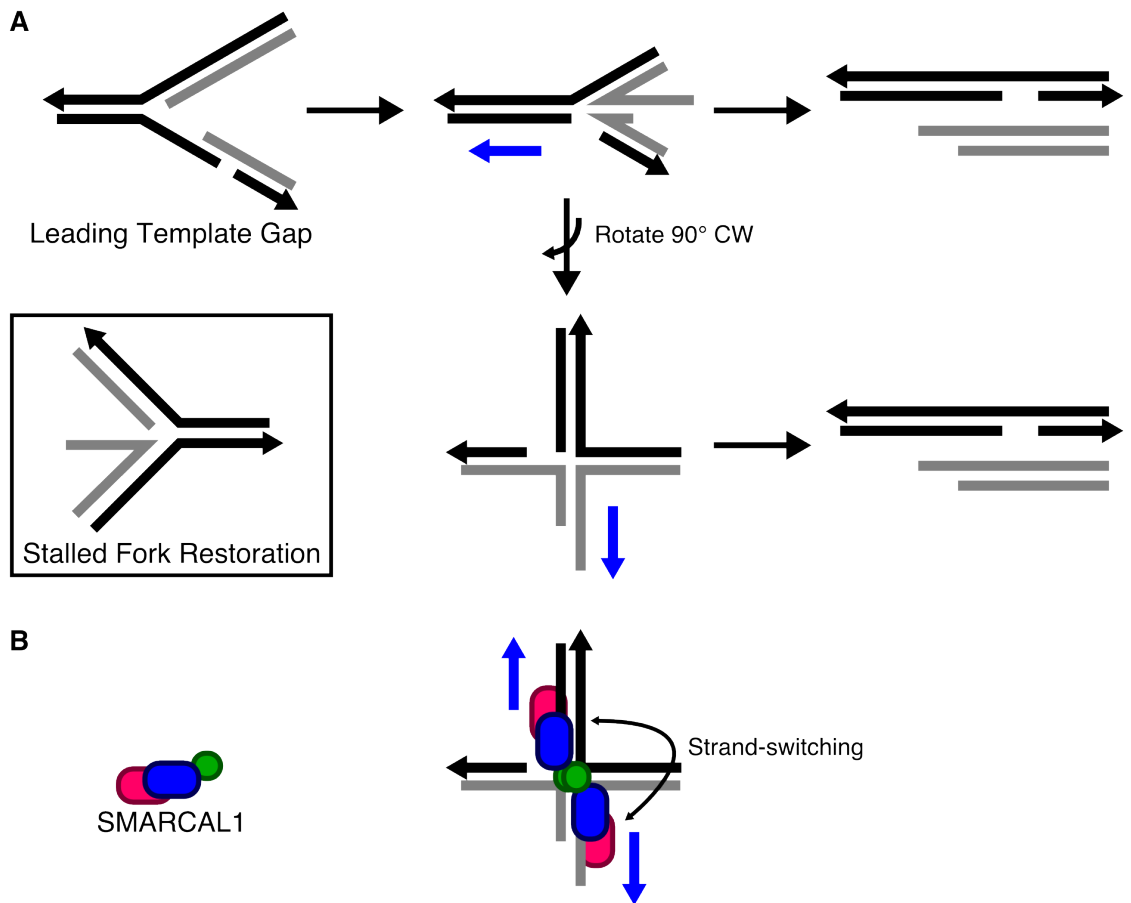


Figure 5.4 Gapped fork regression intermediate resembles fork restoration substrate and SMARCAL1 strand switching. (A) A stalled fork regression substrate with a leading-strand template gap can be regressed until the gap on the template strand reaches the fork junction by SMARCAL1 applying force in the direction of the blue arrow. Continued movement in this direction results in product formation by fork regression. However, by rotating this intermediate 90° clockwise and splaying the arms, we can see that this intermediate resembles the stalled fork restoration substrate (Bétous et al. 2013). If SMARCAL1 applies force in the direction of the blue arrow, translocating on the nascent duplex, the same products are formed from a fork restoration reaction. (B) SMARCAL1 may change strands during regression of these substrates. SMARCAL1 translocation in either orientation shown will produce the same products. As in panel A, blue arrows indicate direction of force exerted on DNA.

Development of a Biotin-Streptavidin Block Assay

Another method used to determine translocation polarity is using a biotin-streptavidin block (Fu et al. 2011; Nelson et al. 2009). Therefore, we constructed substrates containing biotinylated nucleotides. First, we removed the ssDNA at the fork junction to eliminate ssDNA position as a variable. SMARCAL1 binds poorly to fork junctions without ssDNA (Bétous et al. 2012). Therefore, we reduced the size of the substrates from 122 to 62 nucleotides; thus, annealing of only 42 nucleotides, rather than 82 nucleotides, is required to form the products. To add biotin moieties, we constructed substrates containing a nick on either template strand and biotin on either the 5' or 3' end of these nicks.

We tested SMARCAL1 activity on these substrates and found that the nick alone inhibited SMARCAL1 activity, and in no case did addition of streptavidin to the substrate further inhibit SMARCAL1 activity (Fig. 5.5). We reasoned that this inhibition may arise due to the lower affinity of SMARCAL1 for three-way junctions lacking ssDNA combined with some affinity of SMARCAL1 to bind directly to the nick itself instead of the junction (Bétous et al. 2012). To test this hypothesis, we added nicked dsDNA to a reaction containing the unmodified substrate. Indeed, the nicked dsDNA inhibited the reaction (Fig. 5.6), suggesting that the presence of a nick titrates SMARCAL1 away from productive binding to the fork junction.

To eliminate these nicks, we constructed substrates that contain biotin-11-deoxyuridine in the leading, lagging, or both template strands. We tested SMARCAL1 activity on these substrates in the presence and absence of streptavidin. We observed that biotin placed on either the leading or lagging strand was sufficient to inhibit SMARCAL1 activity approximately two-fold, and placing biotin on both strands further inhibited SMARCAL1 another two-fold (Fig. 5.7B-C). This suggests that

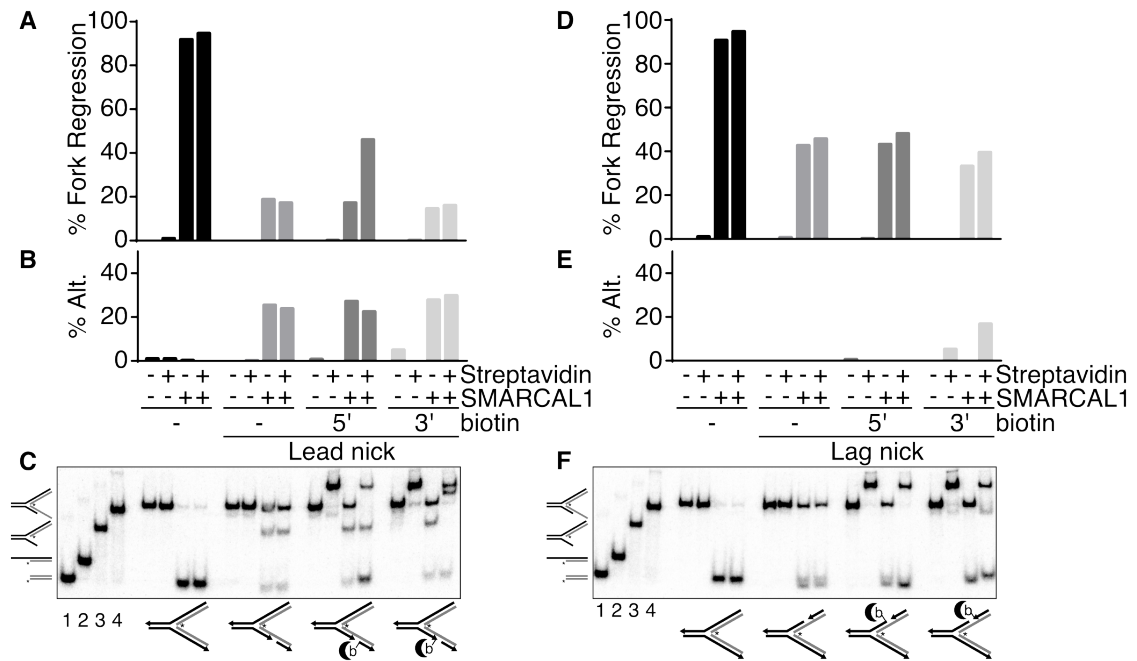


Figure 5.5 Substrates Containing Biotinylated Nicks Inhibit SMARCAL1 Activity.

(A-C) Small, no-gap (sNG) substrates (3nM) containing no modification (“-”), a leading strand nick (“Lead nick, -”), a 5'-biotinylated leading strand nick (“Lead nick, 5'”), or a 3'-biotinylated leading strand nick (“Lead nick, 3'”) were incubated in the presence or absence of streptavidin (12nM) for 10 minutes at room temperature. SMARCAL1 (12nM) was added to the reaction and further incubated for 1 hour at 37°C. DNA products were analyzed by native gel electrophoresis (C) and phosphorimager quantitated (A-B). % Fork Regression is the ratio of product formed to total radioactivity in the lane (A), % Alt. Product is the ratio of intermediate sized products to the total radioactivity in the lane (B). (C) Lanes 1-4 contain markers that correspond to the reaction product (nascent-nascent duplex) and several possible alternative products that retain the labelled DNA strand. (D-F) The same as (A-C) except that the substrates used contained no modification (“-”), a lagging strand nick (“Lag nick, -”), a 5'-biotinylated lagging strand nick (“Lag nick, 5'”), or a 3'-biotinylated lagging strand nick (“Lag nick, 3'”). Data shown are representative of 2 independent experiments (each n=1). Oligos: (No mod) LeadP62 + LagP62 + LeadN42 + LagN42; (Leading nick) LeadP42/LeadP42-3b + LeadP20/LeadP20-5b + LeadN42 + LagN42; (Lagging nick) LeadP62 + LagP42/LagP42-5b + LagP20/LagP20-3b + LeadN42 + LagN42.

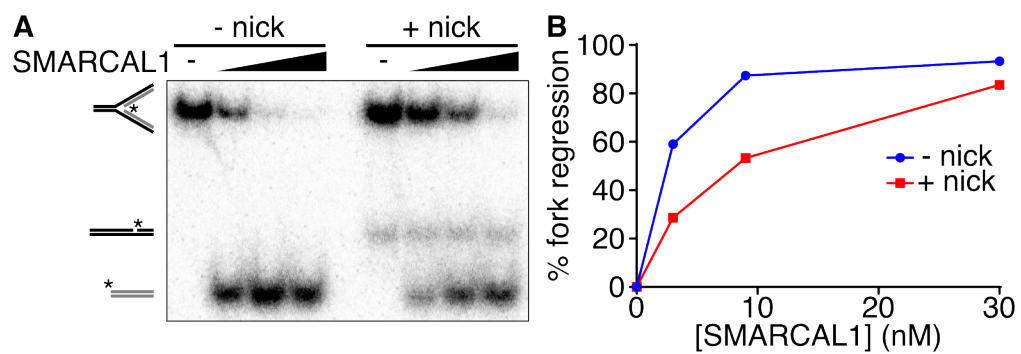


Figure 5.6 Nicked Duplex DNA Inhibits SMARCAL1 activity on No Gap Fork Regression Substrates. No gap substrates (3nM) were incubated in the presence or absence of nicked duplex DNA (“nick”) (3nM) with increasing amounts of SMARCAL1ΔN (0, 3, 9, 30nM) for 1 hour at 37°C. DNA products were analyzed by native gel electrophoresis (A) and phosphorimager quantitation (B). Data shown is a single experiment (n=1). Oligos: (No gap substrate) LeadP62 + LagP62 + LeadN42 + LagN42; (nicked duplex) LeadP42 + LeadP20 + LagP62.

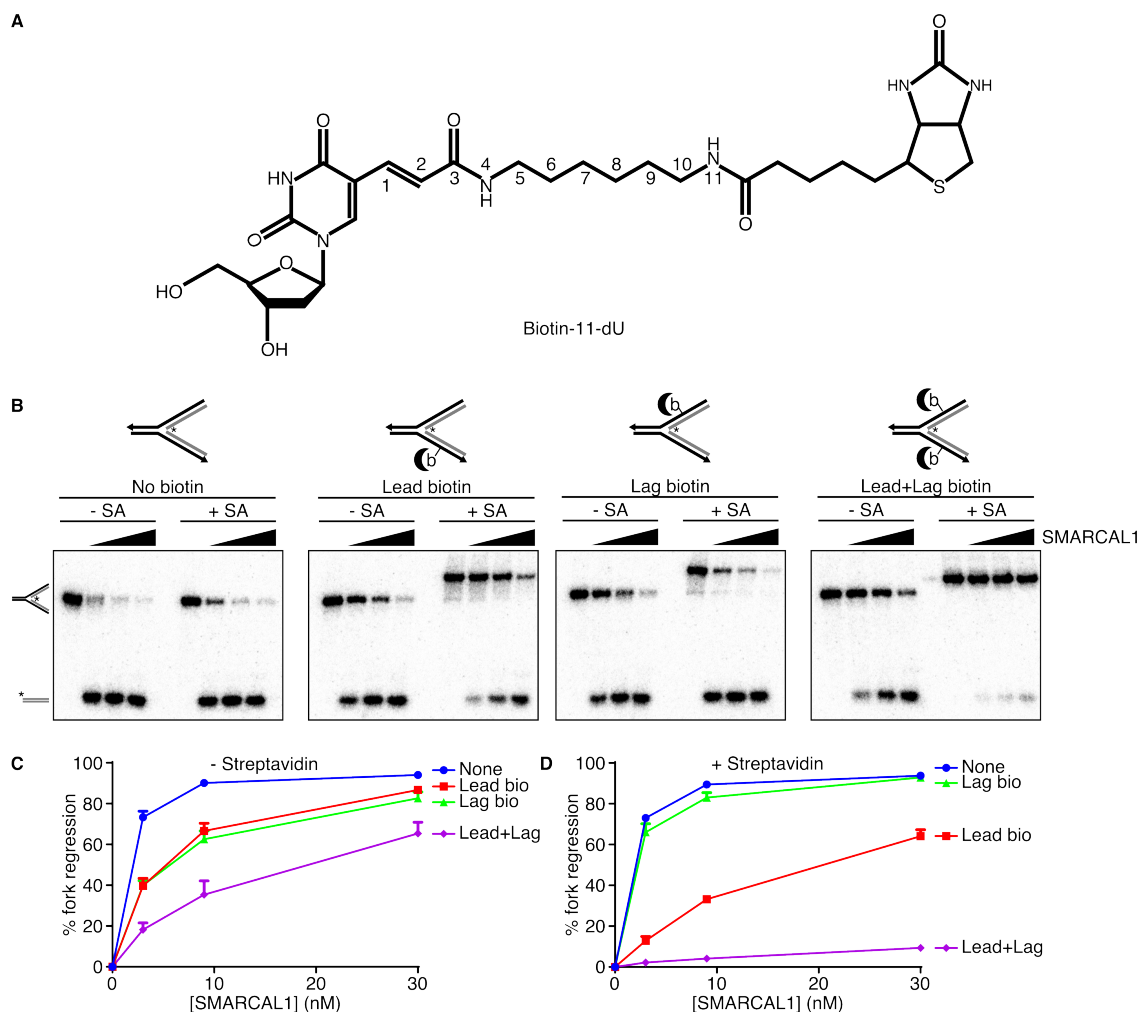


Figure 5.7 Substrates Containing Biotin-dU Bind to Streptavidin Inhibit SMARCAL1 Fork Regression Activity. (A) Chemical structure of Biotin-11-dU. “11” indicates the linker size between uridine and biotin. (B-D) No-gap substrates (3nM) containing no modification (“-”), leading strand biotin-dU (“Lead”), lagging strand biotin-dU (“Lag”), or both (“Lead+Lag”) were incubated in the absence (C) or presence (D) of streptavidin (12nM) for 10 minutes at room temperature. Increasing amounts of SMARCAL1 Δ N (0, 3, 9, 30) were added to the reaction and further incubated for 1 hour at 37°C. DNA products were analyzed by native gel electrophoresis (B) and phosphorimager quantitation (C-D). Graphs represent mean and standard deviation of 3 replicates. Oligos: LeadP62/LeadP62-ib + LagP62/LagP62-ib + LeadN42 + LagN42.

SMARCAL1 may be generally sensitive to base modifications in the major groove of DNA.

When we bound streptavidin to these substrates, SMARCAL1 activity was further inhibited by biotin-streptavidin on the leading template strand, but the addition of streptavidin relieved the inhibitory effect of biotin on the lagging template strand. I don't know why this occurs. Perhaps streptavidin binding causes the base to flip out into solution and no longer occludes the major groove. The presence of biotin-streptavidin on both strands resulted in nearly complete inhibition of SMARCAL1 (Fig. 5.7B and 5.7D). However, this substrate has increased electrophoretic mobility compared to the singly biotinylated substrates bound to streptavidin. Likely, streptavidin cross-links the two strands – a single streptavidin tetramer binds both biotin moieties – and SMARCAL1 cannot break the streptavidin intramolecular interactions to generate products.

To test for streptavidin-specific effects, we repeated these experiments using avidin. Using a time course, we obtained similar results. In this case, avidin bound to both strands inhibited SMARCAL1 only slightly more than avidin bound to the leading strand alone. This suggests that this effect is an artifact of streptavidin (Fig. 5.8). The multiple avidin-bound substrate bands likely reflects either avidin tetramers bound to multiple substrates or multiple oligomerization states of avidin (monomer, dimer, tetramer). As with streptavidin, avidin binding relieved the inhibitory effect of lagging strand biotin on SMARCAL1 activity.

Next, we tested ZRANB3 in this assay. Like SMARCAL1, biotin-avidin bound to the leading strand or both strands strongly inhibited ZRANB3 activity. However, biotin-avidin bound to the lagging strand had an intermediate effect on ZRANB3 (Fig. 5.9). As with SMARCAL1 and ZRANB3, biotin-avidin bound to both strands nearly completely inhibited RecG activity in this assay. However, unlike SMARCAL1 and ZRANB3, RecG was only modestly inhibited by biotin-avidin on either strand alone (Fig.

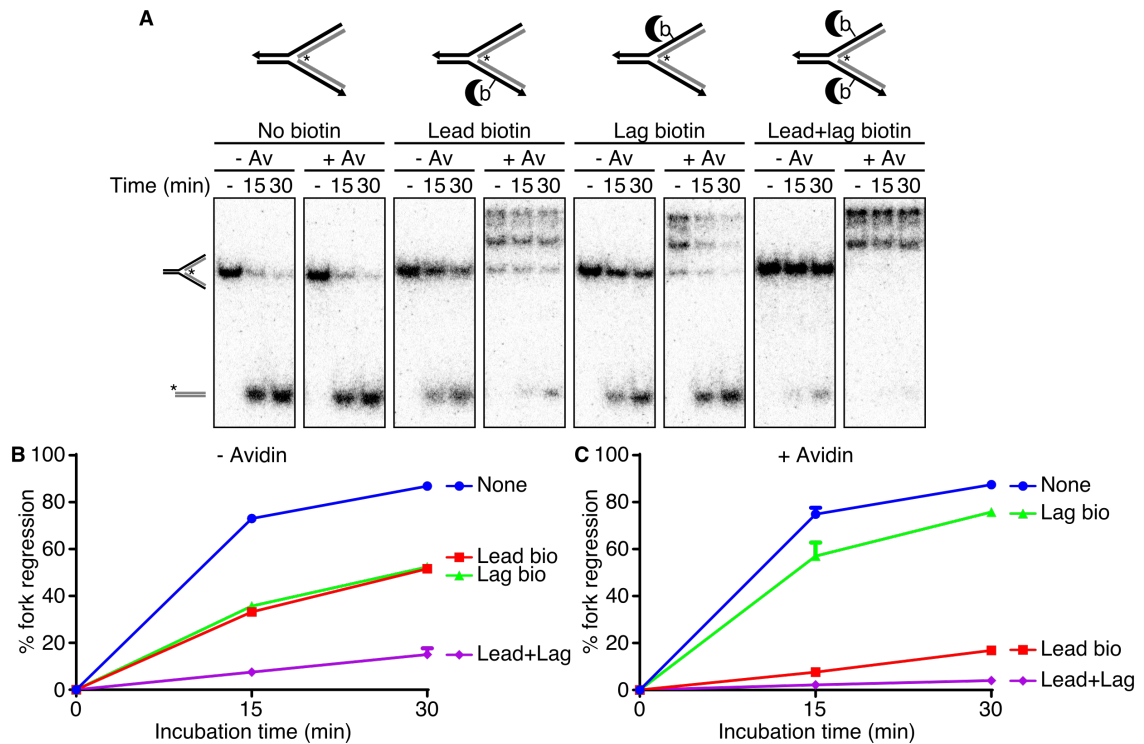


Figure 5.8 Substrates Containing Biotin-dU Bound to Avidin Inhibit SMARCAL1 Fork Regression Activity. No-gap substrates (3nM) containing no modification (“-”), leading strand biotin-dU (“Lead”), lagging strand biotin-dU (“Lag”), or both (“Lead+Lag”) were incubated in the absence (B) or presence (C) of avidin (12nM) for 10 minutes at room temperature as indicated. SMARCAL1ΔN was added to 9nM to the reaction and further incubated for 15 or 30 minutes at 37°C. DNA products were analyzed by native gel electrophoresis and phosphorimager quantitation. Bars represent mean and standard deviation of 3 replicates. Oligos: LeadP62/LeadP62-ib + LagP62/LagP62-ib + LeadN42 + LagN42.

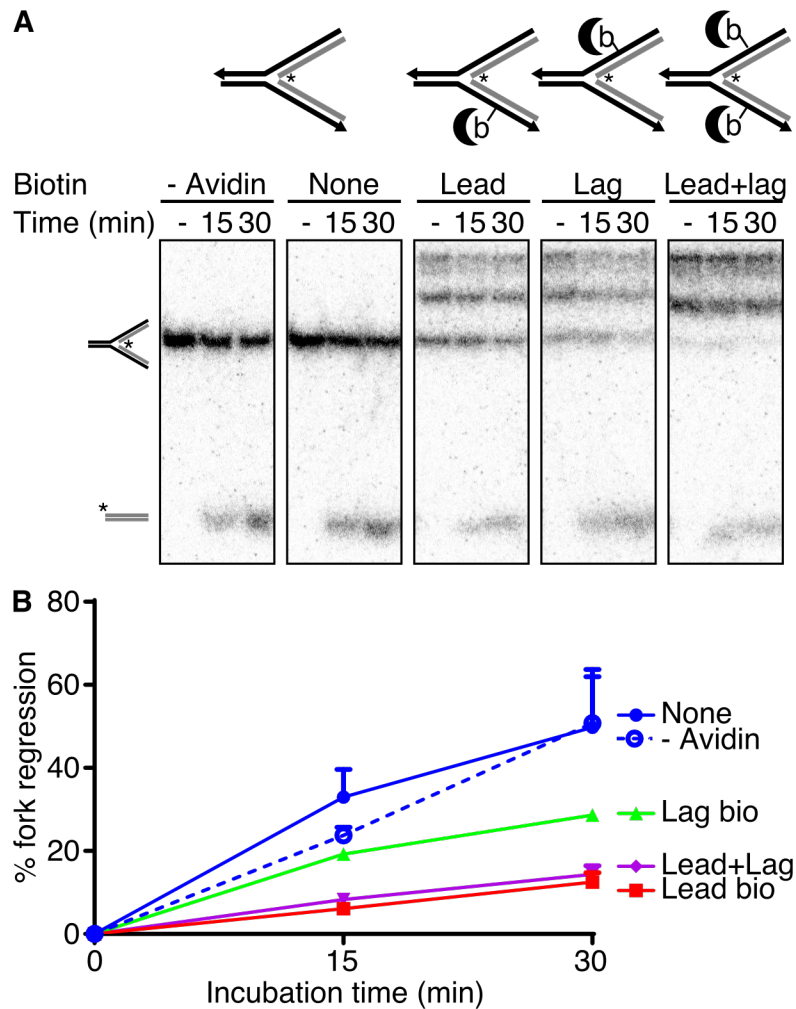


Figure 5.9 Substrates Containing Biotin-dU Bound to Avidin Inhibit ZRANB3 Fork Regression Activity. No-gap substrates (3nM) containing no modification (“-”), leading strand biotin-dU (“Lead”), lagging strand biotin-dU (“Lag”), or both (“Lead+Lag”) were incubated in the absence (B) or presence (C) of avidin (12nM) for 10 minutes at room temperature as indicated. ZRANB3 was added to 3nM to the reaction and further incubated for 15 or 30 minutes at 37°C. DNA products were analyzed by native gel electrophoresis and phosphorimager quantitation. Bars represent mean and standard deviation of 3 replicates. Oligos: LeadP62/LeadP62-ib + LagP62/LagP62-ib + LeadN42 + LagN42.

5.10). Finally, we tested UvsW. As with SMARCAL1 and ZRANB3, leading strand biotin-avidin strongly inhibited UvsW, while biotin-avidin on the lagging strand had an intermediate effect. Again, biotin-avidin bound to both strands resulted in nearly complete inhibition (Fig. 5.11). The common pattern of these results is that biotin-avidin bound to the leading strand has a stronger effect than biotin-avidin bound to the lagging strand, and SMARCAL1, ZRANB3, and UvsW are more sensitive to these modifications than RecG.

Discussion

Previous studies suggested that RecG and UvsW bind and translocate along the dsDNA backbone and make contact with both template DNA strands during fork regression. Nuclease protection assays and reversed polarity experiments suggest that RecG may bind and track along both strands (Manosas et al. 2013; Tanaka and Masai 2006), though perhaps with a preference for 3' → 5' translocation (Whitby et al. 1994). UvsW likely also contacts both strands, though mechanical force may only be applied to the 3' → 5' (lagging) strand (Manosas et al. 2013; Nelson et al. 2009). Our results with fork regression substrates containing a 10 nucleotide gap on either the leading or lagging template strand are consistent with such a model: RecG is inhibited by a gap placed on either template strand, and UvsW is only inhibited when the gap is on the lagging (3' → 5') template strand (Fig. 5.3).

Our previous report demonstrated that SMARCAL1 protects the leading strand in nuclease protection assays (Bétous et al. 2013). Reversed polarity experiments were consistent with SMARCAL1 binding to the leading strand upstream of the fork junction (Maria Manosas, unpublished observations). Consistent with a 5' → 3' translocation polarity for SMARCAL1, both 5-10 nucleotide gaps inhibit SMARCAL1 when placed on the leading (5' → 3') template strand (Fig. 5.2).

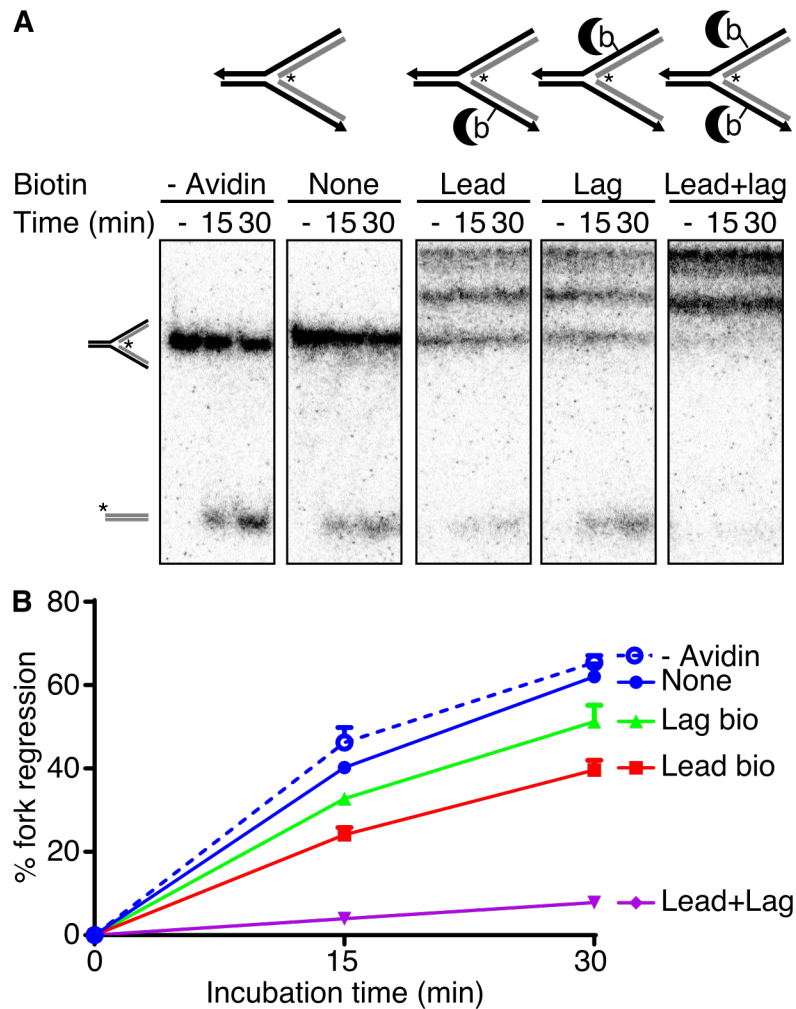


Figure 5.10 Substrates Containing Biotin-dU Bound to Avidin Inhibit RecG Fork Regression Activity. No-gap substrates (3nM) containing no modification (“-”), leading strand biotin-dU (“Lead”), lagging strand biotin-dU (“Lag”), or both (“Lead+Lag”) were incubated in the absence (B) or presence (C) of avidin (12nM) for 10 minutes at room temperature as indicated. RecG was added to 15pM to the reaction and further incubated for 15 or 30 minutes at 37°C. DNA products were analyzed by native gel electrophoresis and phosphorimager quantitation. Bars represent mean and standard deviation of 3 replicates. Oligos: LeadP62/LeadP62-ib + LagP62/LagP62-ib + LeadN42 + LagN42.

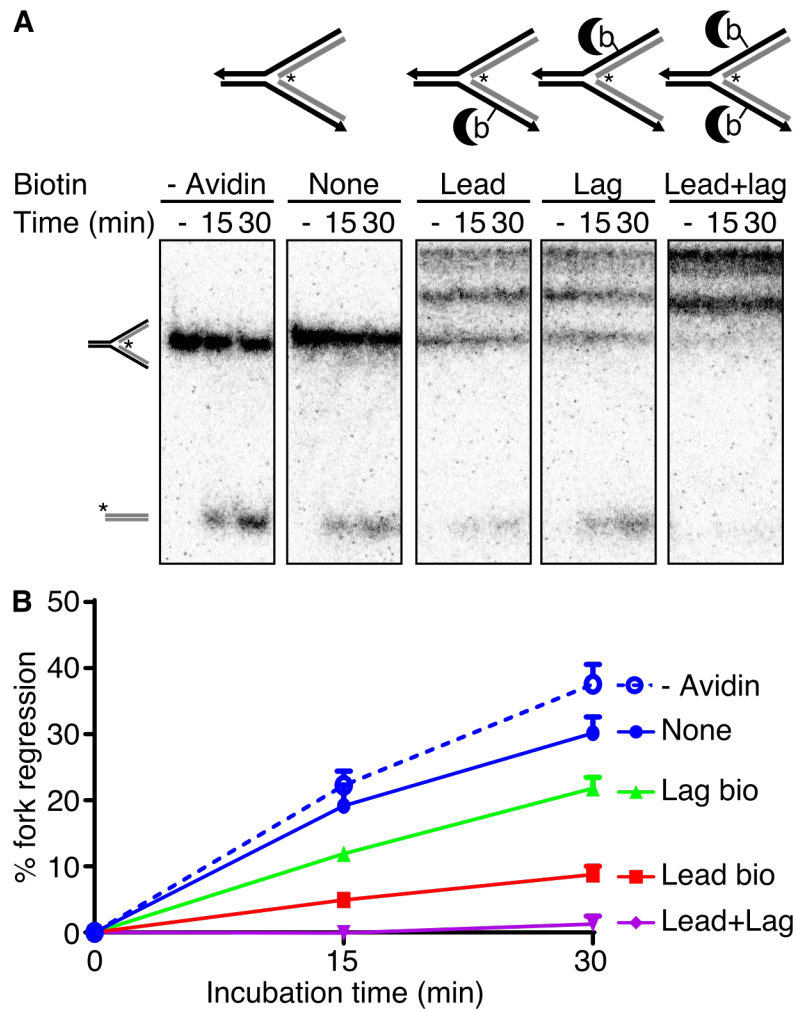


Figure 5.11 Substrates Containing Biotin-dU Bind to Avidin Inhibit UvsW Fork Regression Activity. No-gap substrates (3nM) containing no modification (“-”), leading strand biotin-dU (“Lead”), lagging strand biotin-dU (“Lag”), or both (“Lead+Lag”) were incubated in the absence (B) or presence (C) of avidin (12nM) for 10 minutes at room temperature as indicated. UvsW was added to 0.5nM to the reaction and further incubated for 15 or 30 minutes at 37°C. DNA products were analyzed by native gel electrophoresis and phosphorimager quantitation. Bars represent mean and standard deviation of 3 replicates. Oligos: LeadP62/LeadP62-ib + LagP62/LagP62-ib + LeadN42 + LagN42.

A Helicase Activity for SMARCAL1?

When tested on no-gap substrates containing a nick on the leading template strand, SMARCAL1 activity produced an “alternative” product with an electrophoretic mobility similar to the substrate without the leading nascent strand. How this product forms is a mystery; however, one possibility is that SMARCAL1 changes strands during branch migration across a nick. For example, SMARCAL1 may translocate on the template strands until reaching the nick, then switch to the nascent strands to continue the same annealing reaction. Maria Manosas recently demonstrated in single molecule assays that UvsW and RecG switch strands during translocation (Manosas et al. 2013). It is possible that SMARCAL1 can perform similar strand switching (Fig. 5.4B).

Switching to one of the template-nascent duplex arms may yield the 'alternative' product, but this does not fully explain the appearance of this product. SMARCAL1 has no reported helicase activity, and formation of this product requires unwinding of a short sequence. There is some independent indication that on partial-X junction substrates, SMARCAL1 may perform limited unwinding of the parental duplex (Aaron Mason and Brandt Eichman, unpublished observations). This suggests that SMARCAL1 may have cryptic helicase activity on complex substrates such as partial-X junctions.

Avidin bound substrates reveal commonalities between fork regression enzymes

Our results with avidin blocks showed that all four enzymes tested are more sensitive to a block on the leading strand compared to the lagging strand (Figs. 5.8, 5.9, 5.10, 5.11). Because this result does not match the reported translocation polarity of UvsW and RecG, this suggests that this assay does not, in fact, measure translocation polarity. This is not too surprising, since unlike nicks, gaps, and 5' or 3' biotinylation, the internal biotin modifications reside in the major groove of DNA, not on the backbone. Instead, this assay may tell us something about a common mechanism of fork

regression for these enzymes. Perhaps the substrate specificity domains make more extensive contacts with the leading strand than the lagging strand. In any case, the SWI/SNF family members SMARCAL1, ZRANB3, and UvsW have very similar activities in this assay, while the non-SWI/SNF RecG is less sensitive overall to modifications.

It will be interesting to follow up this study with DNA footprinting assays using hydroxyl-radical cleavage to map both dsDNA and ssDNA protection by these enzymes. If the internal biotin-avidin assay is really measuring something about how the substrate specificity domains bind, we would anticipate greater protection of leading strand ssDNA compared to lagging strand ssDNA. Since we lack any footprinting data for ZRANB3, this would give us an indication for whether ZRANB3 protects the leading or lagging template strand. This is especially interesting given that that on naked DNA substrates, SMARCAL1 and ZRANB3 have similar substrate preferences with respect to the orientation of ssDNA at a replication fork-like junction (Bétous et al. 2013).

Function of Annealing Helicases in Replication

On naked DNA substrates, RecG and SMARCAL1 have opposite substrate preferences with respect to the ssDNA. However, SSB and RPA stimulate RecG and SMARCAL1 activity, respectively, when bound to the leading strand. Furthermore, SSB/RPA inhibit RecG and SMARCAL1 when bound to the lagging strand (Bétous et al. 2013). This reinforces the preference of RecG for leading strand ssDNA, and flips the preference for SMARCAL1 to match RecG. As such, one hypothesis is that in cells, SMARCAL1 and RecG perform fork regression at stalled forks that have ssDNA on the leading strand.

While such careful analysis has not been carried out for UvsW, recent reports suggest that UvsW can perform fork regression to allow lesion bypass in a model T4 replication system (Manosas et al. 2012), and that UvsW may be stimulated by the T4

SSB, gp32, at least in some instances (Perumal et al. 2013). It is possible then, that the function of these divergent SF2 rewinding enzymes is conserved: to regress stalled replication forks to allow tolerance of template DNA damage.

Interestingly, ZRANB3 shares a similar SWI/SNF ATPase core with SMARCAL1 and has a similar substrate preference to SMARCAL1, but ZRANB3 fork regression is inhibited by RPA (Bétous et al. 2013). This suggests that while SMARCAL1 and ZRANB3 share a similar mode of translocation, they perform different functions in the cell. ZRANB3 localizes to stalled replication forks via an interaction with polyubiquitinated PCNA (Ciccia et al. 2012; Weston et al. 2012; Yuan et al. 2012), which is associated with damage tolerance pathways (Blastyák et al. 2007; Lin et al. 2011; Ulrich and Walden 2010; Unk et al. 2010). Further experiments may demonstrate that ZRANB3 also has a protein activator such as PCNA.

One possible model for the function of SMARCAL1 and ZRANB3 is the following: Leading strand template damage stalls the leading strand polymerase, exposing ssDNA on the leading strand. SMARCAL1 is recruited and stimulated by RPA to regress the stalled fork and allow lesion bypass by template switching. SMARCAL1 can also catalyze the reverse reaction and restore a fork that has bypassed the lesion. However, if damage occurs on the lagging strand, this will only reveal limited ssDNA, as the replication fork will likely continue after unwinding and priming another Okazaki fragment. Poly-ubiquitination of PCNA at the stalled polymerase recruits ZRANB3. Thus, ZRANB3 may assist in some step of template switching to ensure replication across the damaged area (see Fig. 6.4). ZRANB3 also contains an ATP-dependent 3'-flap endonuclease activity of unclear significance in cells (Weston et al. 2012).

Another open question is whether SMARCAL1 and ZRANB3 prefer fork regression or fork restoration, since previous analyses relied upon substrates which can only migrate in one direction (Bétous et al. 2013). To address this question, substrates

that resemble partially regressed forks could be used that can migrate in either direction (Fig. 5.12).

Conclusions

From our experiments with gapped substrates, we conclude that SMARCAL1 likely translocates 5' → 3' on the leading template strand, while UvsW uses the 3' → 5' lagging template strand. RecG likely uses both strands, though it may have some preference for 5' → 3' translocation in these assays, in distinction to previous reports. Our experiments with avidin blocks suggest similarities between the enzymes: leading strand biotin-avidin inhibited SMARCAL1, ZRANB3, RecG, and UvsW more strongly than lagging strand biotin-avidin.

Perhaps just as interesting as the substrates that block SMARCAL1 activity is those that do not: neither a nick nor a 1 nucleotide gap affected SMARCAL1 activity on a stalled fork substrate. Furthermore, while SMARCAL1 binding to nicks titrated the enzyme away from the fork junction in the no-gap assay (Fig. 5.6), the presence of biotin or streptavidin at these nicks had no effect on SMARCAL1 activity (Fig. 5.5). This suggests that SMARCAL1 could tolerate both naked single strand breaks and those covalently attached to a protein, such as a Topoisomerase I cleavage complex induced by camptothecin. Therefore, SMARCAL1 is a robust annealing helicase, capable of performing fork regression in a number of circumstances to promote genome stability.

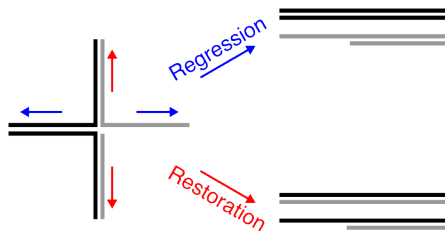


Figure 5.12 Dual Regression/Restoration Substrate Design. A substrate that resembles the fork restoration substrates from (Bétous et al. 2013) with the exception that the sequences are entirely homologous except for a few mismatches that can be strategically placed to prevent spontaneous branch migration. In this way, DNA movement along the red arrows will result in fork restoration (annealing of the ssDNA arm to the parental duplex), and movement along the blue arrows will result in fork regression (annealing of the parental-parental and nascent-nascent duplexes). Products can be distinguished by labelling both of the top strands (one parental and one nascent), thus fork restoration will result in a single band containing both labels, while fork regression results in two bands.

Nomenclature

$\overline{D^{\wedge}5G}$
type lesion

Leading gap, "stalled" fork
Lesions:
^ - nick; ^x - gap of x size
D/G - leading/lagging strand

$\overline{sNG^{\wedge}D5b}$
type lesion

Small, no-gap fork
Lesions:
^Xnb - (n) 5' or 3' biotin on nicked (X) strand
pXb - internal biotin on (D-leading/G-lagging) parental strand
pbb - internal biotin on both parental strands

Lead Gap Substrates

	D, D [^] D	LagP122	CGTCGCAGCGACGATCGCACGTCGCGAACAACCTTCAGCTGATAGACACGTGGCAATTGCCTACATG TATCCTCACACTCTGAATACGCGATATCTTAGGGTTAGGGTTAACATCAAGTCACG
	D [^] G	LagP84	TGATAGACACGTGGCAATTGCCTACATGTATCCTCACACTCTGAATACGCGATATCTTAGGGTTAG GGTTAACATCAAGTCACG
	D [^] 1G	LagP83	GATAGACACGTGGCAATTGCCTACATGTATCCTCACACTCTGAATACGCGATATCTTAGGGTTAGG GTTAACATCAAGTCACG
	D [^] 5G, [^] 10G	LagP79	GACACGTGGCAATTGCCTACATGTATCCTCACACTCTGAATACGCGATATCTTAGGGTTAGGGTTA ACATCAAGTCACG
	D [^] 5G	LagP38	CGTCGCAGCGACGATCGCACGTCGCGAACAACCTTCAGC
	D [^] 10G	LagP33	CGTCGCAGCGACGATCGCACGTCGCGAACAACCTTCAGC
	All	LagD82	TCAGAGTGTGAGGATACATGTAGGCAATTGCCACGTGTCTATCAGCTGAAGTTGTTCCGACGTGC GATCGTCGCTGCGACG
	All	LeadD52	CGTCGCAGCGACGATCGCACGTCGCGAACAACCTTCAGGTGATAGACACGTGG
	D [^] 10D	LeadP33	AGTTGTTCCGACGTGCGATCGTCGCTGCGACG
	D [^] D, [^] 1D, [^] 5D	LeadP38	CCTGAAGTTGTTCCGACGTGCGATCGTCGCTGCGACG
	D [^] 5D, [^] 10D	LeadP79	CGTGACTTGATGTTAACCCCTAACCTAAGATATCGCGTTATCAGAGTGTGAGGATACATGTAGGCA ATTGCCACGTGTC
	D [^] 1D	LeadP83	CGTGACTTGATGTTAACCCCTAACCTAAGATATCGCGTTATCAGAGTGTGAGGATACATGTAGGCA ATTGCCACGTGTCTATC
	D [^] D	LeadP84	CGTGACTTGATGTTAACCCCTAACCTAAGATATCGCGTTATCAGAGTGTGAGGATACATGTAGGCA ATTGCCACGTGTCTATCA
	D, D [^] G	LeadP122	CGTGACTTGATGTTAACCCCTAACCTAAGATATCGCGTTATCAGAGTGTGAGGATACATGTAGGCA ATTGCCACGTGTCTATCACCTGAAGTTGTTCCGACGTGCGATCGTCGCTGCGACG

Small No-Gap Substrates

	sNG, sNG [^] D ⁺	LagP62	CGGACACGTGGCAATTGCCTACATGTATCCTCACACTCTGATAACGCGATATCTTAGGGTGC
	sNG [^] G, [^] G3b	LagP42	ACATGTATCCTCACACTCTGATAACGCGATATCTTAGGGTGC
	sNG [^] G5b	LagP42-5b	/5BiosG/ACATGTATCCTCACACTCTGATAACGCGATATCTTAGGGTGC
	sNG [^] G, [^] G5b	LagP20	CGGACACGTGGCAATTGCCT
	sNG [^] G3b	LagP20-3b	CGGACACGTGGCAATTGCCT/3Bio/
	All	LagN42	ATCAGAGTGTGAGGATACATGTAGGCAATTGCCACGTGTCCG
	All	LeadN42	CGGACACGTGGCAATTGCCACATGTATCCTCACACTCTGAC
	sNG [^] D5b	LeadP20-5b	/5BiosG/GGCAATTGCCACGTGTCCG
	sNG [^] D, [^] D3b	LeadP20	GGCAATTGCCACGTGTCCG
	sNG [^] D3b	LeadP42-3b	GCACCCTAAGATATCGCGTTGTGAGAGTGTGAGGATACATGT/3Bio/
	sNG [^] D, [^] D5b	LeadP42	GCACCCTAAGATATCGCGTTGTGAGAGTGTGAGGATACATGT
	sNG, sNG [^] G ⁺	LeadP62	GCACCCTAAGATATCGCGTTGTGAGAGTGTGAGGATACATGTGGCAATTGCCACGTGTCCG
	sNGpGb	LagP62-ib	CGGACACGTGGCAATTGCC/ibioDT/ACATGTATCCTCACACTCTGATAACGCGATATCTTAGG GTGC
	sNGpDb	LeadP62-ib	GCACCCTAAGATATCGCGTTGTGAGAGTGTGAGGATACATGT/ibioDT/GGCAATTGCCACGTG TCCG

Table 5.1 Construction of Fork Regression Substrates. Lead gap substrates were constructed as previously (Bétous et al. 2013) with nicks and gaps added by substitution of LagP84/83/78 + LagP38/33 for LagP122 or LeadP84/83/78 + LeadP38/33 for LeadP122. Small no-gap substrates were prepared similarly, substituting LagP42 + LagP20/P20-3b for LagP62 and LeadP42 + LeadP20 for LeadP62. Biotin modifications were introduced by substituting biotinylated oligos where appropriate.

CHAPTER VI

DISCUSSION and FUTURE DIRECTIONS[†]

Summary

Human cells must faithfully duplicate billions of base pairs of DNA every cell division cycle. Insufficient precursors, template DNA damage, and difficult to replicate sequences cause replication fork stalling. Even in the best of circumstances hundreds of forks may stall during each S-phase in a human cell and the frequency increases in cells exposed to genotoxic or oncogenic stresses. Cells must resolve these stalled replication forks to complete DNA synthesis, as failure to do so leads to mutations or cell death. Given its importance, multiple pathways exist to recover stalled replication forks including stabilization and restart, repriming and post-replicative repair, template switching, and double-strand break (DSB)-mediated recovery (Yeeles et al. 2013). However, much remains to be learned about these mechanisms and how they coordinate to successfully replicate the genome trillions of times during a human lifetime.

The most important regulator of replication stress responses is the ATR kinase, which phosphorylates hundreds of substrates and is essential for every round of cell division. Many cancer cells have an elevated survival requirement for ATR function, making ATR a good drug target for cancer therapy (Toledo et al. 2011a). In addition, ATR inhibition hypersensitizes cells to many chemotherapeutic agents that work by damaging DNA or interfering with DNA replication.

While I have worked on three very different projects during my dissertation, the overarching theme is to understand how cells protect stalled replication forks. In chapter

[†] Portions of this chapter will be published in (Couch and Cortez 2014).

III, I collaborated with Bianca Sirbu to conduct time-dependent analyses of the DNA damage response at stalled replication forks. In chapter IV, I collaborated with a number of other scientists to elucidate one mechanism by which ATR stabilizes stalled replication forks: phosphorylation of SMARCAL1. In chapter V, I explored further how annealing helicases, especially SMARCAL1, perform fork regression.

iPOND and the DNA Damage Response

iPOND is a useful tool to study protein dynamics at stalled replication forks

Bianca developed iPOND to study proteins that accumulate at replication forks. Using iPOND, we found that a switch occurs in the replication stress response after 2-4 hours of HU treatment. This switch results in accumulation of the KU heterodimer, MRE11, and RAD51. Furthermore, RAD51 accumulation is dependent on MRE11 nuclease activity.

The function of RAD51 at replication forks is an interesting topic. RAD51 likely performs multiple, temporally distinct functions at stalled forks (Petermann et al. 2010). In the absence of RAD51, transiently stalled replication forks are more likely to collapse, unable to resume synthesis (Petermann et al. 2010). RAD51 deficient cells accumulate MRE11-dependent gaps behind replication forks (Hashimoto et al. 2010), and MRE11 degrades the newly synthesized DNA strands in the absence of RAD51 (Schlacher et al. 2011). However, recent reports also suggest that MRE11 is required for full activation of ATR, at least in some circumstances (Duursma et al. 2013; Lee and Dunphy 2013).

The key to understanding this paradox may be our observation that RAD51 recruitment to persistently stalled replication forks is MRE11-dependent (Sirbu et al. 2011). MRE11 has both endonuclease and 3' → 5' exonuclease activities (D'Amours and Jackson 2002). RAD51 is required for fork restart during short HU treatments

(Petermann et al. 2010), and RAD51 recruitment to these forks appears to be MRE11-independent (Sirbu et al. 2011). However, after 2-4 hours of HU treatment, RAD51 accumulates to a greater degree in an MRE11-dependent manner. This may reflect a change in the underlying DNA structure, such as fork regression, where some amount of MRE11-dependent processing is required to load RAD51. RAD51 loading prevents excess degradation of the nascent strands by MRE11 (Hashimoto et al. 2010; Schlacher et al. 2012). Finally, HU treatments in excess of 18 hours produce DSBs, and while RAD51 accumulates at these stalled forks, the forks are unable to resume synthesis (Petermann et al. 2010). This suggests that RAD51 may mediate strand invasion to await rescue of the stalled fork from a nearby origin without re-replicating the region behind the stalled fork (Fig. 6.1).

We also demonstrated that γ H2AX spreads away from the site of replication fork stalling to encompass a large chromatin domain, likely tens of thousands of base pairs in size. We determined that ATR catalyzes the initial H2AX phosphorylation at the replication fork and the early spreading into the surrounding chromatin, and that at later timepoints, ATM/DNA-PK activity are critical for γ H2AX spreading in the surrounding chromatin. ATR inhibition results in hyper-phosphorylation of H2AX and a pan-nuclear γ H2AX phenotype. Kamakoti Bhat, another graduate student in the lab, and I demonstrated that this pan-nuclear γ H2AX phenotype is dependent on DNA-PK but not ATM. Some γ H2AX foci remain after inhibition of ATR, ATM, and DNA-PK; thus, there may be another kinase capable of catalyzing phosphorylation of H2AX-S139 (Fig. 6.2).

Building on the success of iPOND, Bianca set out to identify new replication proteins. Using iPOND coupled to mass spectrometry, she identified 290 proteins enriched at replication forks. Of those identified, only a minority had annotated functions in replication or DNA damage (Sirbu et al. 2013). Huzefa Dungrawala, a post-doctoral

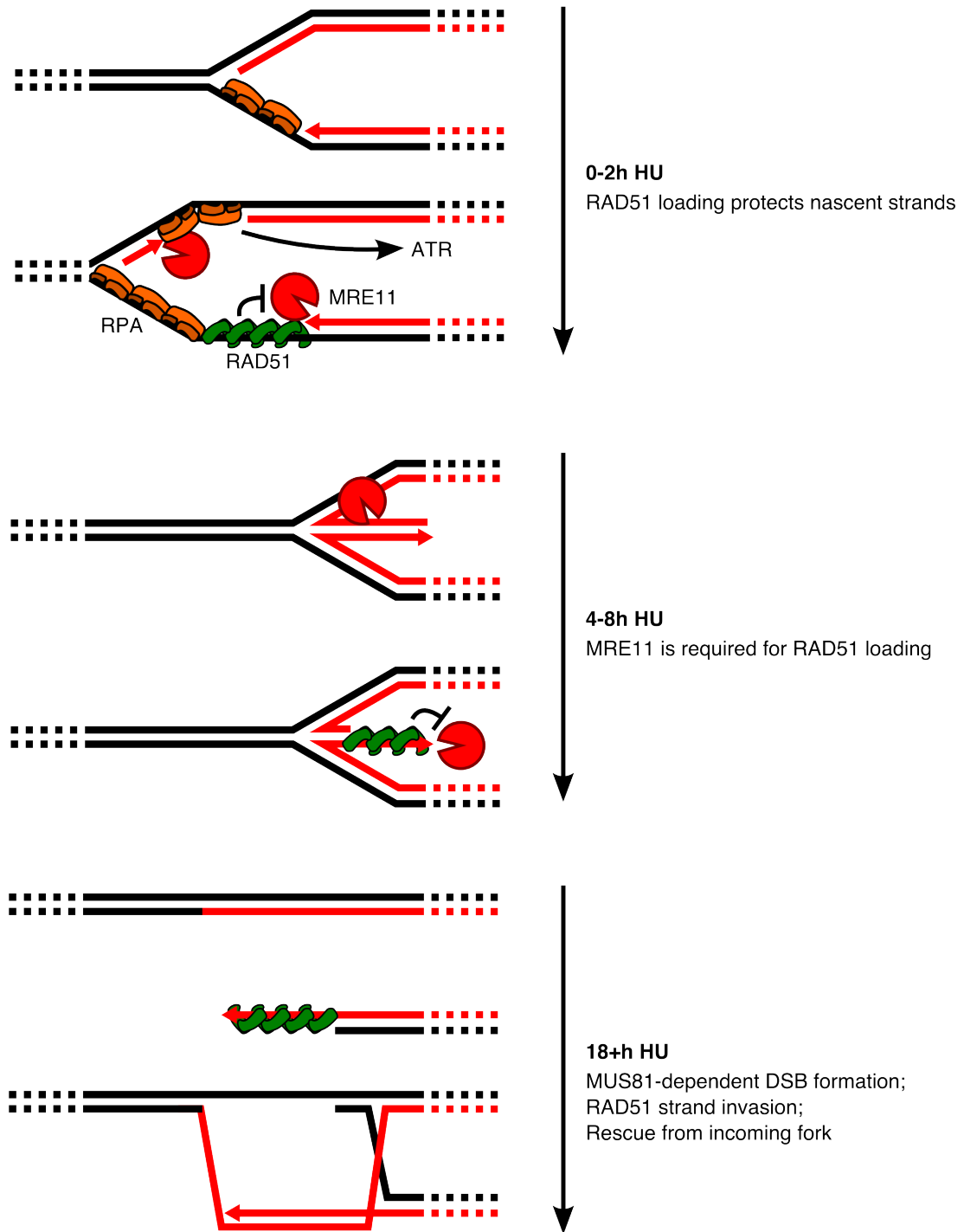


Figure 6.1 MRE11 and RAD51 interplay at stalled replication forks. At early timepoints (0-2h) in HU, MRE11 activity may have some function to promote ATR activity, while RAD51 prevents excess MRE11 degradation of the nascent strands and promotes fork restart. At intermediate times in HU (4-8h), some fork remodeling may occur that requires some MRE11 activity for RAD51 recruitment. At later times in HU (>18h), MUS81-dependent DSBs occur. RAD51 likely promotes strand invasion to await rescue from a nearby origin.

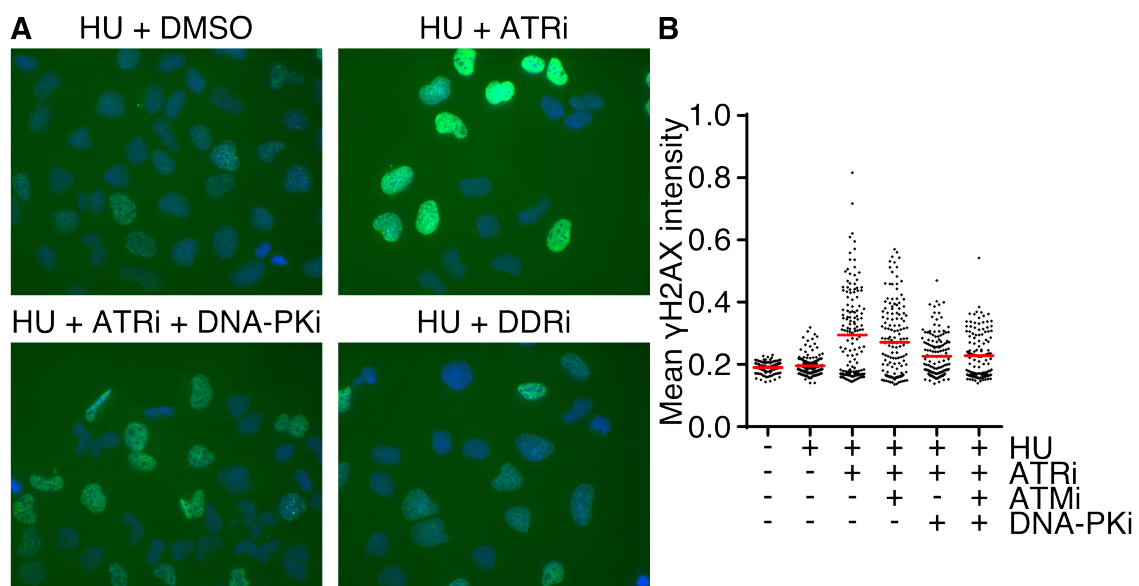


Figure 6.2 ATRi-induced pan-nuclear γ H2AX is DNA-PK-dependent. U2OS cells were treated for 4h with 3mM HU in the presence or absence of 5 μ M ATRi (VE-812 Reaper et al. 2011), 2 μ M ATMi (KU55933 Hickson et al. 2004), 2 μ M DNA-PKi (NU7441 Leahy et al. 2004), or all three together (DDRi = ATRi + ATMi + DNA-PKi) before preparation for immunofluorescence using anti- γ H2AX antibodies. Dot-plot of mean γ H2AX intensity per nucleus is shown in (B).

fellow in our laboratory, is now working to improve the specificity of iPOND and further characterize the protein composition at normal, stalled, and collapsed replication forks.

The post-translational modification landscape at replication forks remains somewhat mysterious. I developed the native iPOND protocol to address this question, and the protocol was since improved (Leung et al. 2013). In theory, native iPOND coupled to mass spectrometry can identify the histone marks at replication forks and how these change over time and distance from the fork and under various conditions of DNA damage. Many of Huzefa's improvements to the iPOND protocol will apply to native iPOND and should further improve the signal-to-noise ratio of n-iPOND.

ATR Regulation of Stalled Replication Forks

ATR activity is critical to prevent replication fork collapse, a situation in which a fork is no longer competent to support DNA synthesis. But what is fork collapse at the molecular level, and how does fork collapse contribute to cell death in ATR deficient cells? These questions have been difficult to answer especially in mammalian systems since deletion of the ATR gene is cell lethal (Brown and Baltimore 2000; de Klein et al. 2000). The development of selective ATR kinase inhibitors has now allowed us and others to begin to answer these questions (Reaper et al. 2011).

As expected, stalled replication forks in ATR inhibited cells rapidly undergo collapse into DSBs (Couch et al. 2013). In addition to DSBs, ATR inhibition results in the formation of excess single-stranded DNA (ssDNA) at the fork including both the template and newly-synthesized strands (Couch et al. 2013). Origin firing is de-repressed in ATR inhibited cells, which exacerbates the aberrant DNA phenotype as these new forks likely undergo similar stalling and degradation (Fig. 6.3A). Importantly, fork collapse into DSBs and excess ssDNA is an active process mediated by SLX4- and CtIP-dependent nucleases (Couch et al. 2013; Ragland et al. 2013).

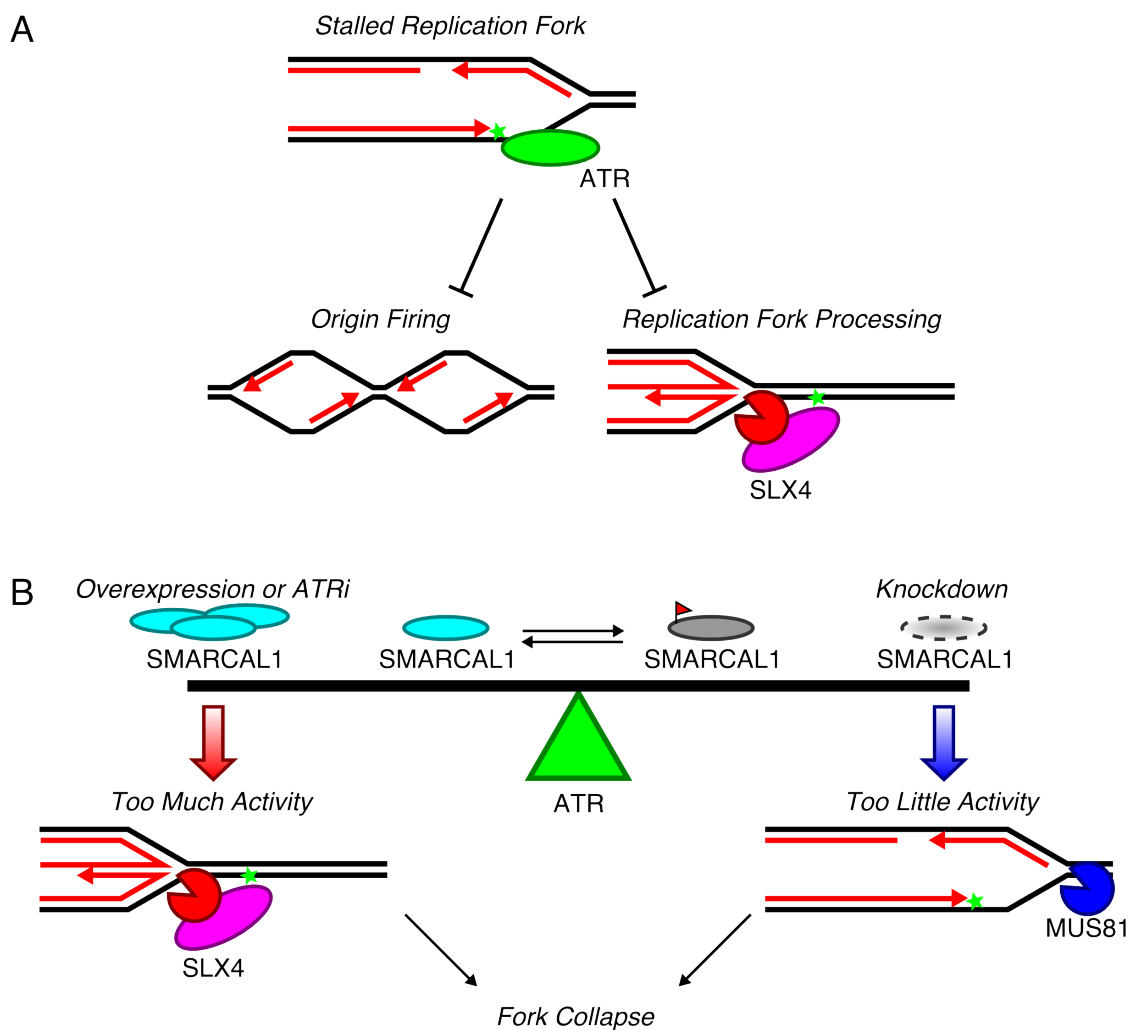


Figure 6.3 SMARCAL1 activity is a balance between too much and too little. (A) A replication fork encounters leading strand template damage (green star) which stalls the polymerase and generates ssDNA. ATR senses this ssDNA, suppresses origin firing, and prevents aberrant processing of the stalled fork. (B) ATR maintains a balance between too much and too little SMARCAL1 activity by phosphorylating SMARCAL1 on S652. Tipping the balance by either inhibiting ATR or overexpressing SMARCAL1 results in fork collapse through an SLX4-dependent cleavage. Conversely, fork collapse is MUS81-dependent when there is too little SMARCAL1 activity. The actual DNA structures that these nucleases cleave in these conditions remain to be experimentally verified.

The DNA structure at the stalled replication fork that is cleaved to create breaks is not known; however, one clue comes from our observation that the SMARCAL1 protein is also involved in the aberrant fork processing that happens in ATR-deficient cells (Couch et al. 2013). SMARCAL1 is a SWI/SNF family DNA-dependent ATPase that catalyzes branch migration of fork junctions (Bétous et al. 2012). In particular, SMARCAL1 is recruited to and active at stalled replication forks that contain ssDNA on the leading template strand (Bétous et al. 2013). On these substrates, SMARCAL1 catalyzes reversal of the replication fork into a chicken-foot structure, potentially the substrate for SLX4-dependent nucleases. SMARCAL1 is also able to catalyze the reverse reaction (fork restoration) when the nascent leading strand is longer than the nascent lagging strand so other models could be envisioned (Bétous et al. 2013).

Importantly, fork reversal is a common event in human cells and is an evolutionarily conserved mechanism of fork stabilization or repair at least in some circumstances (Atkinson and McGlynn 2009; Neelsen et al. 2013; Ray Chaudhuri et al. 2012). Furthermore, SMARCAL1 has fork repair functions important to promote restart in normal cells that have an intact ATR pathway (Bansbach et al. 2009; Ciccia et al. 2009; Yuan et al. 2009). Thus, in ATR-deficient cells, SMARCAL1 catalyzed fork remodeling leads to fork collapse, but in ATR proficient cells, SMARCAL1 maintains fork stability. This paradox is further illustrated by the observation that either too little or too much SMARCAL1 activity in cells leads to replication-associated DSBs (Bansbach et al. 2009).

The solution to this conundrum is that ATR directly regulates SMARCAL1 to maintain the balance between too much and too little SMARCAL1 activity (Fig. 6.3B). Specifically, ATR phosphorylates SMARCAL1 on S652 in a linker region between the two lobes of its ATPase domain. S652 phosphorylation happens after SMARCAL1 binds to DNA at the replication fork and inhibits its fork remodeling activities. Thus, an attractive model is that ATR ensures the right level of SMARCAL1 activity at the damaged

replication fork. Treating cells with an ATR inhibitor causes fork collapse in part because it interferes with SMARCAL1 regulation, sending stalled forks through a pathway that includes SLX4-dependent cleavage. Were this infrequent, recombination could repair the break and restart replication, but the deregulation of origin timing when ATR is inhibited multiplies the number of collapsed forks. This leads to genome-wide problems, evidenced by pan-nuclear γ H2AX staining. Furthermore, addition of replication stress to the system in the presence of an ATR inhibitor for more than 30-45 minutes ensures the cells will be unable to complete replication and die (Couch et al. 2013).

ATR and Fork Repair Pathways

The ATR-SMARCAL1 pathway is certainly not the only mechanism by which ATR prevents fork collapse and cell death. For example, ATR signaling likely regulates the integrity of the replisome proteins themselves, and both RNF4 (RING finger protein 4) and PLK1 (Polo-like kinase 1) have been implicated in this pathway (Ragland et al. 2013). Given the large number of ATR substrates and mechanisms of fork repair, ATR inactivation likely disrupts multiple pathways of fork repair and maintenance, and much remains to be understood about this critical genome maintenance activity.

One possibility is that ATR activity helps to enforce an order of events at stalled replication forks. For example, ATR may stabilize the replisome for some amount of time to allow direct restart or bypass. However, after some time has passed, some fork remodeling may occur, such as fork regression or template switching. In the absence of nucleotides, these repair pathways will also fail. As a backup, ATR may then allow controlled MUS81-dependent collapse of the replication fork into a DSB. Forks could then recover by break-induced replication, or this may simply re-form the replication fork to await rescue from a nearby origin (Fig. 6.1).

In the absence of ATR activity, lack of ordered control of these pathways produces chaos: RNF4-PLK1-dependent degradation of replisome components and SMARCAL1-SLX4-dependent collapse of the replication fork into a DSB (Couch et al. 2013; Ragland et al. 2013). Since these would also occur at any newly fired origins as well in the absence of ATR activity, there is no way to rescue these collapsed forks. Firing excess origins also depletes cellular reserves of RPA, which may also contribute to the lethality of ATR inhibition (Toledo et al. 2013). Thus, cells are unable to recover after HU treatment in the presence of the ATR inhibitor.

Future Directions

Further investigations will likely uncover additional modes of ATR regulation of stalled replication forks. Two post-doctoral fellows in our laboratory have undertaken screens that may prove informative. First, Gina Kavanaugh conducted a high-throughput immunofluorescence screen for ATR-like genes, which she defined as those genes that cause γ H2AX persistence and decreased DNA synthesis after release from hydroxyurea. Second, Kareem Mohni has conducted screens for ATR inhibitor sensitivity. This methodology appears to be especially good at identifying ATR-pathway proteins (Kareem Mohni, personal communication).

Even within the identified SMARCAL1- and SLX4-dependent pathway of ATR fork protection, open questions remain. For example, does ATR phosphorylate SLX4 normally to prevent degradation of the replication forks? Is SLX4-dependent cleavage of the replication fork only a pathogenic process or is there a physiological function for this pathway?

Frustratingly, we have been unable to easily complement SMARCAL1 phenotypes, despite publication of an assay for SMARCAL1 complementation by our lab and others (Bansbach et al. 2009; Ghosal et al. 2011). This likely stems from the

limitations of siRNA technology and exogenous protein expression. The CRISPR-Cas system has enabled efficient genome editing in mammalian cells and can create knockout and knock-in mutants with high efficiency (Cong et al. 2013; Mali et al. 2013; Wang et al. 2013a). Thus, to overcome the technical limitations of siRNA complementation, we should develop a SMARCAL1 knockout cell line and several knock-in mutants including R764Q, S652A, and S652D. These cell lines should give us definitive evidence that S652 phosphorylation is biologically relevant and not an artifact of over-expression.

Knockout cell lines have another advantage: a genetically clean system in which to study genetic interactions with other proteins in the cell. For example, SMARCAL1 and ZRANB3, when co-depleted, give a stronger phenotype than either gene depleted alone (Ciccia et al. 2012; Weston et al. 2012). However, because siRNA depletion reduces but does not eliminate function, we cannot say whether these proteins exist in the same or different pathways. A double knockout developed using CRISPR-Cas would answer this question definitively. Comparing these genetic knockouts could help identify overlapping and specialized functions of these proteins.

We have primarily limited our studies to a single DNA damaging agent, hydroxyurea. While hydroxyurea is valuable because it rapidly stalls replication forks, it may bias our discoveries of fork protection pathways. Thus, another step will be to use other drugs such as UV, MMS, and CPT, and test for replication fork stability, replisome stability, DSB formation, and of course, find the genetic and biochemical requirements for each of these.

Finally, I believe an important experiment is a genome-wide siRNA or cDNA screen for suppressors of ATR inhibitor sensitivity. This could reveal which pathways are deleterious or beneficial using siRNA and cDNA, respectively. Following up on hits from

such a screen will require exclusion of any genes that prevent cell cycle progression, as this is the most obvious mechanism of protection.

The utility of selective inhibitors to ATR and other DDR kinases is not limited to basic scientific discoveries. ATR inhibition sensitizes cells to replication stress, which is a hallmark of cancer cells. As such, several CHK1 inhibitors have entered clinical trials, and as ATR inhibitors become available, they will likely find their way into clinical trials as well (Bartucci et al. 2011; Fokas et al. 2014; Toledo et al. 2011a).

Biochemistry of Annealing Helicases

Rémy Bétous demonstrated that SMARCAL1 activity on model replication fork substrates is regulated by RPA. Namely, he determined that RPA stimulated SMARCAL1 fork regression activity on substrates that resemble stalled replication forks (leading-strand ssDNA) and inhibited SMARCAL1 activity on normal replication forks (lagging-strand ssDNA). Finally, Rémy determined that SMARCAL1 can also perform the reverse reaction, called fork restoration, by re-annealing the template-nascent duplexes of the replication fork. Moreover, RPA stimulated SMARCAL1 restoration of normal forks and inhibited SMARCAL1 restoration of stalled forks (Bétous et al. 2013).

To build on this story, I wanted to answer a biochemical question about SMARCAL1: how it translocates on DNA. Helicases and DNA translocases often track one strand of DNA with a defined directionality: 5' → 3' or 3' → 5'. For example, the related UvsW protein from T4 bacteriophage tracks ssDNA 3' → 5' (Nelson et al. 2009). SMARCAL1 requires the presence of both dsDNA and ssDNA to bind its substrates, thus answering this question is more difficult than for traditional helicases or dsDNA translocases.

Development of an assay for fork regression polarity

To develop an assay for fork regression polarity, I first modified the stalled fork substrate to contain nicks or gaps in either the leading or lagging template strand. SMARCAL1 was able to accommodate substrates containing a nick or 1nt gap without any trouble. When I extended the gap to 5 or 10 nucleotides, however, I observed that SMARCAL1 was less active when the gap was placed on the leading template strand. This suggests a step-size for SMARCAL1 of greater than 1, but less than or equal to 5 nucleotides.

Unfortunately, these substrates come with an important caveat: SMARCAL1 can bind to dsDNA with a gap, and once the gap migrates to the fork junction, SMARCAL1 can bind these substrates differently. Furthermore, it is possible, in principle, that the orientation of ssDNA at the fork junction could affect SMARCAL1 translocation. Therefore, I constructed substrates without ssDNA at the fork junction that contained a nick on either the leading or lagging template strand. I also incorporated biotin moieties on either the 5' or 3' end of those nicks. Unfortunately, a nick on these substrates inhibits SMARCAL1 by titrating the enzyme away from the fork junction. It is interesting to note, however, that in no case did addition of streptavidin to these substrates inhibit SMARCAL1 activity. Therefore SMARCAL1 can tolerate large modifications to the backbone, perhaps even Top1 cleavage complexes.

Next, I constructed substrates containing biotin-11-dU in either the leading, lagging or both template strands. Using these substrates, a biotin-avidin block on the leading strand, but not the lagging strand, inhibited SMARCAL1 activity. This suggests that SMARCAL1 translocates on the leading template strand, 5' → 3'. Unfortunately, while these data are consistent with a leading strand, 5' → 3' ssDNA translocase activity for SMARCAL1, considerations below suggest that this assay may not measure

translocation polarity. Likely, nothing short of crystal structures that capture ATPase cycle intermediates such as for NS3 (Gu and Rice 2010) will provide conclusive answers.

Comparison of SMARCAL1 and other annealing helicases

These data are not convincing or particularly useful in a vacuum. Therefore, I also tested other fork regression enzymes in this assay. ZRANB3, the closest human relative of SMARCAL1, and UvsW, a SWI/SNF family member from T4 phage, had similar preferences to SMARCAL1: they were blocked by a lesion on the leading, but not the lagging strand. RecG, an *E. coli* SF2 helicase, was less inhibited by avidin bound to only one strand, consistent with the literature which suggests that RecG can use both strands for translocation (Manosas et al. 2013; McGlynn and Lloyd 2001; Tanaka and Masai 2006). Still, RecG was inhibited more by avidin bound to the leading template strand than the lagging template strand.

This is an interesting result. It suggests that this assay does not measure translocation polarity. UvsW, which functions similarly to SMARCAL1 in this assay, is a 3' → 5' translocase (Nelson et al. 2009) – in other words, if this assay measured translocation, then a lagging strand lesion should inhibit UvsW more than a leading strand lesion. I suspect that this assay instead measures something about how the substrate specificity domains of these enzymes contact the daughter strands.

RecG has been crystallized with a replication fork junction. In that structure, the wedge domain is inserted between the two daughter strands at the fork junction and makes contacts with both daughter template strands (Singleton et al. 2001). One explanation for the results of the biotin-avidin blocks is that RecG makes contacts with both daughter strands and is thus sensitive to bulky adducts that may not pass over the wedge domain properly.

Since we lack crystal structures of UvsW, SMARCAL1, or ZRANB3 with fork DNA, we can only hypothesize that the substrate specificity domains of these enzymes also make contacts with the daughter strands. Perhaps these make more extensive contacts with the leading strand than the lagging strand, and thus are more sensitive to avidin bound to the leading strand. The HARP2 domain of SMARCAL1 is required for binding to forked DNA and can replace the MotA-like domain of UvsW (Aaron Mason and Brandt Eichman, unpublished observations). This suggests that the SMARCAL1 HARP2 domain and UvsW MotA-like domain function similarly as substrate specificity domains.

The Normal Function of Annealing Helicases

In these studies, SMARCAL1 fork regression has proved quite robust, able to tolerate small modifications to the backbone. This suggests that SMARCAL1 can perform annealing activity on a wide variety of structures *in vivo*. One limitation of these experiments is that these all used fork regression substrates. While useful because of the relative simplicity of the substrate and amenability to modification, it is unclear whether SMARCAL1 uses such a substrate in the cell.

At first blush, SMARCAL1 would seem to prefer fork regression to fork restoration. However, this fails to account for two important facts: (1) the fork restoration substrates tested contain 6 mismatches, compared to the 2 mismatches in fork regression substrates, which provides a higher barrier to fork regression; (2) RPA stimulates “normal” fork restoration to a much greater extent than “stalled” fork regression. Further experiments will be required to solve this mystery. One possibility is that the model put forth by Rémy Bétous is correct: at a stalled fork, SMARCAL1 performs fork regression, then after repair and processing, SMARCAL1 restores the repaired replication fork (Bétous et al. 2013).

It is also possible that SMARCAL1 only performs one or the other of these steps. Further insight into the function of SMARCAL1 in cells could be gained through analysis of replication intermediates in the presence and absence of SMARCAL1. This analysis could be performed using either electron microscopy or using density gradient centrifugation to identify nascent-nascent hybrids. It will prove interesting as well to test whether phosphorylation of SMARCAL1 on S652 alters the preference of SMARCAL1 for fork regression or restoration, given that this damage inducible phosphorylation site reduces SMARCAL1 activity in cells and SMARCAL1 phosphorylation requires DNA-binding activity of the protein (Couch et al. 2013).

A Model for SMARCAL1 and ZRANB3 Function

While ZRANB3 and SMARCAL1 are biochemically similar enzymes, it remains unclear whether these two proteins function in the same or different pathways in cells. Moreover, while the HARP domains of SMARCAL1 function as a substrate specificity domain to the point that chimaeras of the SMARCAL1 HARP domains and other SWI/SNF motor domains can perform annealing helicase activity (Ghosal et al. 2011), it is unclear what domain of ZRANB3 confers substrate specificity to the SWI/SNF motor.

In cells, SMARCAL1 and ZRANB3 localize to replication foci and sites of laser microirradiation (Bansbach et al. 2009; Ciccia et al. 2009, 2012; Weston et al. 2012; Yuan et al. 2009, 2012). Depletion of either protein results in γ H2AX foci formation and sensitivity to replication stress agents including HU, CPT, and MMC (Bansbach et al. 2009; Ciccia et al. 2009, 2012; Yuan et al. 2009, 2012). Interestingly, there are conflicting reports of the damage sensitivity of ZRANB3-depleted cells: one report found ZRANB3-depleted cells sensitive to MMS, but not HU or CPT (compare Weston et al. 2012 to Ciccia et al. 2012; Yuan et al. 2012).

In cells, these two proteins likely function at different places: SMARCAL1 is recruited to stalled forks via an interaction with RPA32, which places SMARCAL1 potentially at the replication fork junction (Bansbach et al. 2009; Ciccio et al. 2009; Yusufzai et al. 2009). On the other hand, ZRANB3 requires PCNA-Ub, which is associated with template switching and likely occurs behind the replication fork (Ciccio et al. 2012; Weston et al. 2012; Yuan et al. 2012; Zeman and Cimprich 2012). The simplest model, then, is that SMARCAL1 and ZRANB3 operate in different pathways. One such case is that SMARCAL1, but not ZRANB3, is required for the nascent-strand ssDNA that occurs in ATR inhibited cells (Couch et al. 2013). Thus, there is at least one separable function of SMARCAL1 and ZRANB3.

One model is as follows: SMARCAL1 is recruited to stalled forks through its interaction with RPA. SMARCAL1 fork regression protects these forks from nucleolytic degradation by MUS81. After repair, SMARCAL1 can restore the functional replication fork, and some unknown mechanism may reload the MCM helicase (Fig. 6.4A). Alternatively, a stalled fork may be reprimed, especially if the damage occurs on the lagging strand, allowing the replisome to continue away from the site of damage. In this case, the PCNA at the lesion may become poly-ubiquitinated by HLTF or SHPRH. Poly-ubiquitinated PCNA then recruits ZRANB3 to aid in some step of the error-free template switching mechanism of repair. What step this may be remains unclear, though ZRANB3 contains an HNH ATP-dependent endonuclease activity. Coupled with the observation that ZRANB3-deficient cells exhibit increased sister-chromatid exchange, this suggests that ZRANB3 aids in dissolution of the junction molecule between the two sister chromatids that forms during template switching (Fig. 6.4B). Of course, this is only a model and will require further experimentation.

How can we test this model? One obvious place to start is to test SMARCAL1 in the sister chromatid exchange assay. This will either indicate that SMARCAL1 deficiency

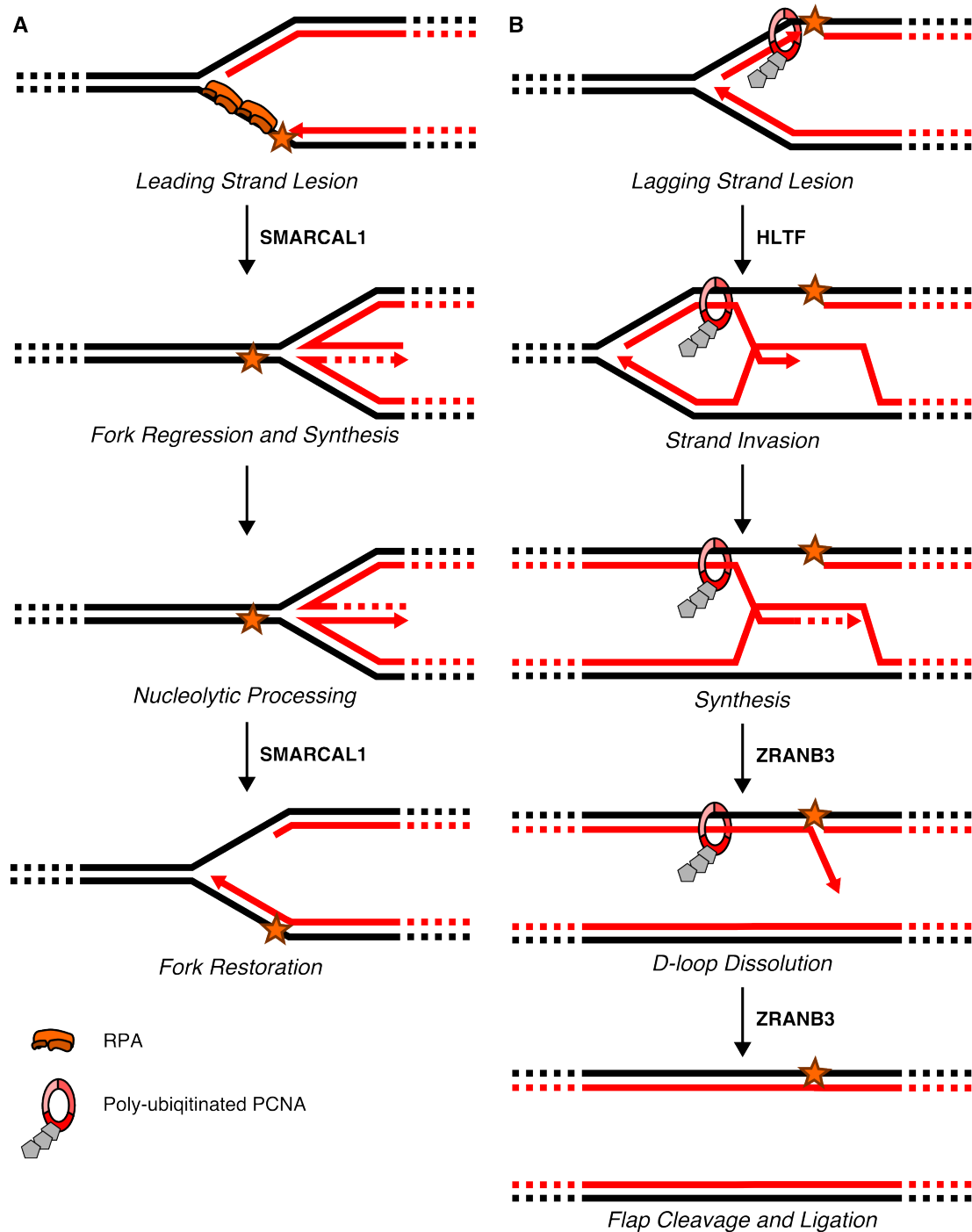


Figure 6.4 Differential functions of SMARCAL1 and ZRANB3. (A) RPA recruits SMARCAL1 to stalled forks, such as a polymerase blocking lesion on the leading strand. SMARCAL1 fork regression and restoration activities can allow lesion bypass by template switching. (B) A lagging strand lesion is unlikely to stall the replisome. Poly-ubiquitinated PCNA marks a lesion for error-free template switching. HLTF may begin this process. After synthesis, both the annealing helicase and nuclease activities of ZRANB3 are required to dissolve the sister chromatid junction. This model awaits experimental verification.

also results in increased sister chromatid exchanges, or that this is a distinct function of ZRANB3. In either case, this is an interesting result. Next, it would be elegant to show that HLTF or SHPRH and ZRANB3 are in the same pathway genetically, while SMARCAL1 and ZRANB3 are in separate pathways.

Regulation of ZRANB3

We demonstrated that SMARCAL1 is a phospho-regulated protein (Carroll et al. 2014; Couch et al. 2013). Notably, the linker region of SMARCAL1 containing S652 is highly conserved in ZRANB3 (Fig. 6.5). One testable hypothesis is that like SMARCAL1, ATR regulates ZRANB3 activity by phosphorylation of this linker region, especially T264. Another question is whether over-expression of ZRANB3 produces similar pan-nuclear and ssDNA phenotypes as SMARCAL1.

Conclusions

This dissertation makes several important contributions to the field of DNA damage repair, and provides a foundation from which we can continue to pull back the curtain on regulation of replication fork repair. In Chapter III, Bianca and I characterized the differences in protein recruitment at early vs late timepoints in HU. In Chapter IV, Carol and I demonstrated that one mechanism by which ATR stabilizes replication forks is through regulation of SMARCAL1. In Chapter V, I demonstrated common themes in the biochemical mechanism of annealing helicases.

I believe that future studies of the replication stress response should “zoom out” and take a systems biology approach to understand the interplay between the different fork repair pathways. To do this, changes in the transcriptome, phospho-proteome, and replication fork associated proteins should be compared over time in HU and with different damaging agents. Integrating all this information should reveal regulatory

pathways and feedback loops that allow time- and damage-dependent regulation of fork repair. One simple example of such a time-dependent regulatory mechanism is likely ATR phosphorylation of SMARCAL1 on S652: at early times in HU, most SMARCAL1 is unphosphorylated on S652 and this prevents MUS81 cleavage of stalled replication forks. However, at later times in HU, S652 may be highly phosphorylated, and the decreased SMARCAL1 activity may no longer be sufficient to prevent MUS81 from cleaving stalled forks (Fig. 6.3B). This is also consistent with the differential requirements for RAD51 at early and late timepoints in HU.

REFERENCES

- Achar YJ, Balogh D, and Haracska L (2011). Coordinated protein and DNA remodeling by human HLTF on stalled replication fork. *Proc. Natl. Acad. Sci. U. S. A.* 2011, 1–6.
- Anand RP, Lovett ST, and Haber JE (2013). Break-induced DNA replication. *Cold Spring Harb. Perspect. Biol.* 5, a010397.
- Anantha RW, Vassin VM, and Borowiec JA (2007). Sequential and synergistic modification of human RPA stimulates chromosomal DNA repair. *J. Biol. Chem.* 282, 35910–35923.
- Atkinson J, and McGlynn P (2009). Replication fork reversal and the maintenance of genome stability. *Nucleic Acids Res.* 37, 3475–3492.
- Van Attikum H, and Gasser SM (2009). Crosstalk between histone modifications during the DNA damage response. *Trends Cell Biol.* 19, 207–217.
- Bakkenist CJ, and Kastan MB (2003). DNA damage activates ATM through intermolecular autophosphorylation and dimer dissociation. *Nature* 421, 499–506.
- Bansbach CE, Bétous R, Lovejoy CA, Glick GG, and Cortez D (2009). The annealing helicase SMARCAL1 maintains genome integrity at stalled replication forks. *Genes Dev.* 23, 2405–2414.
- Bansbach CE, Boerkoel CF, and Cortez D (2010). SMARCAL1 and replication stress: An explanation for SIOD? *Nucleus* 1, 245–248.
- Baradaran-Heravi A, Raams A, Lubieniecka J, Cho KS, DeHaai KA, Basiratnia M, Mari P-O, Xue Y, Rauth M, Olney AH, et al. (2012). SMARCAL1 deficiency predisposes to non-Hodgkin lymphoma and hypersensitivity to genotoxic agents in vivo. *Am. J. Med. Genet.* 158A, 2204–2213.
- Bartucci M, Svensson S, Romania P, Dattilo R, Patrizii M, Signore M, Navarra S, Lotti F, Biffoni M, Pillozzi E, et al. (2011). Therapeutic targeting of Chk1 in NSCLC stem cells during chemotherapy. *Cell Death Differ.* 1–11.
- Bastin-Shanower SA, Fricke WM, Mullen JR, and Brill SJ (2003). The mechanism of Mus81-Mms4 cleavage site selection distinguishes it from the homologous endonuclease Rad1-Rad10. *Mol. Cell. ...* 23, 3487–3496.
- Berkovich E, Monnat RJ, and Kastan MB (2007). Roles of ATM and NBS1 in chromatin structure modulation and DNA double-strand break repair. *Nat. Cell Biol.* 9, 683–690.
- Berkovich E, Monnat RJ, and Kastan MB (2008). Assessment of protein dynamics and DNA repair following generation of DNA double-strand breaks at defined genomic sites. *Nat. Protoc.* 3, 915–922.
- Bétous R, Mason AC, Rambo RP, Bansbach CE, Badu-Nkansah A, Sirbu BM, Eichman BF, and Cortez D (2012). SMARCAL1 catalyzes fork regression and Holliday

- junction migration to maintain genome stability during DNA replication. *Genes Dev.* 26, 151–162.
- Bétous R, Couch FB, Mason AC, Eichman BF, Manosas M, and Cortez D (2013). Substrate-selective repair and restart of replication forks by DNA translocases. *Cell Rep.* 3, 1958–1969.
- Blastyák A, Pintér L, Unk I, Prakash L, Prakash S, and Haracska L (2007). Yeast Rad5 protein required for postreplication repair has a DNA helicase activity specific for replication fork regression. *Mol. Cell* 28, 167–175.
- Boerkoel CF, Takashima H, John J, Yan J, Stankiewicz P, Rosenbarker L, André J-L, Bogdanovic R, Burguet A, Cockfield S, et al. (2002). Mutant chromatin remodeling protein SMARCAL1 causes Schimke immuno-osseous dysplasia. *Nat. Genet.* 30, 215–220.
- Boutros R, Dozier C, and Ducommun B (2006). The when and wheres of CDC25 phosphatases. *Curr. Opin. Cell Biol.* 18, 185–191.
- Branzei D, and Foiani M (2010). Maintaining genome stability at the replication fork. *Nat. Rev. Mol. Cell Biol.* 11, 208–219.
- Brown EJ, and Baltimore D (2000). ATR disruption leads to chromosomal fragmentation and early embryonic lethality. *Genes Dev.* 397–402.
- Brown EJ, and Baltimore D (2003). Essential and dispensable roles of ATR in cell cycle arrest and genome maintenance. *Genes Dev.* 17, 615–628.
- Bryant HE, Schultz N, Thomas HD, Parker KM, Flower D, Lopez E, Kyle S, Meuth M, Curtin NJ, and Helleday T (2005). Specific killing of BRCA2-deficient tumours with inhibitors of poly(ADP-ribose) polymerase. *Nature* 434, 913–917.
- Byun T, Pacek M, Yee M, Walter JC, and Cimprich KA (2005). Functional uncoupling of MCM helicase and DNA polymerase activities activates the ATR-dependent checkpoint. *Genes ...* 1040–1052.
- Carroll C, Badu-Nkansah A, Hunley T, Baradaran-Heravi A, Cortez D, and Frangoul H (2013). Schimke immunoosseous dysplasia associated with undifferentiated carcinoma and a novel SMARCAL1 mutation in a child. *Pediatr. Blood Cancer* 60, E88–E90.
- Carroll C, Bansbach CE, Zhao R, Jung SY, Qin J, and Cortez D (2014). Phosphorylation of a C-terminal auto-inhibitory domain increases SMARCAL1 activity. *Nucleic Acids Res.* 42, 918–925.
- Chapman JR, and Jackson SP (2008). Phospho-dependent interactions between NBS1 and MDC1 mediate chromatin retention of the MRN complex at sites of DNA damage. *EMBO Rep.* 9, 795–801.
- Charrier J-D, Durrant SJ, Golec JMC, Kay DP, Knegtel RM a, MacCormick S, Mortimore M, O'Donnell ME, Pinder JL, Reaper PM, et al. (2011). Discovery of potent and

- selective inhibitors of ataxia telangiectasia mutated and Rad3 related (ATR) protein kinase as potential anticancer agents. *J. Med. Chem.* *54*, 2320–2330.
- Chen BPC, Uematsu N, Kobayashi J, Lerenthal Y, Krempler A, Yajima H, Löbrich M, Shiloh Y, and Chen DJ (2007). Ataxia telangiectasia mutated (ATM) is essential for DNA-PKcs phosphorylations at the Thr-2609 cluster upon DNA double strand break. *J. Biol. Chem.* *282*, 6582–6587.
- Chen T, Stephens P a, Middleton FK, and Curtin NJ (2012). Targeting the S and G2 checkpoint to treat cancer. *Drug Discov. Today* *17*, 194–202.
- Ciccio A, and Elledge SJ (2010). The DNA Damage Response: Making It Safe to Play with Knives. *Mol. Cell* *40*, 179–204.
- Ciccio A, Bredemeyer AL, Sowa ME, Terret M-E, Jallepalli P V, Harper JW, and Elledge SJ (2009). The SOD disorder protein SMARCAL1 is an RPA-interacting protein involved in replication fork restart. *Genes Dev.* *23*, 2415–2425.
- Ciccio A, Nimonkar A V, Hu Y, Hajdu I, Achar YJ, Izhar L, Petit S a, Adamson B, Yoon JC, Kowalczykowski SC, et al. (2012). Polyubiquitinated PCNA recruits the ZRANB3 translocase to maintain genomic integrity after replication stress. *Mol. Cell* *47*, 396–409.
- Cimprich KA, and Cortez D (2008). ATR: an essential regulator of genome integrity. *Nat. Rev. Mol. Cell Biol.* *9*, 616–627.
- Cobb JA, Bjergbaek L, Shimada K, Frei C, and Gasser SM (2003). DNA polymerase stabilization at stalled replication forks requires Mec1 and the RecQ helicase Sgs1. *EMBO J.* *22*, 4325–4336.
- Cobb JA, Schleker T, Rojas V, Bjergbaek L, Tercero JA, and Gasser SM (2005). Replisome instability, fork collapse, and gross chromosomal rearrangements arise synergistically from Mec1 kinase and RecQ helicase mutations. *Genes Dev.* *19*, 3055.
- Cong L, Ran F, Cox D, Lin S, and Barretto R (2013). Multiplex genome engineering using CRISPR/Cas systems. *Science* (80-.). *339*, 819–823.
- Cortez D, Guntuku S, Qin J, and Elledge SJ (2001). ATR and ATRIP: partners in checkpoint signaling. *Science* *294*, 1713–1716.
- Cotta-Ramusino C, Fachinetti D, Lucca C, Doksan Y, Lopes M, Sogo J, and Foiani M (2005). Exo1 processes stalled replication forks and counteracts fork reversal in checkpoint-defective cells. *Mol. Cell* *17*, 153–159.
- Couch FB, and Cortez D (2014). Fork reversal, too much of a good thing. *Cell Cycle* *13*, -1.
- Couch FB, Bansbach CE, Driscoll R, Luzwick JW, Glick GG, Bétous R, Carroll CM, Jung SY, Qin J, Cimprich KA, et al. (2013). ATR phosphorylates SMARCAL1 to prevent replication fork collapse. *Genes Dev.* *27*, 1610–1623.

- Coward P, Wada HG, Falk MS, Chan SD, Meng F, Akil H, and Conklin BR (1998). Controlling signaling with a specifically designed Gi-coupled receptor. *Proc. Natl. Acad. Sci. U. S. A.* *95*, 352–357.
- Cui X, Yu Y, Gupta S, Cho Y, Lees-miller SP, and Meek K (2005). Autophosphorylation of DNA-Dependent Protein Kinase Regulates DNA End Processing and May Also Alter Double-Strand Break Repair Pathway Choice Autophosphorylation of DNA-Dependent Protein Kinase Regulates DNA End Processing and May Also Alter Double-Strand.
- D'Amours D, and Jackson SP (2002). The Mre11 complex: at the crossroads of dna repair and checkpoint signalling. *Nat. Rev. Mol. Cell Biol.* *3*, 317–327.
- Deans AJ, and West SC (2011). DNA interstrand crosslink repair and cancer. *Nat. Rev. Cancer* *11*, 467–480.
- Deindl S, Hwang WL, Hota SK, Blosser TR, Prasad P, Bartholomew B, and Zhuang X (2013). ISWI remodelers slide nucleosomes with coordinated multi-base-pair entry steps and single-base-pair exit steps. *Cell* *152*, 442–452.
- Duggin IG, Wake RG, Bell SD, and Hill TM (2008). The replication fork trap and termination of chromosome replication. *Mol. Microbiol.* *70*, 1323–1333.
- Dupré A, Boyer-Chatenet L, Sattler RM, Modi AP, Lee J-H, Nicolette ML, Kopelovich L, Jasin M, Baer R, Paull TT, et al. (2008). A forward chemical genetic screen reveals an inhibitor of the Mre11-Rad50-Nbs1 complex. *Nat. Chem. Biol.* *4*, 119–125.
- Dürr H, Körner C, Müller M, Hickmann V, and Hopfner K-P (2005). X-ray structures of the *Sulfolobus solfataricus* SWI2/SNF2 ATPase core and its complex with DNA. *Cell* *121*, 363–373.
- Duursma AM, Driscoll R, Elias JE, and Cimprich K a (2013). A role for the MRN complex in ATR activation via TOPBP1 recruitment. *Mol. Cell* *50*, 116–122.
- Errico A, and Costanzo V (2010). Differences in the DNA replication of unicellular eukaryotes and metazoans: known unknowns. *EMBO Rep.* *11*, 270–278.
- Farmer H, McCabe N, Lord CJ, Tutt ANJ, Johnson D a, Richardson TB, Santarosa M, Dillon KJ, Hickson I, Knights C, et al. (2005). Targeting the DNA repair defect in BRCA mutant cells as a therapeutic strategy. *Nature* *434*, 917–921.
- Fekairi S, Scaglione S, Chahwan C, Taylor ER, Tissier A, Coulon S, Dong M-Q, Ruse C, Yates JR, Russell P, et al. (2009). Human SLX4 is a Holliday junction resolvase subunit that binds multiple DNA repair/recombination endonucleases. *Cell* *138*, 78–89.
- Flaus A, Martin DM a, Barton GJ, and Owen-Hughes T (2006). Identification of multiple distinct Snf2 subfamilies with conserved structural motifs. *Nucleic Acids Res.* *34*, 2887–2905.

- Fokas E, Prevo R, Hammond EM, Brunner TB, McKenna WG, and Muschel RJ (2014). Targeting ATR in DNA damage response and cancer therapeutics. *Cancer Treat. Rev.* *40*, 109–117.
- Forment J V, Blasius M, Guerini I, and Jackson SP (2011). Structure-specific DNA endonuclease mus81/eme1 generates DNA damage caused by chk1 inactivation. *PLoS One* *6*, e23517.
- Franchitto A, Pirzio LM, Prosperi E, Sabora O, Bignami M, and Pichierri P (2008). Replication fork stalling in WRN-deficient cells is overcome by prompt activation of a MUS81-dependent pathway. *J. Cell Biol.* *183*, 241–252.
- Fricke WM, Bastin-Shanower S a, and Brill SJ (2005). Substrate specificity of the *Saccharomyces cerevisiae* Mus81-Mms4 endonuclease. *DNA Repair (Amst.)* *4*, 243–251.
- Friedel AM, Pike BL, and Gasser SM (2009). ATR/Mec1: coordinating fork stability and repair. *Curr. Opin. Cell Biol.* *21*, 237–244.
- Fu D, Calvo J, and Samson L (2012). Balancing repair and tolerance of DNA damage caused by alkylating agents. *Nat. Rev. Cancer* *12*, 104–120.
- Fu YV, Yardimci H, Long DT, Guainazzi A, Bermudez VP, Hurwitz J, van Oijen A, Schärer OD, and Walter JC (2011). Selective Bypass of a Lagging Strand Roadblock by the Eukaryotic Replicative DNA Helicase. *Cell* *146*, 931–941.
- Gangaraju VK, and Bartholomew B (2007). Mechanisms of ATP-dependent chromatin remodelling. *Mutat. Res.* *618*, 3–17.
- Gari K, Décaillot C, Delannoy M, Wu L, and Constantinou A (2008a). Remodeling of DNA replication structures by the branch point translocase FANCM. *Proc. Natl. Acad. Sci. U. S. A.* *105*, 16107–16112.
- Gari K, Décaillot C, Stasiak AZ, Stasiak A, and Constantinou A (2008b). The Fanconi anemia protein FANCM can promote branch migration of Holliday junctions and replication forks. *Mol. Cell* *29*, 141–148.
- Ghosal G, Yuan J, and Chen J (2011). The HARP domain dictates the annealing helicase activity of HARP/SMARCAL1. *EMBO Rep.* *12*, 574–580.
- Gilad O, Nabet BY, Ragland RL, Schoppy DW, Smith KD, Durham AC, and Brown EJ (2010). Combining ATR suppression with oncogenic Ras synergistically increases genomic instability, causing synthetic lethality or tumorigenesis in a dosage-dependent manner. *Cancer Res.* *70*, 9693–9702.
- Goldberg M, Stucki M, Falck J, D'Amours D, Rahman D, Pappin D, Bartek J, and Jackson SP (2003). MDC1 is required for the intra-S-phase DNA damage checkpoint. *Nature* *421*, 952–956.
- Gu M, and Rice CM (2010). Three conformational snapshots of the hepatitis C virus NS3 helicase reveal a ratchet translocation mechanism. *Proc. Natl. Acad. Sci. U. S. A.* *107*, 521–528.

- Halazonetis TD, Gorgoulis VG, and Bartek J (2008). An oncogene-induced DNA damage model for cancer development. *Science* 319, 1352–1355.
- Hanada K, Budzowska M, Davies SL, van Drunen E, Onizawa H, Beverloo HB, Maas A, Essers J, Hickson ID, and Kanaar R (2007). The structure-specific endonuclease Mus81 contributes to replication restart by generating double-strand DNA breaks. *Nat. Struct. Mol. Biol.* 14, 1096–1104.
- Hanahan D, and Weinberg RA a (2011). Hallmarks of cancer: the next generation. *Cell* 144, 646–674.
- Harper JW, and Elledge SJ (2007). The DNA damage response: ten years after. *Mol. Cell* 28, 739–745.
- Hartlerode AJ, and Scully R (2009). Mechanisms of double-strand break repair in somatic mammalian cells. *Biochem. J.* 423, 157–168.
- Hashimoto Y, Chaudhuri AR, Lopes M, and Costanzo V (2010). Rad51 protects nascent DNA from Mre11-dependent degradation and promotes continuous DNA synthesis. *Nat. Struct. Mol. Biol.* 17, 1305–1311.
- Hashimoto Y, Puddu F, and Costanzo V (2011). RAD51- and MRE11-dependent reassembly of uncoupled CMG helicase complex at collapsed replication forks. *Nat. Struct. Mol. Biol.* 1–9.
- Helleday T (2011). The underlying mechanism for the PARP and BRCA synthetic lethality: Clearing up the misunderstandings. *Mol. Oncol.* 1–7.
- Hickson I, Zhao Y, Richardson CJ, Green SJ, Martin NMB, Orr AI, Reaper PM, Jackson SP, Curtin NJ, and Smith GCM (2004). Identification and characterization of a novel and specific inhibitor of the ataxia-telangiectasia mutated kinase ATM. *Cancer Res.* 64, 9152–9159.
- Huang J, Liu S, Bellani M, and Thazhathveetil A (2013). The DNA Translocase FANCM/MHF Promotes Replication Traverse of DNA Interstrand Crosslinks. *Mol. Cell* 52, 434–446.
- Huertas P, and Jackson SP (2009). Human CtIP mediates cell cycle control of DNA end resection and double strand break repair. *J. Biol. Chem.* 284, 9558–9565.
- Ichijima Y, Ichijima M, Lou Z, Nussenzweig A, Camerini-Otero RD, Chen J, Andreassen PR, and Namekawa SH (2011). MDC1 directs chromosome-wide silencing of the sex chromosomes in male germ cells. *Genes Dev.* 25, 959–971.
- Jones RM, and Petermann E (2012). Replication fork dynamics and the DNA damage response. *Biochem. J.* 443, 13–26.
- Kaidi A, Weinert BT, Choudhary C, and Jackson SP (2010). Human SIRT6 Promotes DNA End Resection Through CtIP Deacetylation. *Science* (80-.). 329, 1348–1353.
- Kakarougkas A, and Jeggo PA (2013). DNA DSB repair pathway choice: an orchestrated handover mechanism. *Br. J. Radiol.* 87.

- De Klein A, Muijtjens M, van Os R, Verhoeven Y, Smit B, Carr AM, Lehmann AR, and Hoesjmakers JHJ (2000). Targeted disruption of the cell-cycle checkpoint gene ATR leads to early embryonic lethality in mice. *Curr. Biol.* 10, 479–482.
- Kobayashi M, Hayashi N, Takata M, and Yamamoto K-I (2013). NBS1 directly activates ATR independently of MRE11 and TOPBP1. *Genes Cells* 18, 238–246.
- Leahy JJJ, Golding BT, Griffin RJ, Hardcastle IR, Richardson C, Rigoreau L, and Smith GCM (2004). Identification of a highly potent and selective DNA-dependent protein kinase (DNA-PK) inhibitor (NU7441) by screening of chromenone libraries. *Bioorg. Med. Chem. Lett.* 14, 6083–6087.
- Lebofsky R, Takahashi T, and Walter J (2009). DNA replication in nucleus-free *Xenopus* egg extracts. *Methods Mol. Biol.* 521, 229–252.
- Lee J, and Dunphy WG (2013). The Mre11-Rad50-Nbs1 (MRN) complex has a specific role in the activation of Chk1 in response to stalled replication forks. *Mol. Biol. Cell* 24, 1343–1353.
- Leung KHT, El Hassan MA, and Bremner R (2013). A rapid and efficient method to purify proteins at replication forks under native conditions. *Biotechniques* 55, 204–206.
- Lewis R, Dürr H, Hopfner K-P, and Michaelis J (2008). Conformational changes of a Swi2/Snf2 ATPase during its mechano-chemical cycle. *Nucleic Acids Res.* 36, 1881–1890.
- Li X, Corsa CAS, Pan PW, Wu L, Ferguson D, Yu X, Min J, and Dou Y (2010). MOF and H4 K16 acetylation play important roles in DNA damage repair by modulating recruitment of DNA damage repair protein Mdc1. *Mol. Cell. Biol.* 30, 5335–5347.
- Lin J-R, Zeman MK, Chen J-Y, Yee M-C, and Cimprich K a (2011). SHPRH and HLTF Act in a Damage-Specific Manner to Coordinate Different Forms of Postreplication Repair and Prevent Mutagenesis. *Mol. Cell* 42, 1–13.
- Lopes M, Cotta-Ramusino C, Pelliccioli a, Liberi G, Plevani P, Muzi-Falconi M, Newlon CS, and Foiani M (2001). The DNA replication checkpoint response stabilizes stalled replication forks. *Nature* 412, 557–561.
- López-Contreras AJ, Gutierrez-Martinez P, Specks J, Rodrigo-Perez S, and Fernandez-Capetillo O (2012). An extra allele of Chk1 limits oncogene-induced replicative stress and promotes transformation. *J. Exp. Med.*
- Lovejoy CCA, and Cortez D (2009). Common mechanisms of PIKK regulation. *DNA Repair (Amst)*. 8, 1004–1008.
- Lucca C, Vanoli F, Cotta-Ramusino C, Pelliccioli A, Liberi G, Haber J, and Foiani M (2004). Checkpoint-mediated control of replisome-fork association and signalling in response to replication pausing. *Oncogene* 23, 1206–1213.
- Lukas C, Melander F, Stucki M, Falck J, Bekker-Jensen S, Goldberg M, Lerenthal Y, Jackson SP, Bartek J, and Lukas J (2004). Mdc1 couples DNA double-strand break

- recognition by Nbs1 with its H2AX-dependent chromatin retention. *EMBO J.* **23**, 2674–2683.
- MacAlpine DM, and Almouzni G (2013). Chromatin and DNA replication. *Cold Spring Harb. Perspect. Biol.* **5**, a010207.
- Machwe A, Xiao L, Groden J, and Orren D (2006). The Werner and Bloom syndrome proteins catalyze regression of a model replication fork. *Biochemistry* **45**.
- Machwe A, Xiao L, Lloyd RG, Bolt E, and Orren DK (2007). Replication fork regression in vitro by the Werner syndrome protein (WRN): holliday junction formation, the effect of leading arm structure and a potential role for WRN exonuclease activity. *Nucleic Acids Res.* **35**, 5729–5747.
- Mali P, Yang L, Esvelt K, and Aach J (2013). RNA-guided human genome engineering via Cas9. *Science* (80-.). **339**, 823–826.
- Manosas M, Perumal SK, Croquette V, and Benkovic SJ (2012). Direct Observation of Stalled Fork Restart via Fork Regression in the T4 Replication System. *Science* (80-.). **338**, 1217–1220.
- Manosas M, Perumal SK, Bianco P, Ritort F, Benkovic SJ, and Croquette V (2013). RecG and UvsW catalyze robust DNA rewinding critical for stalled DNA replication fork rescue. *Nat. Commun.* **4**, 2368.
- Matsuoka S, Ballif B a, Smogorzewska A, McDonald ER, Hurov KE, Luo J, Bakalarski CE, Zhao Z, Solimini N, Lerenthal Y, et al. (2007). ATM and ATR substrate analysis reveals extensive protein networks responsive to DNA damage. *Science* **316**, 1160–1166.
- McGlynn P, and Lloyd RG (2001). Rescue of stalled replication forks by RecG: simultaneous translocation on the leading and lagging strand templates supports an active DNA unwinding model of fork reversal and Holliday junction formation. *Proc. Natl. Acad. Sci. U. S. A.* **98**, 8227–8234.
- McGlynn P, and Lloyd RG (2002). Genome stability and the processing of damaged replication forks by RecG. *Trends Genet.* **18**, 413–419.
- Meek K, Dang V, and Lees-Miller SP (2008). DNA-PK: the means to justify the ends? *Adv. Immunol.* **99**, 33–58.
- Mimitou EP, and Symington LS (2009). DNA end resection: many nucleases make light work. *DNA Repair (Amst)*. **8**, 983–995.
- Mordes DA, Glick GG, Zhao R, and Cortez D (2008). TopBP1 activates ATR through ATRIP and a PIKK regulatory domain. *Genes Dev.* **22**, 1478–1489.
- Morrison AJ, and Shen X (2009). Chromatin remodelling beyond transcription: the INO80 and SWR1 complexes. *Nat. Rev. Mol. Cell Biol.* **10**, 373–384.
- Moses JE, and Moorhouse AD (2007). The growing applications of click chemistry. *Chem. Soc. Rev.* **36**, 1249–1262.

- Motegi A, Liaw H-J, Lee K-Y, Roest HP, Maas A, Wu X, Moinova H, Markowitz SD, Ding H, Hoeijmakers JHJ, et al. (2008). Polyubiquitination of proliferating cell nuclear antigen by HLTF and SHPRH prevents genomic instability from stalled replication forks. *Proc. Natl. Acad. Sci. U. S. A.* *105*, 12411–12416.
- Mourón S, Rodriguez-Acebes S, Martínez-Jiménez MI, García-Gómez S, Chocrón S, Blanco L, and Méndez J (2013). Repriming of DNA synthesis at stalled replication forks by human PrimPol. *Nat. Struct. Mol. Biol.* *1*.
- Mulcair MD, Schaeffer PM, Oakley AJ, Cross HF, Neylon C, Hill TM, and Dixon NE (2006). A molecular mousetrap determines polarity of termination of DNA replication in *E. coli*. *Cell* *125*, 1309–1319.
- Myers JS, and Cortez D (2006). Rapid activation of ATR by ionizing radiation requires ATM and Mre11. *J. Biol. Chem.* *281*, 9346–9350.
- Nam EA, and Cortez D (2011). ATR signalling: more than meeting at the fork. *Biochem. J.* *436*, 527–536.
- Nam EA, Zhao R, Glick GG, Bansbach CE, Friedman DB, and Cortez D (2011a). T1989 phosphorylation is a marker of active ataxia telangiectasia-mutated and rad3-related (ATR) kinase. *J. Biol. Chem.* *286*, 28707–28714.
- Nam EA, Zhao R, and Cortez D (2011b). Analysis of mutations that dissociate G(2) and essential S phase functions of human ataxia telangiectasia-mutated and Rad3-related (ATR) protein kinase. *J. Biol. Chem.* *286*, 37320–37327.
- Neelsen KJ, Zanini IMY, Herrador R, and Lopes M (2013). Oncogenes induce genotoxic stress by mitotic processing of unusual replication intermediates. *J. Cell Biol.* *200*, 699–708.
- Nelson S, Perumal S, and Benkovic S (2009). Processive and Unidirectional Translocation of Monomeric UvsW Helicase on Single-Stranded DNA. *Biochemistry* *48*, 1036–1046.
- O'Donnell M, Langston L, and Stillman B (2013). Principles and concepts of DNA replication in bacteria, archaea, and eukarya. *Cold Spring Harb. Perspect. Biol.* *5*.
- O'Driscoll M, Ruiz-Perez VL, Woods CG, Jeggo PA, and Goodship JA (2003). A splicing mutation affecting expression of ataxia-telangiectasia and Rad3-related protein (ATR) results in Seckel syndrome. *Nat. Genet.* *33*, 497–501.
- Oshima J, Huang S, Pae C, Campisi J, and Schiestl RH (2002). Lack of WRN results in extensive deletion at nonhomologous joining ends. *Cancer Res.* *62*, 547.
- Osman F, and Whitby MC (2007). Exploring the roles of Mus81-Eme1/Mms4 at perturbed replication forks. *DNA Repair (Amst).* *6*, 1004–1017.
- Paciotti V, Clerici M, Scotti M, Longhese MP, Lucchini G, and Longhese MPIA (2001). Characterization of mec1 Kinase-Deficient Mutants and of New Hypomorphic mec1 Alleles Impairing Subsets of the DNA Damage Response Pathway Characterization

of *mec1* Kinase-Deficient Mutants and of New Hypomorphic *mec1* Alleles Impairing Subsets of the DNA D.

- Paull TT (2010). Making the best of the loose ends: Mre11/Rad50 complexes and Sae2 promote DNA double-strand break resection. *DNA Repair (Amst)*. 9, 1283–1291.
- Perumal SK, Nelson SW, and Benkovic SJ (2013). Interaction of T4 UvsW helicase and single-stranded DNA binding protein gp32 through its carboxy-terminal acidic tail. *J. Mol. Biol.* 425, 2823–2839.
- Petermann E, and Helleday T (2010). Pathways of mammalian replication fork restart. *Nat. Rev. Mol. Cell Biol.* 11, 683–687.
- Petermann E, Issaeva N, Orta ML, Schultz N, and Helleday T (2010). Hydroxyurea-stalled replication forks become progressively inactivated and require two different RAD51-mediated pathways for restart and repair. *Mol. Cell* 37, 492–502.
- Pommier Y (2006). Topoisomerase I inhibitors: camptothecins and beyond. *Nat. Rev. Cancer* 6, 789–802.
- Postow L, Woo EM, Chait BT, and Funabiki H (2009). Identification of SMARCAL1 as a component of the DNA damage response. *J. Biol. Chem.* 284, 35951–35961.
- Ragland RL, Patel S, Rivard RS, Smith K, Peters AA, Bielinsky A-K, and Brown EJ (2013). RNF4 and PLK1 are required for replication fork collapse in ATR-deficient cells. *Genes Dev.* 27, 2259–2273.
- Ralf C, Hickson ID, and Wu L (2006). The Bloom's syndrome helicase can promote the regression of a model replication fork. *J. Biol. Chem.* 281, 22839–22846.
- Ray Chaudhuri A, Hashimoto Y, Herrador R, Neelsen KJ, Fachinetti D, Bermejo R, Cocito A, Costanzo V, and Lopes M (2012). Topoisomerase I poisoning results in PARP-mediated replication fork reversal. *Nat. Struct. Mol. Biol.*
- Reaper PM, Griffiths MR, Long JM, Charrier J-D, MacCormick S, Charlton P a, Golec JMC, and Pollard JR (2011). Selective killing of ATM- or p53-deficient cancer cells through inhibition of ATR. *Nat. Chem. Biol.* 1–4.
- Regairaz M, Zhang Y-W, Fu H, Agama KK, Tata N, Agrawal S, Aladjem MI, and Pommier Y (2011). Mus81-mediated DNA cleavage resolves replication forks stalled by topoisomerase I-DNA complexes. *J. Cell Biol.* 195, 739–749.
- Rodrigue A, Lafrance M, Gauthier M-C, McDonald D, Hendzel M, West SC, Jasin M, and Masson J-Y (2006). Interplay between human DNA repair proteins at a unique double-strand break in vivo. *EMBO J.* 25, 222–231.
- Rossetto D, Truman AW, Kron SJ, and Côté J (2010). Epigenetic modifications in double-strand break DNA damage signaling and repair. *Clin. Cancer Res.* 16, 4543–4552.

- Rudin N, and Haber JE (1988). Efficient repair of HO-induced chromosomal breaks in *Saccharomyces cerevisiae* by recombination between flanking homologous sequences. *Mol. Cell. Biol.* 8, 3918–3928.
- Salic A, and Mitchison TJ (2008). A chemical method for fast and sensitive detection of DNA synthesis in vivo. *Proc. Natl. Acad. Sci. U. S. A.* 105, 2415–2420.
- Sarkaria JN, Busby EC, Tibbetts RS, Roos P, Taya Y, Karnitz LM, and Abraham RT (1999). Inhibition of ATM and ATR kinase activities by the radiosensitizing agent, caffeine. *Cancer Res.* 59, 4375–4382.
- Sartori A a, Lukas C, Coates J, Mistrik M, Fu S, Bartek J, Baer R, Lukas J, and Jackson SP (2007). Human CtIP promotes DNA end resection. *Nature* 450, 509–514.
- Savic V, Yin B, Maas NL, Bredemeyer AL, Carpenter AC, Helmink B a, Yang-iott KS, Sleckman BP, and Bassing CH (2009). Formation of dynamic gamma-H2AX domains along broken DNA strands is distinctly regulated by ATM and MDC1 and dependent upon H2AX densities in chromatin. *Mol. Cell* 34, 298–310.
- Schlacher K, Christ N, Siaud N, Egashira A, Wu H, and Jasin M (2011). Double-Strand Break Repair-Independent Role for BRCA2 in Blocking Stalled Replication Fork Degradation by MRE11. *Cell* 145, 529–542.
- Schlacher K, Wu H, and Jasin M (2012). A Distinct Replication Fork Protection Pathway Connects Fanconi Anemia Tumor Suppressors to RAD51-BRCA1/2. *Cancer Cell* 22, 106–116.
- Schoppy DW, Ragland RL, Gilad O, Shastri N, Peters AA, Murga M, Fernandez-Capetillo O, Diehl JA, and Brown EJ (2012). Oncogenic stress sensitizes murine cancers to hypomorphic suppression of ATR. *J. Clin. ...* 122, 241–252.
- Seiler JA, Conti C, Syed A, Aladjem MI, and Pommier Y (2007). The intra-S-phase checkpoint affects both DNA replication initiation and elongation: single-cell and -DNA fiber analyses. *Mol. Cell. Biol.* 27, 5806–5818.
- Shao RG, Cao CX, Zhang H, Kohn KW, Wold MS, and Pommier Y (1999). Replication-mediated DNA damage by camptothecin induces phosphorylation of RPA by DNA-dependent protein kinase and dissociates RPA:DNA-PK complexes. *EMBO J.* 18, 1397–1406.
- Sharma GG, So S, Gupta A, Kumar R, Cayrou C, Avvakumov N, Bhadra U, Pandita RK, Porteus MH, Chen DJ, et al. (2010). MOF and histone H4 acetylation at lysine 16 are critical for DNA damage response and double-strand break repair. *Mol. Cell. Biol.* 30, 3582–3595.
- Shen X, Do H, Li Y, Chung W-H, Tomasz M, de Winter JP, Xia B, Elledge SJ, Wang W, and Li L (2009). Recruitment of fanconi anemia and breast cancer proteins to DNA damage sites is differentially governed by replication. *Mol. Cell* 35, 716–723.

- Shibata A, Conrad S, Birraux J, Geuting V, Barton O, Ismail A, Kakarougkas A, Meek K, Taucher-Scholz G, Löbrich M, et al. (2011). Factors determining DNA double-strand break repair pathway choice in G2 phase. *EMBO J.* 1–14.
- Shimura T, Torres MJ, Martin MM, Rao VA, Pommier Y, Katsura M, Miyagawa K, and Aladjem MI (2008). Bloom's syndrome helicase and Mus81 are required to induce transient double-strand DNA breaks in response to DNA replication stress. *J. Mol. Biol.* 375, 1152–1164.
- Siddiqui K, On KF, and Diffley JFX (2013). Regulating DNA replication in eukarya. *Cold Spring Harb. Perspect. Biol.* 5.
- Singleton MR, Scaife S, and Wigley DB (2001). Structural Analysis of DNA Replication Fork Reversal by RecG. *Cell* 107, 79–89.
- Singleton MR, Dillingham MS, and Wigley DB (2007). Structure and mechanism of helicases and nucleic acid translocases. *Annu. Rev. Biochem.* 76, 23–50.
- Sirbu BM, Couch FB, Feigerle JT, Bhaskara S, Hiebert SW, and Cortez D (2011). Analysis of protein dynamics at active, stalled, and collapsed replication forks. *Genes Dev.* 25, 1320–1327.
- Sirbu BM, Couch FB, and Cortez D (2012). Monitoring the spatiotemporal dynamics of proteins at replication forks and in assembled chromatin using isolation of proteins on nascent DNA. *Nat. Protoc.* 7, 594–605.
- Sirbu BM, McDonald WH, Dungalwala H, Badu-Nkansah A, Kavanaugh GM, Chen Y, Tabb DL, and Cortez D (2013). Identification of proteins at active, stalled, and collapsed replication forks using isolation of proteins on nascent DNA (iPOND) coupled with mass spectrometry. *J. Biol. Chem.* 288, 31458–31467.
- Sobel RE, Cook RG, Perry CA, Annunziato AT, and Allis CD (1995). Conservation of deposition-related acetylation sites in newly synthesized histones H3 and H4. *Proc. Natl. Acad. Sci. U. S. A.* 92, 1237–1241.
- Sogo JM, Lopes M, and Foiani M (2002). Fork reversal and ssDNA accumulation at stalled replication forks owing to checkpoint defects. *Science* 297, 599–602.
- Soutoglou E, Dorn JF, Sengupta K, Jasin M, Nussenzweig A, Ried T, Danuser G, and Misteli T (2007). Positional stability of single double-strand breaks in mammalian cells. *Nat. Cell Biol.* 9, 675–682.
- Sprouse RO, Brenowitz M, and Auble DT (2006). Snf2/Swi2-related ATPase Mot1 drives displacement of TATA-binding protein by gripping DNA. *EMBO J.* 25, 1492–1504.
- Spycher C, Miller ES, Townsend K, Pavic L, Morrice N a, Janscak P, Stewart GS, and Stucki M (2008). Constitutive phosphorylation of MDC1 physically links the MRE11-RAD50-NBS1 complex to damaged chromatin. *J. Cell Biol.* 181, 227–240.
- Stanley LK, Seidel R, van der Scheer C, Dekker NH, Szczelkun MD, and Dekker C (2006). When a helicase is not a helicase: dsDNA tracking by the motor protein EcoR124I. *EMBO J.* 25, 2230–2239.

- Svendsen JM, Smogorzewska A, Sowa ME, O'Connell BC, Gygi SP, Elledge SJ, and Harper JW (2009). Mammalian BTBD12/SLX4 assembles a Holliday junction resolvase and is required for DNA repair. *Cell* 138, 63–77.
- Taddei A, Roche D, Sibarita JB, Turner BM, and Almouzni G (1999). Duplication and maintenance of heterochromatin domains. *J. Cell Biol.* 147, 1153–1166.
- Tanaka T, and Masai H (2006). Stabilization of a stalled replication fork by concerted actions of two helicases. *J. Biol. Chem.* 281, 3484–3493.
- Tibbetts RS, Brumbaugh KM, Williams JM, Sarkaria JN, Cliby WA, Shieh S, Taya Y, Prives C, and Abraham RT (1999). A role for ATR in the DNA damage-induced phosphorylation of p53 A role for ATR in the DNA phosphorylation of p53. 152–157.
- Toledo LI, Murga M, and Fernandez-Capetillo O (2011a). Targeting ATR and Chk1 kinases for cancer treatment: a new model for new (and old) drugs. *Mol. Oncol.* 5, 368–373.
- Toledo LI, Murga M, Zur R, Soria R, Rodriguez A, Martinez S, Oyarzabal J, Pastor J, Bischoff JR, and Fernandez-Capetillo O (2011b). A cell-based screen identifies ATR inhibitors with synthetic lethal properties for cancer-associated mutations. *Nat. Struct. Mol. Biol.* 18, 721–727.
- Toledo LI, Altmeyer M, Rask M-B, Lukas C, Larsen DH, Povlsen LK, Bekker-Jensen S, Mailand N, Bartek J, and Lukas J (2013). ATR prohibits replication catastrophe by preventing global exhaustion of RPA. *Cell* 155, 1088–1103.
- Trenz K, Smith E, Smith S, and Costanzo V (2006). ATM and ATR promote Mre11 dependent restart of collapsed replication forks and prevent accumulation of DNA breaks. *EMBO J.* 25, 1764–1774.
- Ulrich HD, and Walden H (2010). Ubiquitin signalling in DNA replication and repair. *Nat. Rev. Mol. Cell Biol.* 11, 479–489.
- Unk I, Hajdú I, Blastyák A, and Haracska L (2010). Role of yeast Rad5 and its human orthologs, HLF1 and SHPRH in DNA damage tolerance. *DNA Repair (Amst)*. 9, 257–267.
- Venkitaraman AR (2010). Modifying chromatin architecture during the response to DNA breakage. *Crit. Rev. Biochem. Mol. Biol.* 45, 2–13.
- Wang H, Zhao Y, Li L, McNutt M a, Wu L, Lu S, Yu Y, Zhou W, Feng J, Chai G, et al. (2008). An ATM- and Rad3-related (ATR) signaling pathway and a phosphorylation-acetylation cascade are involved in activation of p53/p21Waf1/Cip1 in response to 5-aza-2'-deoxycytidine treatment. *J. Biol. Chem.* 283, 2564–2574.
- Wang J, Gong Z, and Chen J (2011). MDC1 collaborates with TopBP1 in DNA replication checkpoint control. *J. Cell Biol.* 193, 267–273.
- Wang T, Wei J, Sabatini D, and Lander E (2013a). Genetic Screens in Human Cells Using the CRISPR/Cas9 System. *Science* (80-.). 1–8.

- Wang Y, Ji P, Liu J, Broaddus RR, Xue F, and Zhang W (2009). Centrosome-associated regulators of the G(2)/M checkpoint as targets for cancer therapy. *Mol. Cancer* 8, 8.
- Wang Y, Leung JW, Jiang Y, Lowery MG, Do H, Vasquez KM, Chen J, Wang W, and Li L (2013b). FANCM and FAAP24 maintain genome stability via cooperative as well as unique functions. *Mol. Cell* 49, 997–1009.
- Ward IM, and Chen J (2001). Histone H2AX is phosphorylated in an ATR-dependent manner in response to replicational stress. *J. Biol. Chem.* 276, 47759–47762.
- Weston R, Peeters H, and Ahel D (2012). ZRANB3 is a structure-specific ATP-dependent endonuclease involved in replication stress response. *Genes Dev.* 26, 1558–1572.
- Whitby MC, Vincent SD, and Lloyd RG (1994). Branch migration of Holliday junctions: identification of RecG protein as a junction specific DNA helicase. *EMBO J.* 13, 5220–5228.
- Whitehouse I, and Stockdale C (2003). Evidence for DNA translocation by the ISWI chromatin-remodeling enzyme. ... *Cell. Biol.* 23.
- Wu L, Luo K, Lou Z, and Chen J (2008). MDC1 regulates intra-S-phase checkpoint by targeting NBS1 to DNA double-strand breaks. *Proc. Natl. Acad. Sci. U. S. A.* 105, 11200–11205.
- Wysocka J, Reilly P, and Herr W (2001). Loss of HCF-1—chromatin association precedes temperature-induced growth arrest of tsBN67 cells. *Mol. Cell. Biol.* 21, 3820–3829.
- Yeeles JTP, and Marians KJ (2013). Dynamics of Leading-Strand Lesion Skipping by the Replisome. *Mol. Cell* 1–11.
- Yeeles JTP, Poli J, Marians KJ, and Pasero P (2013). Rescuing stalled or damaged replication forks. *Cold Spring Harb. Perspect. Biol.* 5, a012815.
- You Z, and Bailis JM (2010). DNA damage and decisions: CtIP coordinates DNA repair and cell cycle checkpoints. *Trends Cell Biol.* 20, 402–409.
- You Z, Bailis JM, Johnson SA, Dilworth SM, and Hunter T (2007). Rapid activation of ATM on DNA flanking double-strand breaks. *Nat. Cell Biol.* 9, 1311–1318.
- Yuan J, Ghosal G, and Chen J (2009). The annealing helicase HARP protects stalled replication forks. *Genes Dev.* 23, 2394–2399.
- Yuan J, Ghosal G, and Chen J (2012). The HARP-like Domain-Containing Protein AH2/ZRANB3 Binds to PCNA and Participates in Cellular Response to Replication Stress. *Mol. Cell* 47, 1–12.
- Yusufzai T, and Kadonaga JT (2008). HARP is an ATP-driven annealing helicase. *Science* 322, 748–750.
- Yusufzai T, and Kadonaga JT (2010). Annealing helicase 2 (AH2), a DNA-rewinding motor with an HNH motif. *Proc. Natl. Acad. Sci. U. S. A.* 107, 20970–20973.

- Yusufzai T, Kong X, Yokomori K, and Kadonaga JT (2009). The annealing helicase HARP is recruited to DNA repair sites via an interaction with RPA. *Genes Dev.* *23*, 2400–2404.
- Zeman MK, and Cimprich K a (2012). Finally, polyubiquitinated PCNA gets recognized. *Mol. Cell* *47*, 333–334.
- Zeman MK, and Cimprich K a (2013). Causes and consequences of replication stress. *Nat. Cell Biol.* *16*, 2–9.
- Zhong Y, Nellimoottil T, Peace JM, Knott SR V, Villwock SK, Yee JM, Jancuska JM, Rege S, Tecklenburg M, Sclafani R a, et al. (2013). The level of origin firing inversely affects the rate of replication fork progression. *J. Cell Biol.* *201*, 373–383.